

**Synchronization Analysis of Winner-Take-All Neuronal  
Networks**

by

**Brandon Bernard Jennings**

B.S. Computer Engineering, University of Maryland, Baltimore County, 2013

M.S. Computer Engineering, University of Pittsburgh, 2016

Submitted to the Graduate Faculty of  
Swanson School of Engineering in partial fulfillment  
of the requirements for the degree of  
Doctor of Philosophy

University of Pittsburgh

2019

UNIVERSITY OF PITTSBURGH  
SWANSON SCHOOL OF ENGINEERING

This dissertation was presented

by

**Brandon Bernard Jennings**

It was defended on

March 28, 2019

and approved by

Murat Akcakaya, PhD, Assistant Professor, Department of Electrical and Computer Engineering

Samuel Dickerson, PhD, Assistant Professor, Department of Electrical and Computer  
Engineering

Ervin Sejdic, PhD, Associate Professor, Department of Electrical and Computer Engineering

Sylvanus Wosu, PhD, Associate Professor, Department of Mechanical Engineering & Materials  
Science

Dissertation Co-Director: Ahmed Dallal, PhD, Assistant Professor, Department of Electrical and  
Computer Engineering

Dissertation Co-Director: Zhi-Hong Mao, PhD, Professor, Department of Electrical and  
Computer Engineering

Copyright © by Brandon Bernard Jennings

2019

# **Synchronization Analysis of Winner-Take-All Neuronal Networks**

Brandon Bernard Jennings, PhD

University of Pittsburgh, 2019

With the physical limitations of current CMOS technology, it becomes necessary to design and develop new methods to perform simple and complex computations. Nature is efficient, so many in the scientific community attempt to mimic it when optimizing or creating new systems and devices. The human brain is looked to as an efficient computing device, inspiring strong interest in developing powerful computer systems that resemble its architecture and behavior such as neural networks. There is much research focusing on both circuit designs that behave like neurons and arrangement of these electromechanical neurons to compute complex operations.

It has been shown previously that the synchronization characteristics of neural oscillators can be used not only for primitive computation functions such as convolution but for complex non-Boolean computations. With strong interest in the research community to develop biologically representative neural networks, this dissertation analyzes and simulates biologically plausible networks, the four-dimensional Hodgkin-Huxley and the simpler two-dimensional Fitzhugh-Nagumo neural models, fashioned in winner-take-all neuronal networks. The synchronization behavior of these neurons coupled together is studied in detail. Different neural network topologies are considered including lateral inhibition and inhibition via a global interneuron. Then, this dissertation analyzes the winner-take-all behaviors, in terms of both firing rates and phases, of neuronal networks with different topologies. A technique based on phase response curve is suggested for the analysis of synchronization phase characteristics of winner-take-all networks.

Simulations are performed to validate the analytical results. This study promotes the understanding of winner-take-all operations in biological neuronal networks and provides a fundamental basis for applications of winner-take-all networks in modern computing systems.

## Table of Contents

Preface.....	xix
1.0 Introduction.....	1
1.1 Motivation .....	2
1.2 Neuron Models .....	5
1.2.1 Hodgkin-Huxley.....	6
1.2.2 Fitzhugh-Nagumo .....	11
1.3 Contributions .....	13
2.0 Winner-Take-All Networks .....	14
2.1 Biological Lateral Inhibition .....	14
2.2 Nonbiological Lateral Inhibition .....	17
2.3 Winner-Take-All Via Lateral Inhibition .....	19
2.4 Nonbiological Winner-Take-All .....	20
2.5 Winner-Take-All Model.....	23
3.0 Analysis of Neruonal Dynamics .....	27
3.1 Equilibrium Points.....	27
3.1.1 Fitzhugh-Nagumo Model .....	30
3.2 Limit Cycles .....	35
3.2.1 Fitzhugh-Nagumo Model.....	36
4.0 Winner-Take-All in Firing Rate Competition.....	41
4.1 Lateral Inhibition Equations .....	41
4.2 Characteristics of the Equilibrium Point .....	43

4.2.1 Existence of Equilibrium Point .....	43
4.2.2 Isolation and Uniqueness Characteristics.....	44
4.2.3 Stability .....	45
4.3 Winner-Take-All Equations .....	46
4.3.1 Order Preserving Characteristics .....	47
4.3.2 Increased Differences Between Neuronal Activities .....	48
4.4 Simulation.....	49
5.0 Winner-Take-All in Phase Competition .....	53
5.1 Simulation Model .....	53
5.2 Synchronization Analysis .....	54
5.2.1 Frequency and Amplitude Analysis .....	54
5.2.2 Phase Analysis .....	56
5.2.2.1 Determining Amount of Phase Change .....	57
5.2.2.2 Types of Phase Responses and the Poincare Phase Map.....	59
5.2.2.3 Determining Fixed Points .....	60
5.2.2.4 Synchronization .....	60
5.2.2.5 Phase Locking and Phase Lock Regions .....	61
5.3 Feedback Models.....	63
5.3.1 Applied Weights.....	63
5.3.2 Low-Pass Filter .....	63
5.3.3 Lateral Inhibition vs Global interneuron.....	64
5.4 Hodgkin-Huxley Model.....	65
5.4.1 Lateral Inhibition Weighted Feedback Model .....	69

5.4.2 Lateral Inhibition Low-Pass Filter Feedback .....	76
5.4.3 Global Interneuron Weighted Feedback .....	83
5.4.4 Global Interneuron Low-Pass Filter .....	90
5.5 Fitzhugh-Nagumo .....	96
5.5.1 Lateral Inhibition Weighted Feedback .....	99
5.5.2 Lateral Inhibition Low-Pass Filter Feedback .....	106
5.5.3 Global Interneuron Weighted Feedback .....	113
5.5.4 Global Interneuron Low-Pass Filter .....	120
6.0 Conclusions .....	128
Appendix A .....	131
Appendix B .....	135
Bibliography .....	152

## List of Tables

Table 5-1: Hodgkin-Huxley Model Parameters [93] .....	65
Table 5-2: Fitzhugh-Nagumo Parameters .....	96

## List of Figures

Figure 1-1: Circuit representation of membrane voltage of the Hodgkin-Huxley model. ....	7
Figure 2-1: Basic winner-take-all structure using a global interneuron. This example is a three-neuron network with a single global neuron. The three neurons receive input current and as they become active, their output is received by the global neuron. The global neuron uses the outputs and computes a feedback to return to the neurons in the network. ....	24
Figure 2-2: Basic winner-take-all network structure using lateral inhibition. This is example is a three-neuron network in which all neurons receive input current and distribute their output as feedback to all other neurons in the network. ....	24
Figure 3-1: Example of hyperbolic saddle point. ....	29
Figure 3-2: Example of nonhyperbolic saddle point. ....	29
Figure 3-3: Direction fields for source equilibrium point. ....	30
Figure 3-4: Direction fields for sink equilibrium point. ....	30
Figure 3-5: Direction fields for saddle equilibrium point. ....	30
Figure 3-6: For small $I_{app}$ , the equilibrium point lies on the positive slope of the cubic function. ....	33
Figure 3-7: For large $I_{app}$ , the equilibrium point lies on the positive slope of the cubic function. ....	34
Figure 3-8: Stable limit cycle (bold) with two trajectories converging into it. ....	35
Figure 3-9: Graphical example of the Poincarè-Bendixson Theorem. ....	37
Figure 3-10: Regions where trajectories diverge $dHdt > 0$ and converge $dHdt < 0$ . Within the gray region, $xt$ could either diverge or converge, but beyond the gray region $vm$ and $\omega m$ $xt$ is guaranteed to converge into the region. ....	38
Figure 4-1: Example of sigmoidal function. ....	48
Figure 4-2: Activation function $f(u) = 1/(1 + e^{-(u - 1)/(1/3)})$ . ....	49
Figure 4-3: Five-neuron winner-take-all network modeled by (4.1) and (4.2) where $I = 2$ . ....	50

Figure 4-4: Five-neuron winner-take-all network modeled by (4.1) and (4.2) where $I_1 = 3; I_2 = I_5 = 2$ .....	51
Figure 4-5: Five-neuron winner-take-all network modeled by (4.1) and (4.2) where $I_1 = 3; I_2 = I_4 = I_5 = 2; I_3 = 1$ .....	51
Figure 4-6: Five-neuron winner-take-all network modeled by (4.1) and (4.2) where $I_1 = 3; I_2 = 1.3; I_3 = 1.9; I_4 = 2.5; I_5 = 1$ .....	51
Figure 4-7: Frequency of Hodgkin-Huxley neuron as the input increases. As the input increases, so does the frequency in a way that resembles the continuous and monotonic activation function used in the simplified postsynaptic membrane winner-take-all model.....	52
Figure 5-1: Phase-shift example. Two sin waves start at the same point but over time, a phase shift develops. ....	58
Figure 5-2: Synchronization examples. ....	60
Figure 5-3: Synchronizing phase locking .....	61
Figure 5-4: Sample p:q-phase locked regions.....	62
Figure 5-5: Low-pass filter example using a simple sine wave as the input and tuning the time constant. ....	64
Figure 5-6: Two uncoupled Hodgkin-Huxley neurons where $I_1 = I_2 = 25$ .....	67
Figure 5-7: Two uncoupled Hodgkin-Huxley neurons where $I_1 = 25, I_2 = 25.5$ . ....	67
Figure 5-8: Two uncoupled Hodgkin-Huxley neurons where $I_1 = 25, I_2 = 27$ .....	68
Figure 5-9: Two uncoupled Hodgkin-Huxley neurons where $I_1 = 25, I_2 = 30$ .....	68
Figure 5-10: Five-neuron Hodgkin-Huxley inhibition winner-take-all network with weighted feedback of 1 where $I_1 = 25.5, I_2 = I_3 = I_4 = I_5 = 25$ .....	70
Figure 5-11: Five-neuron Hodgkin-Huxley inhibition winner-take-all network with weighted feedback of 1 where $I_1 = 27, I_2 = I_3 = I_4 = I_5 = 25$ .....	70
Figure 5-12: Five-neuron Hodgkin-Huxley inhibition winner-take-all network with weighted feedback of 1 where $I_1 = 30, I_2 = I_3 = I_4 = I_5 = 25$ .....	71
Figure 5-13: Five-neuron Hodgkin-Huxley inhibition winner-take-all network with weighted feedback of 1 where $I_1 = 30, I_2 = 27, I_3 = 25.5, I_4 = I_5 = 25$ . ....	71

Figure 5-14: Five-neuron Hodgkin-Huxley inhibition winner-take-all network with weighted feedback of 0.5 where $I_1 = 25.5, I_2 = I_3 = I_4 = I_5 = 25$ .....	72
Figure 5-15: Five-neuron Hodgkin-Huxley inhibition winner-take-all network with weighted feedback of 0.5 where $I_1 = 27, I_2 = I_3 = I_4 = I_5 = 25$ .....	72
Figure 5-16: Five-neuron Hodgkin-Huxley inhibition winner-take-all network with weighted feedback of 0.5 where $I_1 = 30, I_2 = I_3 = I_4 = I_5 = 25$ .....	73
Figure 5-17: Five-neuron Hodgkin-Huxley inhibition winner-take-all network with weighted feedback of 0.5 where $I_1 = 30, I_2 = 27, I_3 = 25.5, I_4 = I_5 = 25$ .....	73
Figure 5-18: Five-neuron Hodgkin-Huxley inhibition winner-take-all network with weighted feedback of 0.1 where $I_1 = 25.5, I_2 = I_3 = I_4 = I_5 = 25$ .....	74
Figure 5-19: Five-neuron Hodgkin-Huxley inhibition winner-take-all network with weighted feedback of 0.1 where $I_1 = 27, I_2 = I_3 = I_4 = I_5 = 25$ .....	74
Figure 5-20: Five-neuron Hodgkin-Huxley inhibition winner-take-all network with weighted feedback of 0.1 where $I_1 = 30, I_2 = I_3 = I_4 = I_5 = 25$ .....	75
Figure 5-21: Five-neuron Hodgkin-Huxley inhibition winner-take-all network with weighted feedback of 0.1 where $I_1 = 30, I_2 = 27, I_3 = 25.5, I_4 = I_5 = 25$ .....	75
Figure 5-22: Five-neuron Hodgkin-Huxley inhibition winner-take-all network with low-pass filter feedback where $\tau = 0.1; I_1 = 25.5, I_2 = I_3 = I_4 = I_5 = 25$ .....	77
Figure 5-23: Five-neuron Hodgkin-Huxley inhibition winner-take-all network with low-pass filter feedback where $\tau = 0.1; I_1 = 27, I_2 = I_3 = I_4 = I_5 = 25$ .....	77
Figure 5-24: Five-neuron Hodgkin-Huxley inhibition winner-take-all network with low-pass filter feedback where $\tau = 0.1; I_1 = 30, I_2 = I_3 = I_4 = I_5 = 25$ .....	78
Figure 5-25: Five-neuron Hodgkin-Huxley inhibition winner-take-all network with low-pass filter feedback where $\tau = 0.1; I_1 = 30, I_2 = 27, I_3 = 25.5, I_4 = I_5 = 25$ .....	78
Figure 5-26: Five-neuron Hodgkin-Huxley inhibition winner-take-all network with low-pass filter feedback where $\tau = 10; I_1 = 25.5, I_2 = I_3 = I_4 = I_5 = 25$ .....	79
Figure 5-27: Five-neuron Hodgkin-Huxley inhibition winner-take-all network with low-pass filter feedback where $\tau = 10; I_1 = 27, I_2 = I_3 = I_4 = I_5 = 25$ .....	79
Figure 5-28: Five-neuron Hodgkin-Huxley inhibition winner-take-all network with low-pass filter feedback where $\tau = 10; I_1 = 30, I_2 = I_3 = I_4 = I_5 = 25$ .....	80

Figure 5-29: Five-neuron Hodgkin-Huxley inhibition winner-take-all network with low-pass filter feedback where $\tau = 10$ ; $I_1=30, I_2 = 27, I_3 = 25.5, I_4 = I_5 = 25$ .....	80
Figure 5-30: Five-neuron Hodgkin-Huxley inhibition winner-take-all network with low-pass filter feedback where $\tau = 100$ ; $I_1 = 25.5, I_2 = I_3 = I_4 = I_5 = 25$ .....	81
Figure 5-31: Five-neuron Hodgkin-Huxley inhibition winner-take-all network with low-pass filter feedback where $\tau = 100$ ; $I_1 = 27, I_2 = I_3 = I_4 = I_5 = 25$ .....	81
Figure 5-32: Five-neuron Hodgkin-Huxley inhibition winner-take-all network with low-pass filter feedback where $\tau = 100$ ; $I_1 = 30, I_2 = I_3 = I_4 = I_5 = 25$ .....	82
Figure 5-33: Five-neuron Hodgkin-Huxley inhibition winner-take-all network with low-pass filter feedback where $\tau = 100$ ; $I_1 = 30, I_2 = 27, I_3 = 25.5, I_4 = I_5 = 25$ .....	82
Figure 5-34: Five-neuron Hodgkin-Huxley interneuron winner-take-all network with weighted feedback of 1 where $I_1 = 25.5, I_2 = I_3 = I_4 = I_5 = 25$ .....	84
Figure 5-35: Five-neuron Hodgkin-Huxley interneuron winner-take-all network with weighted feedback of 1 where $I_1 = 27, I_2 = I_3 = I_4 = I_5 = 25$ .....	84
Figure 5-36: Five-neuron Hodgkin-Huxley interneuron winner-take-all network with weighted feedback of 1 where $I_1 = 30, I_2 = I_3 = I_4 = I_5 = 25$ .....	85
Figure 5-37: Five-neuron Hodgkin-Huxley interneuron winner-take-all network with weighted feedback of 1 where $I_1 = 30, I_2 = 27, I_3 = 25.5, I_4 = I_5 = 25$ .....	85
Figure 5-38: Five-neuron Hodgkin-Huxley interneuron winner-take-all network with weighted feedback of 0.5 where $I_1 = 25.5, I_2 = I_3 = I_4 = I_5 = 25$ .....	86
Figure 5-39: Five-neuron Hodgkin-Huxley interneuron winner-take-all network with weighted feedback of 0.5 where $I_1 = 27, I_2 = I_3 = I_4 = I_5 = 25$ .....	86
Figure 5-40: Five-neuron Hodgkin-Huxley interneuron winner-take-all network with weighted feedback of 0.5 where $I_1 = 30, I_2 = I_3 = I_4 = I_5 = 25$ .....	87
Figure 5-41: Five-neuron Hodgkin-Huxley interneuron winner-take-all network with weighted feedback of 0.5 where $I_1 = 30, I_2 = 27, I_3 = 25.5, I_4 = I_5 = 25$ .....	87
Figure 5-42: Five-neuron Hodgkin-Huxley interneuron winner-take-all network with weighted feedback of 0.1 where $I_1 = 25.5, I_2 = I_3 = I_4 = I_5 = 25$ .....	88
Figure 5-43: Five-neuron Hodgkin-Huxley interneuron winner-take-all network with weighted feedback of 0.1 where $I_1 = 27, I_2 = I_3 = I_4 = I_5 = 25$ .....	88

Figure 5-44: Five-neuron Hodgkin-Huxley interneuron winner-take-all network with weighted feedback of 0.1 where $I_1 = 30, I_2 = I_3 = I_4 = I_5 = 25$ .	89
Figure 5-45: Five-neuron Hodgkin-Huxley interneuron winner-take-all network with weighted feedback of 0.1 where $I_1 = 30, I_2 = 27, I_3 = 25.5, I_4 = I_5 = 25$ .	89
Figure 5-46: Five-neuron Hodgkin-Huxley interneuron winner-take-all network with low-pass filter feedback where $\tau = 0.1; I_1 = 25.5, I_2 = I_3 = I_4 = I_5 = 25$ .	90
Figure 5-47: Five-neuron Hodgkin-Huxley interneuron winner-take-all network with low-pass filter feedback where $\tau = 0.1; I_1 = 27, I_2 = I_3 = I_4 = I_5 = 25$ .	91
Figure 5-48: Five-neuron Hodgkin-Huxley interneuron winner-take-all network with low-pass filter feedback where $\tau = 0.1; I_1 = 30, I_2 = I_3 = I_4 = I_5 = 25$ .	91
Figure 5-49: Five-neuron Hodgkin-Huxley interneuron winner-take-all network with low-pass filter feedback where $\tau = 0.1; I_1 = 30, I_2 = 27, I_3 = 25.5, I_4 = I_5 = 25$ .	92
Figure 5-50: Five-neuron Hodgkin-Huxley interneuron winner-take-all network with low-pass filter feedback where $\tau = 10; I_1 = 25.5, I_2 = I_3 = I_4 = I_5 = 25$ .	92
Figure 5-51: Five-neuron Hodgkin-Huxley interneuron winner-take-all network with low-pass filter feedback where $\tau = 10; I_1 = 27, I_2 = I_3 = I_4 = I_5 = 25$ .	93
Figure 5-52: Five-neuron Hodgkin-Huxley interneuron winner-take-all network with low-pass filter feedback where $\tau = 10; I_1 = 30, I_2 = I_3 = I_4 = I_5 = 25$ .	93
Figure 5-53: Five-neuron Hodgkin-Huxley interneuron winner-take-all network with low-pass filter feedback where $\tau = 10; I_1 = 30, I_2 = 27, I_3 = 25.5, I_4 = I_5 = 25$ .	94
Figure 5-54: Five-neuron Hodgkin-Huxley interneuron winner-take-all network with low-pass filter feedback where $\tau = 100; I_1 = 25.5, I_2 = I_3 = I_4 = I_5 = 25$ .	94
Figure 5-55: Five-neuron Hodgkin-Huxley interneuron winner-take-all network with low-pass filter feedback where $\tau = 100; I_1 = 27, I_2 = I_3 = I_4 = I_5 = 25$ .	95
Figure 5-56: Five-neuron Hodgkin-Huxley interneuron winner-take-all network with low-pass filter feedback where $\tau = 100; I_1 = 30, I_2 = I_3 = I_4 = I_5 = 25$ .	95
Figure 5-57: Five-neuron Hodgkin-Huxley interneuron winner-take-all network with low-pass filter feedback where $\tau = 100; I_1 = 30, I_2 = 27, I_3 = 25.5, I_4 = I_5 = 25$ .	96
Figure 5-58: Two uncoupled Fitzhugh-Nagumo neurons where $I_1 = I_2 = 0.1$ .	97
Figure 5-59: Two uncoupled Fitzhugh-Nagumo neurons where $I_1 = 0.15; I_2 = 0.1$ .	98

Figure 5-60: Two uncoupled Fitzhugh-Nagumo neurons where $I_1 = 0.3$ ; $I_2 = 0.1$ .....	98
Figure 5-61: Two uncoupled Fitzhugh-Nagumo neurons where $I_1 = 0.5$ ; $I_2 = 0.1$ .....	99
Figure 5-62: Five-neuron Fitzhugh-Nagumo inhibition winner-take-all network with weighted feedback of 1 where $I_1 = 0.15$ ; $[I_2, I_3, I_4, I_5] = 0.1$ .....	100
Figure 5-63: Five-neuron Fitzhugh-Nagumo inhibition winner-take-all network with weighted feedback of 1 where $I_1 = 0.3$ ; $[I_2, I_3, I_4, I_5] = 0.1$ .....	101
Figure 5-64: Five-neuron Fitzhugh-Nagumo inhibition winner-take-all network with weighted feedback of 1 where $I_1 = 0.5$ ; $[I_2, I_3, I_4, I_5] = 0.1$ .....	101
Figure 5-65: Five-neuron Fitzhugh-Nagumo inhibition winner-take-all network with weighted feedback of 1 where $I_1 = 0.5$ ; $I_2 = 0.3$ ; $I_3 = 0.15$ ; $[I_4, I_5] = 0.1$ .....	102
Figure 5-66: Five-neuron Fitzhugh-Nagumo inhibition winner-take-all network with weighted feedback of 0.5 where $I_1 = 0.15$ ; $[I_2, I_3, I_4, I_5] = 0.1$ .....	102
Figure 5-67: Five-neuron Fitzhugh-Nagumo inhibition winner-take-all network with weighted feedback of 0.5 where $I_1 = 0.3$ ; $[I_2, I_3, I_4, I_5] = 0.1$ .....	103
Figure 5-68: Five-neuron Fitzhugh-Nagumo inhibition winner-take-all network with weighted feedback of 0.5 where $I_1 = 0.5$ ; $[I_2, I_3, I_4, I_5] = 0.1$ .....	103
Figure 5-69: Five-neuron Fitzhugh-Nagumo inhibition winner-take-all network with weighted feedback of 0.5 where $I_1 = 0.5$ ; $I_2 = 0.3$ ; $I_3 = 0.15$ ; $[I_4, I_5] = 0.1$ .....	104
Figure 5-70: Five-neuron Fitzhugh-Nagumo inhibition winner-take-all network with weighted feedback of 0.1 where $I_1 = 0.15$ ; $[I_2, I_3, I_4, I_5] = 0.1$ .....	104
Figure 5-71: Five-neuron Fitzhugh-Nagumo inhibition winner-take-all network with weighted feedback of 0.1 where $I_1 = 0.3$ ; $[I_2, I_3, I_4, I_5] = 0.1$ .....	105
Figure 5-72: Five-neuron Fitzhugh-Nagumo inhibition winner-take-all network with weighted feedback of 0.1 where $I_1 = 0.5$ ; $[I_2, I_3, I_4, I_5] = 0.1$ .....	105
Figure 5-73: Five-neuron Fitzhugh-Nagumo inhibition winner-take-all network with weighted feedback of 0.1 where $I_1 = 0.5$ ; $I_2 = 0.3$ ; $I_3 = 0.15$ ; $[I_4, I_5] = 0.1$ .....	106
Figure 5-74: Five-neuron Fitzhugh-Nagumo inhibition winner-take-all network with low-pass filter feedback where $\tau = 0.1$ ; $I_1 = 0.15$ ; $[I_2, I_3, I_4, I_5] = 0.1$ .....	107
Figure 5-75: Five-neuron Fitzhugh-Nagumo inhibition winner-take-all network with low-pass filter feedback where $\tau = 0.1$ ; $I_1 = 0.3$ ; $[I_2, I_3, I_4, I_5] = 0.1$ .....	108

Figure 5-76: Five-neuron Fitzhugh-Nagumo inhibition winner-take-all network with low-pass filter feedback where $\tau = 0.1$ ; $I_1 = 0.5$ ; $[I_2, I_3, I_4, I_5] = 0.1$ .	108
Figure 5-77: Five-neuron Fitzhugh-Nagumo inhibition winner-take-all network with low-pass filter feedback where $\tau = 0.1$ ; $I_1 = 0.5$ ; $I_2 = 0.3$ ; $I_1 = 0.15$ ; $[I_4, I_5] = 0.1$ .	109
Figure 5-78: Five-neuron Fitzhugh-Nagumo inhibition winner-take-all network with low-pass filter feedback where $\tau = 10$ ; $I_1 = 0.15$ ; $[I_2, I_3, I_4, I_5] = 0.1$ .	109
Figure 5-79: Five-neuron Fitzhugh-Nagumo inhibition winner-take-all network with low-pass filter feedback where $\tau = 10$ ; $I_1 = 0.3$ ; $[I_2, I_3, I_4, I_5] = 0.1$ .	110
Figure 5-80: Five-neuron Fitzhugh-Nagumo inhibition winner-take-all network with low-pass filter feedback where $\tau = 10$ ; $I_1 = 0.5$ ; $[I_2, I_3, I_4, I_5] = 0.1$ .	110
Figure 5-81: Five-neuron Fitzhugh-Nagumo inhibition winner-take-all network with low-pass filter feedback where $\tau = 10$ ; $I_1 = 0.5$ ; $I_2 = 0.3$ ; $I_1 = 0.15$ ; $[I_4, I_5] = 0.1$ .	111
Figure 5-82: Five-neuron Fitzhugh-Nagumo inhibition winner-take-all network with low-pass filter feedback where $\tau = 100$ ; $I_1 = 0.15$ ; $[I_2, I_3, I_4, I_5] = 0.1$ .	111
Figure 5-83: Five-neuron Fitzhugh-Nagumo inhibition winner-take-all network with low-pass filter feedback where $\tau = 100$ ; $I_1 = 0.3$ ; $[I_2, I_3, I_4, I_5] = 0.1$ .	112
Figure 5-84: Five-neuron Fitzhugh-Nagumo inhibition winner-take-all network with low-pass filter feedback where $\tau = 100$ ; $I_1 = 0.5$ ; $[I_2, I_3, I_4, I_5] = 0.1$ .	112
Figure 5-85: Five-neuron Fitzhugh-Nagumo inhibition winner-take-all network with low-pass filter feedback where $\tau = 100$ ; $I_1 = 0.5$ ; $I_2 = 0.3$ ; $I_1 = 0.15$ ; $[I_4, I_5] = 0.1$ .	113
Figure 5-86: Five-neuron Fitzhugh-Nagumo interneuron winner-take-all network with weighted feedback of 1 where $I_1 = 0.15$ ; $[I_2, I_3, I_4, I_5] = 0.1$ .	114
Figure 5-87: Five-neuron Fitzhugh-Nagumo interneuron winner-take-all network with weighted feedback of 1 where $I_1 = 0.3$ ; $[I_2, I_3, I_4, I_5] = 0.1$ .	115
Figure 5-88: Five-neuron Fitzhugh-Nagumo interneuron winner-take-all network with weighted feedback of 1 where $I_1 = 0.5$ ; $[I_2, I_3, I_4, I_5] = 0.1$ .	115
Figure 5-89: Five-neuron Fitzhugh-Nagumo interneuron winner-take-all network with weighted feedback of 1 where $I_1 = 0.5$ ; $I_2 = 0.3$ ; $I_1 = 0.15$ ; $[I_4, I_5] = 0.1$ .	116
Figure 5-90: Five-neuron Fitzhugh-Nagumo interneuron winner-take-all network with weighted feedback of 0.5 where $I_1 = 0.15$ ; $[I_2, I_3, I_4, I_5] = 0.1$ .	116

Figure 5-91: Five-neuron Fitzhugh-Nagumo interneuron winner-take-all network with weighted feedback of 0.5 where $I_1 = 0.3$ ; $[I_2, I_3, I_4, I_5] = 0.1$ .	117
Figure 5-92: Five-neuron Fitzhugh-Nagumo interneuron winner-take-all network with weighted feedback of 0.5 where $I_1 = 0.5$ ; $[I_2, I_3, I_4, I_5] = 0.1$ .	117
Figure 5-93: Five-neuron Fitzhugh-Nagumo interneuron winner-take-all network with weighted feedback of 0.5 where $I_1 = 0.5$ ; $I_2 = 0.3$ ; $I_3 = 0.15$ ; $[I_4, I_5] = 0.1$ .	118
Figure 5-94: Five-neuron Fitzhugh-Nagumo interneuron winner-take-all network with weighted feedback of 0.1 where $I_1 = 0.15$ ; $[I_2, I_3, I_4, I_5] = 0.1$ .	118
Figure 5-95: Five-neuron Fitzhugh-Nagumo interneuron winner-take-all network with weighted feedback of 0.1 where $I_1 = 0.3$ ; $[I_2, I_3, I_4, I_5] = 0.1$ .	119
Figure 5-96: Five-neuron Fitzhugh-Nagumo interneuron winner-take-all network with weighted feedback of 0.1 where $I_1 = 0.5$ ; $[I_2, I_3, I_4, I_5] = 0.1$ .	119
Figure 5-97: Five-neuron Fitzhugh-Nagumo interneuron winner-take-all network with weighted feedback of 0.1 where $I_1 = 0.5$ ; $I_2 = 0.3$ ; $I_3 = 0.15$ ; $[I_4, I_5] = 0.1$ .	120
Figure 5-98: Five-neuron Fitzhugh-Nagumo interneuron winner-take-all network with low-pass filter feedback where $\tau = 0.1$ ; $I_1 = 0.15$ ; $[I_2, I_3, I_4, I_5] = 0.1$ .	121
Figure 5-99: Five-neuron Fitzhugh-Nagumo interneuron winner-take-all network with low-pass filter feedback where $\tau = 0.1$ ; $I_1 = 0.3$ ; $[I_2, I_3, I_4, I_5] = 0.1$ .	122
Figure 5-100: Five-neuron Fitzhugh-Nagumo interneuron winner-take-all network with low-pass filter feedback where $\tau = 0.1$ ; $I_1 = 0.5$ ; $[I_2, I_3, I_4, I_5] = 0.1$ .	122
Figure 5-101: Five-neuron Fitzhugh-Nagumo interneuron winner-take-all network with low-pass filter feedback where $\tau = 0.1$ ; $I_1 = 0.5$ ; $I_2 = 0.3$ ; $I_3 = 0.15$ ; $[I_4, I_5] = 0.1$ .	123
Figure 5-102: Five-neuron Fitzhugh-Nagumo interneuron winner-take-all network with low-pass filter feedback where $\tau = 10$ ; $I_1 = 0.15$ ; $[I_2, I_3, I_4, I_5] = 0.1$ .	123
Figure 5-103: Five-neuron Fitzhugh-Nagumo interneuron winner-take-all network with low-pass filter feedback where $\tau = 10$ ; $I_1 = 0.3$ ; $[I_2, I_3, I_4, I_5] = 0.1$ .	124
Figure 5-104: Five-neuron Fitzhugh-Nagumo interneuron winner-take-all network with low-pass filter feedback where $\tau = 10$ ; $I_1 = 0.5$ ; $[I_2, I_3, I_4, I_5] = 0.1$ .	124
Figure 5-105: Five-neuron Fitzhugh-Nagumo interneuron winner-take-all network with low-pass filter feedback where $\tau = 10$ ; $I_1 = 0.5$ ; $I_2 = 0.3$ ; $I_3 = 0.15$ ; $[I_4, I_5] = 0.1$ .	125

Figure 5-106: Five-neuron Fitzhugh-Nagumo interneuron winner-take-all network with low-pass filter feedback where $\tau = 100$ ; $I_1 = 0.15$ ; $[I_2, I_3, I_4, I_5] = 0.1$ .....	125
Figure 5-107: Five-neuron Fitzhugh-Nagumo interneuron winner-take-all network with low-pass filter feedback where $\tau = 100$ ; $I_1 = 0.3$ ; $[I_2, I_3, I_4, I_5] = 0.1$ .....	126
Figure 5-108: Five-neuron Fitzhugh-Nagumo interneuron winner-take-all network with low-pass filter feedback where $\tau = 100$ ; $I_1 = 0.5$ ; $[I_2, I_3, I_4, I_5] = 0.1$ .....	126
Figure 5-109: Five-neuron Fitzhugh-Nagumo interneuron winner-take-all network with low-pass filter feedback where $\tau = 100$ ; $I_1 = 0.5$ ; $I_2 = 0.3$ ; $I_3 = 0.15$ ; $[I_4, I_5] = 0.1$ .....	127
Figure 6-1: Hodgkin-Huxley neuron with feedback.....	131
Figure 6-2: Fitzhugh-Nagumo neuron with feedback.....	131
Figure 6-3: Low-pass filter feedback.....	132
Figure 6-4: Weighted feedback.....	132
Figure 6-5: Five-neuron network.....	133
Figure 6-6: Interneuron coupling.....	133
Figure 6-7: Inhibitory coupling.....	134

## **Preface**

I would like to thank my advisors Dr. Zhi-Hong Mao and Dr. Ahmed Hassan Sayed Dallal for supporting my work and challenging me to work harder and think creatively. I would like to also thank Dr. Sylvanus N. Wosu for his guidance and mentorship throughout my graduate studies. Lastly, I would like to thank my family and friends for their encouragement and emotional support.

## 1.0 Introduction

Physical limitations of current integrated circuit design using complementary metal-oxide-semiconductor (CMOS) have motivated research into viable new technology for computing. Despite the vast amount of work improving CMOS, there are still major key factors impeding the progression of Boolean based computing. Transistor size can only be so small before the physical characteristics can no longer function properly. Efficient heat dissipation is still a major concern, especially as devices become smaller and more powerful. Clock speed and computation power is also limited by the physical characteristics of CMOS.

Nano-oscillators have shown promise as an alternative to CMOS. Instead of using many logic gates for computations, the intrinsic physical properties of the oscillators can be used to perform non-Boolean computations. Arranged in different architectures, oscillators can be used for various computations such as edge detection, associative memory, and neurocomputing [1] [2] [3]. Simpler than entire processes, fundamental primitive computations can be performed, for example convolution. Weakly coupled oscillators have been shown to be capable of approximating convolution [4], and later shown to compute an exact convolution [5], by using the characteristics of their synchronization behavior. Oscillatory designs could then be extended to be used in convolution-based computations such as discrete cosine transforms, discrete Fourier transforms, Gabor filtering, and image processing [6]. This is just one example of how oscillators can impact hardware design, as their utility can be expanded beyond convolution.

The oscillatory characteristic of the behavior of oscillators is reminiscent of the oscillatory behavior of brain neurons. This makes them particularly useful in neuronal-based computations and applications such as artificial intelligence and neuronal networks [84] [86]. Some of these

oscillators are biologically inspired but not necessarily biologically plausible. The neuronal networks emulate the brain but are not modeled after its neuronal units, such as ionic channels. With a need for developing efficient and accurate neuronal networks, there is a strong interest among the research community in developing creative biological and biologically inspired neuronal network models. A very useful and prevalent concept of neural networks is winner-take-all [86], which is a mechanism used to make a selection out of group of neurons. It is a fundamental basis in many neural network applications such as decision-making and motor function selection [31] [72].

## 1.1 Motivation

Christian Huygens [7] is considered the first person to observe the phenomena of synchronizing coupled pendulums. He noted that pendulums connected on the same platform will synchronize with one another, despite initial frequencies and phases. This observation has inspired many studies about coupled oscillators. Oscillators have shown useful in a broad array of fields of non-Boolean computations in different domains such as magnetic, electric, and biological [1] [2] [3].

CMOS is the current standard technology used in designing integrated circuits, composed of tiny devices known as transistors. These transistors dictate the flow of electricity through circuits. This current control property of the transistors enables the design of logic gates such as AND, OR, and inverter gates to perform Boolean algebra. In Boolean algebra, the values are denoted by 1's and 0's representing the on (1) and off (0) switching of the transistors. A wide

variety of multiple logic gates can be arranged in different architectures to perform different types of operations. This is essentially the framework of modern computers.

Although there has been a vast amount of research into improving CMOS technology and computer architecture to make more powerful and efficient systems, the trends of decreasing sizes and energy while increasing power and speed are plateauing. Major roadblocks hindering the progression of Boolean logic-based computing are transistor size, heat dissipation, clock speed, and computation power.

Rairigh [8] reviews some of the challenges in scaling CMOS technologies. One of the problems with smaller transistor sizes is the hard limit set by the size atoms of molecules, as devices could not possibly be fabricated at dimensions smaller than a single molecule and there are rising costs of equipment to scale at that level. There is also an issue of maintaining performance with devices at that scale, in particular the mobility of electrons and holes in transistors. The negative impact on the physical properties of transistors will diminish the returns on newer devices to the extent that they will no longer be significantly better than previous versions. More specifically, issues such as junction leakage, gate induced drain leakage, and sub-threshold channel current, significantly increase the problem of off-state power consumption as transistor dimensions decrease.

This has inspired investigation into new methods for performing complex operations not based on logic gates, also called non-Boolean computations. One such method is coupled oscillator arrays. Instead of a logic gates to compute complex functions, the intrinsic physical properties of the coupled oscillators can be used for computation.

Horvath [1] models the interaction of spin torque coupled oscillators via their magnetic field and demonstrate the use of this dynamic in an edge detection application. By passing current

through a ferromagnetic material, spin-polarized current can be generated which can switch the magnetization of the current. Under certain conditions, this current induces steady precession of the magnetization at various frequencies which are used for detection. Shibata [2] emulated the behavior of oscillators using CMOS ring oscillators and supporting CMOS circuitry to produce associative memory function. This work demonstrated how the emerging technology of oscillators can be integrated in current architectures by developing supportive circuitries. The associative memory function was implemented in image recognition via HSPICE simulation. Hoppensteadt [3] proposed that coupled microelectromechanical oscillators can be useful to efficiently process analog information and theorize that they can function as a neurocomputer having oscillatory autocorrelative associative memory.

Nikonov [4] proposed using weakly coupled voltage-controlled oscillators to approximate convolution. They demonstrate the use of oscillators through Gabor filtering, using a phase-shift keying scheme. Chiarulli [5] improved on this work and demonstrated using oscillators to perform an exact convolution based on a coupled oscillator degree of match (DOM) metric. Simulation of the DOM circuit showed that the behavior of the coupled oscillators was similar to that of a squared Euclidean distance metric ( $L^2$ ), which can be a computational primitive for template matching and distance metrics, like the ones used in image processing pipelines such as HMAX [21]. Jennings [6] took the work of Chiarulli and analyzed the effects of parameters on the output of convolution using the oscillators and demonstrated their application in convolution-based image processing computations. This work showed that oscillators are a viable technology to perform complex computations and with mitigation against the effects of the parameters, yield as accurate results as current technologies.

Studies have been done to model and characterize neurons, which generally can be considered as oscillators [93]. Different types of oscillators have different behavioral characteristics which may make some better for certain purposes than others. This dissertation strives to examine how the behavior of neurons configured in different architectures might be characterized and offer insight into better architectural design. More specifically, this work will simulate the winner-take-all behavior via neuronal networks based on the Hodgkin-Huxley and Fitzhugh-Nagumo neuron models [94] [14]. This dissertation will observe and analyze winner-take-all by synchronization behavior of the neurons in terms of phase, using different architectures of both models and different topologies of feedback. In addition, it will also analyze winner-take-all in terms of firing rate, using a simplified model [37]. The analysis could provide further understanding of how winner-take-all works in biological neuronal networks and insight into better circuit design.

## **1.2 Neuron Models**

The work in this dissertation focuses particularly on the Hodgkin-Huxley model Fitzhugh-Nagumo neuron models, though it also examines a simplified neuronal network model that uses a function of firing rate to achieve winner-take-all as opposed to action potential. The Hodgkin-Huxley neuron is a renowned biological model that quantitatively represents experimental data of a real neuron and, as such, it is a complex four-dimensional model [15]. The Fitzhugh-Nagumo model is a simplified version of the Hodgkin-Huxley model with half the dimensionality making it a commonly used model because of its reduced complexity and ease of simulation [9] [18]. The firing rate model will be discussed in a later chapter.

### 1.2.1 Hodgkin-Huxley

Alan Hodgkin and Andrew Huxley [11] [92] came up with first known model of action potential of an axon in a squid neuron. The two scientists conducted series of experiments in the late 1940s and 1950s on the neuron of a squid. Specifically, they examined the squid's giant axon. This is an axon of the squid that is specialized for conducting action potentials fast. This allows for quickly controlling the water jet propulsion that allows the squid to escape from predators.

What made the squid giant axon valuable was its unusually large size, typically 0.5mm where most axons in other nervous systems are significantly smaller [28]. This proved beneficial for research as it allowed them to perform experiments and manipulate the axon in ways infeasible on anything smaller. Electrical voltage exists between the inside and outside the membrane of all living cells. The difference between these two voltages is referred to as membrane potential, which changes during an action potential, or spiking. An increase in membrane potential is caused by an inward current, which corresponds to positively charged ions such as  $\text{Na}^+$  entering the cell and depolarizes the cell. Conversely, outward current decreases the membrane potential and corresponds to positively charged ions such as  $\text{K}^+$  leaving the cell or negatively charged ions such as  $\text{Cl}^-$  entering the cell, causing the cell to become hyperpolarized. A large enough depolarization will lead to an action potential.

It is the concentrations of these ions inside and outside the cell that influence the membrane potential difference, which are impacted by factors such as the transport of ions across the cell membrane and the permeability of the membrane to these ions.  $\text{Na}^+$  and  $\text{Cl}^-$  concentrations are typically higher outside of the cell, whereas  $\text{K}^+$  concentrations are higher inside the cell. The membrane of the cell itself is not a particularly strong conductor of ionic currents, however there are specialized proteins that behave as channels through which the ions can enter and exit the cell.

The channels can be gated or nongated. Gated channels are usually ion specific, opening and closing with a probability dependent on the membrane potential. Nongated channels are always open and primarily involved in the resting potential of a cell as most of the gated channels are closed at rest. Channels opening and allowing ions to flow across the membrane generate action potential.

What resulted from Hodgkin and Huxley was a set of differential equations that became their model of the action potential behavior. They realized that ionic currents in the giant axon could be understood by observing the changes in  $\text{Na}^+$  and  $\text{K}^+$  conductance in the axon membrane, leading to a mathematical model of voltage-dependent and time-dependent properties of the conductance.

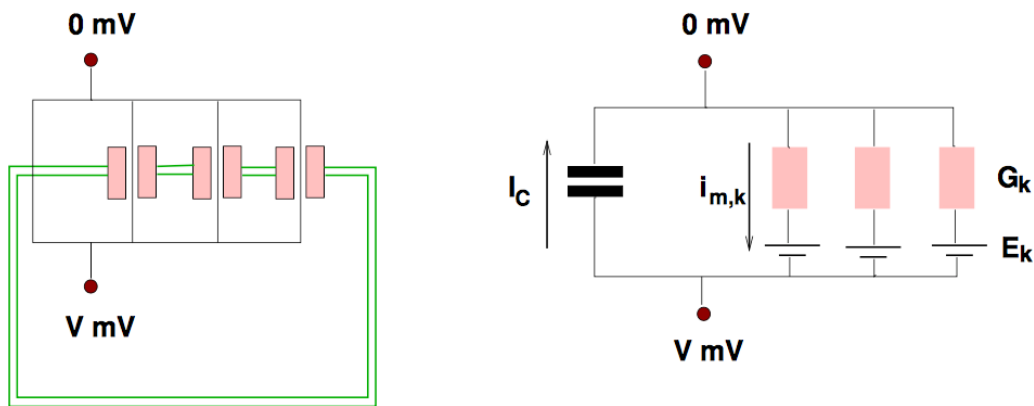


Figure 1-1: Circuit representation of membrane voltage of the Hodgkin-Huxley model.

Figure 1-1 [27] shows the circuit model based on the Hodgkin-Huxley model. The total current in the system is a summation of both the current contributed by membrane capacitance and the individual ions that pass through the membrane.

$$I(t) = I_C + I_k, \quad (1.1)$$

where

$$I_C = C_m \frac{dV}{dt} \quad (1.2)$$

and

$$I_k = \sum_k i_{m,k}, \quad (1.3)$$

where  $I_C$  is the membrane capacitance contribution,  $I_k$  is the current from ions passing through the membrane,  $C_m$  is membrane capacitance, and  $i_{m,k}$  is the membrane current from ion  $k$ . Using Ohm's law, the currents from the individual ions can be characterized using

$$i_{m,k} = G_k(V - E_k), \quad (1.4)$$

where  $G_k$  is the ionic membrane conductance for a particular ion  $k$  and  $E_k$  is the Nernst equilibrium potential for a particular ion  $k$ . Kirchoff's current law states that the current flowing into a junction or node has to be equal to the current flowing out of it, or in other words the net current at a junction or node in a circuit is zero,  $I(t) = 0$ . From this we can obtain the membrane voltage equation

$$C_m \frac{dV}{dt} = - \sum_k G_k(V - E_k). \quad (1.5)$$

Experimental observations from Hodgkin and Huxley showed that there are three channels, one for sodium current, one for potassium current, and one for leakage current contributed by all other ions.

$$\begin{aligned}\sum_k i_{m,k} &= I_{Na} + I_K + I_L \\ &= \bar{G}_{Na} m^3 h (V - E_{Na}) + \bar{G}_K n^4 (V - E_K) + \bar{G}_L (V - E_L),\end{aligned}\tag{1.6}$$

where  $I_{Na}$  is sodium current,  $I_K$  is potassium current,  $I_L$  is leakage current from all other ions,  $m$ ,  $n$ , and  $h$  are all variables bounded by 0 and 1 and each have their own differential equation of the forms

$$\begin{aligned}\frac{dn}{dt} &= \alpha_n(V)(1 - n) - \beta_n(V)n = \frac{n_\infty(V) - n}{\tau_n(V)}, \\ \frac{dm}{dt} &= \alpha_m(V)(1 - m) - \beta_m(V)m = \frac{m_\infty(V) - m}{\tau_m(V)}, \\ \frac{dh}{dt} &= \alpha_h(V)(1 - h) - \beta_h(V)h = \frac{h_\infty(V) - h}{\tau_h(V)},\end{aligned}\tag{1.7}$$

where the gating functions are defined as [92]

$$\alpha_n = 0.01 \frac{V + 55}{1 - e^{-\frac{V+55}{10}}},$$

$$\alpha_m = 0.1 \frac{V + 40}{1 - e^{-\frac{V+40}{10}}},$$

$$\alpha_h = 0.07e^{-\frac{V+65}{20}},$$

$$\beta_n = 0.125e^{-\frac{V+65}{80}},$$

$$\beta_m = 4e^{-\frac{V+65}{18}},$$

$$\beta_h = \frac{1}{1 + e^{-\frac{V+35}{10}}}.$$

More generally, if  $X = n, m$ , or  $h$ , then the equations of (1.7) can be written as

$$\frac{dX}{dt} = \alpha_X(V)(1 - X) - \beta_X(V)X = \frac{X_\infty(V) - X}{\tau_X(V)}, \quad (1.8)$$

where

$$x_\infty(v) = \frac{\alpha_x V}{\alpha_x V + \beta_x V} \quad (1.9)$$

and

$$\tau_X = \frac{1}{\alpha_X(V) + \beta_X(V)}. \quad (1.10)$$

Variable  $m$  drives the activation of the sodium current,  $h$  drives the inactivation of the sodium current, and  $n$  drives the activation of the potassium current. The transition rates between open and closed states of the individual gates of each ionic channel is described by  $\alpha_X(V)$  and  $\beta_X(V)$ .  $X_\infty$  is a steady state variable and  $\tau_x$  is a time-constant.

At this point, the model has not taken into account the impact of injecting some external current into the model. Neurons in any nervous system are not simply self-excited. In the real world there is usually some sort of stimulating injection that triggers and activates neural spike. In consideration of current contributed by some external entity, the observed equation becomes

$$\begin{aligned}
 C_m \frac{dV}{dt} &= - \sum_k i_{m,k} + I_e \\
 &= -[\bar{G}_{Na} m^3 h (V - E_{Na}) + \bar{G}_K n^4 (V - E_K) + \bar{G}_L (V - E_L)] + I_e,
 \end{aligned} \tag{1.11}$$

where  $I_e$  is some externally produced current that is injected into the system. When  $I_e = 0$ , the neural state is said to be at rest, however excitable if the perturbation from the steady state is sufficiently large. For  $I_e \neq 0$ , there is a range of  $I_e$  values that will stimulate periodic neural firing.

### 1.2.2 Fitzhugh-Nagumo

It is noted that because  $V(t)$  and  $m(t)$  change similarly during an action potential and  $h(t)$  and  $n(t)$  change slower during an action potential,  $V$  and  $m$  can be combined into a single variable that will represent activation of the neuron, potential  $V$ . In fact,  $n$  and  $h$  can be combined as well (really  $n$  and  $1 - h$ ) into a single variable refractoriness  $\omega$ , thus drastically

reducing the complexity of the neural model from four dimensions to two. This results in the mathematical representation of the Fitzhugh-Nagumo model, which has the general form [91]

$$\begin{cases} \dot{v} = f(V) - \omega + I \\ \dot{\omega} = a(\beta v - \gamma \omega) \end{cases} \quad (1.12)$$

where  $\alpha$ ,  $\beta$ , and  $\gamma$  are chosen positive values,  $v$  models membrane potential,  $\omega$  is accommodation and refractoriness, and  $I$  is external stimulating current. There are two common versions of  $f(V)$ , one where  $f(V) = v(\alpha - v)(v - 1)$  [90] and one where  $f(V) = v - \frac{v^3}{3}$  [10]. In this dissertation, we will use the latter because there are less terms and will make future computations simpler

$$\begin{cases} \dot{v} = v - \frac{v^3}{3} - \omega + I, \\ \dot{\omega} = \beta v - \gamma \omega \end{cases} \quad (1.13)$$

where  $\alpha$  is set to 1.

Winner-take-all neuronal networks using both the Hodgkin-Huxley and Fitzhugh-Nagumo models will be simulated and analyzed.

### 1.3 Contributions

This dissertation models winner-take-all networks of different neuronal models, in addition to different inhibition and feedback topologies. Our simulations use the complex Hodgkin-Huxley and simpler Fitzhugh-Nagumo neuronal models, each of which is simulated as via lateral inhibition and global interneuron networks with weighted feedback and low-pass filter feedback. In addition, unlike traditional inhibition in which signals are suppressed, the behavior of these model variations was studied in terms of phase. We analyzed how winner-take-all can be achieved by comparing the phase shift of coupled neurons. We also simulated and analyzed an even simpler winner-take-all model previously studied, modeled instead by the postsynaptic membrane potential. This model was also studied comparing lateral inhibition and global interneuron. Though it is not a true biological network since the output is a function of firing rate as opposed to membrane potential, simulations show how it relates to the biological networks and represents an even simpler model than the Fitzhugh-Nagumo. Since the feedback is a function of the firing rate, there is no oscillatory behavior to experience any phase shifts. This dissertation provides a more exhaustive study of these neuronal networks and further insight into how they behave.

## **2.0 Winner-Take-All Networks**

Lateral inhibition is an important phenomenon found in nature. In many neural processes the action potential of an excited neuron will promote stimulation in neighboring neuron, increasing sensory perception. Lateral inhibition however does the opposite; the action potential of an excited neuron suppresses, or inhibits, the action potentials of its neighbors. It is a key mechanism in many neural systems for fundamental computations for different tasks. Commonly used in visual processes, lateral inhibition can also be used in neural processes for sense of hearing, smell, sight, and touch [38][46][48]. Because of its commonplace in natural processes and importance in fundamental biological and neural computations, this has inspired the realization of circuits and devices [39] [40].

In fact, it is the characteristic of lateral inhibition that makes it an ideal to compute winner-take-all. Winner-take-all is a particular principle usually applied in neural networks in which the neurons compete against each other to be chosen as a winner. This is a principle that is commonly fundamental to artificial neural networks for learning algorithms and computational models of the brain for simulating fast human processes such as decision making, pattern recognition, and competitive learning.

### **2.1 Biological Lateral Inhibition**

Lateral inhibition is a concept that has been around for a long time, as far back as the 1600s [41]. However, Hartline et al. [42] progressed the research in lateral inhibition by experimenting

on and studying the ommatidia, or photoreceptor cells, in the compound eyes of *Limulus Polyphemus*, known as the horseshoe crab. The photoreceptors of these compound eyes behave like those of a human eye and are similar in anatomy, though larger and histologically simpler. Like the squid axon Hodgkin and Huxley used, the larger size makes them easy to experiment on and observe. They observed lateral inhibition by illuminating regions of the *Limulus* compound eye. What they discovered was that when a region of the compound eye was illuminated, any ommatidium within a close enough range of the region had its ability to respond to the light reduced. In fact, the illumination increased the threshold by which the photoreceptors reacted was increased. Furthermore, the surrounding ommatidium experienced a reduction in the number of impulses discharged in response to flashes of light and in the discharging frequency during steady illumination. It was also noted that the discharge of photoreceptors during inhibition was similar to the discharge of a photoreceptor operating at a comparable frequency from a weaker stimulus, with no inhibition taking place.

Since then, there have been more discoveries of lateral inhibition in other biological and neurological systems. Arthur et al. [45] examined inhibition in the auditory system of mammals. More specifically they looked at a phenomenon known as two-tone inhibition in cats. Two-tone inhibition is when the discharge rate for a particular auditory neuron activated by a continuous tone is reduced by the stimulus of a tone burst. What they found was that, under the right conditions, inhibitory areas were observed on both sides of the best frequency of a neuron when a tone burst was present with a continuous tone. In a sense, it is similar to a saliency map in that an important or interesting section of a larger field can be identified among background noise which is critical for the advanced hearing that many animals have in order to identify prey and predators.

It also the reason why many alarm systems vary multiple tones as oppose to a single monotonous tone that can easily be drowned out in white noise or become too passive to notice.

Lateral inhibition is also present in the hippocampus, which is heavily responsible for important functions such as short-term, long-term, and spatial memory. Sayer e al. [47] studied synaptic plasticity between neurons in the hippocampus. Although their work focused on the excitory postsynaptic potential connection between neurons in the hippocampus as it pertains to synaptic plasticity, they reference the importance of not blocking synaptic inhibition in order to preserve any inhibitory postsynaptic potential that may arise as that inhibition is relevant in the study of the strength of synapses. Lateral inhibition is also very prevalent in a section of the somatosensory system in vertebrate known as the somatosensory cortex, which processes information related to tactile feedback such as temperature, touch, and even the perception of the movement of one's body [44].

An extremely important neurological system that utilizes lateral inhibition is the basal ganglia [50] [77] [74]. The basal ganglia are located in the in the middle of the brain and responsible for many cognitive abilities. However, they have a particularly pivotal role in motor control [51] [52]. Movement is extremely complex and in any given motion, there are many other mechanisms that can become active that could potentially interfere with the intended action. Imagine a person dropped a pencil and wanted to pick it up. There are not only movements that need to happen (bending down, opening hand), but also movements that should not happen (shaking of the hands, bending too far to one side). The basal ganglia aid in this suppression of these other actions to allow maximum efficiency of the desired motion [50]. This explains why

there has been a strong relationship between the neurological diseases such as Huntington's disease (procedural learning), schizophrenia (emotional behavior), and Parkinson's disease (tremors) [54] [55] [53].

## **2.2 Nonbiological Lateral Inhibition**

With the inspiration from the discovery of lateral inhibition, the concept has been applied to many real-world applications. Lyon [43] proposed a mechanism for designing a high-reliable digital mouse that utilized lateral inhibition in two ways. First, lateral inhibiting light sensors on a circuit are used to produce a bitmap, or digital image, of bright features in a dark field. This map is used by the mouse to track its location relative to itself, making it reliable regardless of orientation. Then an inhibition network that matches the bitmap pattern, in conjunction with the bitmap and detector array, was used to develop a tracking algorithm. This mechanism proved to be efficient and reliable.

Of course, one of the bigger applications of lateral inhibition is neural networks [40]. In fact, neuromorphic engineering is an important and growing research area in which lateral inhibition can serve as a vital basis in developing biologically inspired devices to perform complex computations. There are a couple different learning paradigms used in neural networks, namely supervised and unsupervised training [89]. Supervised learning is a commonly used and researched method in which a network is trained on specific data with known outputs. The network is tasked with producing results as close to the real response as possible. However, the more interesting and

complex method of learning is unsupervised training. The goal of this type of learning is not to yield a necessarily correct answer, but to utilize the input data given to make pattern correlations and group or categorize these correlations.

There are examples of lateral inhibition being used in both supervised and unsupervised training [88], however there is much to research about effective ways to design neural networks to optimally learn. For example, when at a time the algorithm with which neural networks self-organized was unknown, Kunihiko [87] hypothesized a new method for organizing synapses between neurons and ultimately deduced a new algorithm to effectively organize multilayered neural networks. It was known that layered neural network capabilities enlarged with an increased number of layers and his hypothesis proposed is that the synaptic connection between some cell A and some cell B is reinforced under the conditions that cell A fires and no other cell about cell B fires stronger than B. They demonstrate this for both excitory and inhibitory synapses.

Lateral inhibition has encouraged the development of complex circuitries such as vision chips, integrated circuits designed such that the circuitry for image processing and image sensing are both on the same die as opposed to their own individual circuits [39]. Cao et al. [59] further progressed the utilization of lateral inhibition in this area by demonstrating its use in a convolution neural network. It was shown that lateral inhibition can be used to aid in saliency detection and the development of category-specific attention maps, which contributes to many real-world applications such as x-ray surveillance [60]. One of the most critical parts of artificial intelligence is training algorithms and Gregor et al. [58] demonstrated the impact of lateral inhibition in learning larger sparse codes and developing faster and more efficient algorithms.

### 2.3 Winner-Take-All via Lateral Inhibition

Because of the inherent competitive behavior of lateral inhibition, it can be easily used to realize winner-take-all. The concept of winner-take-all can be found in the natural world, as shown in the work of Bechara [31]. In their work on the impact of drug use on a person's ability to long term decisions, he suggests that during the process of considering a number of decisions, a drug addict will experience a daunting number of affective responses triggered by all the options being considered. Over time, numerous and conflicting signals could be triggering but only the stronger ones will have precedent, regardless of whether they will positively or negatively impact the person. This dominating signal can then manipulate the cognitive and behavioral parts of the neural system. In fact, it has been proposed that lateral inhibition is the base mechanism of the competitive behavior of neurons like the basal ganglia, and that winner-take-all is the base mechanism for deciphering the correct motor function among competing programs [71][72][50].

Coultrip et al. [61] simulated a biologically plausible model of winner-take-all based on a section of the hippocampus. Specifically, the neural network studied was simulated to represent a naturally-occurring rhythmic activity called the hippocampal theta rhythm. They were able to achieve a near-ideal biologically plausible winner-take-all mechanism in which only the most strongly-activated cell of a neuron group responded with spiking activity. This mechanism also closely parallels specific physiological and anatomical features of particular cortical circuits. Ermentrout [62] investigated winner-take-all neural networks by examining the impact the speed of inhibition has on the network's behavior. A network mimicking a small piece of cortex is simulated, where there is a significantly larger number of excitatory pyramidal cells than inhibitory interneurons. What was shown was that for faster inhibitions, which is necessary for some types of cortical processing (i.e. short-term memory), the network exhibited behavior that of a winner-

take-all network. However, as the inhibition is slowed, the network begins to experience synchronous oscillations. Hahnloser [80] used simulations to show how global inhibition, along with self-excitation will give rise to multi stable winner-take-all mechanisms.

Fukai et al. [63] offered a comparison of the strength of lateral inhibition to the strength of self-inhibition to observe the impact that the ratio has the network behavior. It was determined that the ratio of later inhibition strength to self-inhibition strength is in fact very important to the network in terms of steady states. Winner-take-all behavior is achieved when both strengths are equal. When self-inhibition is weaker, however, there is only one active neuron and there is no guarantee that the neuron is the neuron that is accepting the largest input. When lateral inhibition is weaker, the network experiences a winners-share-all behavior where there is a group of activated neurons. Xie et al. [64] expands upon the concept of winner-take-all by using lateral inhibition to realize competition between groups of neurons. Much research revolves around a single neuron being the winner among a group. This work instead looks at how competition among potentially overlapping groups can result in the coactivation of a subset of neurons given an input, which is useful in areas such as unsupervised learning. The selected group of neurons represents a patten, where each neuron is activated by a particular feature in the pattern. This encoding becomes useful for sparsely distributed representations.

## **2.4 Nonbiological Winner-Take-All**

Of course, there have been different winner-take-all based analog circuits implemented in real applications [69] that demonstrate the computation can be manifested physically. But there has been an abundance of research into creative ways to realize and apply winner-take-all. Feldman

et al. [65] demonstrated the use of winner-take-all to develop building block for connectionist model. The main principle of connectionism is that any mental phenomenon can be represented by some artificial neural network. This work offers methods of developing connectionist models to solve general problems that appear in the intelligent behavior field, providing a framework for models that address problems in connectionist models such as stability and noise-sensitivity, distributed decision-making, time and sequence problems, and the representation of complex concepts. Unlike previous model proposals, the abstraction of their model makes them more applicable to a wide range of uses. Koch et al. [66] examine biological phenomena related to image processing computations within primates and humans. The visual systems in primates and humans have been found to have developed over time a special way of focusing on specific objects, however there is a process that occurs beforehand that analyzes simple features in a field of space. Their work studies how neural networks can be used to emulate the phenomena associated with these processes such as developing topographical maps that represent elements of a visual field (color, movement direction, orientation, density, etc.). The selection rules used to build these maps are implemented using winner-take-all.

Indiveri [13] implemented a real-time model of stimulus-driven selective attention in an analog VLSI 2D architecture. This work was inspired by biological systems that can discern the important parts of various sensory inputs, specifically images, by observing the relevant sub-regions of the input while suppressing the noise and irrelevant sub-regions. They were able to mimic neural spike trains in hardware, proposing an architecture that receives inputs from synaptic circuits and then projects outputs to local inhibitory neurons. A chip designed specifically for the selective attention contains a cell designated for winner-take-all that monitors the voltage of itself and its neighbors to determine the winners. In competitive learning, there is much unknown about

the data and winner-take-all has proven to be useful in approximating the probability of a classification based on the activation responses of the neurons in the network. Lemmon and Kumar [30] used a generalized form of winner-take-all to model competitive learning paradigms and demonstrated how their model, can be used to design algorithms which estimate the modes of unknown probability density functions.

Beyond just the standard winner-take-all network in which there is one clear winner, there is also a model variation in which there can be multiple winner. Majani et al. [67] thoroughly analyzed such a model known as the  $k$ -winner-take-all network, in which the network determines  $k$  winners out of  $n$  neurons. They base their neural model from the continuous Hopfield network [57] and provide an extensive theoretical analysis of the  $k$ -winner-take-all network, illustrating the capability of the Hopfield network to solve interesting decision problems. Where their approach is primarily based on choosing an appropriate external input that is to be the same for all neurons, Wolfe et al. [81] expands upon this work by allowing external inputs to be different, among a few other things.

Another variation of winner-take-all uses a slightly different form of lateral inhibition. Sum et al. [68] provide a thorough theoretical analysis of an algorithm called Maxnet, in which a neuron uses its output to not only inhibit other neurons in the network but boost its own signal. In other words, every neuron's output is positively fed back into its own input and negatively fed back into the other neurons' inputs. One of the problems with Maxnet however is its slow convergence rate, especially when values from the data are similar. Yen et al. [83] proposed an improved model (iMax) in which it tackles the slow convergence rate problem of Maxnet by dynamically updating the inhibitory strength between neurons at every iteration in the algorithm. This causes the output of the algorithm to decrease quicker and thus converge faster.

## 2.5 Winner-Take-All Model

There are multiple ways to design a winner-take-all architecture, however the idea remains the same that the stronger signals dominate over the weaker signals. Neurons could have an awareness of other neural states, shown in Figure 2-1, or a central neuron could be used to decipher the prevailing signal, shown in Figure 2-2. This dissertation considers both models. It is also important to mitigate influence on the network from external noise. Some stronger systems are capable of having noise drowned out by the inputs to the system whereas some weaker systems need to initialize with uniform output activity [17]. This work assumes more ideal conditions, in which there is no external noise impacting the neuronal behavior. Commonly, winner-take-all is represented by the suppression of weaker neurons by a stronger neuron, typically causing the weaker neurons to become inactive. However, it may be worthwhile to examine other possible representations of winner-take-all, utilizing some other reaction in the system that will differentiate winners from the losers.

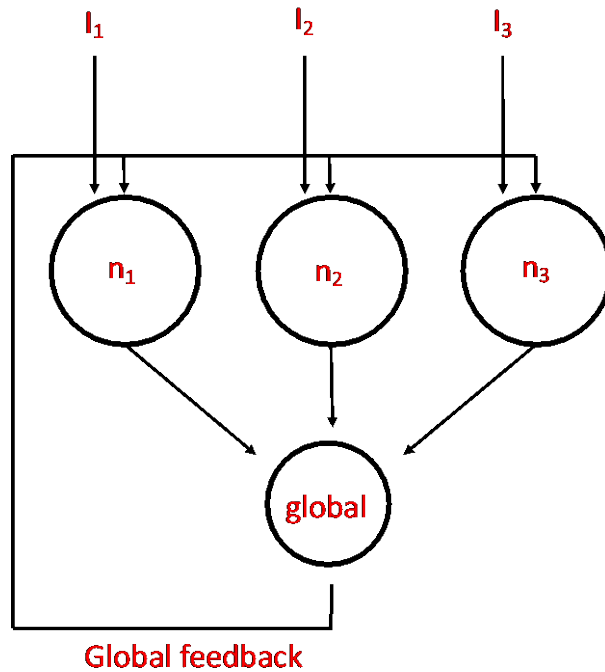


Figure 2-1: Basic winner-take-all structure using a global interneuron. This example is a three-neuron network with a single global neuron. The three neurons receive input current and as they become active, their output is received by the global neuron. The global neuron uses the outputs and computes a feedback to return to the neurons in the network.

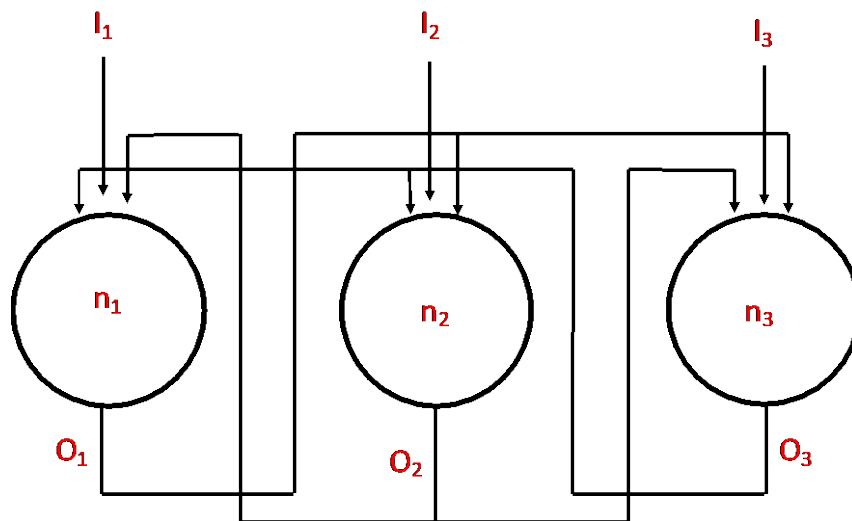


Figure 2-2: Basic winner-take-all network structure using lateral inhibition. This is example is a three-neuron network in which all neurons receive input current and distribute their output as feedback to all other neurons in the network.

The dynamics of the Hodgkin-Huxley and Fitzhugh-Nagumo neurons are modified to reflect winner-take-all, including an additional  $z$  term in their potential equations. In some works that consider models with global inhibitory neurons,  $z$  is an inhibition current from the global neuron, reflecting the dynamics of its charging and discharging modes [14]. As the neurons in the network spike, the global inhibitory neuron enters into a charging state and after some time (saturation), starts to discharge until the next spike. This charging/discharging state is defined as

$$\dot{z} = \begin{cases} -k_c(z - z_0) \\ -k_d z \end{cases}, \quad (2.1)$$

where  $z_0$  is the saturation threshold,  $k_c$  is the charging rate, and  $k_d$  is the discharging rate.  $k_c$  is set to be some large value and  $k_d$  is set to be some small value. As a neuron in the network spikes, the strength of the inhibition current increases to the saturation level quickly, such that it leaves little opportunity for other neurons to spike. The potential of the neurons decreases sharply, converging to an equilibrium point, and then the inhibition current discharges slowly as the neurons enter the oscillation region. The winner is determined as the neuron that enters this oscillation region first, as it will be the neuron with the largest input.

For simplicity, this dissertation defines  $z$  as a coupling function that is a summation of the feedbacks from the neurons in the network. Therefore, the new dynamical equations for the Hodgkin-Huxley and Fitzhugh-Nagumo neurons are

$$C_m \frac{dV}{dt} = -[\bar{G}_{Na} m^3 h (V - E_{Na}) + \bar{G}_K n^4 (V - E_K) + \bar{G}_L (V - E_L)] + I_e - z \quad (2.2)$$

and

$$\dot{v}_i = v_i - \frac{v_i^3}{3} - \omega_i + I_i - z \quad (2.3)$$

respectfully, where  $z_i = \sum_{k=1}^n v_k, k \neq i$  for lateral inhibition and  $z_i = \sum_{i=1}^n v_i$  for global interneuron.

### 3.0 Analysis of Neuronal Dynamics

Nonlinear dynamical systems are complex and can be tricky to characterize and analyze. There are different ways to go about this, however it is best to start by calculating the equilibrium (also known as critical) points of a nonlinear system and examine the behavior of the system about this point. True for oscillatory systems, limit cycles can be used to model behavior in that they are a closed solution curve in the phase space that is not a critical point [26].

#### 3.1 Equilibrium Points

An equilibrium point is a point representing a constant solution to some given differential equation, the point where the derivative, or partial derivatives if there are multiple variables in the differential equation, is zero. A good place to start analyzing nonlinear systems is examining the equilibrium point. This is because the behavior about the equilibrium point of some given nonlinear system

$$\dot{x} = f(x) \tag{3.1}$$

can be quantitatively determined by linearizing around the equilibrium point

$$\dot{\bar{x}} = A\bar{x}, \quad (3.2)$$

where  $\bar{x} = x - x_0$ . Jacobian matrix  $A = Df(x_0)$ , a matrix of partial derivatives with respect to each variable in each nonlinear system. It is defined that for some point  $x_0$ , that if  $f(x_0) = 0$  then  $x_0$  is an equilibrium point of (1.1). The equilibrium point is a constant solution where the nonlinear equations intersect and can be of various types depending on matrix A. More specifically, if none of the eigenvalues of the partial derivative matrix  $Df(x_0)$  have a zero real-part, or all eigenvalues have a nonzero real part, then  $x_0$  is considered to be a hyperbolic equilibrium point.

Nonhyperbolic equilibrium points have a center manifold that is a set of orbits that have a behavior about the equilibrium point that influenced by the stable (convergence) and unstable (divergence) manifolds. Hyperbolic equilibrium points, however, do not have a center manifold, thus the behavior of their orbits is strictly determined by the stable or unstable manifolds. In Figure 3-1 [32], the green represents the stable manifold and the blue represents the unstable manifold. Figure 3-2 [33] shows a center manifold in red. The distinction between hyperbolic and nonhyperbolic equilibrium points is important because it has been shown that when  $x_0$  is a hyperbolic equilibrium point, then the local behavior of the nonlinear system about the point is topologically equivalent to the local behavior of the linear system.

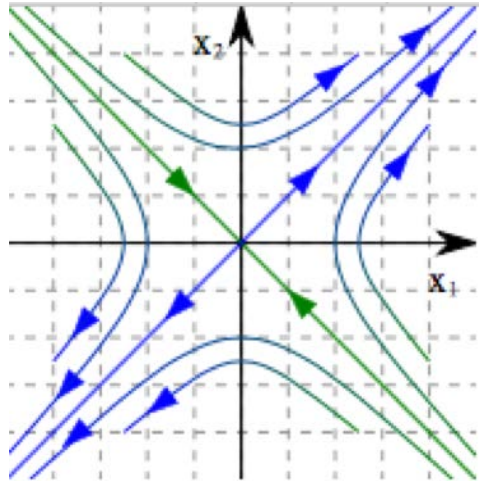


Figure 3-1: Example of hyperbolic saddle point.

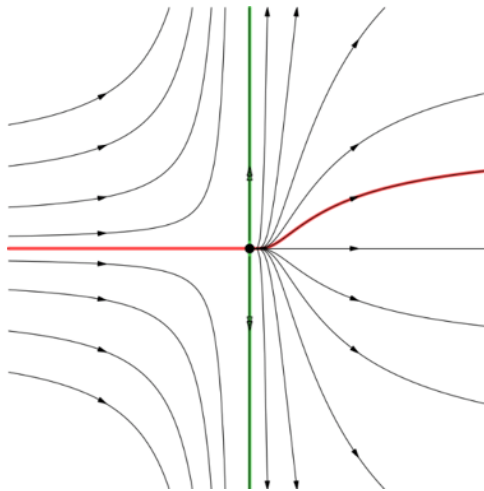


Figure 3-2: Example of nonhyperbolic saddle point.

As stated earlier, the equilibrium points of a nonlinear system can be categorized based on their eigenvalues determined by matrix  $A$ . If all of the eigenvalues of the Jacobian matrix  $Df(x_0)$  have positive real parts, then the equilibrium point is referred to as a source. If the eigenvalues are all negative, then it known as a sink. The equilibrium point is known as a saddle if there are both positive and negative real parts and it is also hyperbolic. Figure 3-3 to Figure 3-5 [34] show the directional fields about these types of equilibrium points.

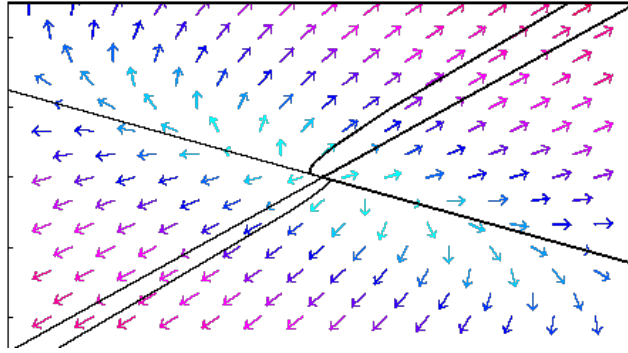


Figure 3-3: Direction fields for source equilibrium point.

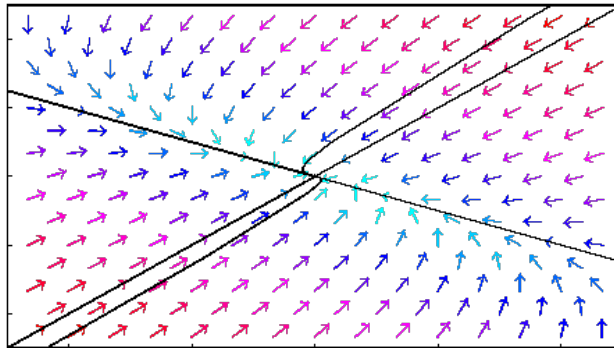


Figure 3-4: Direction fields for sink equilibrium point.

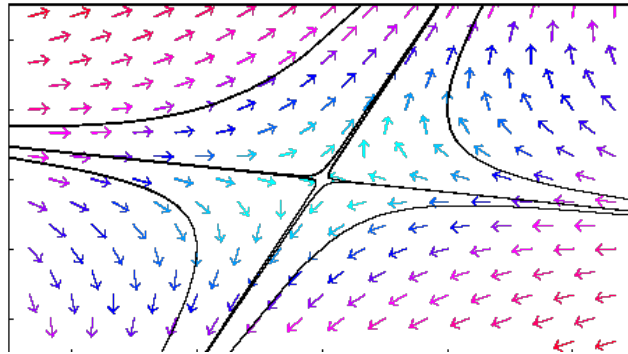


Figure 3-5: Direction fields for saddle equilibrium point.

### 3.1.1 Fitzhugh-Nagumo Model

Using the characterization of the model in this dissertation, we can study the behavior of the system around the equilibrium point. Given the nonlinear system representation of the Fitzhugh-Nagumo neural model

$$\begin{cases} \dot{v} = v - \frac{v^3}{3} - \omega + I_{app}, \\ \dot{\omega} = \beta v - \gamma \omega \end{cases} \quad (3.3)$$

where  $\beta, \gamma > 0$ , the behavior of the nonlinear system can be determined by using (3.2) to calculate the Jacobian matrix  $A$  by computing the partial derivatives of  $\dot{v}$  and  $\dot{\omega}$ :

$$\frac{\partial \dot{v}}{\partial v} = 1 - v_0^2, \quad (3.4)$$

$$\frac{\partial \dot{v}}{\partial \omega} = -1, \quad (3.5)$$

$$\frac{\partial \dot{\omega}}{\partial v} = \beta, \quad (3.6)$$

$$\frac{\partial \dot{\omega}}{\partial \omega} = -\gamma, \quad (3.7)$$

$$A = \begin{bmatrix} \frac{\partial \dot{v}}{\partial v} & \frac{\partial \dot{v}}{\partial \omega} \\ \frac{\partial \dot{\omega}}{\partial v} & \frac{\partial \dot{\omega}}{\partial \omega} \end{bmatrix} = \begin{bmatrix} 1 - v_0^2 & -1 \\ \beta & -\gamma \end{bmatrix}. \quad (3.8)$$

Now that the Jacobian matrix has been determined, it can be used to calculate the eigenvalues for (3.3). To compute the eigenvalues, a solution needs to be found such that the determinant of the summation of the eigenvalue identify matrix and the Jacobian matrix is zero, or  $\det(\lambda I - A) = 0$ :

$$\lambda I - A = \lambda \begin{bmatrix} 1 & 0 \\ 0 & 1 \end{bmatrix} - \begin{bmatrix} 1 - v_0^2 & -1 \\ \beta & -\gamma \end{bmatrix} = \begin{bmatrix} \lambda - 1 + v_0^2 & 1 \\ -\beta & \lambda + \gamma \end{bmatrix}, \quad (3.9)$$

where for simplicity,  $\varepsilon = 1 - v_0^2$ , giving

$$\begin{aligned} \det(\lambda I - A) &= \det \left( \begin{bmatrix} \lambda - \varepsilon & 1 \\ -\beta & \lambda + \gamma \end{bmatrix} \right) = (\lambda - \varepsilon)(\lambda + \gamma) + \beta \\ &= \lambda^2 + (\gamma - \varepsilon)\lambda + (\beta - \varepsilon\gamma). \end{aligned} \quad (3.10)$$

The solution for  $\lambda$  is found to be

$$\lambda = \frac{(\varepsilon - \gamma) \pm \sqrt{(\gamma - \varepsilon)^2 - 4(\beta - \varepsilon\gamma)}}{2} \quad (3.11)$$

and considering that the equilibrium point represents where the two functions intersect, (3.3) can be manipulated algebraically represent that intersection:

$$\begin{cases} \dot{v} = v - \frac{v^3}{3} - \omega + I_{app} = 0, \\ \dot{\omega} = \beta v - \gamma \omega = 0 \end{cases}$$

$$\begin{cases} \omega = v - \frac{v^3}{3} + I_{app} \\ \omega = \frac{\beta}{\gamma} v \end{cases} \quad (3.12)$$

Since one function is cubic and the other is linear, there are two possible cases of intersection: one where the linear equation intersects the cubic function along its negative slope and one where it intersects along the positive slope.

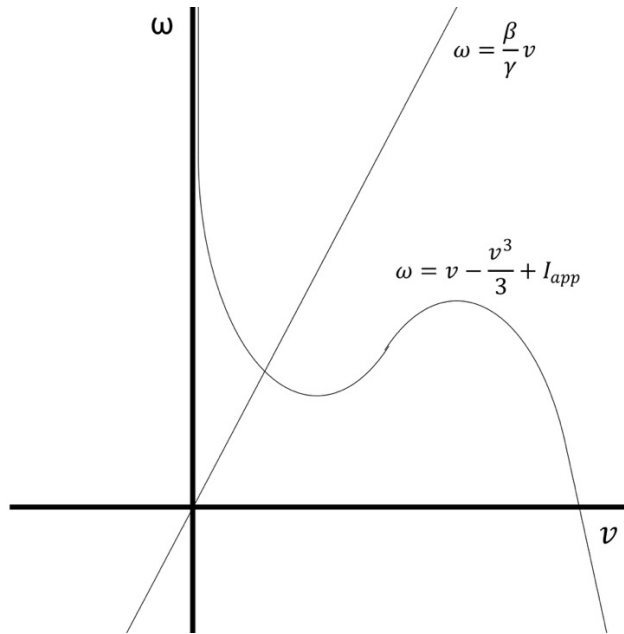


Figure 3-6: For small  $I_{app}$ , the equilibrium point lies on the positive slope of the cubic function.

In the first case shown in Figure 3-6, the slope of the cubic function is negative meaning the derivative is negative. The derivative of the cubic function in (3.12) was found in (3.8),  $1 - v^2$

which we refer to as  $\varepsilon$ . With  $\varepsilon < 0$ ,  $(\varepsilon - \gamma)$  is negative and  $|\varepsilon - \gamma| > \sqrt{(\gamma - \varepsilon)^2 - 4(\beta - \varepsilon\gamma)}$  thus the real component of (3.11) is strictly negative, and according to the previous definition in Section 3.1, the equilibrium point is considered a sink and is stable. This means all neighboring orbits about the equilibrium point will converge to the equilibrium point.

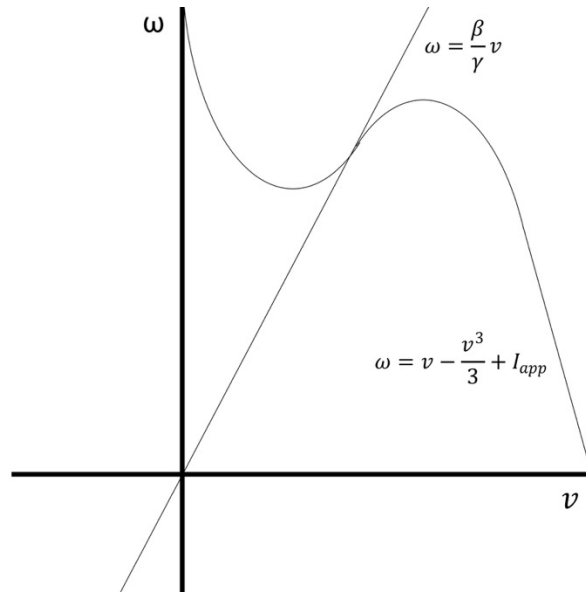


Figure 3-7: For large  $I_{app}$ , the equilibrium point lies on the positive slope of the cubic function.

In the second case shown in Figure 3-7, the slope  $\varepsilon$  is greater than 0, but also smaller than the slope of the linear function, which is  $\frac{\beta}{\gamma}$ . With  $\varepsilon > 0$ , the real part of the eigenvalue is no longer guaranteed to be negative, making the equilibrium point unstable. In fact, when  $\gamma > \varepsilon$ , the eigenvalues are strictly positive classifying the equilibrium point as a source. As such, this source has a characteristic where all trajectories in the region about the equilibrium point diverge away from it, which will be necessary to establish a limit cycle.

### 3.2 Limit Cycles

A limit cycle is a closed trajectory that has the property of at least one other trajectory converging into it as  $t$  approaches infinity. It also does not include an equilibrium point. An example is shown in Figure 3-8. There is some neighborhood region that separates the equilibrium point from the limit cycle region. It is defined by its property of having at least one other trajectory that converges to it, whether interior or exterior, as time approaches positive or negative infinity. Similar to equilibrium points, limit cycles describe solutions to nonlinear systems, but they correspond to period solutions, hence why they are used for oscillatory systems.

A limit cycle is considered stable if all neighboring trajectories converge to the limit cycle as time approaches positive infinity. It is unstable otherwise. A limit cycle is defined as asymptotically stable if it is stable and the limit of all neighboring trajectories approaches zero as time approaches infinity. Figure 3-8 shows an example of a limit cycle [35], where two other trajectories converge into it.

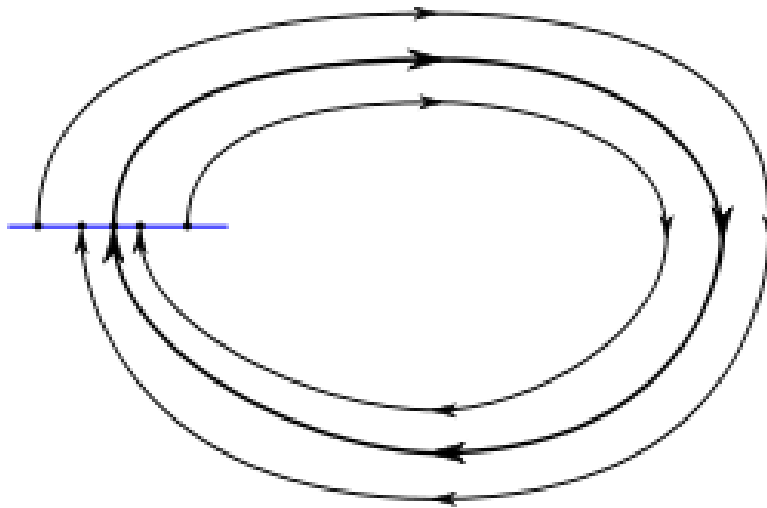


Figure 3-8: Stable limit cycle (bold) with two trajectories converging into it.

Limit cycles are important because they are used to describe the oscillatory behavior of nonlinear dynamical systems. Systems with a stable limit cycle will settle into a steady trajectory in the phase plane. This indicates a steady state of the nonlinear system, for example a fixed amplitude and period, which is important when analyzing neuronal networks.

### 3.2.1 Fitzhugh-Nagumo Model

In general, oscillatory systems have limit cycles and to demonstrate the existence of a limit cycle, we use the Poincarè-Bendixson Theorem [26]:

*Suppose that  $f \in C^1(E)$  where  $E$  is an open subset of  $R^2$  and that  $\dot{x} = f(x)$  has a trajectory  $\Gamma$  with  $\Gamma^+$  contained in a compact subset  $F$  of  $E$ . Then if  $\omega(\Gamma)$  contains no critical point of  $\dot{x} = f(x)$ , then  $\omega(\Gamma)$  is a periodic orbit of  $\dot{x} = f(x)$ .*

What this means is that there is some region  $E$  which contains all feasible values of  $x$  and that there is some trajectory that continues to be contained inside some bounded closed region  $F$ , which is a subset of  $E$ . If the  $\omega$ -limit set, that is the set of solutions of the trajectory as  $t$  approaches infinity, of that trajectory does not contain an equilibrium point within it, then that  $\omega$ -limit set is a limit cycle. A graphic example is shown in Figure 3-9.

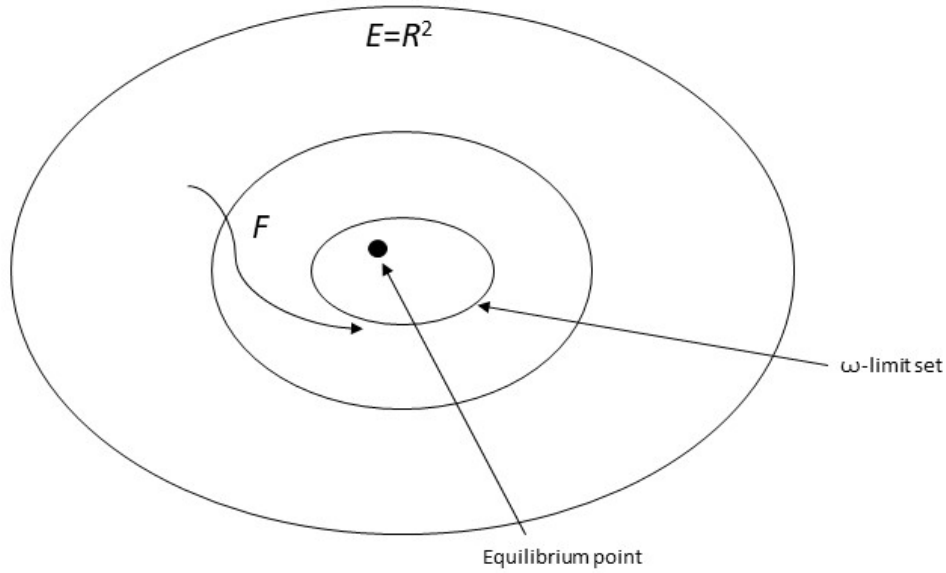


Figure 3-9: Graphical example of the Poincaré-Bendixson Theorem.

Using (3.3), we determine a region  $F$  using a Lyapunov function defined as

$$H(v, \omega) = \frac{j}{2}v^2 + \frac{k}{2}\omega^2, \quad (3.13)$$

where  $j$  and  $k$  are positive constant values to be chosen later. When an unstable equilibrium point exists, there is a neighborhood about the equilibrium point, excluding it, where trajectories diverge away from the equilibrium point into a surrounding closed region  $F$ . Therefore, to prove boundedness of region  $F$ , it needs to be shown that the region for  $\frac{dH}{dt} > 0$  is in fact bounded; that there exists some outer region in which  $\frac{dH}{dt} < 0$  implying convergence of trajectories.

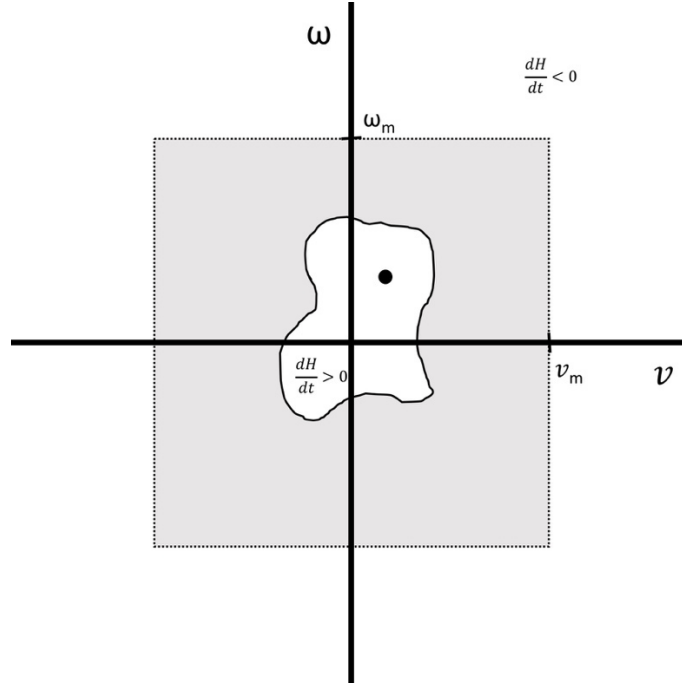


Figure 3-10: Regions where trajectories diverge ( $\frac{dH}{dt} > 0$ ) and converge ( $\frac{dH}{dt} < 0$ ). Within the gray region,  $x(t)$  could either diverge or converge, but beyond the gray region ( $v_m$  and  $\omega_m$ )  $x(t)$  is guaranteed to converge into the region.

Taking the derivative and using chain rule,

$$\begin{aligned}
 \frac{dH}{dt} &= (jv)\dot{v} + (k\omega)\dot{\omega} \\
 &= jv\left(v - \frac{v^3}{3} - \omega + I\right) + k\omega(\beta v - \gamma\omega) \\
 &= jv^2 - \frac{jv^4}{3} - jv\omega + jvI + k\omega\beta v - k\omega^2\gamma,
 \end{aligned} \tag{3.14}$$

however, to help simplify the equation,  $j$  and  $k$  are chosen to be 1 and  $\frac{1}{\beta}$  respectively,

$$\frac{dH}{dt} = v^2 - \frac{v^4}{3} + vI - \frac{\gamma}{\beta}\omega^2. \quad (3.15)$$

To prove the Poincarè-Bendixson Theorem, a value  $v_m > 0$  needs to be determined such that for any  $(v, \omega)$  where  $|v| > v_m$ ,  $\frac{dH}{dt} < 0$ . Since  $\omega$  is squared, it is irrelevant whether it is positive or negative:

$$v^2 - \frac{v^4}{3} + vI - \frac{\gamma}{\beta}\omega^2 < 0. \quad (3.16)$$

Since the quartic portion of the equation is negative and contributes heavily to the value of the equation, choosing a sufficiently positive value such as  $v_m = 5$  would ensure  $\frac{dH}{dt}$  is negative. It is not known how the region behaves inside our arbitrary  $v_m = 5$  (the gray region in Figure 3-10) so in the case where  $|v| < v_m$ , a  $\omega_m < |\omega|$  needs to be chosen such that

$$v_m^2 - \frac{v_m^4}{3} + v_m I < \frac{\gamma}{\beta}\omega_m^2. \quad (3.17)$$

Thus, we establish a region  $F$  as defined by  $|v| > v_m$  and  $|\omega| < \omega_m$  excluding the neighborhood about the equilibrium point. Any trajectory  $x(t)$  starting outside of region  $F$  will converge into the region, and any trajectory  $x(t)$  starting inside region  $F$  will remain inside the region. According to the Poincarè-Bendixson Theorem, there exists a limit cycle inside region  $F$ . This limit cycle can then be used to help characterize the synchronization behavior of the winner-take-all neuronal network.

## 4.0 Winner-Take-All in Firing Rate Competition

This chapter presents a study of winner-take-all in firing rate competition. The analysis is based on the investigation of winner-take-all behavior and dynamics of the biological networks in the basal ganglia [37]. The neuronal model considered in this chapter is a simplified version of Fitzhugh-Nagumo model with the postsynaptic firing rate as its output. The focus here is the intensity of neuronal firing and how this is reshaped by winner-take-all competition in a network with lateral inhibition, and next chapter will concentrate on winner-take-all competition in the aspect of timing of neuronal firing.

### 4.1 Lateral Inhibition Equations

Equations (4.1) and (4.2) represent the dynamics of a neuronal lateral inhibition network. It is considered to be an  $n$ -neuron network where  $x_i$  represents the postsynaptic membrane potential,  $y_i$  represents the firing rate of a particular neuron  $i$ ,  $v_i > 0$  represents the synaptic strength of the connection between neuron  $i$  and some neuron  $k$  where  $k \neq i$ , and  $d_i$  represents the external input to neuron  $i$ , in which  $i$  ranges from 1 to  $n$ .  $\tau$  is a time constant and  $f_i(\cdot)$  is some nonnegative and continuous activation function with a continuous and nonnegative first derivative that describes the relationship between the membrane potential and firing rate of a particular neuron  $i$ . In this analysis we are assuming the synaptic strength is the same between any particular neuron and all others in the network. It is noted that though this analysis is on a lateral inhibition model, simulations later will also include an interneuron variation.

$$\tau \frac{dx_i}{dt} = -x_i - \sum_{k \neq i} v_k y_k + d_i, \quad (4.1)$$

$$y_i = f_i(x_i). \quad (4.2)$$

Equation (4.1) actually can be represented in a more concise form when considering the matrix-vector form of its variables, where  $x = [x_1, \dots, x_n]^T$ ,  $y = [y_1, \dots, y_n]^T$ ,  $d = [d_1, \dots, d_n]^T$ , and  $V = [v_{ik}]_{\{n \times n\}}$  with  $v_{ii} = 0$  and  $v_{ik} = v_k$  for  $i \neq k$ .

$$\tau \frac{dx_i}{dt} = -x - Vy + d. \quad (4.3)$$

If the topology was that of a global interneuron instead of lateral inhibition, the model would instead be defined as

$$\tau \frac{dx_i}{dt} = -x_i - z + d_i, \quad (4.4)$$

where  $z$  represents the dynamics of the global interneuron. This global interneuron sends the same feedback to all other neurons in the network based on the input it receives from the neurons. Its dynamics can be expressed as

$$\tau_z \frac{dz}{dt} = -z + \sum_{i=1}^n y_i, \quad (4.5)$$

where  $\tau_z$  is a time-constant for the global interneuron and  $y_i$  is remains a function for firing rate of a particular neuron  $i$ , the notable difference that the summation is over the firing rate for all neurons in the work. Characteristic analysis in this chapter can similarly be done for the global interneuron topology.

## 4.2 Characteristics of the Equilibrium Point

This section will analyze some of the key characteristics of dynamic equations as they relate to a neuronal winner-take-all network, as opposed to the previous section that looked at the characteristics from an individual neuron perspective.

### 4.2.1 Existence of Equilibrium Point

As stated before, an important concept of dynamics of nonlinear systems is equilibrium points. An Equilibrium point  $x^*$  is a constant solution such that any system state that begins at it will stay in it indefinitely. In this case, to determine the equilibrium of this model comprised of (4.1) and (4.2), there would need to be found a solution to  $-x - Vy + d = 0$ , i.e.,

$$x_i = d_i - \sum_{k \neq i} v_k f_k(x_k), \quad i = 1, \dots, n, \quad (4.6)$$

and because  $f_i(\cdot)$  is nonnegative as stated before, (4.6) then implies

$$x_i^* \leq d_i, \quad i = 1, \dots, n. \quad (4.7)$$

The existence of an equilibrium point can be shown by using the Brouwer Fixed Point Theorem [70], which states a continuous function  $f$  that maps a compact convex set to itself contains a fixed point  $x_0$  (possibly more) such that  $f(x_0) = x_0$ . In this case, if a function is defined as  $h_i(x) = d_i - \sum_{k \neq i} v_k f_k(x_k)$  and a compact convex set is defined as  $D = [d_1 - \sum_{k \neq 1} v_k f_k(d_k), d_1] \times \dots \times [d_n - \sum_{k \neq n} v_k f_k(d_k), d_n]$ , then it can be shown that the function  $h(x)$  can map to  $D$  and there  $x = h(x)$  is in  $D$ . This can be applied using any activation function that as long as it is continuous, nonnegative, and monotone nondecreasing.

#### 4.2.2 Isolation and Uniqueness Characteristics

Isolation is a characteristic that describes an equilibrium point where there is a small neighborhood about it that does not contain any other equilibrium points. Uniqueness simply describes whether or not there is only one equilibrium point in the system. Both of these characteristics are important because they help to ensure predictability of the system, as it is critical to understand future states based on the current state at a given time.

The equilibrium point  $x^*$  can be described as an isolated equilibrium point by using the determinant of the Jacobian matrix  $A$  of the network. If  $\det(A) \neq 0$ , then  $x^*$  is considered isolated. The Jacobian matrix can then be used to determine uniqueness of  $x^*$ . It can be shown that there

does exist an open set of solutions such that the determinant does not equal zero. If it was to be assumed that there did in fact exist another equilibrium point  $x'$  that satisfied (4.6), an equation describing the relationship between those two equilibrium points can be used to make substitutions, i.e.  $u = x' - x^*$ . Using the mean value theorem [70], it can be deduced that in fact  $x' = x^*$  and thus there is only one equilibrium point.

### 4.2.3 Stability

The stability of an equilibrium point is important, and we previously mentioned before the different ways to categorize a stable equilibrium point. It is important because a system needs to be stable to be observable, to provide any useful information about future predictions based on current state and time. Expanding a further and applying to this model, a stable equilibrium point  $x^*$  is where for each  $\epsilon > 0$ , there is  $\delta > 0$  such that

$$\|x(0) - x^*\| < \delta \Rightarrow \|x(t) - x^*\| < \epsilon \text{ for any } t \geq 0, \quad (4.8)$$

an asymptotically stable equilibrium point  $x^*$  is where the point is stable and  $\delta$  can be chosen such that

$$\|x(0) - x^*\| < \delta \Rightarrow \lim_{t \rightarrow \infty} \|x(t) - x^*\| = 0, \quad (4.9)$$

and a globally asymptotically stable equilibrium point is where the point is stable and  $x(t)$  approaches  $x^*$  as  $t \rightarrow \infty$  for any  $x(0)$ .

These nuances of stability can be used to characterize the strength of the stability of the system. An equilibrium point is stable when the trajectories of the system remain inside a bounded region about it. It becomes asymptotically stable when those trajectories not only remain inside the region but converge to the equilibrium point. Even further, an equilibrium point becomes globally asymptotically stable when all trajectories converge to it, not just the ones within the region. Similar as before we can turn to a Lyapunov function of the system to determine the stability of this system. What is found is that given the condition  $v_i \dot{f}_i(x_i^*) < 1$ , the slope of this Lyapunov function is strictly negative, indicating an asymptotically stable equilibrium point. In fact, it shown that the system as a globally asymptotically stable equilibrium point.

### 4.3 Winner-Take-All Equations

In the interest in fairness between the neurons in the network, we will now consider  $f_i(\cdot) = f(\cdot)$  and  $v_i = v$  for  $i = 1, \dots, n$ . This is done so that all of the neurons in the network have the same synaptic strengths and activation functions. So (4.1 becomes

$$\tau \frac{dx_i}{dt} = -x_i - \sum_{k \neq i} v f(x_k) + d_i, \quad i = 1, \dots, n, \quad (4.10)$$

where  $f(\cdot)$  is nonnegative and globally Lipschitz continuous,

$$0 \leq \frac{f(u_1) - f(u_2)}{u_1 - u_2} \leq M_i \quad (4.11)$$

for any two different  $u_1, u_2$ .

### 4.3.1 Order Preserving Characteristics

Order preservation with respect to the network input is maintained when the ordering of the postsynaptic membrane potential of the neurons in the network corresponds to the ordering of the inputs to those neurons. In other words, if a neuron receives a greater input than another its potential will be greater. It is important to maintain order in the system because it is a characteristic that helps drive the inhibition of the winner-take-all network. With neurons receiving feedback from other neurons in the network, those with greater inputs should yield greater outputs in order to deliver larger feedback to suppress the other neurons.

It can be shown that as long as  $f(\cdot)$  is continuous (though not necessarily Lipschitz continuous), nonnegative, and monotone nondecreasing, (4.10) is ensured to have an order preserving equilibrium. Considering the ordering of neuron inputs  $d_1 \leq d_2 \leq \dots \leq d_n$  and outputs  $x_1 \leq \dots \leq x_n$ , following an analysis similar to the one in Section 4.2.1 and defining a function  $h_i(x) = d_i - \sum_{k \neq i} v f(x_k)$  and compact convex set  $D = \{x \mid d_i - \sum_{k \neq i} v f(d_k) \leq x_i \leq d_i\}$  it can be shown that there is an equilibrium point  $x^*$  such that  $x_1^* \leq x_2^* \leq \dots \leq x_n^*$ . In regard to stability of an order preserving equilibrium point, it is asymptotically stable following Section 4.2.3 provided  $f(\cdot)$  is nonnegative and continuous with a continuous and nonnegative first

derivative. However, if in fact  $f(\cdot)$  is considered to be Lipschitz continuous, then following an analysis similar to Section 4.2.3 it is determined that this order-preserving equilibrium point is globally asymptotically stable.

### 4.3.2 Increased Differences between Neuronal Activities

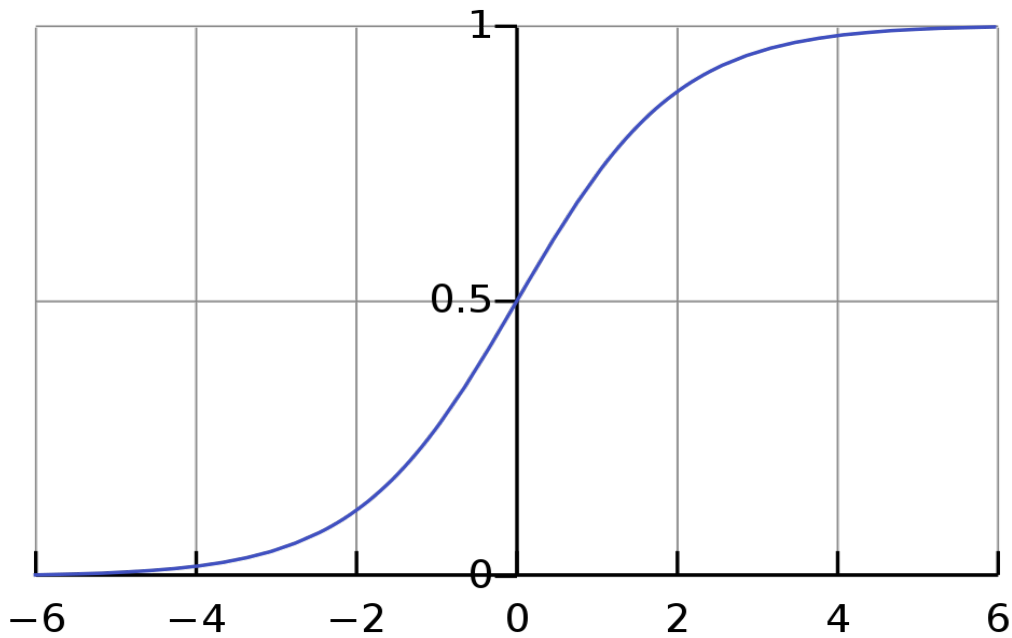


Figure 4-1: Example of sigmoidal function.

In this model, the activation function plays a critical role in the winner-take-all behavior. In fact, it is the very mechanism that drives it. Figure 4-1 shows an example of a continuous and monotonic function. Applying to your model, the x-axis is the input to the function, and the y-axis is the firing rate for that particular neuron, though as stated before we will consider all neurons to have the same activating function for fairness. It can be observed in Figure 4-1 that there becomes an increase in the differences between neuronal activity as the inputs increase. As stated in the previous section,  $d_1 \leq d_2 \leq \dots \leq d_n$  and  $x_1 \leq \dots \leq x_n$ . This means that since  $x$  is the input to

the activation function, lower valued  $x$  will result in significantly lower firing rates because of the shape of the activation function. Hence, larger inputs cause larger inhibitions to the neurons in the network they are connected to.

#### 4.4 Simulation

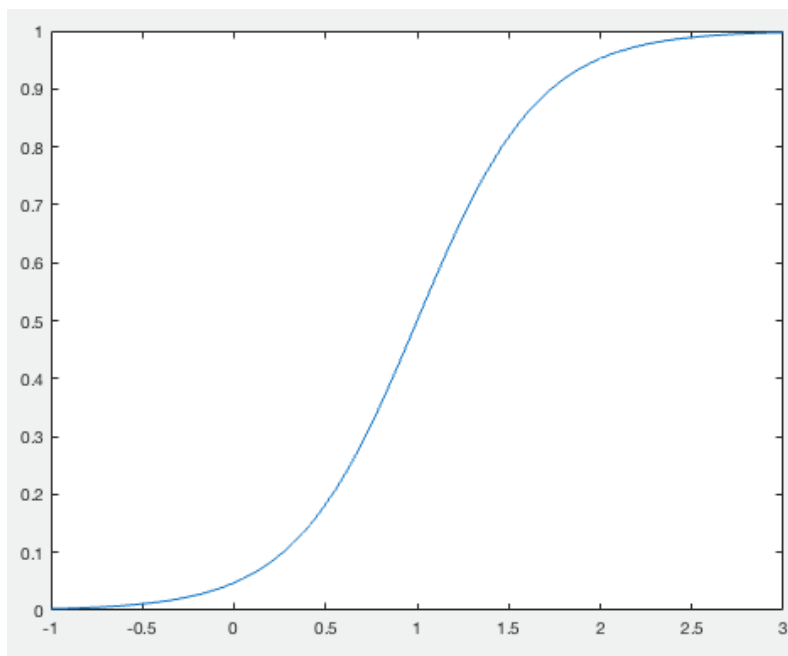


Figure 4-2: Activation function  $f(u) = 1/(1 + e^{-(u - 1)/(1/3)})$ .

Simulations were performed on reproduced versions of the model based on (4.1) and (4.2) from [37]. With the original based on lateral inhibition topology, a modified global interneuron model is simulated as well. The activation function used in these simulations is of the form

$$f(u) = \frac{1}{1 + e^{-\frac{u-b}{a}}} \quad (4.12)$$

where  $a = 1/3$ ,  $b = 1$ , and  $\tau = 0.1$ . Increasing or decreasing  $b$  shifts the function along the x-axis right or left, respectively, and will impact the amount of inhibition returned to the neurons in the network. Increasing or decreasing  $a$  will increase or decrease, respectively, the slope the function. This will impact the network's sensitivity to distinguish a winner.

Figure 4-3 through Figure 4-6 show the simulation results of the reproduced model from [37] using the activation function (4.12). On the left of each figure are the results from the lateral inhibition model. On the right of each figure are the results from the global interneuron model. Over all, they are pretty similar in characteristics. Though, the winner of the global interneuron model has a slightly smaller value than the winner of the lateral inhibition model. This is due to the global interneuron model having a greater amount of inhibition in the network.

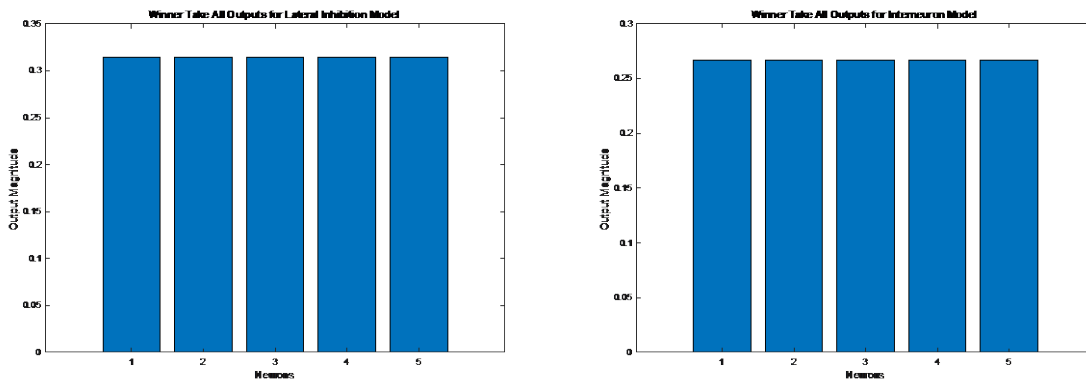


Figure 4-3: Five-neuron winner-take-all network modeled by (4.1) and (4.2) where  $I = 2$ .

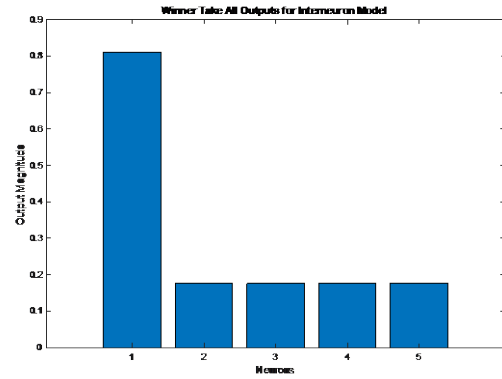
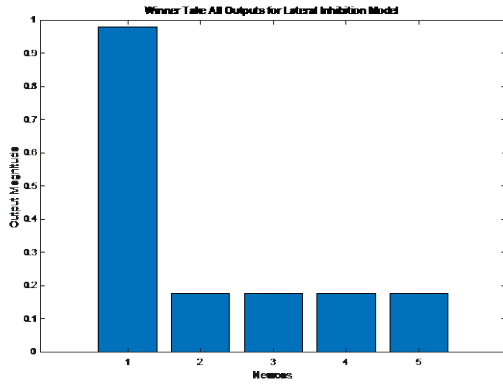


Figure 4-4: Five-neuron winner-take-all network modeled by (4.1) and (4.2) where  $I_1 = 3$ ;  $I_2 = I_5 = 2$ .

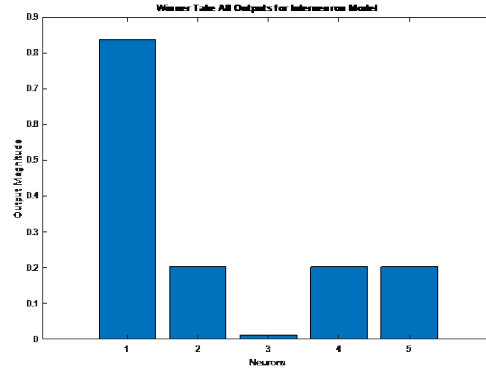
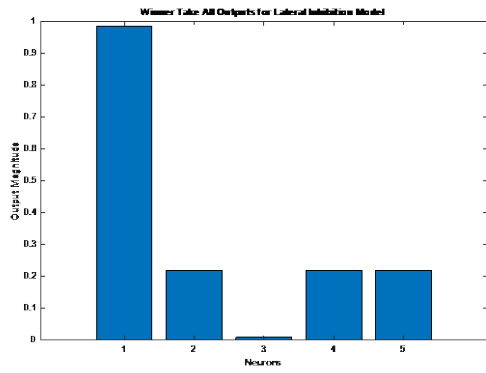


Figure 4-5: Five-neuron winner-take-all network modeled by (4.1) and (4.2) where  $I_1 = 3$ ;  $I_2 = I_4 = I_5 = 2$ ;  $I_3 =$

1.

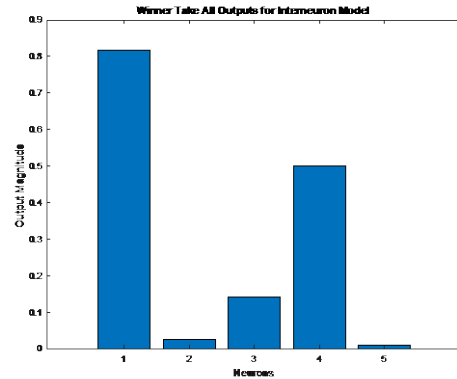
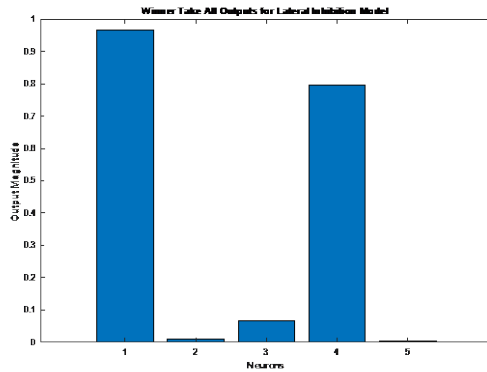


Figure 4-6: Five-neuron winner-take-all network modeled by (4.1) and (4.2) where  $I_1 = 3$ ;  $I_2 = 1.3$ ;  $I_3 = 1.9$ ;  $I_4 =$   
2.5;  $I_5 = 1$ .

Even though this postsynaptic membrane potential model is a simplified representation of a true biological network (i.e. Hodgkin-Huxley), we can observe a connection between the two in terms of activation functions. Figure 4-7 shows the results from a single Hodgkin-Huxley neuron that was simulated for a wide range of increasing inputs. The output frequency, or firing rate, was determined for each input value resulting in a plot that appears similar to the continuous and monotonically increasing activation function used for the postsynaptic membrane potential model.

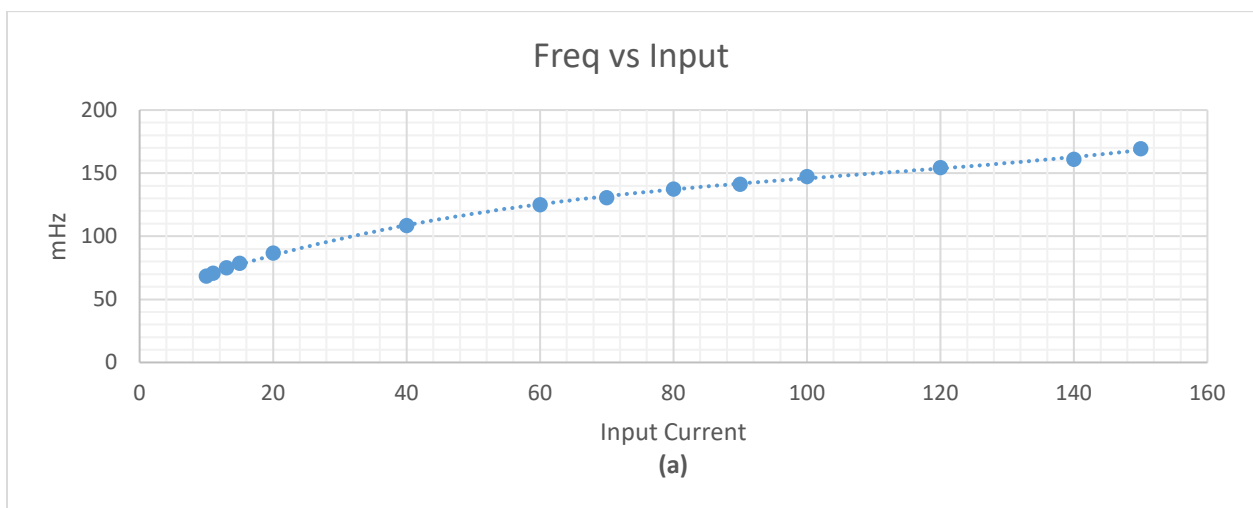


Figure 4-7: Frequency of Hodgkin-Huxley neuron as the input increases. As the input increases, so does the frequency in a way that resembles the continuous and monotonic activation function used in the simplified postsynaptic membrane winner-take-all model.

## 5.0 Winner-Take-All in Phase Competition

In this section, the architectures of the neural networks are defined. The parameters of both the Hodgkin-Huxley and the Fitzhugh-Nagumo models are established as well as the simulation parameters. Next, the synchronization characteristics are discussed. Amplitude and frequency are relevant; however, this dissertation focuses on phase. Finally, the models are simulated, and the results are discussed. Simulations were first run on the neurons without feedback to demonstrate the neurons' individual behavior before coupling. Simulations were then run on the neurons coupled in networks of five. In addition to observing the impact of the neurons' input current on the output of the network, other parameters such as feedback weights and filter time constants are also studied. When analyzing the behavior of winner-take-all, it is more informative to examine models using input values that are relatively close together. It is important to observe how sensitive a system to similar inputs and its ability to distinguish a winner.

### 5.1 Simulation Model

To model and simulate Hodgkin-Huxley and Fitzhugh-Nagumo neuron based winner-take-all networks, Simulink is used to create block diagrams of both the neurons and neural network, as depicted in Appendix A. MATLAB is also used to provide simulation settings and control logic. A modification has been made to the original coupling term for the winner-take-all model.

The Hodgkin-Huxley neuron simulated is based on (2.2) and the Fitzhugh-Nagumo neuron is simulated using (2.3). Each neuron takes two inputs, input voltage and voltage from the coupling

related to winner-take-all. The global neuron essentially computes the coupling function  $z$ , receiving the voltages from coupled neurons and summing them to return as feedback input to the neurons in the network. Since neuron voltages oscillate in the model, negative voltage values have been eliminated by setting the lower bound of voltages used for coupling to 0, further simplifying the model. Figure 6-6 and Figure 6-7 show how the coupling voltage are summed and supplied to the neurons.

## **5.2 Synchronization Analysis**

In this section we discuss some characteristics involved with analyzing phase synchronization of neurons. Different types of analyses have been done to mathematical express and characterize neural behavior, especially oscillatory synchronization. The three common attributes used to describe synchronization, or wave forms in general, are frequency, amplitude, and phase. Although mentioned here, a more thorough analysis using frequency and amplitude characteristics can be done in the future. A technique based on phase response curve is suggested for the analysis of synchronization phase characteristics of winner-take-all networks.

### **5.2.1 Frequency and Amplitude Analysis**

Frequency is a common and popular method to characterize synchronization, as many systems studied show that neuronal devices oscillating at different frequency will tend to agree on a common frequency at which to resonate. Chiarulli [5] used the behavior of the frequency to

develop a mathematical model of clustered oscillators. Specifically, their work was able to show that given the frequency synchronization behavior of their generic oscillator model, the oscillators act as a degree of match circuit when coupled together. They were then able to make implications about the types of computations could be done. Extending the previous work, Jennings [6] used frequency synchronization to compute convolutions, and therefore convolution-based operations. These computations were modeled in applications in image processing.

A neural spike in a network could impact the frequency of an individual neuron or across the entire network. Neurons that individually resonate at different frequencies might find that when coupled together, and with the right parameters, will synchronized to a new common frequency. Conversely, it is possible that the neurons coupled together could be synchronized at a particular frequency and any neural spike would cause them to them to become unsynchronized or change the synchronous frequency value.

Amplitude, although not directly related to synchronization, is a useful characteristic, especially when considering biologically plausible neural networks where the amplitude of the true output can influence the feedback propagated in the network. There may be some useful information provided by the amplitudes of the neural responses, or at least some correlation between the amplitudes and frequency or phase.

Sase [19] analyzed a type of synchronization that combines both phase and amplitude, phase-amplitude coupling. This is where the phase of the lower frequency oscillation drives the power of the coupled higher frequency oscillation. This synchronizes the amplitude of faster rhythms with the phase of slower rhythms. Gambuzza [22] conducted an analysis comparison between amplitude and phase dynamics to show that in fact, phase synchronization may be enhanced when amplitude dynamics is no negligible. They find that regardless of network

topology, synchronization in random complex networks is enhanced by the amplitude dynamics. Urazhdin [25] examined the synchronization behavior of spin torque nano-oscillators. These particular oscillators are one of the smallest and also have a complex nonlinear dynamical system whose frequency depends on the amplitude of the oscillation.

### **5.2.2 Phase Analysis**

Phase is another characteristic to describe synchronization and the focus. Phase is a particularly interesting form of inhibition because it is not necessarily a traditional inhibition where one neuron becomes active while others are not. Instead winner-take-all can be represented by phase shifts. Shuai and Durand [20] presented a flexible definition of phase of a chaotic neuron and considers the application of phase synchronization in the brain. This work specifically analyzes the phase of a Hindmarsh-Rose neuron model, reconsidering its chaotic dynamics. Yang et. al. [23] developed a simplified phase model to perform phase and frequency synchronization prediction, in order to speed up the simulation of coupled oscillator systems. Their work showed that a new model can be provided that simplifies the analysis of larger system. Syrjala et. al. [24] analyzed the impact of phase noise on self-interference cancellation capabilities of radio transceivers. In this regard, their work looks at the fluctuations in the phase of the radio wave forms and analyzing how that impacts the communication abilities of full-duplex direct-conversion radio transceivers, which transmit and receive signals simultaneously at the same center-frequency.

A spike from one neuron in a network could cause a phase shift in its own oscillatory pattern or in others, impacting the entire system. Depending on the fashion in which the neurons in the network are coupled together, the phase shift may be more drastic in some neural responses

than others. It could be that after a neural spike, phase differences among neural responses will increase or decrease depending on the spike. Though it is possible that phase differences will remain uniform for any spike, and thus is worth investigating. The following sections further describe the characteristics of phase synchronization [95].

#### **5.2.2.1 Determining Amount of Phase Change**

Typically, when a neuron receives some amount of current ( $I_{app}$  in (3.3)), for example a pulse, its membrane potential increases and spiking occurs. However, sometimes this perturbation will not necessarily result in a spike immediately after being injected. Instead, this burst of current can influence when the spiking occurs. That is, there is a difference in the timing of subsequent spikes, or the phase of the spiking behavior has shifted. Figure 5-1 shows an example of a phase-shift, where if a neuron were to receive some sort of perturbation, the resulting phase-shift would cause the spiking of the neuron to occur earlier.

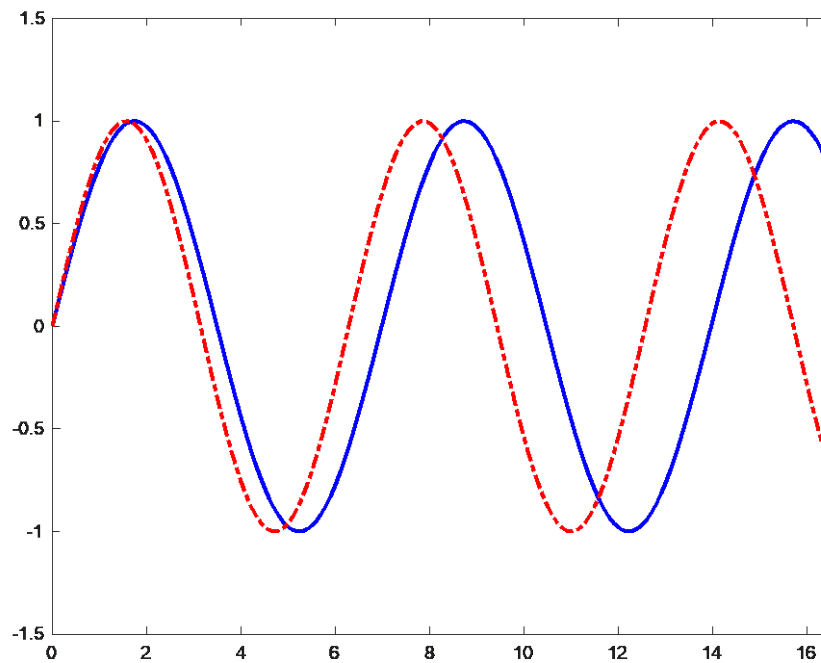


Figure 5-1: Phase-shift example. Two sin waves start at the same point but over time, a phase shift develops.

The phase after the perturbation  $\vartheta_p$  is said to be greater than the phase of the original spike  $\vartheta$ , the magnitude of which is determined by the timing of the current pulse (or other stimuli) relative to the phase experienced by the spike. The phase response curve can be used to measure these phase-shifts and is represented as a function described by  $PRC(\vartheta) = \{\vartheta_p - \vartheta\}$ , where  $\vartheta_p > \vartheta$  correspond to phase advances and  $\vartheta_p < \vartheta$  correspond to phase delays, in terms of the timing of the following spikes. Not only can the phase response curve be measured for a brief or weak stimulus such as a pulse, but it can be measured for any type of stimulus. The spiking behavior simply needs to occur long enough such that the transients from the stimulus subside and the spiking becomes stable enough to observe. This is particularly important for more biologically plausible neuronal networks because, as seen later, certain models need time for the phase shift to occur.

In addition to phase response curves, there is another type of phase measurement that can be used called the phase transition curve [96] defined as  $\vartheta_p = PTC(\vartheta)$ . Although the two methods of measurements are equivalent, because  $PTC(\vartheta) = \{\vartheta + PRC(\vartheta)\} \bmod T$ , PRCs are typically used when there are smaller phase shifts occurring and phase transition curves are usually used when the phase shifts become so large they can be compared with the period  $T$  of the oscillatory behavior. Such large phase shifts will be shown later in the simulation results.

### 5.2.2.2 Types of Phase Responses and the Poincare Phase Map

There are two types of phase responses for both the phase response curve and phase transition curve. The first is Type 0 (strong), where the response results in discontinuous phase response curves and phase transition curves with mean slope 0. The second is Type 1 (weak), where the response results in continuous phase response curves and phase transition curves with mean slope 1. In addition, there is a parametrized version of the phase response curve and phase transition curve that considers the amplitude, or magnitude, of the stimulus causing the perturbation described as  $PRC(\vartheta, A)$  and  $PTC(\vartheta, A)$ , respectively.

Phase response curves are not only limited to describing neuronal responses to single pulses, but they can also be used to study responses to periodic pulse trains. Consider the phase of the neural behavior,  $\vartheta_n$ , at the time the  $n$ th pulse of the train arrives. Using  $PRC(\vartheta_n)$ , the new phase following the perturbation becomes  $\vartheta_n + PRC(\vartheta_n)$ . If we consider the period of the pulsed stimulation  $T_s$ , the phase of oscillation before the following  $(n+1)$ th pulse is  $\vartheta_n + PRC(\vartheta_n) + T_s$ . This results in a stroboscopic mapping of a circle to itself referred to as the Poincare phase map, defined as

$$\vartheta_{n+1} = (\vartheta_n + PRC(\vartheta_n) + T_s) \bmod T. \quad (5.1)$$

### 5.2.2.3 Determining Fixed Points

Generalizing the Poincare phase map (5.1) as

$$\vartheta_{n+1} = f(\vartheta_n), \quad (5.2)$$

the fixed points  $\vartheta = f(\vartheta_n)$  can be used to understand the orbits of the map, as these points are similar to the usual equilibria of continuous dynamical systems such as described in Section 3.1. Continuing the same concept, the fixed point represents the intersection of  $f(\vartheta_n)$  and the line describing where  $\vartheta_{n+1} = \vartheta_n$  and the orbit  $\vartheta_{n+1} = f(\vartheta_n) = \vartheta_n$  is fixed at that intersection. As mentioned previously, a fixed point is asymptotically stable when all nearby trajectories converge to it. Given a fixed point  $\vartheta$ , it is asymptotically stable if for all  $\vartheta_n$  within a sufficiently small neighborhood about  $\vartheta$ ,  $\vartheta_n \rightarrow \vartheta$  as  $n \rightarrow \infty$ . A fixed point is unstable if any of the points  $\vartheta_n$  within a sufficiently small neighborhood about the point  $\vartheta$  diverges away from it. Again, we can use the slope  $m = f'(\vartheta)$  to determine the stability of the fixed point.

### 5.2.2.4 Synchronization

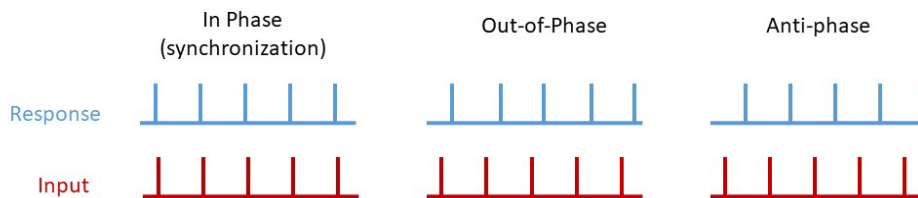


Figure 5-2: Synchronization examples.

Figure 5-2 shows different types of synchronization between the input pulse train on the bottom and the spiking output of the neuron. This synchronization corresponds to stable fixed point on

the Poincare phase map, where in-phase corresponds to  $\vartheta = 0$ , anti-phase corresponds to  $\vartheta = T/2$ , and out-of-phase corresponds to any other value. A fixed point of (5.1) satisfies  $PRC(\vartheta) = T - T_s$  if the stimulation period  $T_s$  is close to the period of the unperturbed oscillation  $T$ . This is the intersection between the phase response curve and the horizontal line  $T - T_s$ . Maxima and minima values on the phase response curve correspond to thresholds in which the oscillation becomes stable or unstable.

### 5.2.2.5 Phase Locking and Phase Lock Regions

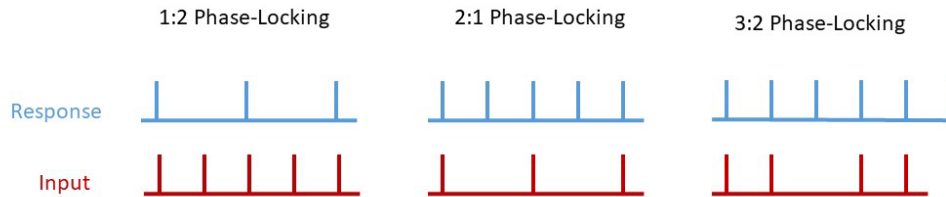


Figure 5-3: Synchronizing phase locking

Phase locking describes the relationship between the input perturbation and the spiking output. It is expressed as  $p:q$ -phase-locking, where the neuron will fire  $p$  times for every  $q$  input pulse as shown in Figure 5-3. 1:1-phase locking (synchronization) or any other  $p:1$ -phase-locking relates to the Poincare phase map (5.1) with  $p$  fired spikes per input pulse. This is important as the Poincare phase map provides information strictly about the phase of the neuron at a particular input pulse, but it does not provide information about the number of spikes between pulses.

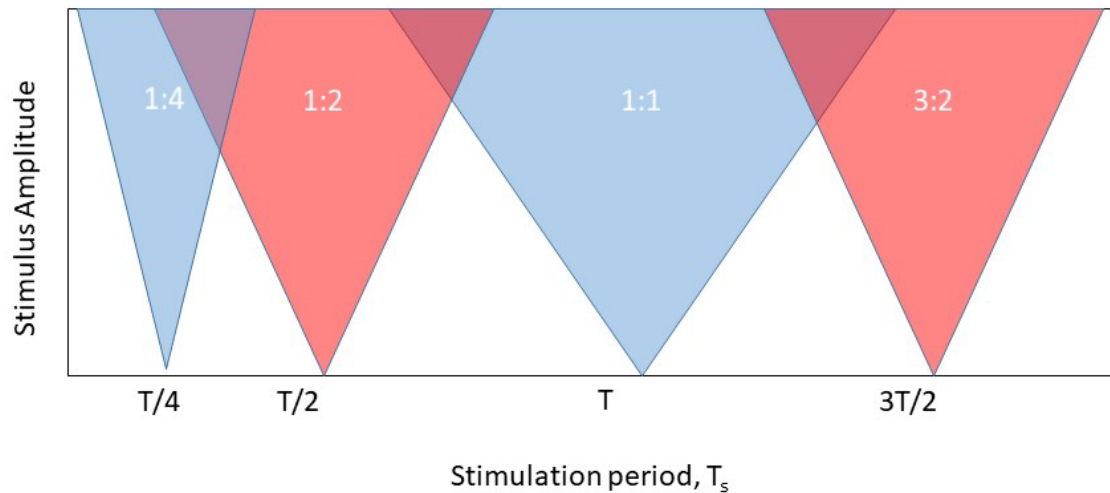


Figure 5-4: Sample  $p:q$ -phase locked regions.

We can somewhat predict the phase-lock state of a network by determining the regions of existences for the states based on the magnitude of the input stimuli. As the amplitude of the stimuli increases, it produces a stringer phase-shift. As mentioned previously, synchronization occurs during a 1:1-phase locked state. An input stimulus train would need a period  $T_s$  sufficiently close to the normal period of the neuron's oscillatory behavior  $T$ . So as the amplitude increases, this difference  $T_s - T$  becomes greater and phase-shift region of existence increases, as shown in Figure 5-4. Every state has its own region and overlapping can occur, meaning multiple states can coexist. The lower the locking order ( $p + q$ ) the wider the phase state region is, making it easier to observe. We will show through simulation how the magnitude of the input stimuli, along with other model parameters, impact the ability of the neuronal networks to synchronize in phase.

## 5.3 Feedback Models

There are two topologies of feedback tested in these simulations. One is a simple weight applied to the output of each neuron. The other topology sends the output of each neuron through a low-pass filter. In both cases, the results from every neuron in the network is summed, according to either an interneuron or inhibitory design, and then sent back as feedback input to the neurons.

### 5.3.1 Applied Weights

Applying weights to the feedback of neurons controls the strength of the signal. It is essentially a form of coupling strength between neurons. In any given neuronal network, depending on the type of neurons used and the parameter settings of the model, the connection between neurons can be strong (the output of the neuron contribute significantly to the network) or weak (the impact of neuron outputs is small). There are numerous factors that can affect this coupling strength, but these simulations focus on the only the feedback weights. The weights range between 0 and 1, with 1 representing 100% of the signal.

### 5.3.2 Low-Pass Filter

A low-pass filter attenuates high frequency signals greater than some threshold value controlled by the time constant  $\tau$ . It is defined by

$$H(s) = \frac{1}{1 + \tau s}, \quad (5.3)$$

which can be tuned such that the output of the neuron approximates a DC signal, as shown in Figure 5-5. The blue line us the original signal and the red, yellow, and purple lines are the same signal when  $\tau$  is 1, 5, and 100, respectively. Because the signal approaches a DC signal for larger time constants, it can be interpreted as a constant value similar to the input current and be fed back into the neurons.

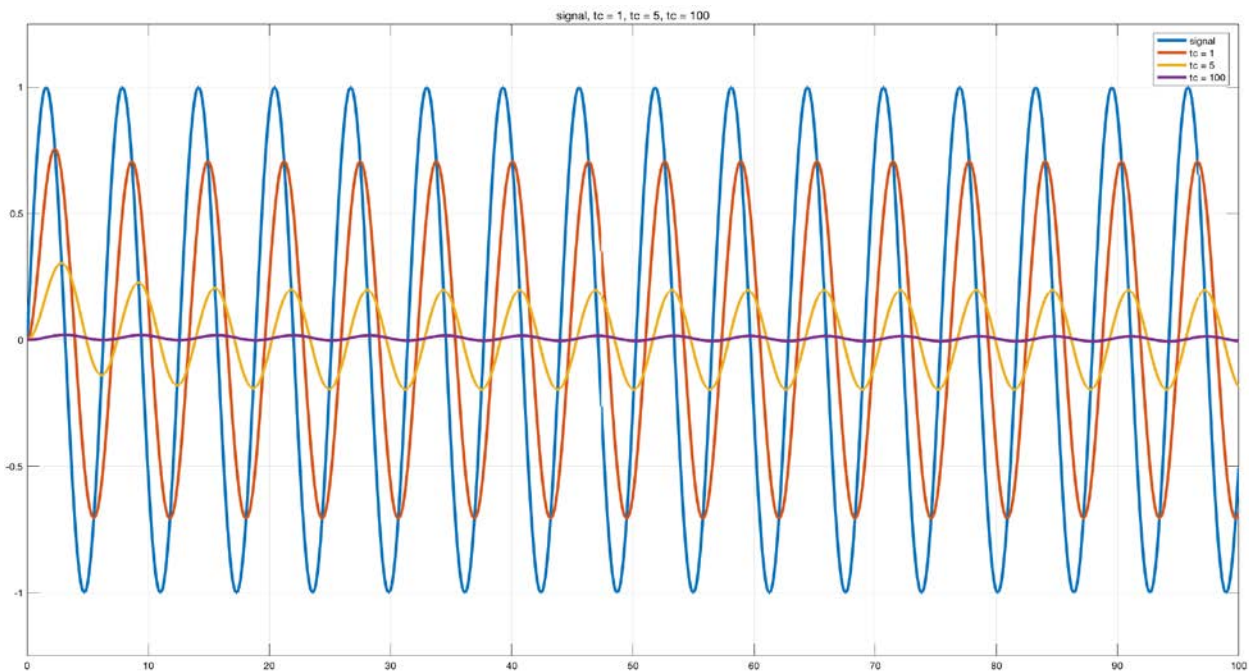


Figure 5-5: Low-pass filter example using a simple sine wave as the input and tuning the time constant.

### 5.3.3 Lateral Inhibition vs Global interneuron

There are two topologies of inhibition simulated in this dissertation: Lateral inhibition and global interneuron. The lateral inhibition neuronal network excludes a neurons own output from its feedback, which gives every neuron in the network potentially different feedbacks depending on the input currents received by them. In a global interneuron neuronal network, every neuron in

the network receives feedback that considers its own output. Effectively, this means all neurons in the network will receive the same amount of feedback.

### 5.4 Hodgkin-Huxley Model

Referring to the model equations of the Hodgkin-Huxley model, more specifically equations (1.7) and (1.11), the following values were chosen for the parameters:

Table 5-1: Hodgkin-Huxley Model Parameters [92]

Parameter	Value
$\bar{G}_{Na}$	120
$E_{Na}$	50
$\bar{G}_K$	36
$E_K$	-77
$\bar{G}_L$	0.3
$E_L$	-54.4
$C_m$	1
$\alpha_n$	$0.01 \frac{V + 55}{1 - e^{-\frac{V+55}{10}}}$
$\alpha_m$	$0.1 \frac{V + 40}{1 - e^{-\frac{V+40}{10}}}$
$\alpha_h$	$0.07e^{-\frac{V+65}{20}}$
$\beta_n$	$0.125e^{-\frac{V+65}{80}}$
$\beta_m$	$4e^{-\frac{V+65}{18}}$
$\beta_h$	$\frac{1}{1 + e^{-\frac{V+35}{10}}}$

According to simulations tested, the Hodgkin-Huxley neuron operates with an input range of about 10 to 150. For these experiments, the input current values used range from 25 to 30. In addition, weighted feedback model, the values for the weights range from 0.1 to 1. The low-pass filter feedback simulations have time-constant values ranging from 0.1 to 100.

Before simulating the network, simulations were run to show how the neurons behave individually when uncoupled and Figure 5-6 to Figure 5-9 show the results of those simulations. The input current to neuron 1 is held constant while the input current to neuron 2 is incrementally increased. What is observed, as expected, is that as the input current to neuron 2 increases, its frequency also increases, while there is also a decrease in amplitude. These characteristics become important when coupling the neurons together depending on how they are coupled together. In addition to comparing simulations between different parameter values, a comparison was also made between the interneuron model and the inhibitory model, the key difference being that the output of a neuron is not contributed to its own feedback. Therefore, in the inhibitory model, the neurons receive potentially different amounts of feedback. Whereas in the interneuron model, all the neurons are receiving the same feedback.

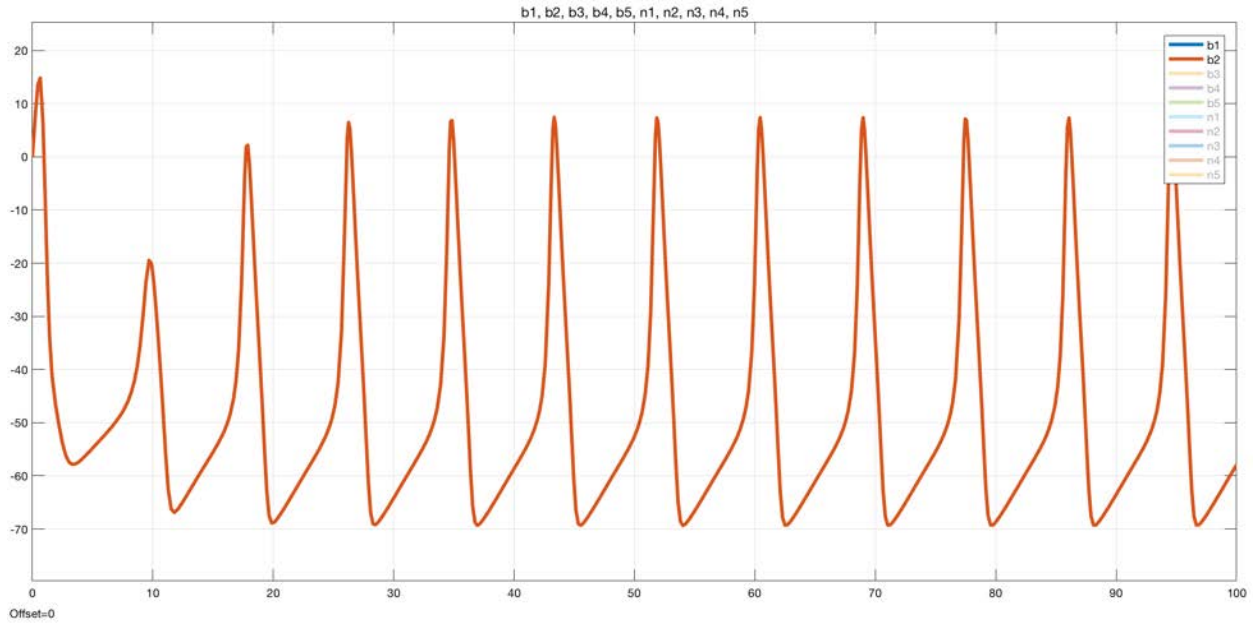


Figure 5-6: Two uncoupled Hodgkin-Huxley neurons where  $I_1 = I_2 = 25$ .

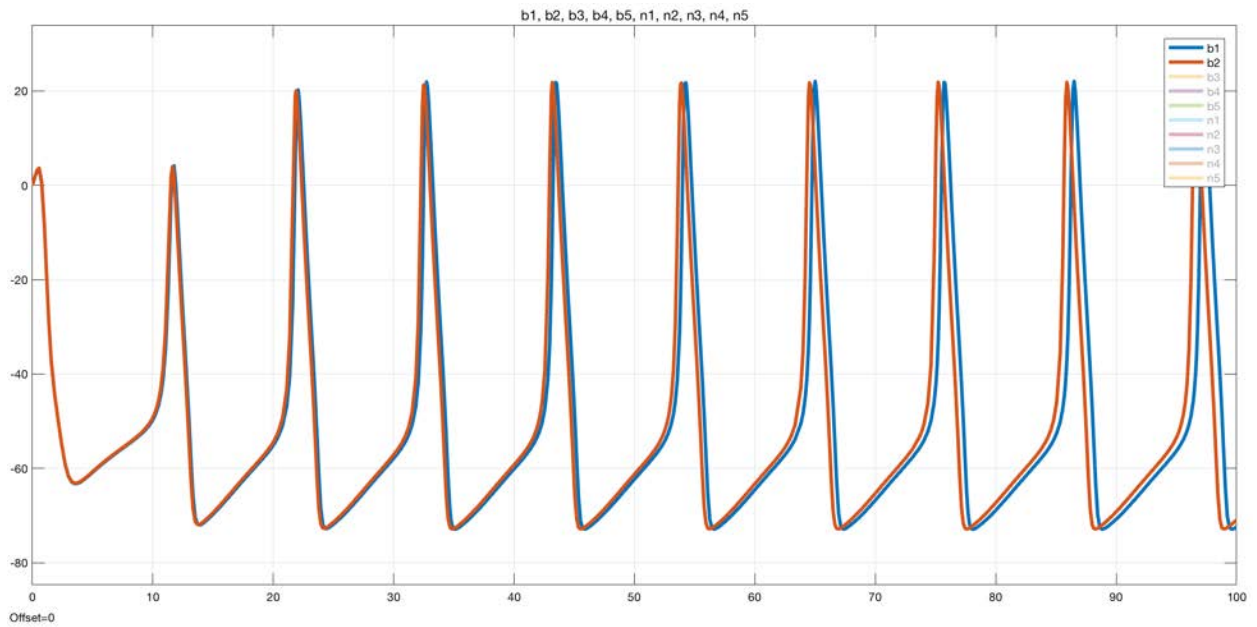


Figure 5-7: Two uncoupled Hodgkin-Huxley neurons where  $I_1 = 25, I_2 = 25.5$ .

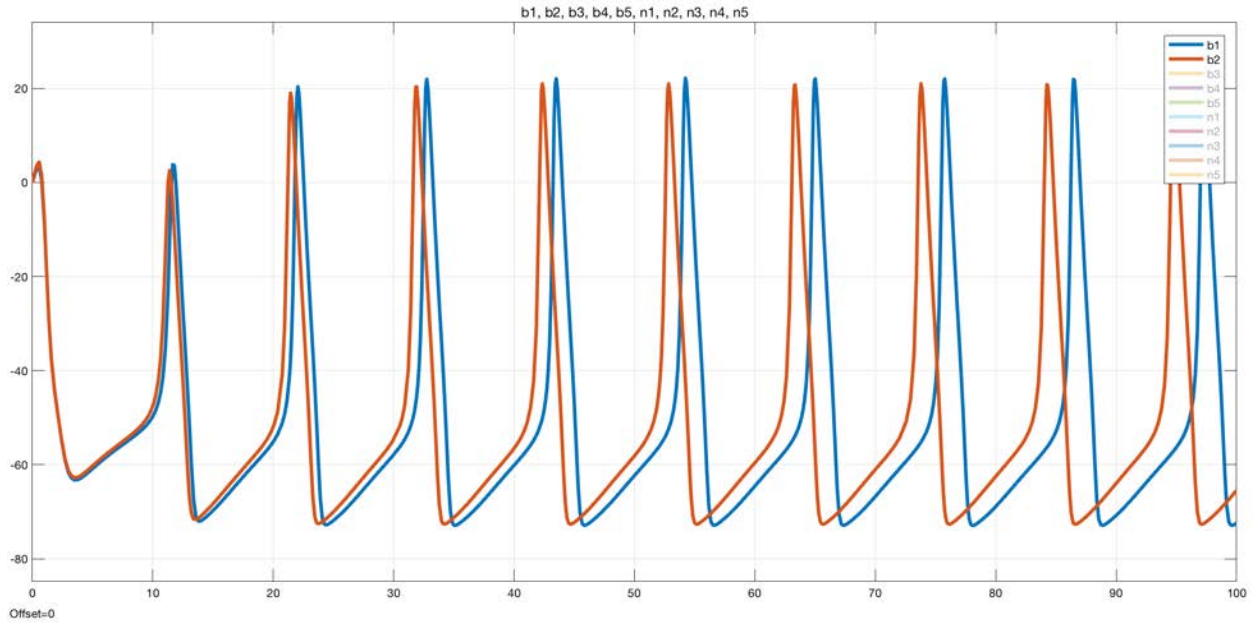


Figure 5-8: Two uncoupled Hodgkin-Huxley neurons where  $I_1 = 25, I_2 = 27$ .

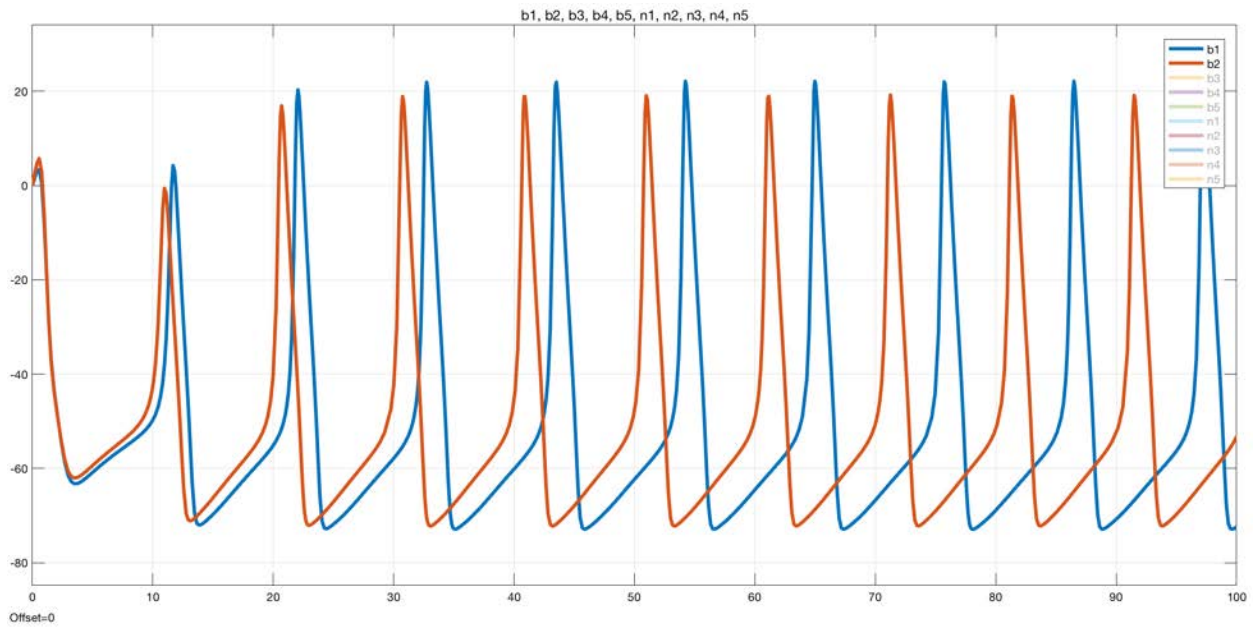


Figure 5-9: Two uncoupled Hodgkin-Huxley neurons where  $I_1 = 25, I_2 = 30$ .

### 5.4.1 Lateral Inhibition Weighted Feedback Model

Figure 5-10 through Figure 5-12 show simulation results of a 5-neuron network with a weighted feedback value of 1. As the input current to neuron 1 is increased, and the difference between input currents becomes larger, the time it takes for the neurons to lock and synchronize is decreased. The neurons shift phases almost by 180 degrees, however they synchronize right before neuron 1 passes the group. When the feedback weight is decreased to 0.5 as shown in Figure 5-14 through Figure 5-16, for closer input values ( $I_1 = 25.5$ ) the lower weight causes the feedback to have less impact, as it takes significantly longer for the neurons to synchronize. As the input current of neuron 1 is increased, there is a delay before synchronization compared to when the weight is 1, however it is not as significant as for closer input values.

Decreasing the weight even further to 0.1 as shown in Figure 5-18 through Figure 5-20, we observe that there is a significantly delay in synchronization for closer input currents. In fact, as the input current of neuron 1 increases, there is no longer synchronization and the neuron 1 oscillates at a faster frequency than the rest of the network (Figure 5-19 would show the mismatched frequencies if it were viewed at a later time). Figure 5-13, Figure 5-17, and Figure 5-21 show simulation results when the neurons in the network have varying input currents for feedback weights of 1, 0.5, and 0.1, respectively. These results show that unlike the other simulations where only one input current differed from the other, varying the feedback weights does not impact the output of the neurons. The neurons are not synchronized, although the frequency at which the neurons oscillate correspond to the order of winners and losers. The higher the input current, the faster the frequency.

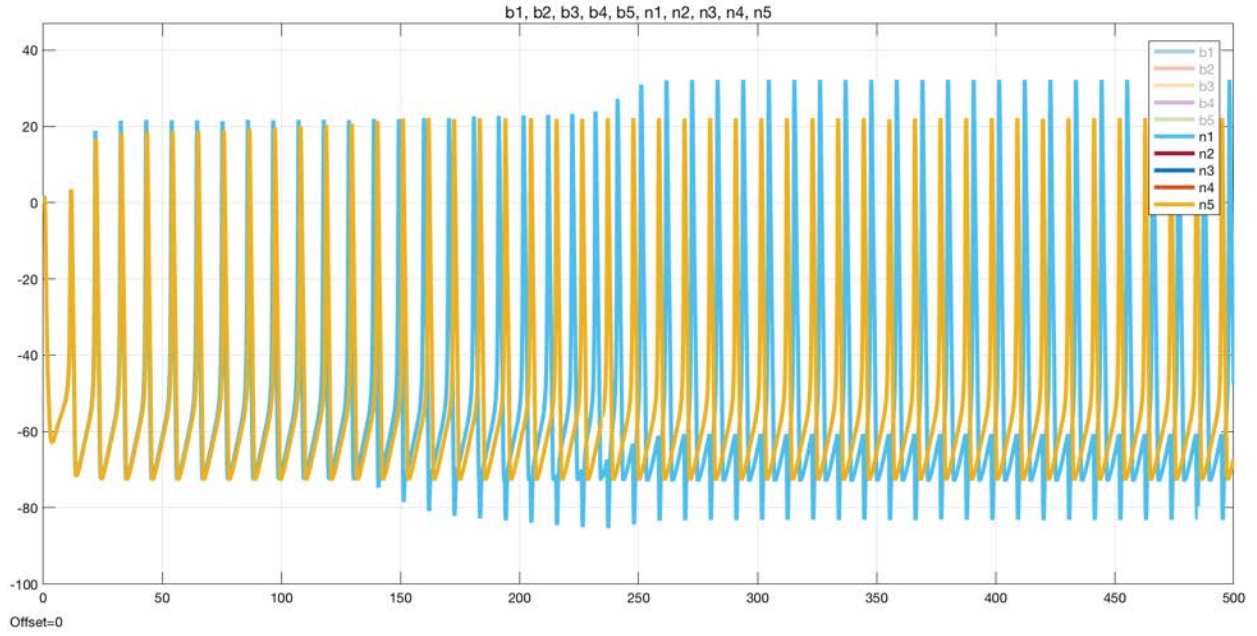


Figure 5-10: Five-neuron Hodgkin-Huxley inhibition winner-take-all network with weighted feedback of 1 where  $I_1 = 25.5, I_2 = I_3 = I_4 = I_5 = 25$ .

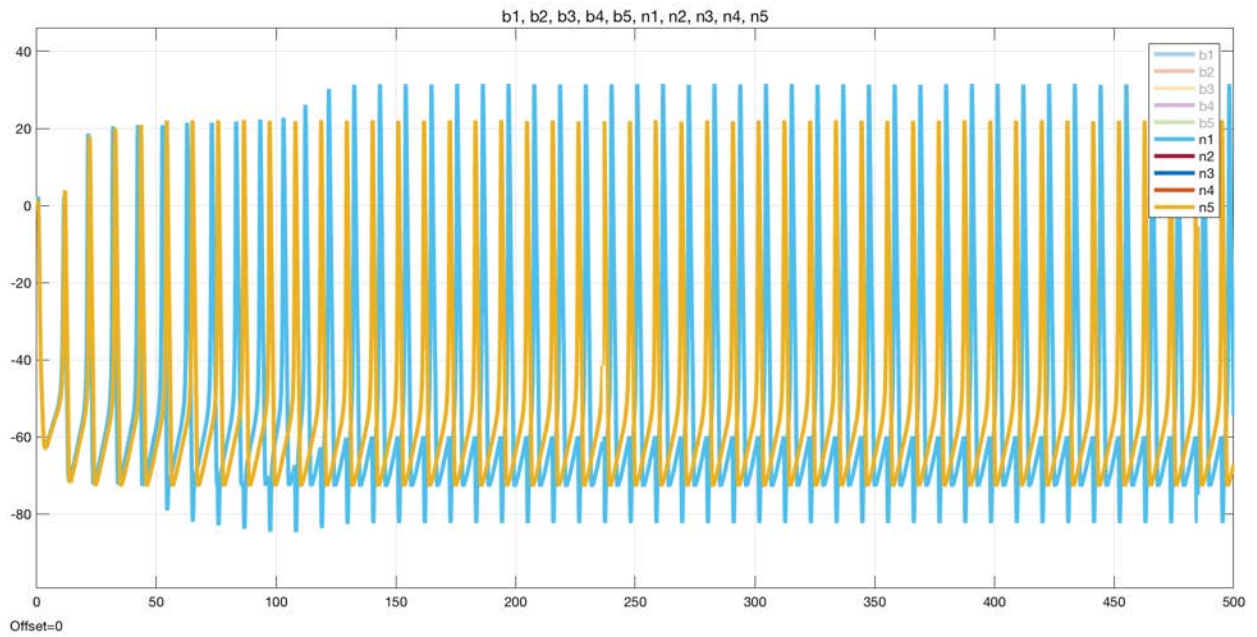


Figure 5-11: Five-neuron Hodgkin-Huxley inhibition winner-take-all network with weighted feedback of 1 where  $I_1 = 27, I_2 = I_3 = I_4 = I_5 = 25$ .

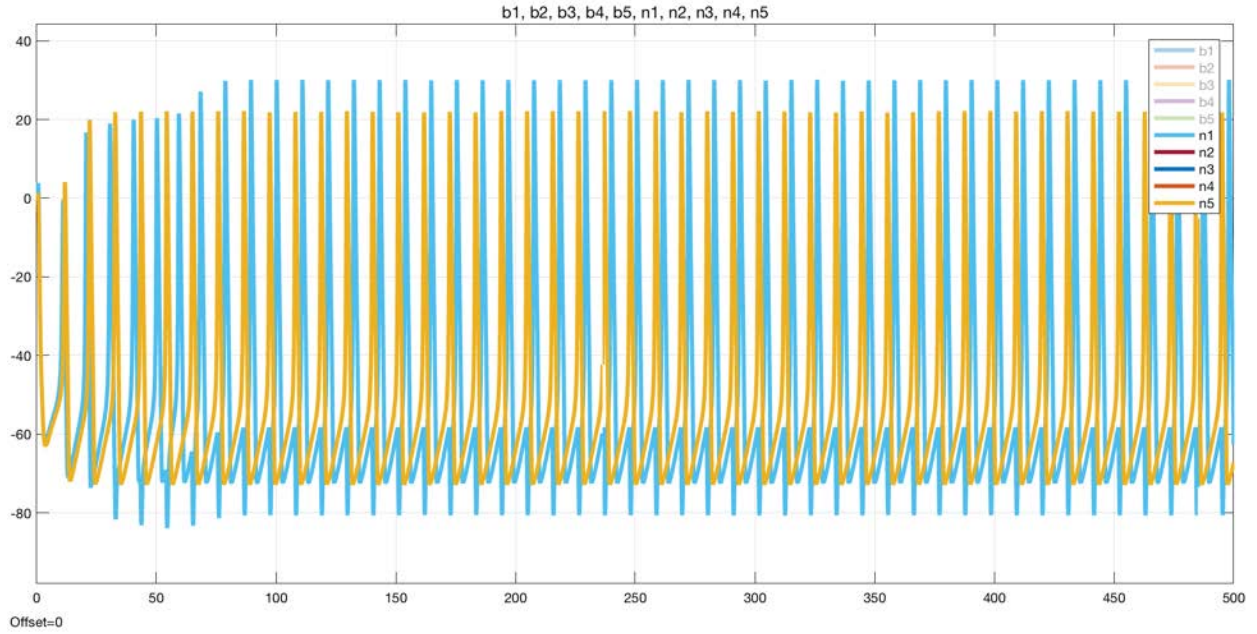


Figure 5-12: Five-neuron Hodgkin-Huxley inhibition winner-take-all network with weighted feedback of 1 where  $I_1 = 30, I_2 = I_3 = I_4 = I_5 = 25$ .

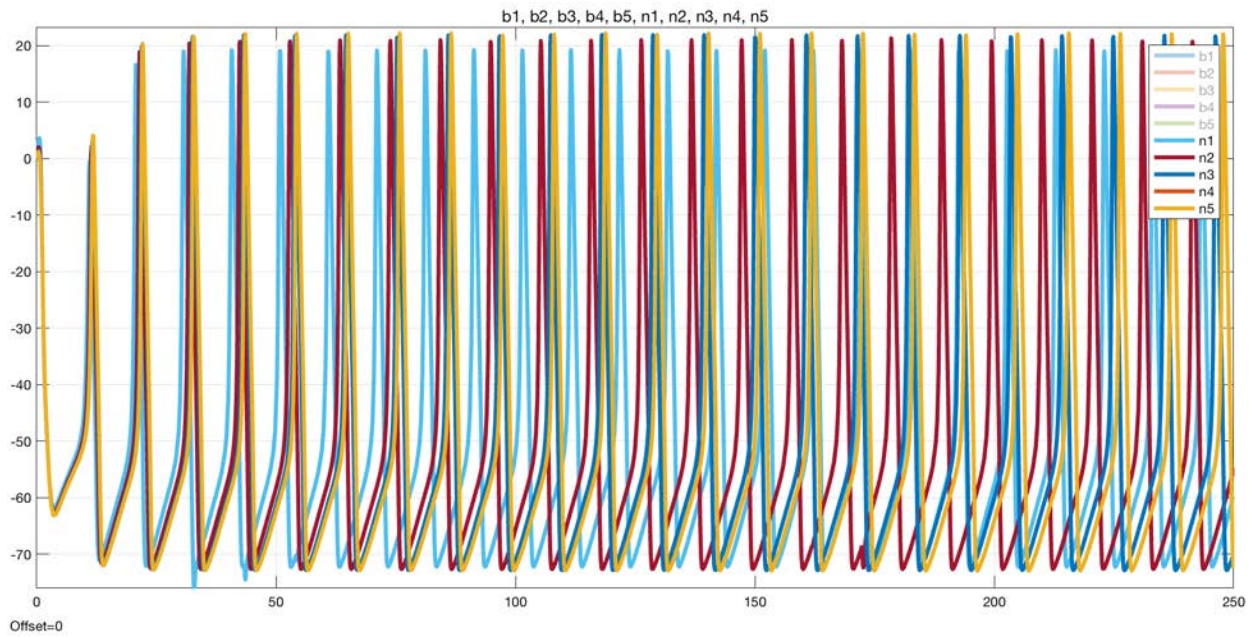


Figure 5-13: Five-neuron Hodgkin-Huxley inhibition winner-take-all network with weighted feedback of 1 where  $I_1 = 30, I_2 = 27, I_3 = 25.5, I_4 = I_5 = 25$ .

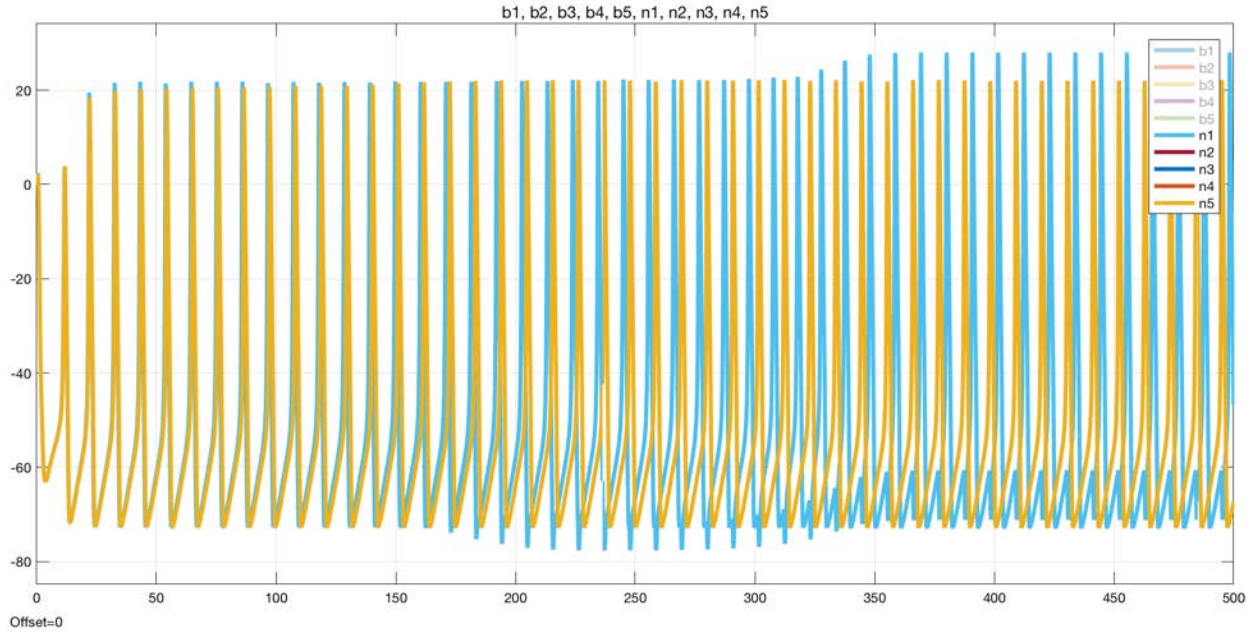


Figure 5-14: Five-neuron Hodgkin-Huxley inhibition winner-take-all network with weighted feedback of 0.5 where  $I_1 = 25.5, I_2 = I_3 = I_4 = I_5 = 25$ .

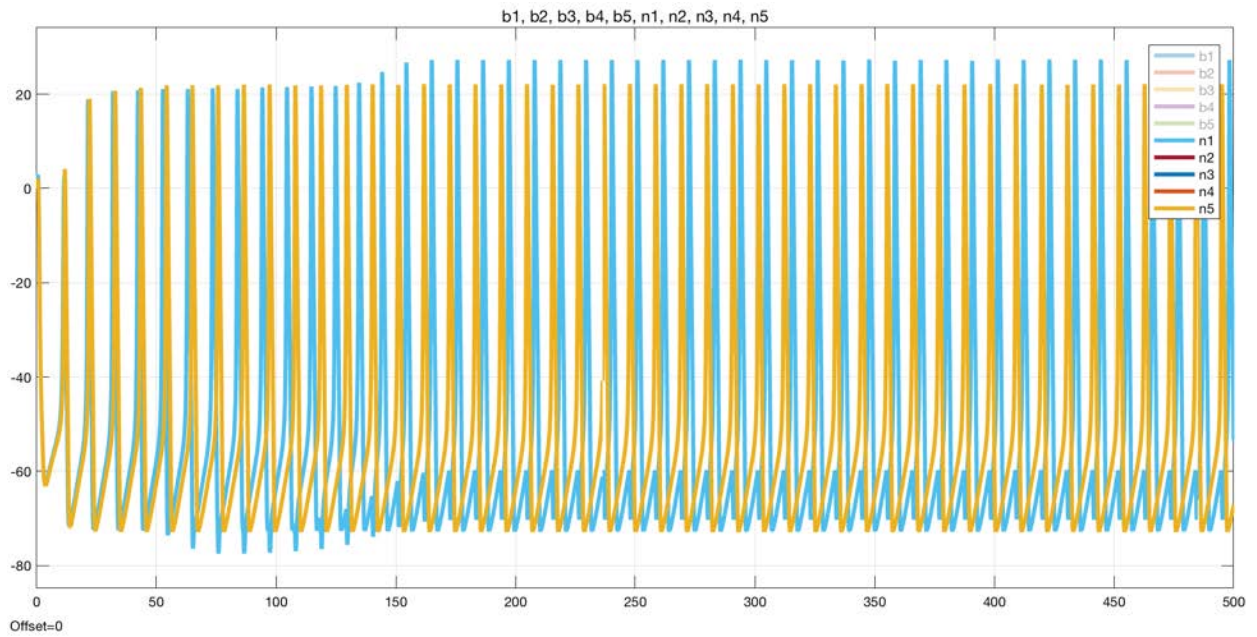


Figure 5-15: Five-neuron Hodgkin-Huxley inhibition winner-take-all network with weighted feedback of 0.5 where  $I_1 = 27, I_2 = I_3 = I_4 = I_5 = 25$ .

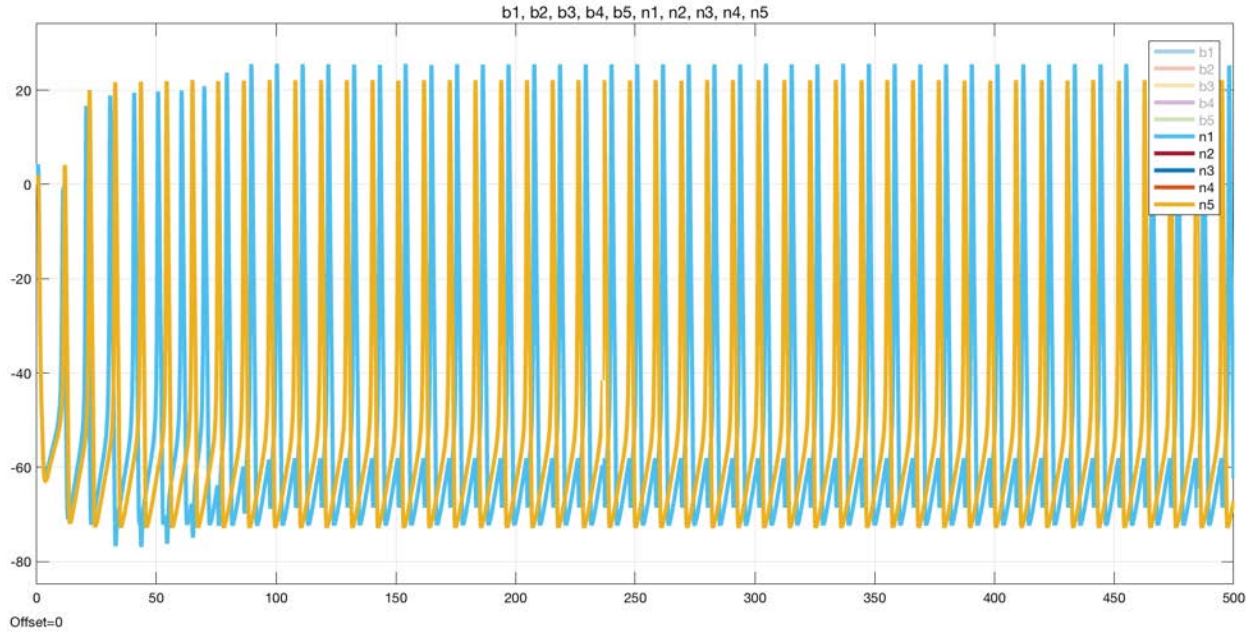


Figure 5-16: Five-neuron Hodgkin-Huxley inhibition winner-take-all network with weighted feedback of 0.5 where  $I_1 = 30, I_2 = I_3 = I_4 = I_5 = 25$ .

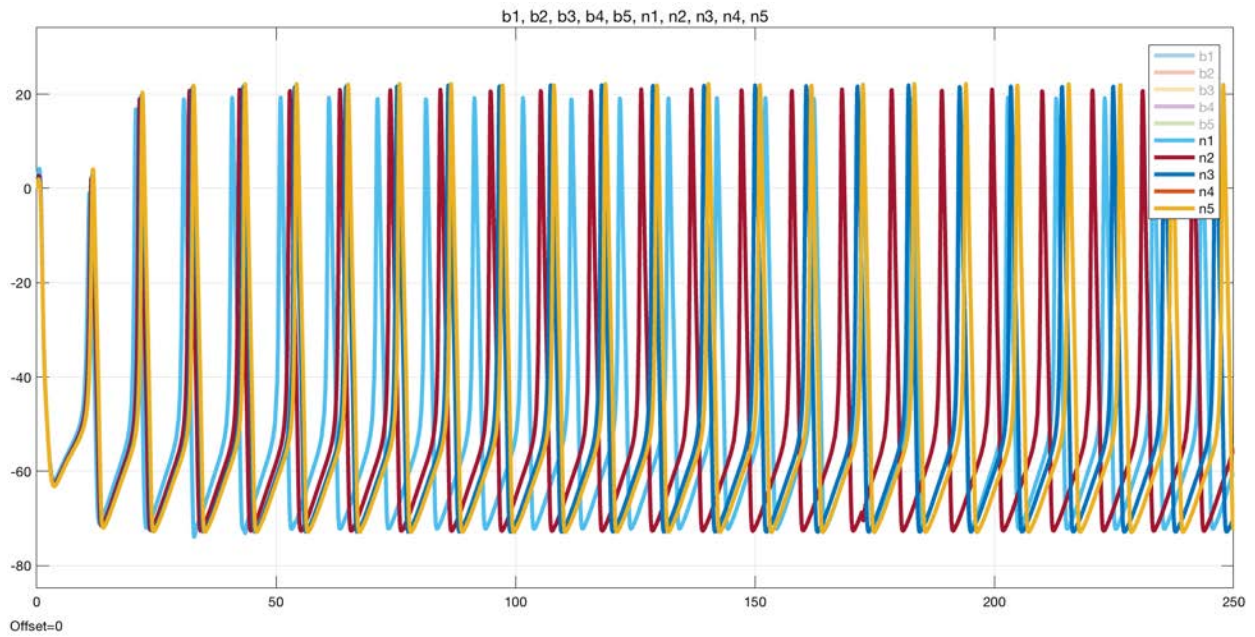


Figure 5-17: Five-neuron Hodgkin-Huxley inhibition winner-take-all network with weighted feedback of 0.5 where  $I_1 = 30, I_2 = 27, I_3 = 25.5, I_4 = I_5 = 25$ .

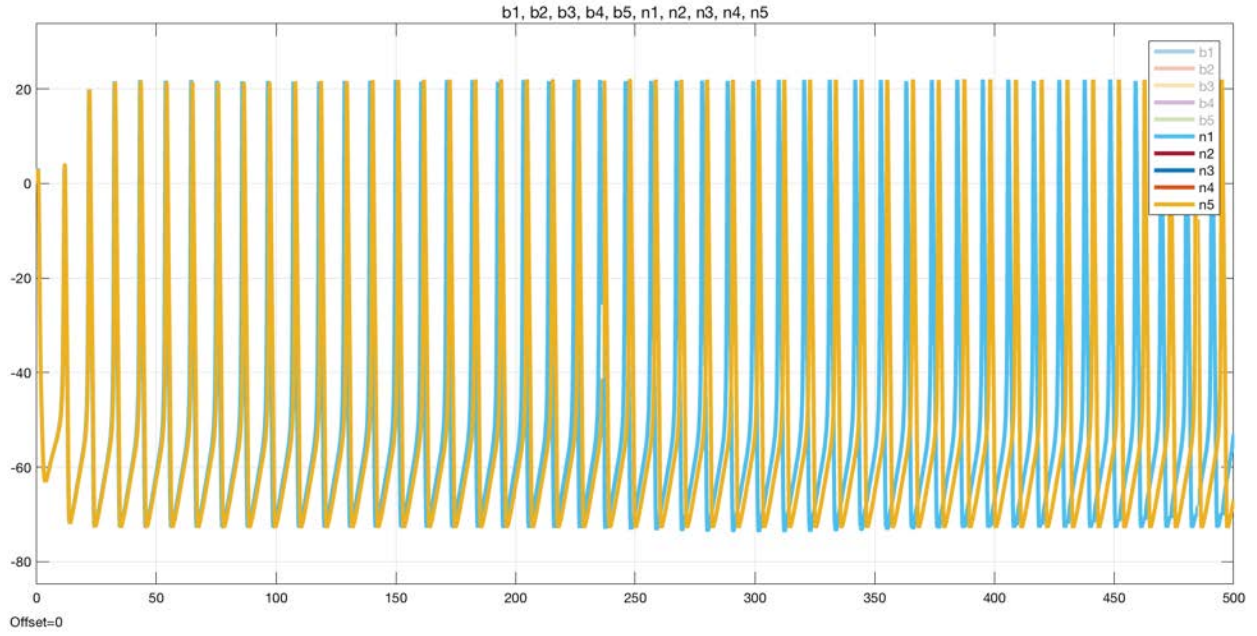


Figure 5-18: Five-neuron Hodgkin-Huxley inhibition winner-take-all network with weighted feedback of 0.1 where  $I_1 = 25.5, I_2 = I_3 = I_4 = I_5 = 25$ .

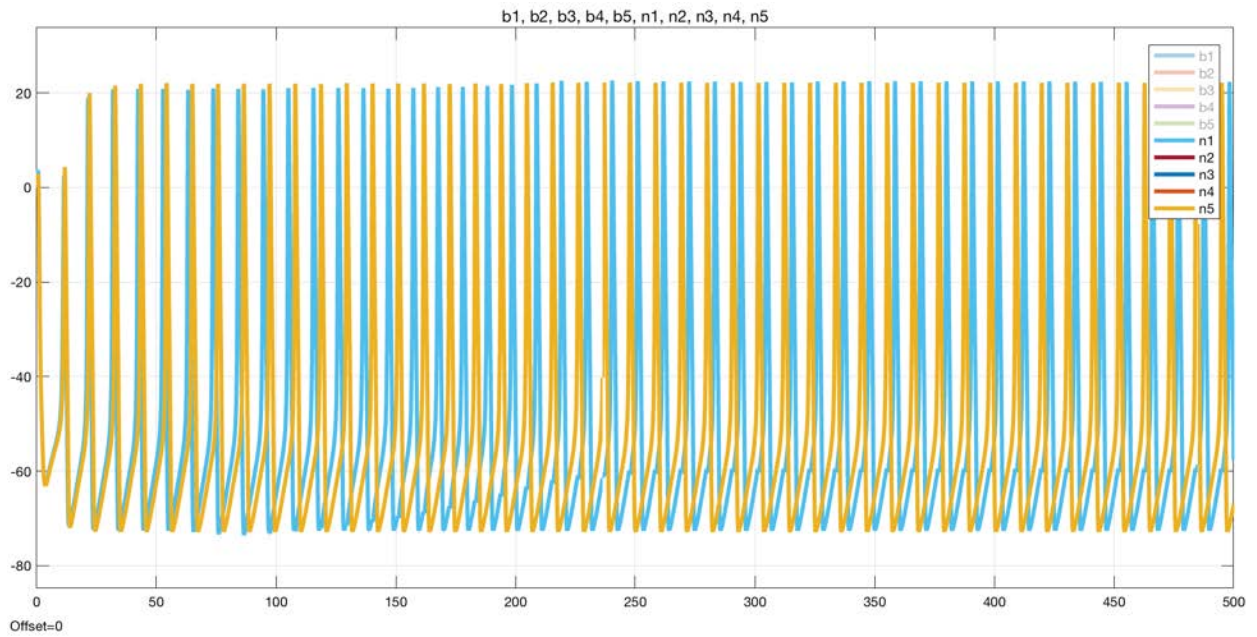


Figure 5-19: Five-neuron Hodgkin-Huxley inhibition winner-take-all network with weighted feedback of 0.1 where  $I_1 = 27, I_2 = I_3 = I_4 = I_5 = 25$ .

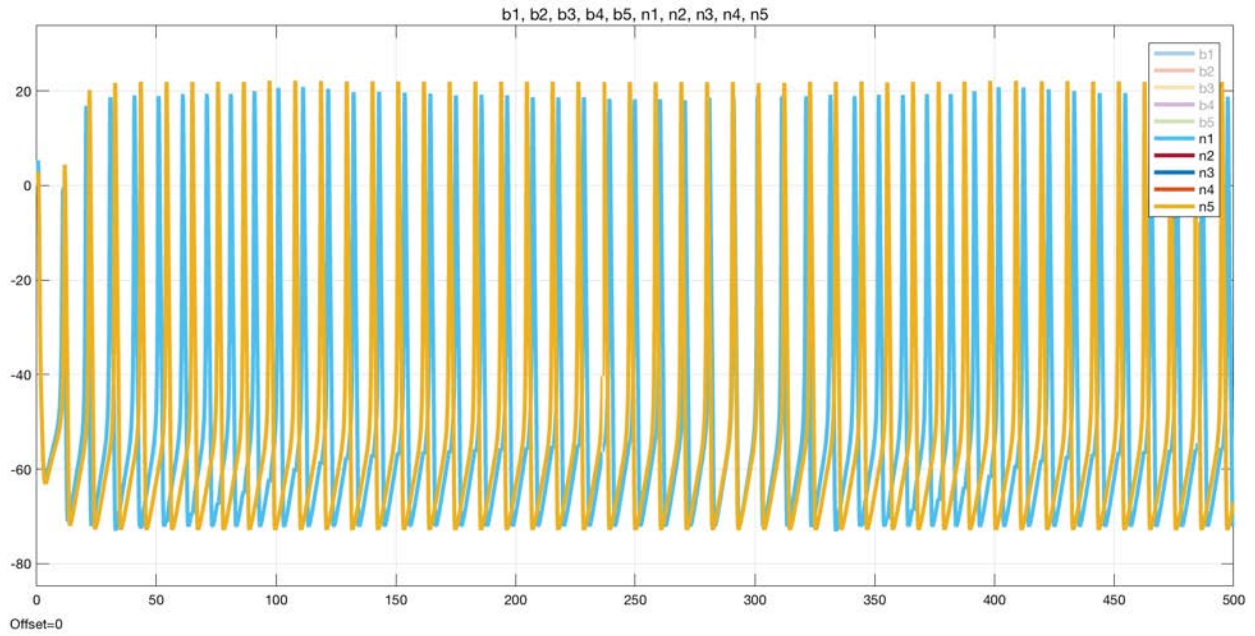


Figure 5-20: Five-neuron Hodgkin-Huxley inhibition winner-take-all network with weighted feedback of 0.1 where  $I_1 = 30, I_2 = I_3 = I_4 = I_5 = 25$ .

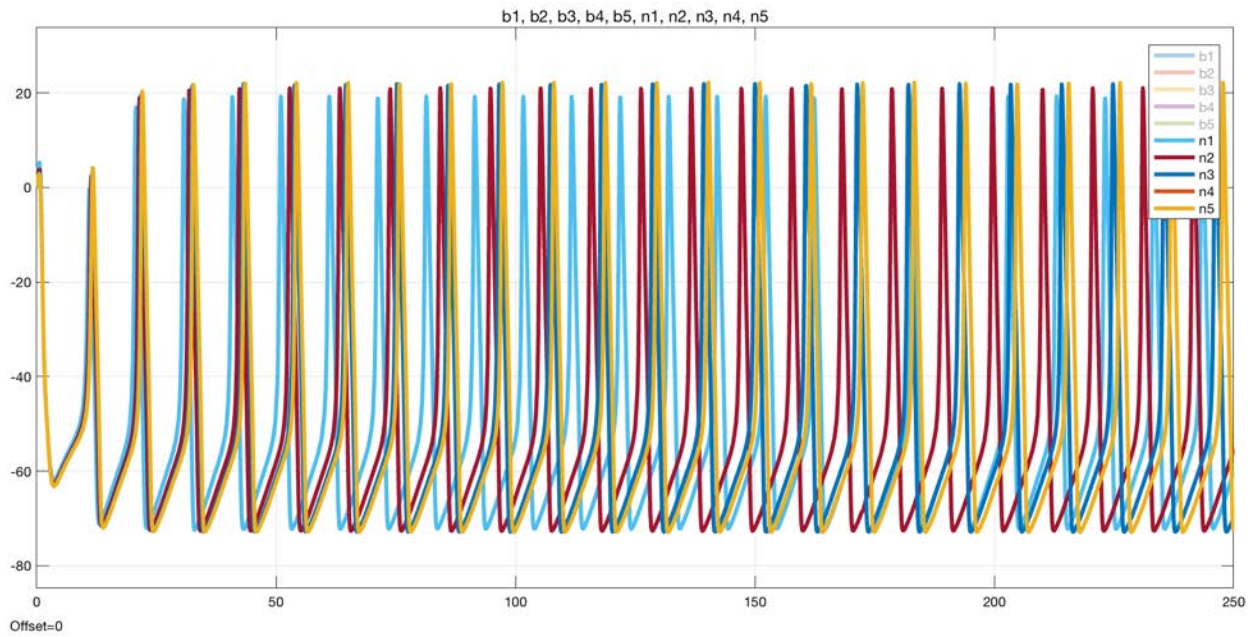


Figure 5-21: Five-neuron Hodgkin-Huxley inhibition winner-take-all network with weighted feedback of 0.1 where  $I_1 = 30, I_2 = 27, I_3 = 25.5, I_4 = I_5 = 25$ .

## 5.4.2 Lateral Inhibition Low-Pass Filter Feedback

Figure 5-22 through Figure 5-24 show simulations of a 5-neuron low-pass feedback network with a time constant value of 0.1. Again, it is observed that as the input current to neuron 1 is increased, the time it takes for the network to achieve synchronization is decreased. The phase shift between neuron 1 and the rest of the network is almost 180 degrees. However, as the time-constant of the low-pass filter is increased to 10 (Figure 5-26 through Figure 5-28) and 100 (Figure 5-30 through Figure 5-32) approximate a DC signal, the network no longer synchronizes. As the input current to neuron 1 is increased, the difference in frequencies between neuron 1 and the network becomes significantly greater. Similarly as with the weighted feedback model,

Figure 5-25 ( $\tau = 0.1$ ), Figure 5-29 ( $\tau = 0.1$ ), and Figure 5-33 ( $\tau = 0.1$ ), show that with varying input currents the model does not synchronize, but there is little impact that the value of the time-constant has on the neuron outputs.

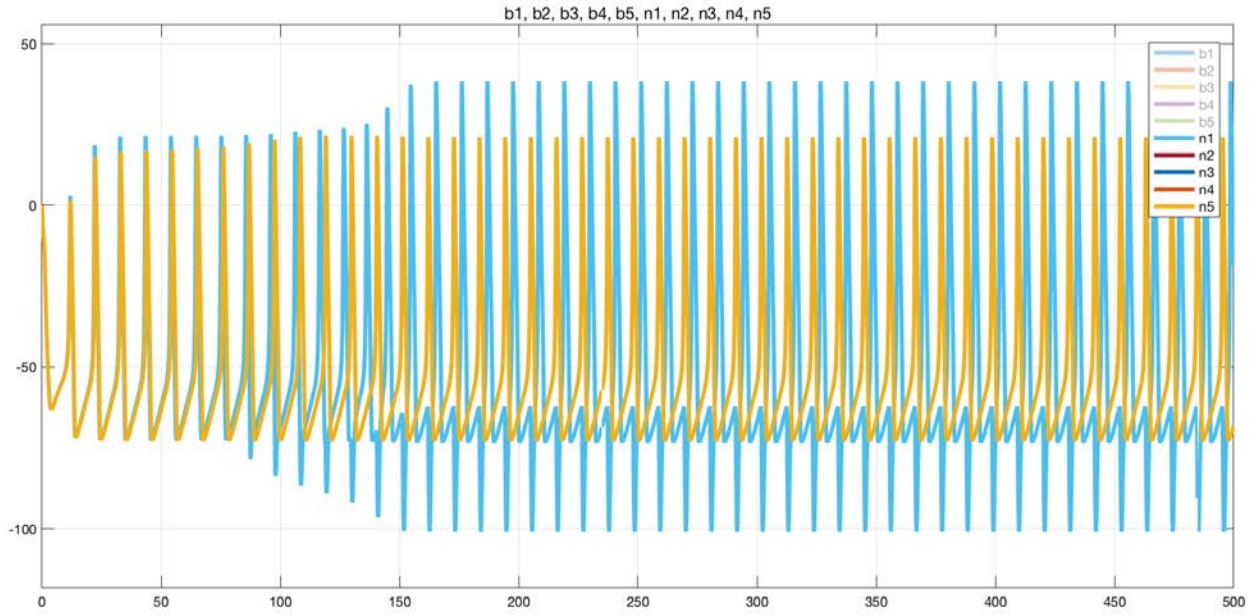


Figure 5-22: Five-neuron Hodgkin-Huxley inhibition winner-take-all network with low-pass filter feedback where  $\tau = 0.1$ ;  $I_1 = 25.5, I_2 = I_3 = I_4 = I_5 = 25$ .

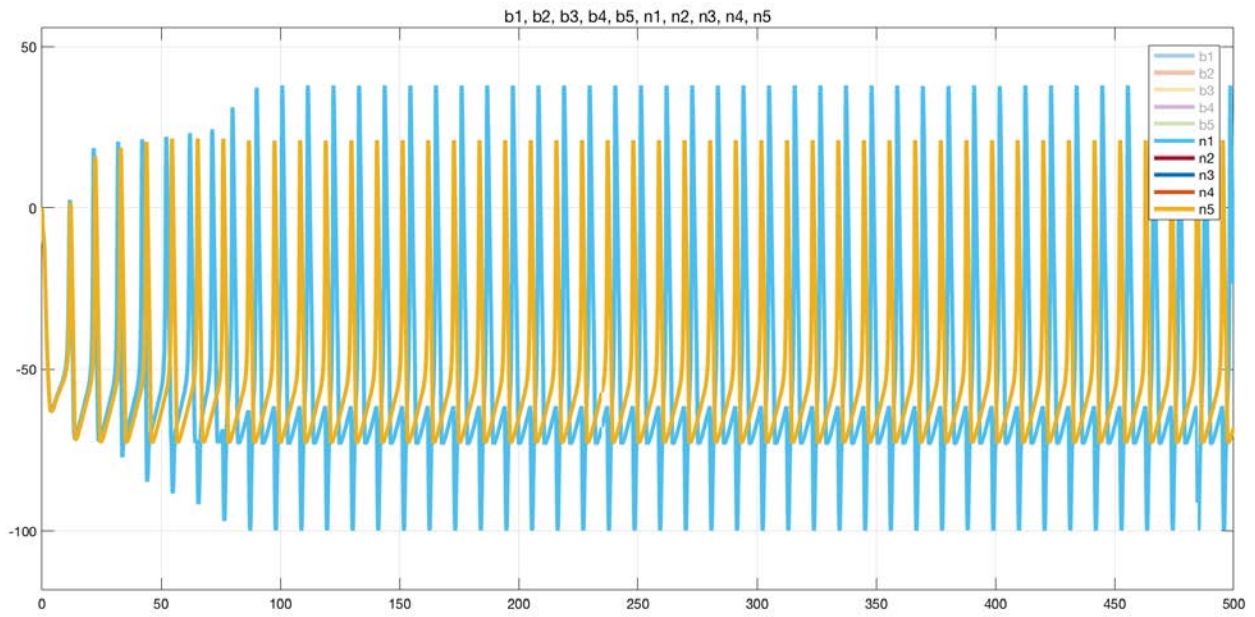


Figure 5-23: Five-neuron Hodgkin-Huxley inhibition winner-take-all network with low-pass filter feedback where  $\tau = 0.1$ ;  $I_1 = 27, I_2 = I_3 = I_4 = I_5 = 25$ .

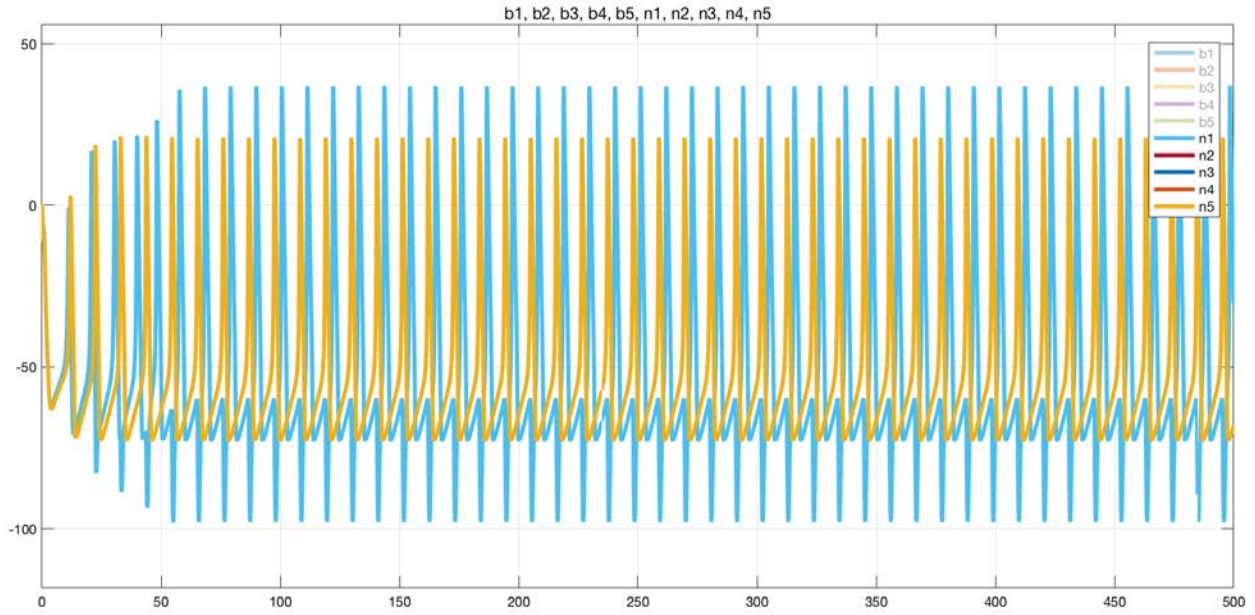


Figure 5-24: Five-neuron Hodgkin-Huxley inhibition winner-take-all network with low-pass filter feedback where  $\tau = 0.1$ ;  $I_1 = 30, I_2 = I_3 = I_4 = I_5 = 25$ .

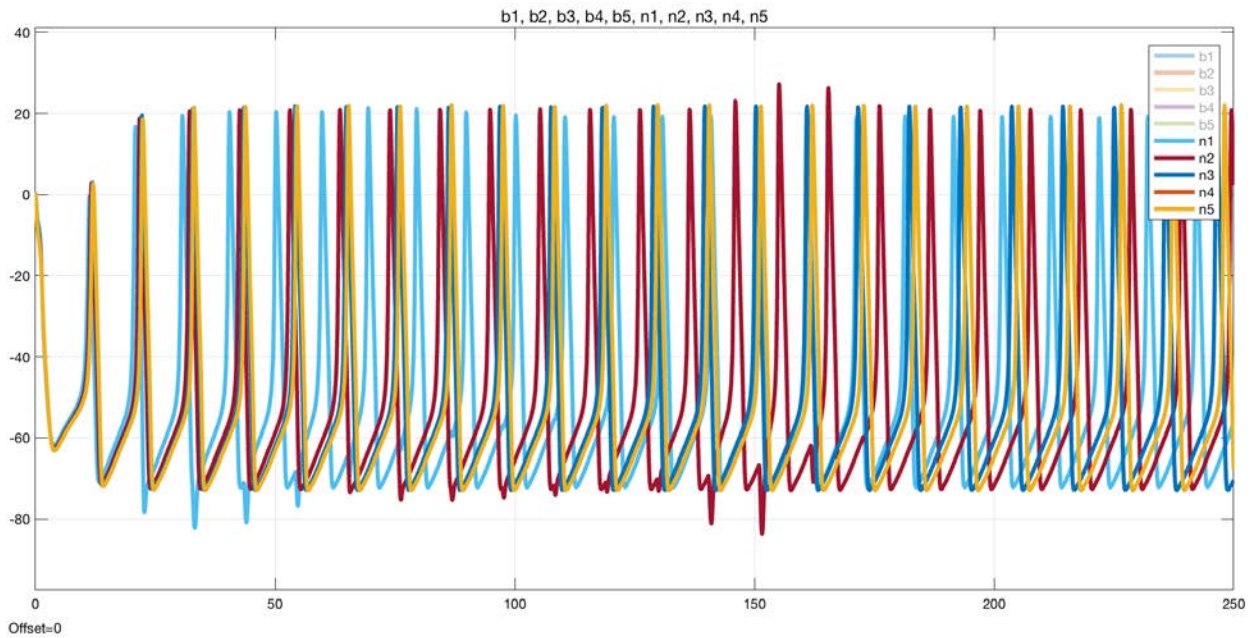


Figure 5-25: Five-neuron Hodgkin-Huxley inhibition winner-take-all network with low-pass filter feedback where  $\tau = 0.1$ ;  $I_1 = 30, I_2 = 27, I_3 = 25.5, I_4 = I_5 = 25$ .

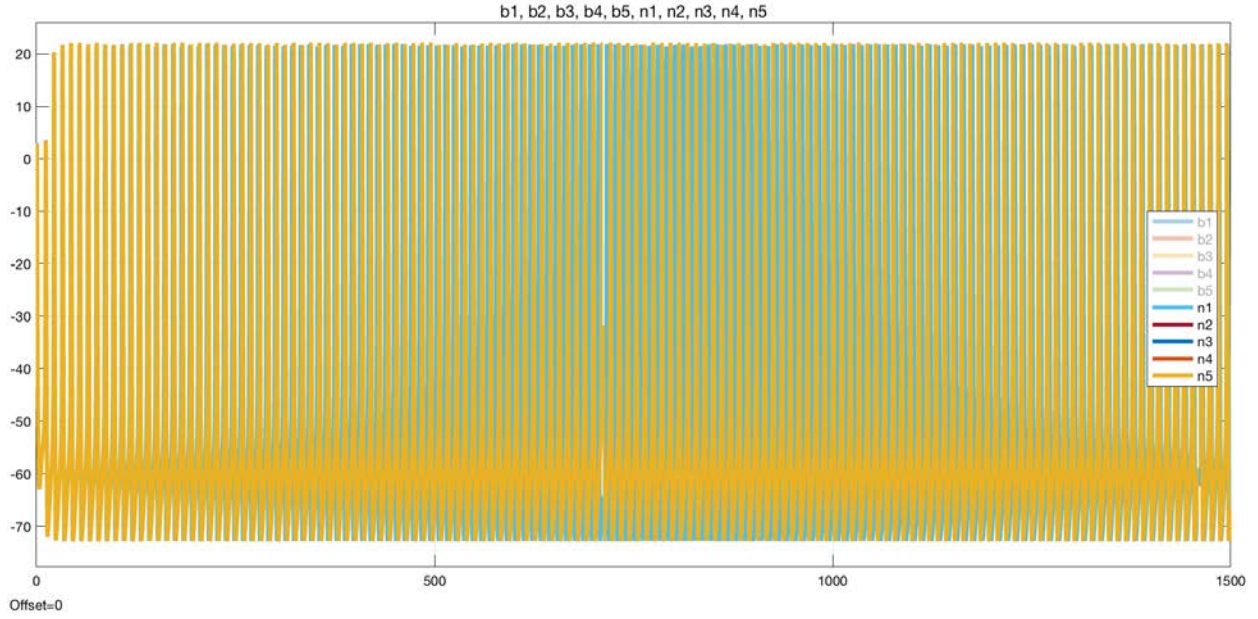


Figure 5-26: Five-neuron Hodgkin-Huxley inhibition winner-take-all network with low-pass filter feedback where  $\tau = 10; I_1 = 25.5, I_2 = I_3 = I_4 = I_5 = 25$ .

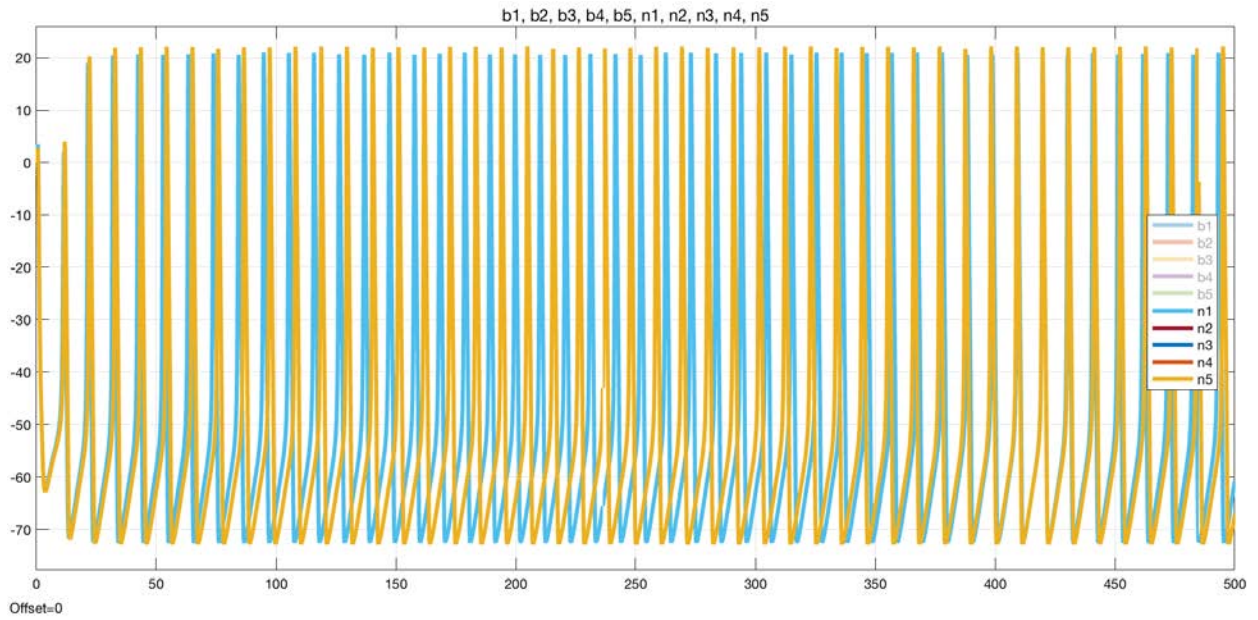


Figure 5-27: Five-neuron Hodgkin-Huxley inhibition winner-take-all network with low-pass filter feedback where  $\tau = 10; I_1 = 27, I_2 = I_3 = I_4 = I_5 = 25$ .

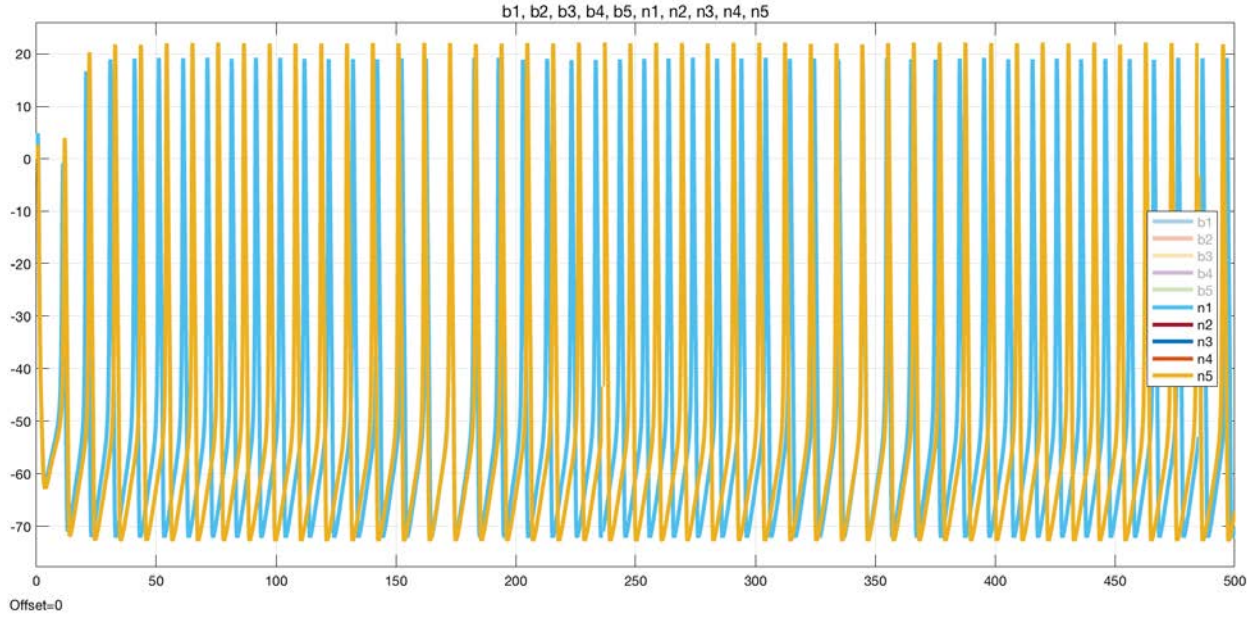


Figure 5-28: Five-neuron Hodgkin-Huxley inhibition winner-take-all network with low-pass filter feedback where  $\tau = 10$ ;  $I_1 = 30, I_2 = I_3 = I_4 = I_5 = 25$ .

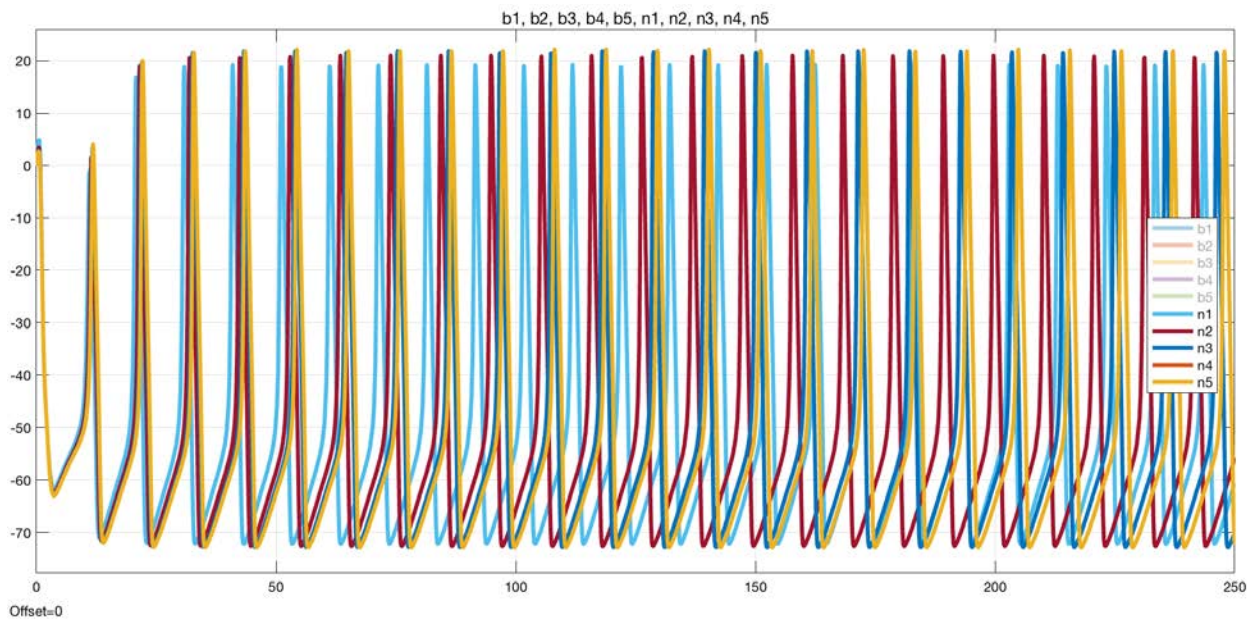


Figure 5-29: Five-neuron Hodgkin-Huxley inhibition winner-take-all network with low-pass filter feedback where  $\tau = 10$ ;  $I_1=30, I_2 = 27, I_3 = 25.5, I_4 = I_5 = 25$ .

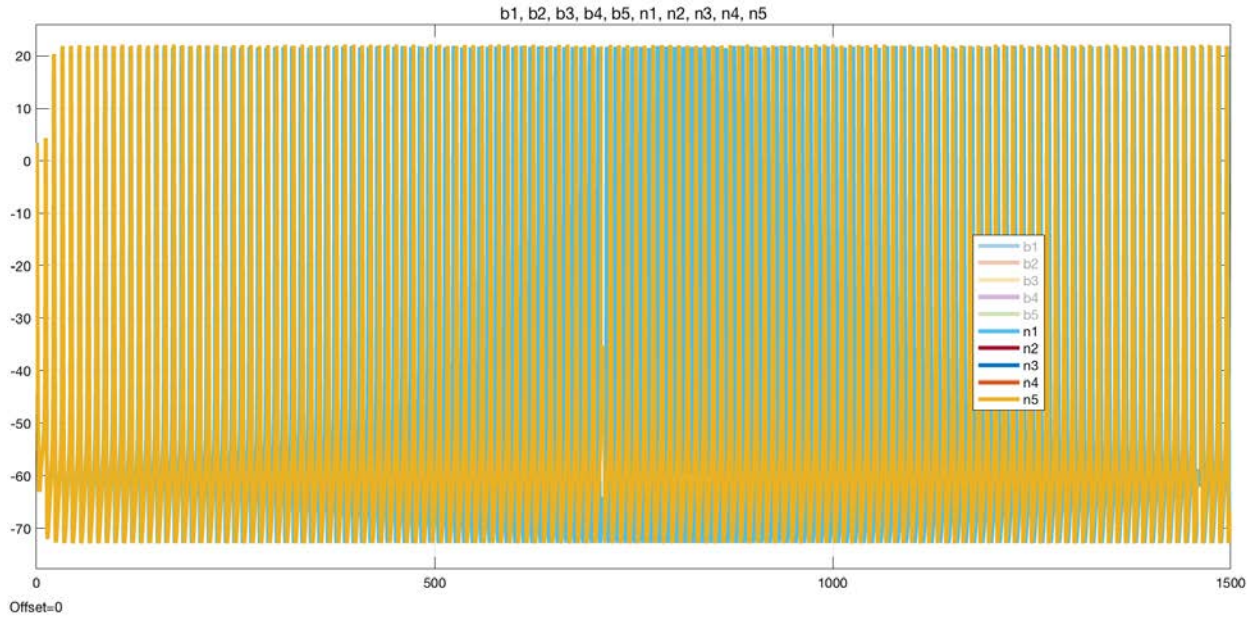


Figure 5-30: Five-neuron Hodgkin-Huxley inhibition winner-take-all network with low-pass filter feedback where  $\tau = 100$ ;  $I_1 = 25.5, I_2 = I_3 = I_4 = I_5 = 25$ .

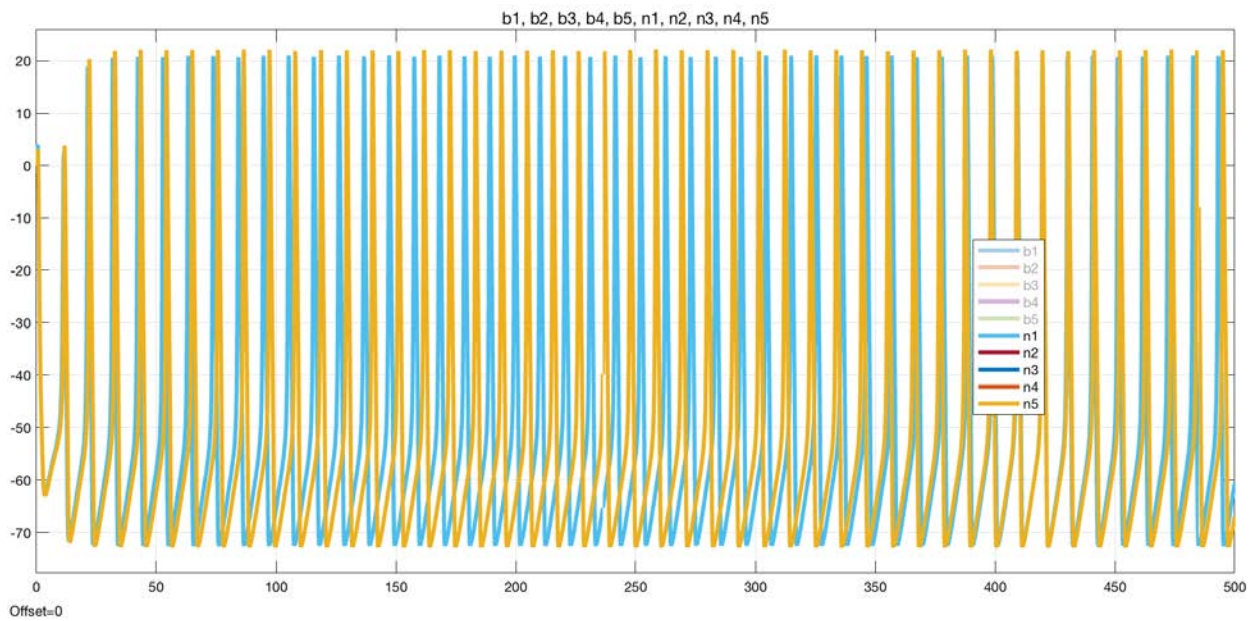


Figure 5-31: Five-neuron Hodgkin-Huxley inhibition winner-take-all network with low-pass filter feedback where  $\tau = 100$ ;  $I_1 = 27, I_2 = I_3 = I_4 = I_5 = 25$ .

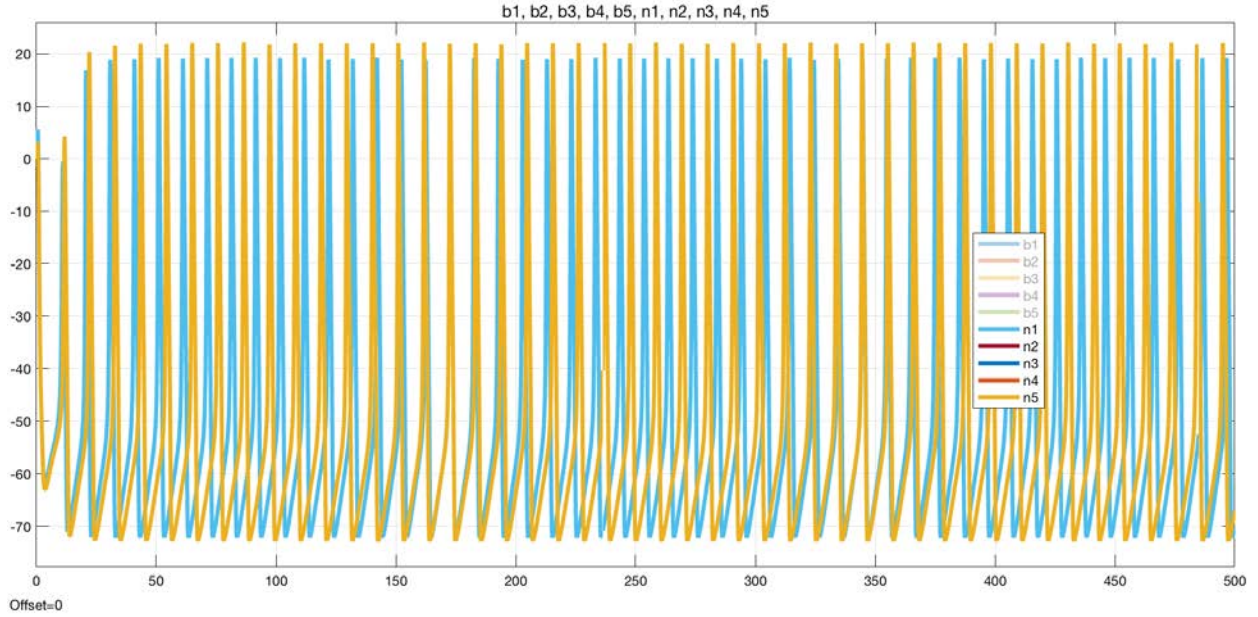


Figure 5-32: Five-neuron Hodgkin-Huxley inhibition winner-take-all network with low-pass filter feedback where  $\tau = 100$ ;  $I_1 = 30, I_2 = I_3 = I_4 = I_5 = 25$ .

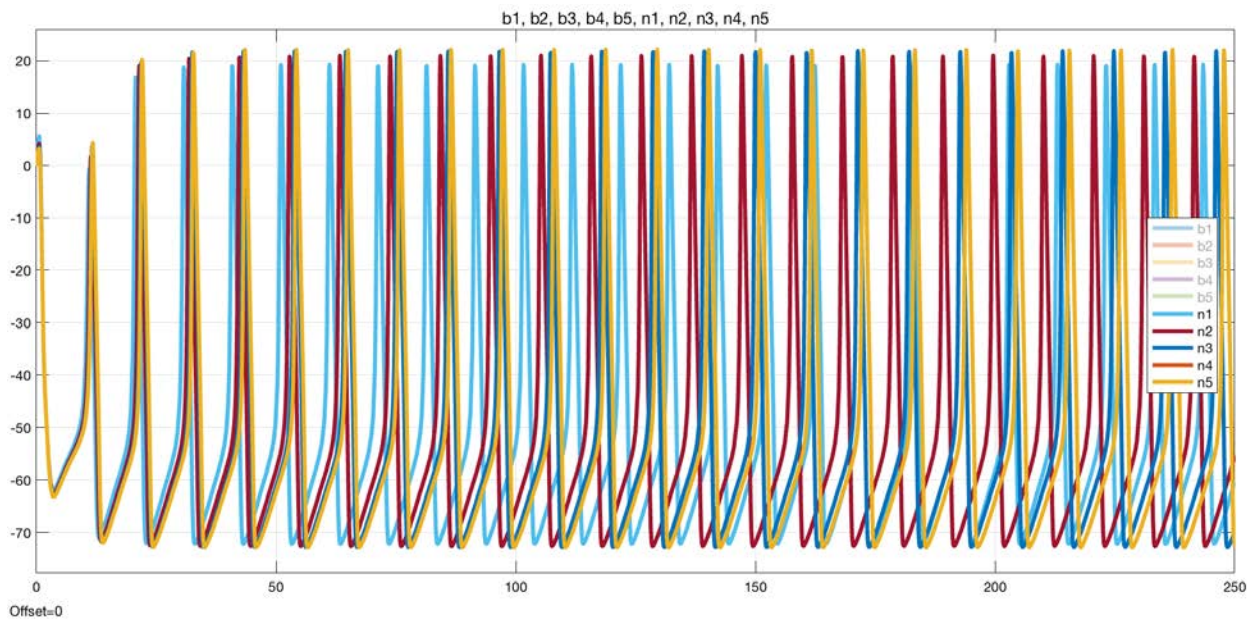


Figure 5-33: Five-neuron Hodgkin-Huxley inhibition winner-take-all network with low-pass filter feedback where  $\tau = 100$ ;  $I_1 = 30, I_2 = 27, I_3 = 25.5, I_4 = I_5 = 25$ .

### 5.4.3 Global Interneuron Weighted Feedback

Figure 5-34 through Figure 5-36 show simulations of a 5-neuron weighted feedback network with a weight of 1. The network achieves synchronization and a phase shift of almost 180 degrees. As the input current to neuron 1 is increased, the faster the network is able to synchronize. When the weight of the feedback is increased to 0.5 as shown in Figure 5-38 through Figure 5-40, for closer input current values, the network is able to synchronize, however it is unable to for larger input current differences. Because the weight is smaller, the system takes longer to synchronize. Increasing the input current of neuron 1 to 0.1 (Figure 5-42 through Figure 5-44), the network synchronizes for close input current values. The network is unable to synchronize as the input current of neuron 1 gets even larger. The difference in frequencies between neuron 1 and the rest of the network increases as the input current of neuron 1 increases. When varying the frequencies, there is no difference in impact between the weights of the feedback as shown in Figure 5-37 (weight = 1), Figure 5-41 (weight = 0.5), and Figure 5-45 (weight = 0.1)

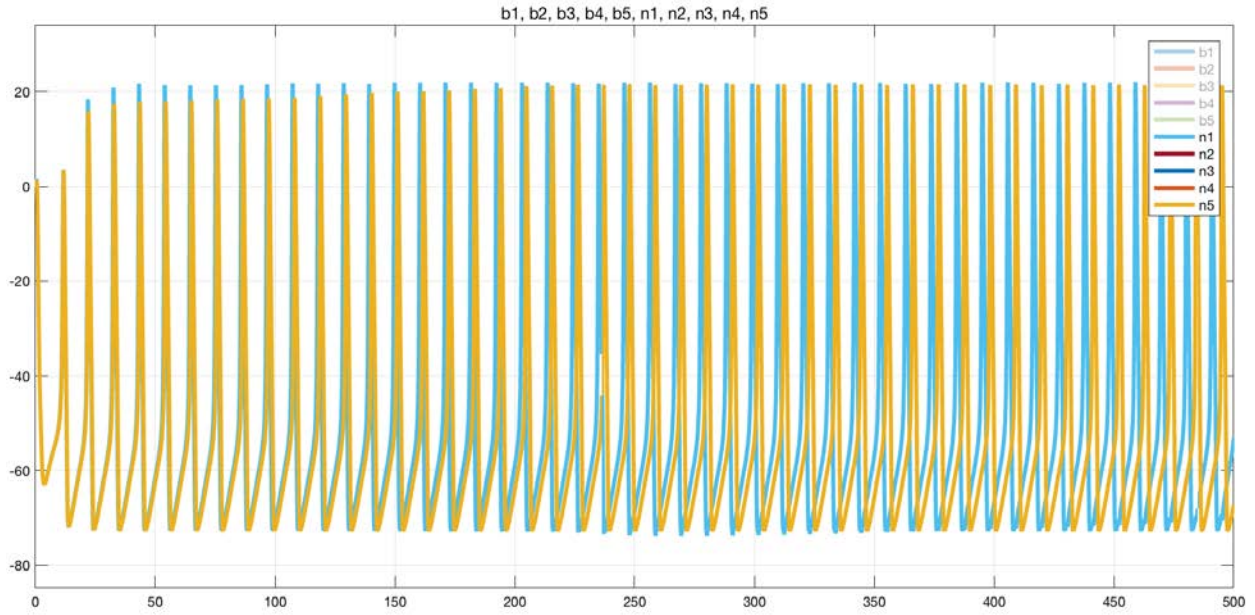


Figure 5-34: Five-neuron Hodgkin-Huxley interneuron winner-take-all network with weighted feedback of 1 where  $I_1 = 25.5, I_2 = I_3 = I_4 = I_5 = 25$ .

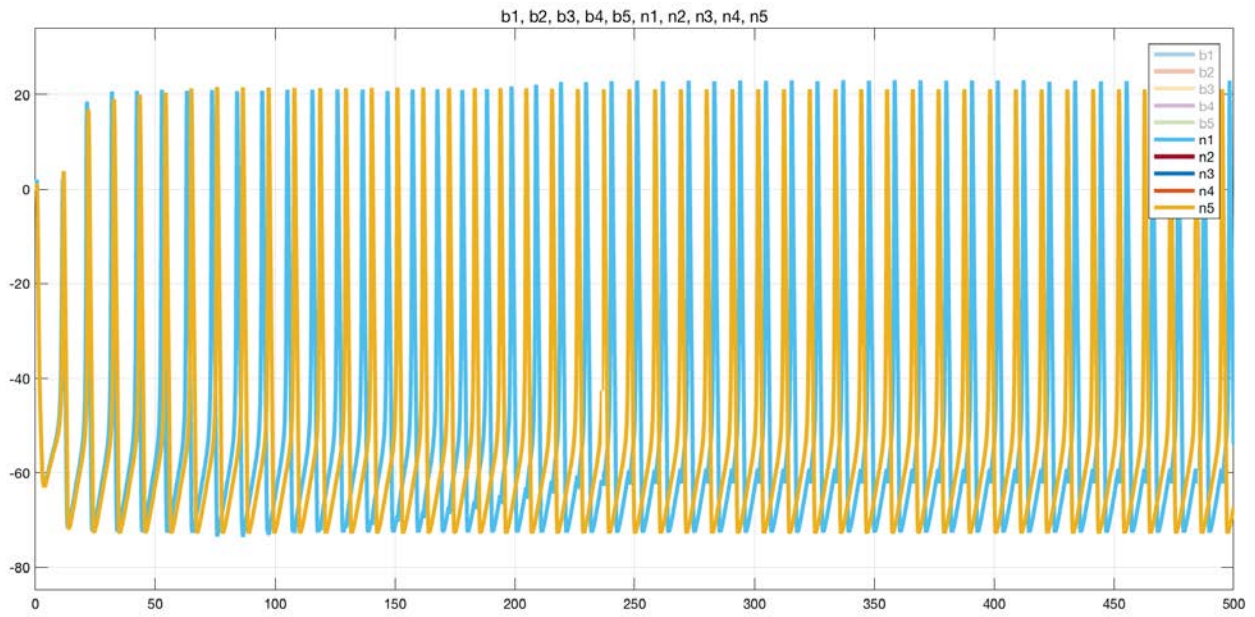


Figure 5-35: Five-neuron Hodgkin-Huxley interneuron winner-take-all network with weighted feedback of 1 where  $I_1 = 27, I_2 = I_3 = I_4 = I_5 = 25$ .

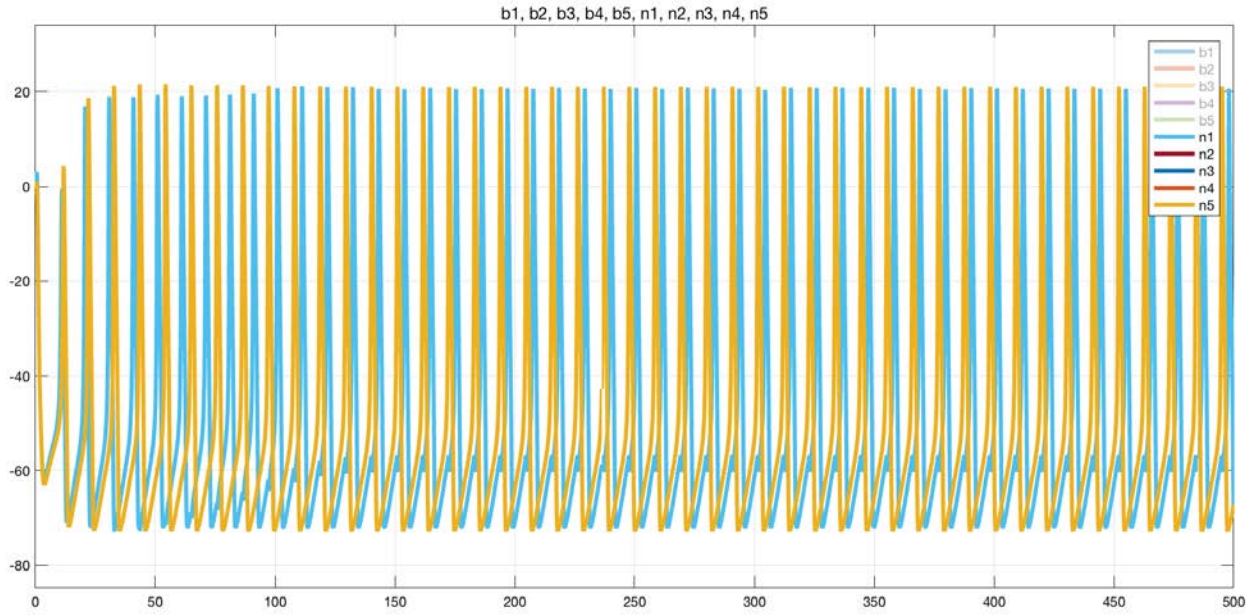


Figure 5-36: Five-neuron Hodgkin-Huxley interneuron winner-take-all network with weighted feedback of 1 where  $I_1 = 30, I_2 = I_3 = I_4 = I_5 = 25$ .

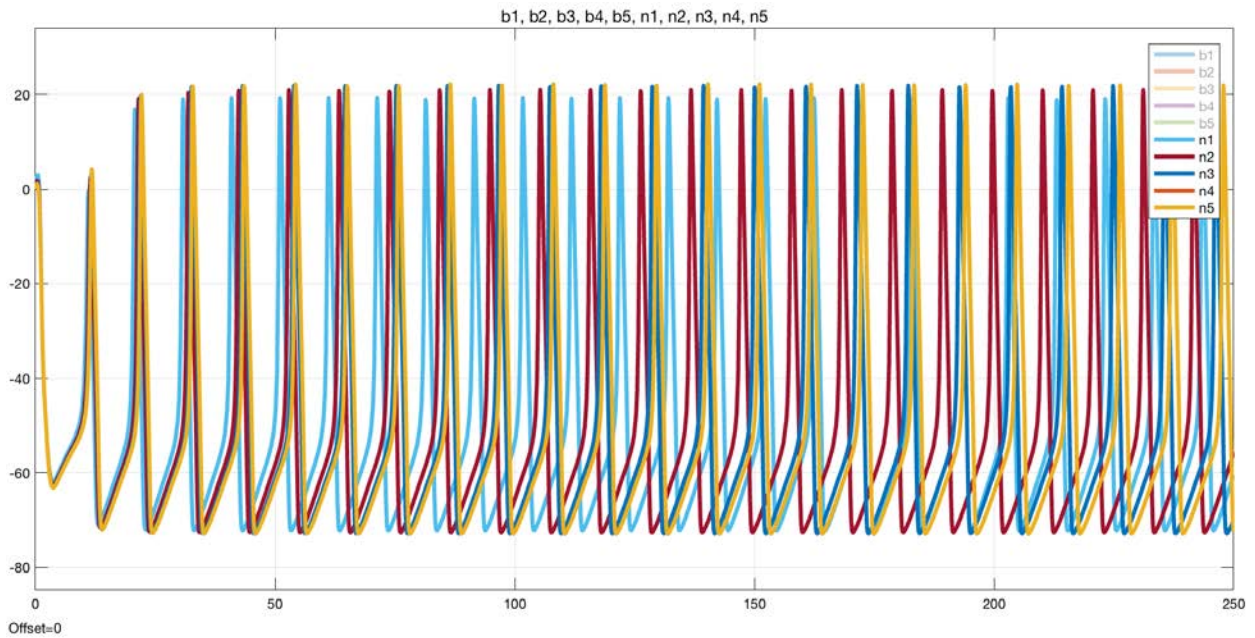


Figure 5-37: Five-neuron Hodgkin-Huxley interneuron winner-take-all network with weighted feedback of 1 where  $I_1 = 30, I_2 = 27, I_3 = 25.5, I_4 = I_5 = 25$ .

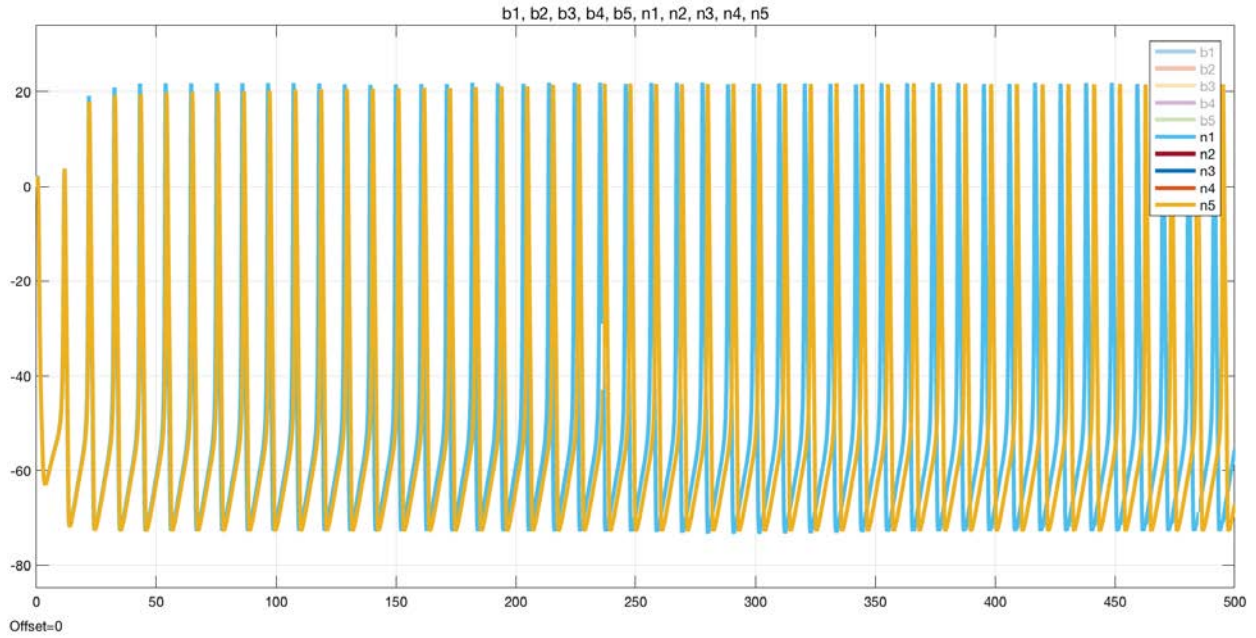


Figure 5-38: Five-neuron Hodgkin-Huxley interneuron winner-take-all network with weighted feedback of 0.5 where  $I_1 = 25.5, I_2 = I_3 = I_4 = I_5 = 25$ .

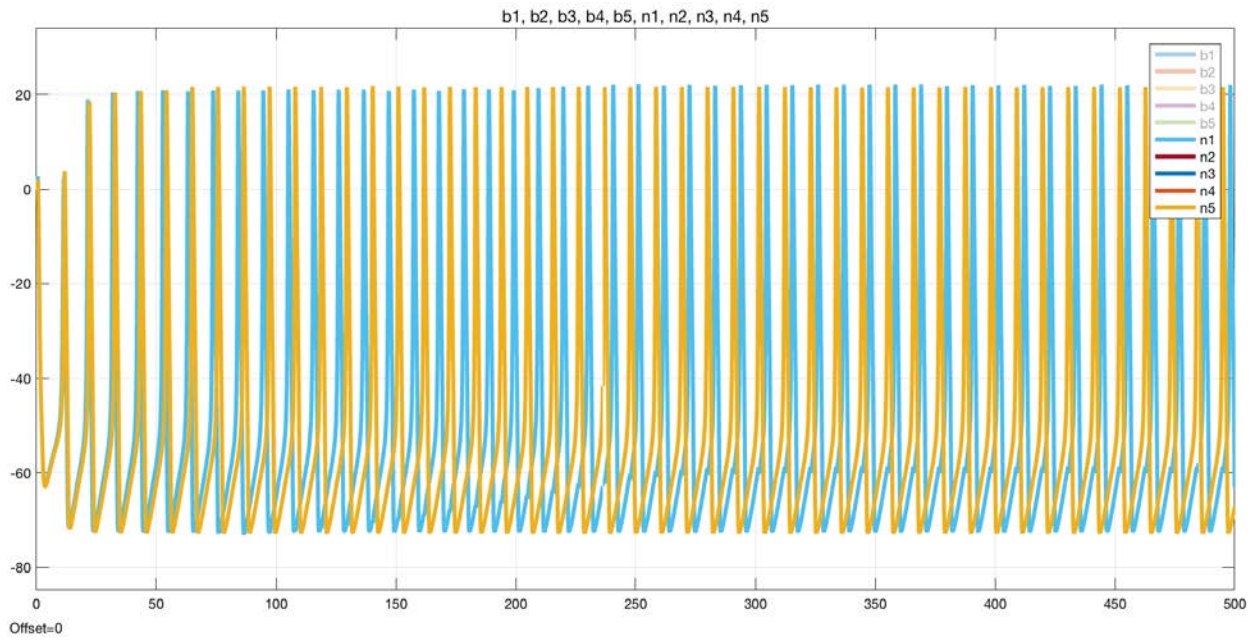


Figure 5-39: Five-neuron Hodgkin-Huxley interneuron winner-take-all network with weighted feedback of 0.5 where  $I_1 = 27, I_2 = I_3 = I_4 = I_5 = 25$ .

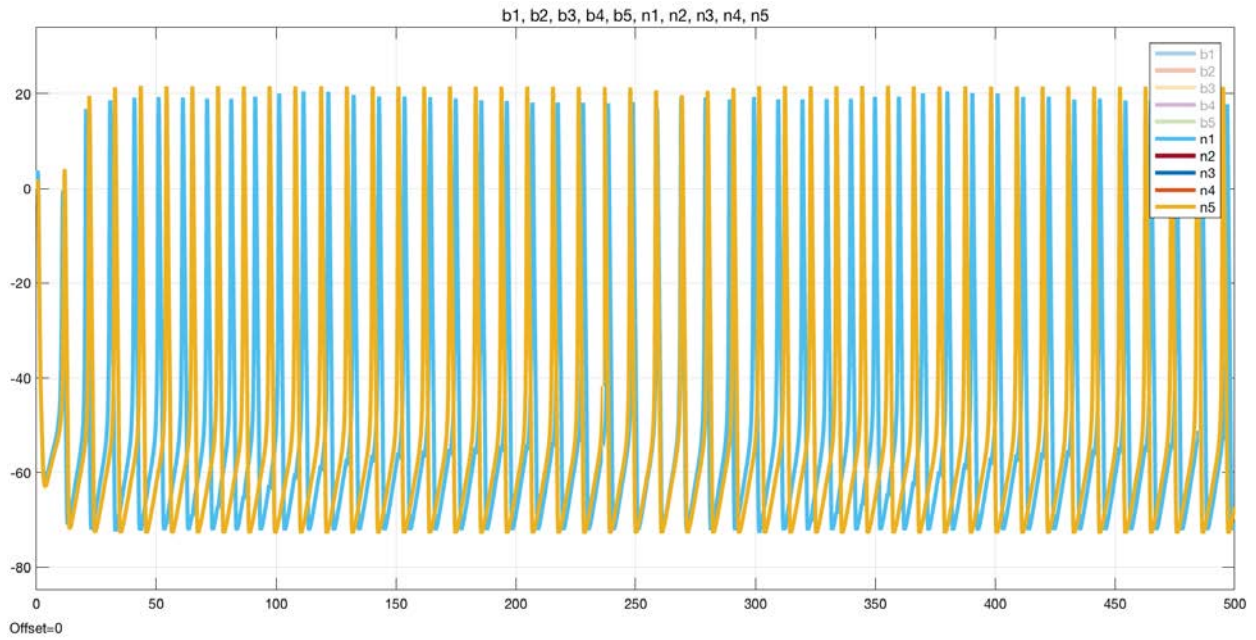


Figure 5-40: Five-neuron Hodgkin-Huxley interneuron winner-take-all network with weighted feedback of 0.5 where  $I_1 = 30, I_2 = I_3 = I_4 = I_5 = 25$ .

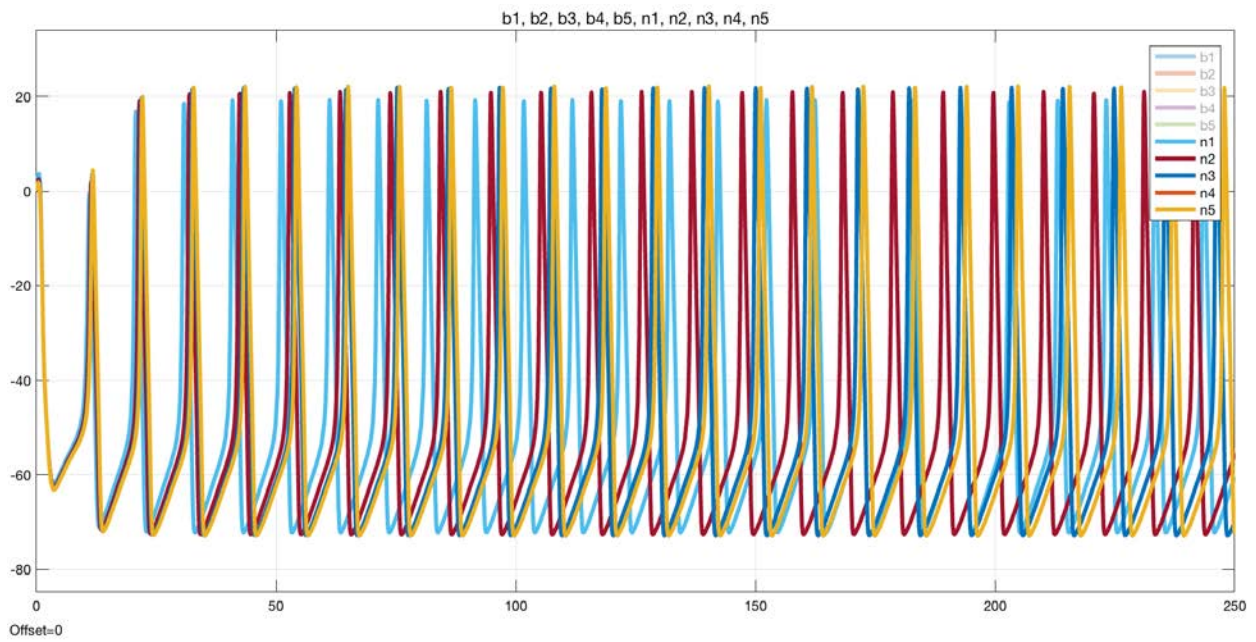


Figure 5-41: Five-neuron Hodgkin-Huxley interneuron winner-take-all network with weighted feedback of 0.5 where  $I_1 = 30, I_2 = 27, I_3 = 25.5, I_4 = I_5 = 25$ .

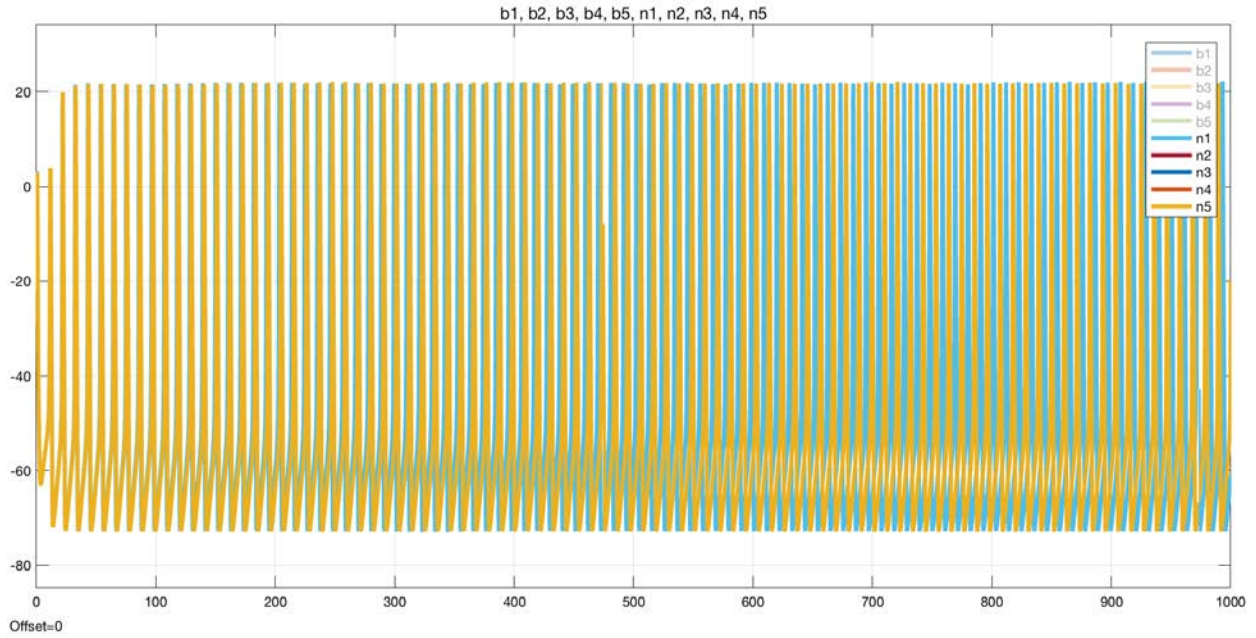


Figure 5-42: Five-neuron Hodgkin-Huxley interneuron winner-take-all network with weighted feedback of 0.1 where  $I_1 = 25.5, I_2 = I_3 = I_4 = I_5 = 25$ .

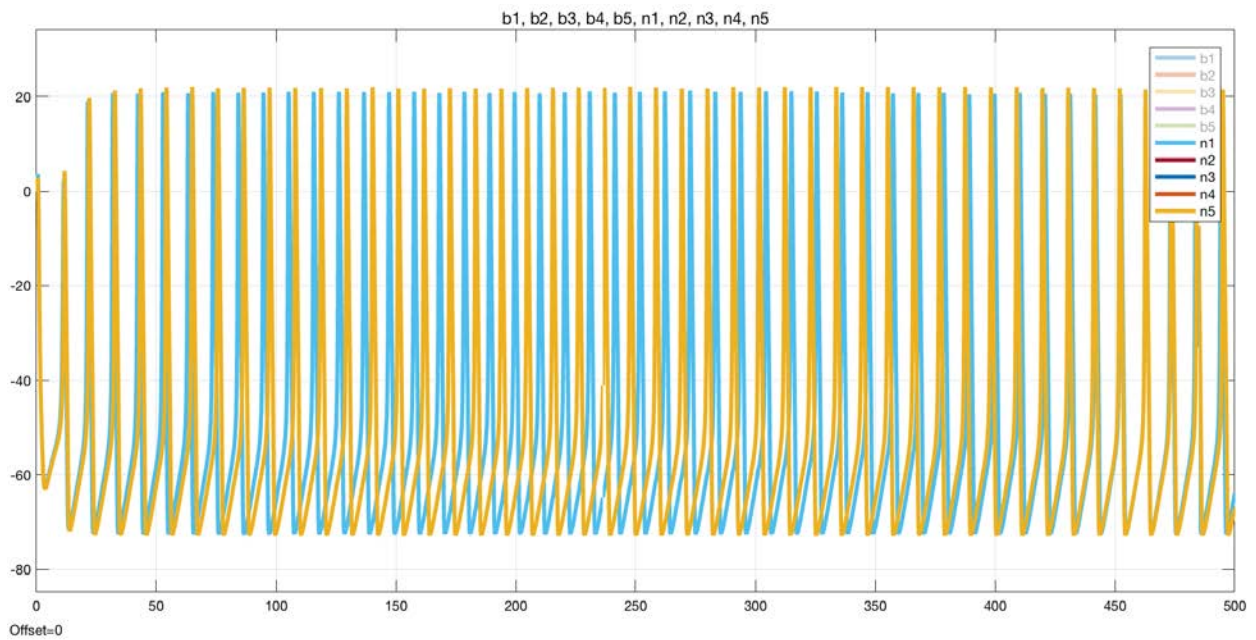


Figure 5-43: Five-neuron Hodgkin-Huxley interneuron winner-take-all network with weighted feedback of 0.1 where  $I_1 = 27, I_2 = I_3 = I_4 = I_5 = 25$ .

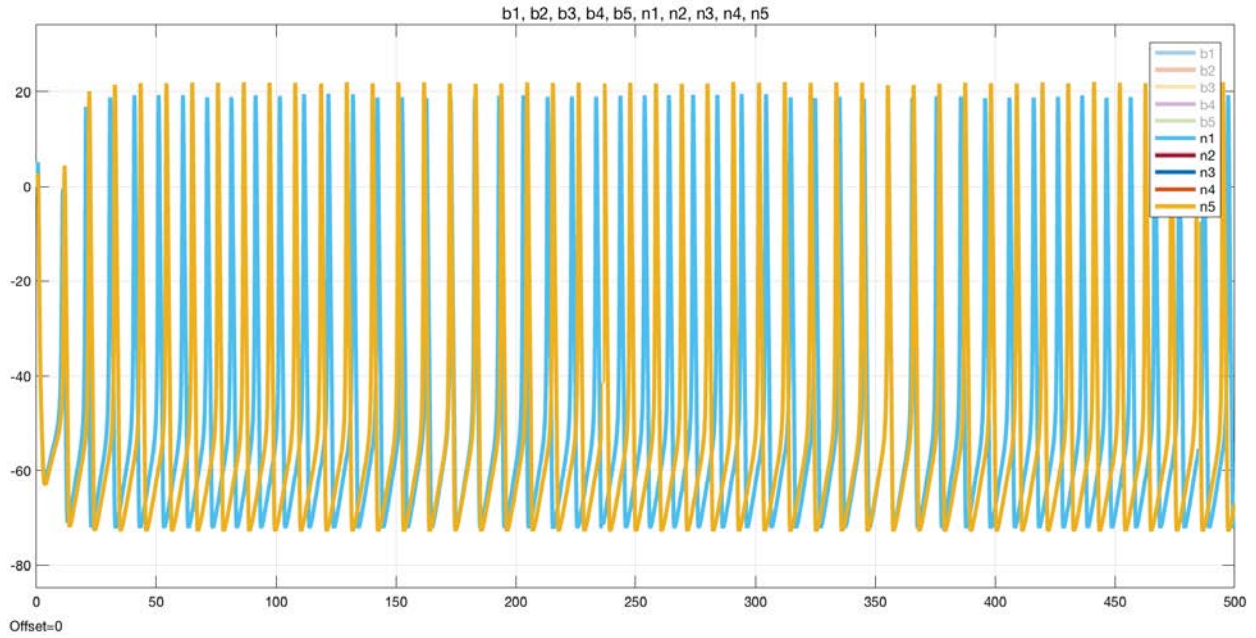


Figure 5-44: Five-neuron Hodgkin-Huxley interneuron winner-take-all network with weighted feedback of 0.1 where  $I_1 = 30, I_2 = I_3 = I_4 = I_5 = 25$ .

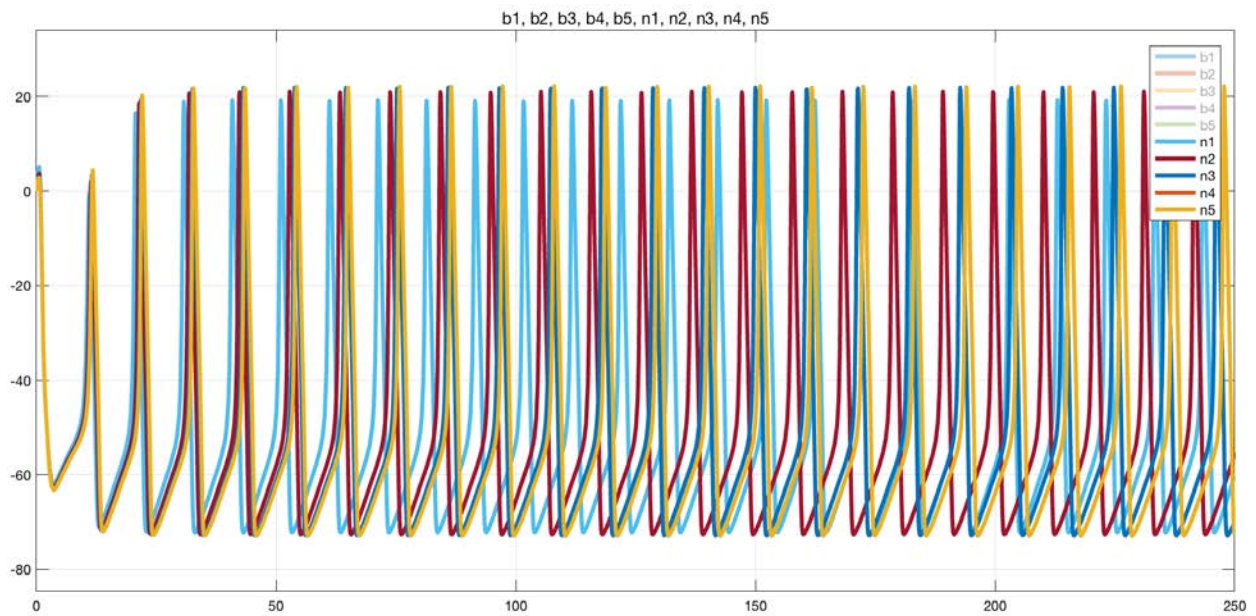


Figure 5-45: Five-neuron Hodgkin-Huxley interneuron winner-take-all network with weighted feedback of 0.1 where  $I_1 = 30, I_2 = 27, I_3 = 25.5, I_4 = I_5 = 25$ .

#### 5.4.4 Global Interneuron Low-Pass Filter

Figure 5-46 through Figure 5-48 show simulation results of a 5-neuron low-pass feedback network with a time constant value of 0.1. As expected, the network synchronizes with about 180-degree phase shift and as the input current in neuron 1 increases, the time it takes to achieve synchronization decreases. However, when the time-constant is increased to 10 (Figure 5-50 through Figure 5-52) and 100 (Figure 5-54 through Figure 5-56), the network cannot synchronize. Though as the input current to neuron 1 increases, its frequency also increases. Figure 5-49, Figure 5-53, and Figure 5-57 again show that increasing the time constant has little impact on the network when the input current to the neurons vary.

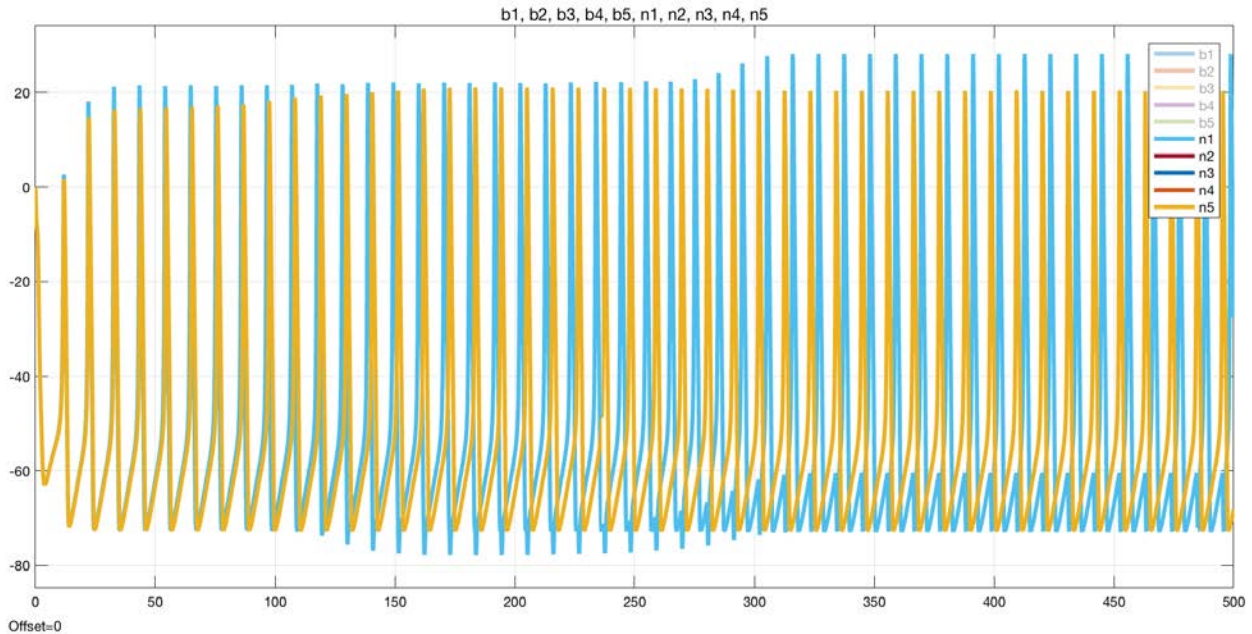


Figure 5-46: Five-neuron Hodgkin-Huxley interneuron winner-take-all network with low-pass filter feedback where  $\tau = 0.1$ ;  $I_1 = 25.5, I_2 = I_3 = I_4 = I_5 = 25$ .

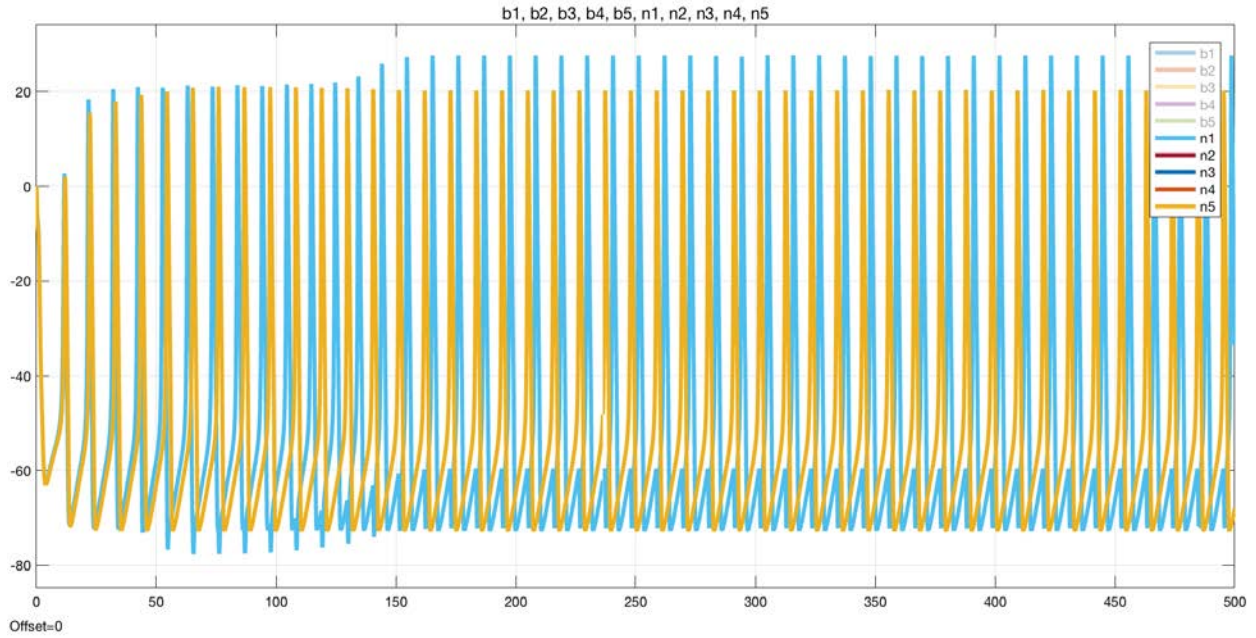


Figure 5-47: Five-neuron Hodgkin-Huxley interneuron winner-take-all network with low-pass filter feedback where  $\tau = 0.1$ ;  $I_1 = 27, I_2 = I_3 = I_4 = I_5 = 25$ .

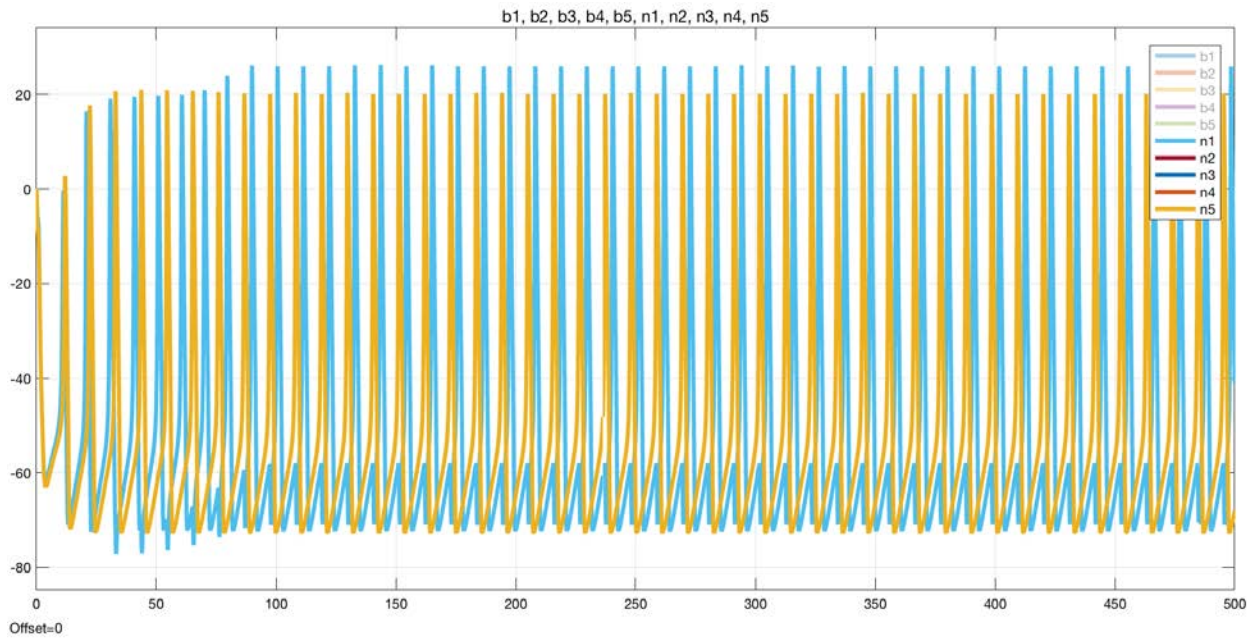


Figure 5-48: Five-neuron Hodgkin-Huxley interneuron winner-take-all network with low-pass filter feedback where  $\tau = 0.1$ ;  $I_1 = 30, I_2 = I_3 = I_4 = I_5 = 25$ .

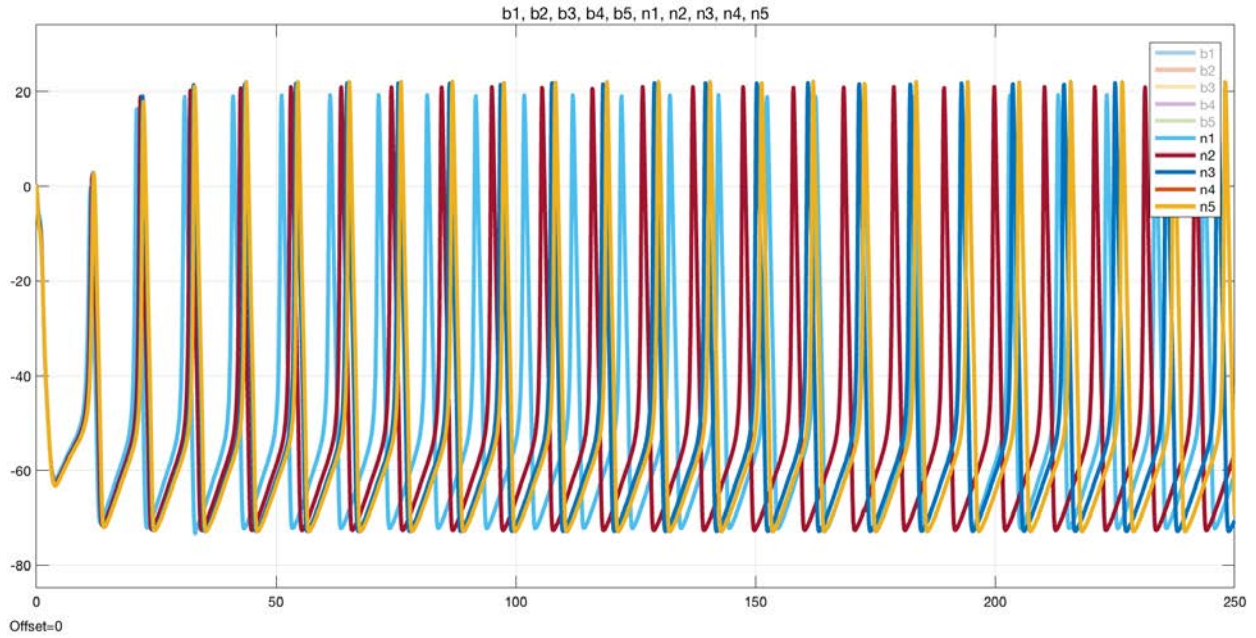


Figure 5-49: Five-neuron Hodgkin-Huxley interneuron winner-take-all network with low-pass filter feedback where  $\tau = 0.1$ ;  $I_1 = 30, I_2 = 27, I_3 = 25.5, I_4 = I_5 = 25$ .

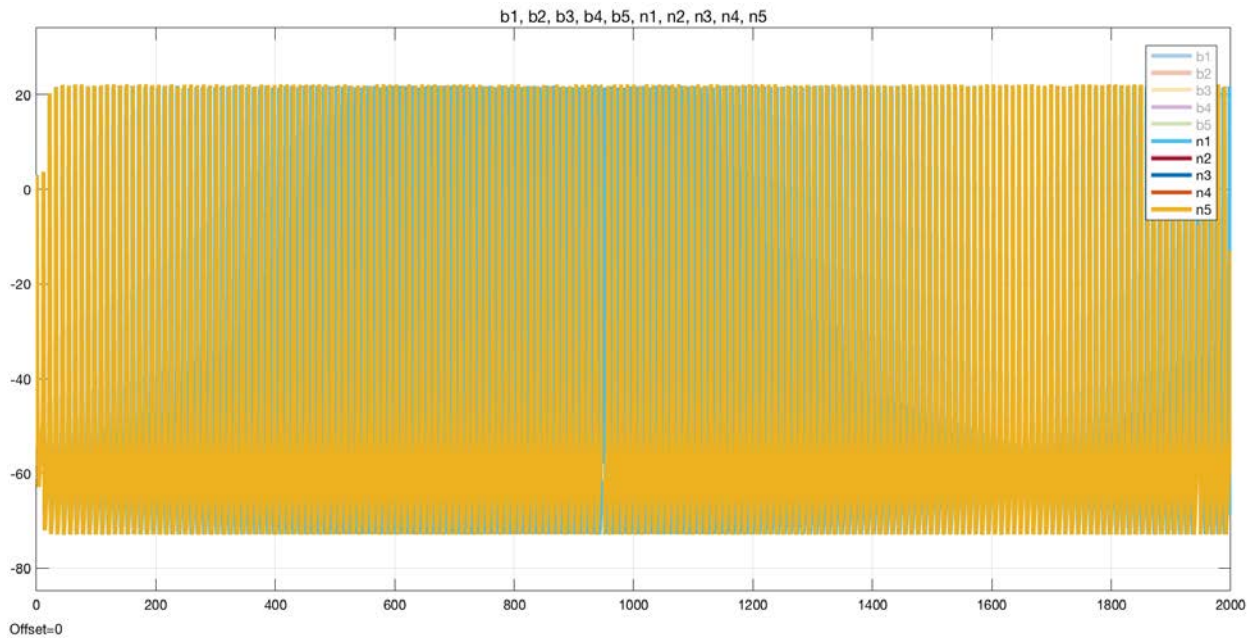


Figure 5-50: Five-neuron Hodgkin-Huxley interneuron winner-take-all network with low-pass filter feedback where  $\tau = 10$ ;  $I_1 = 25.5, I_2 = I_3 = I_4 = I_5 = 25$ .

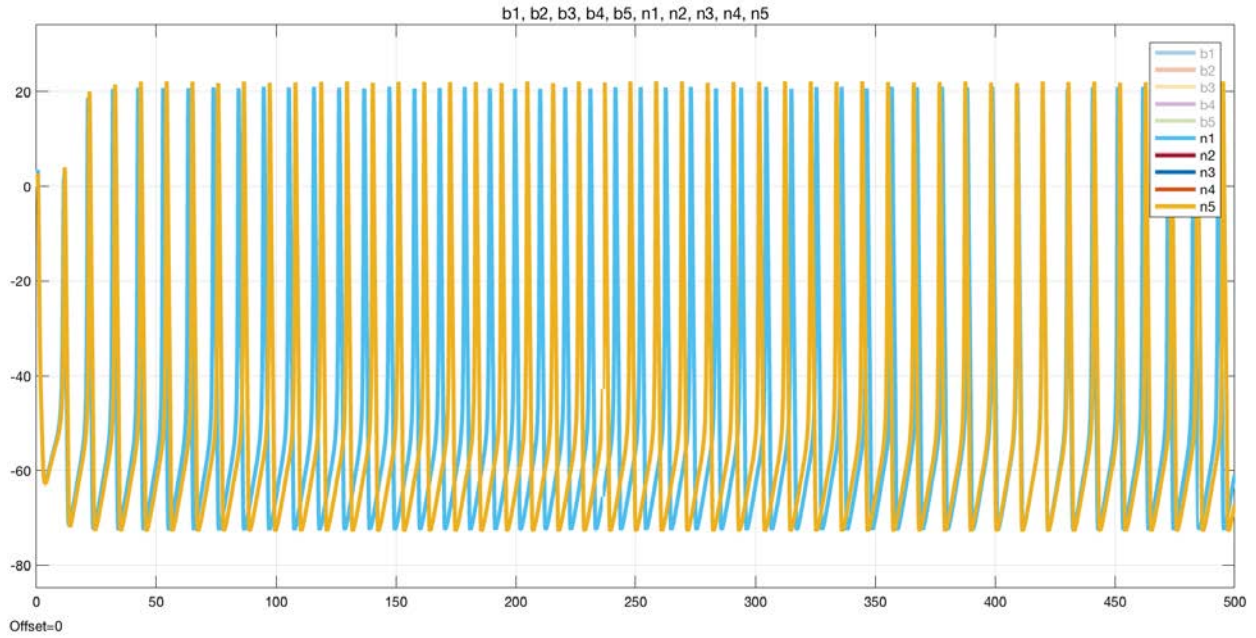


Figure 5-51: Five-neuron Hodgkin-Huxley interneuron winner-take-all network with low-pass filter feedback where  $\tau = 10$ ;  $I_1 = 27, I_2 = I_3 = I_4 = I_5 = 25$ .

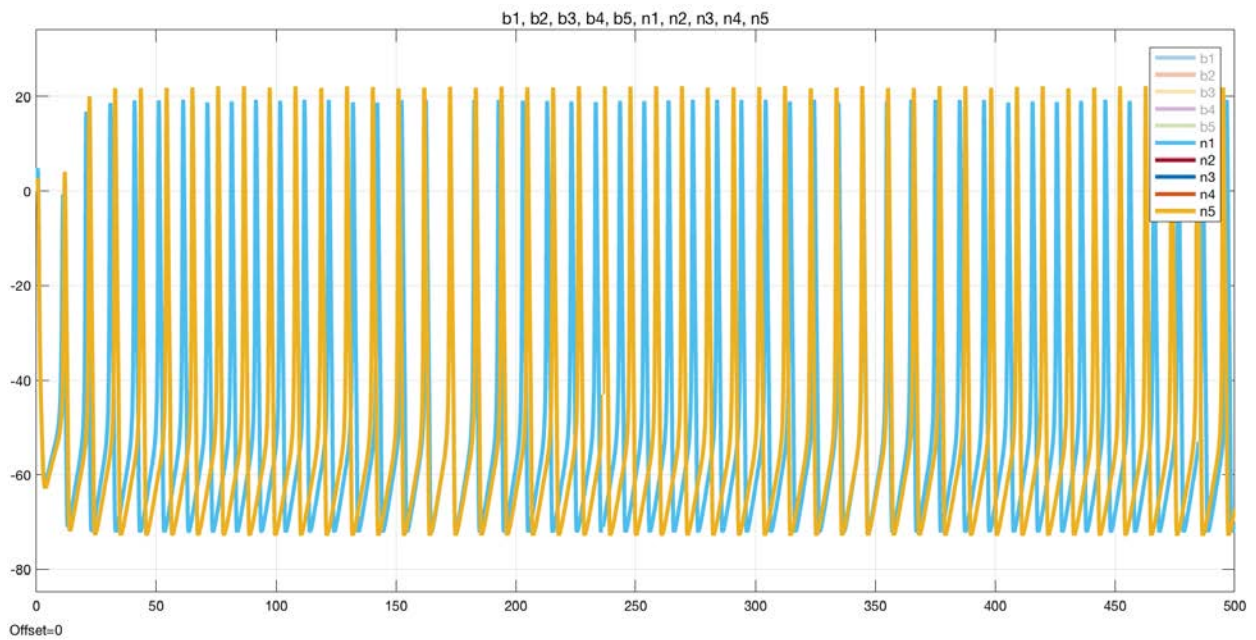


Figure 5-52: Five-neuron Hodgkin-Huxley interneuron winner-take-all network with low-pass filter feedback where  $\tau = 10$ ;  $I_1 = 30, I_2 = I_3 = I_4 = I_5 = 25$ .

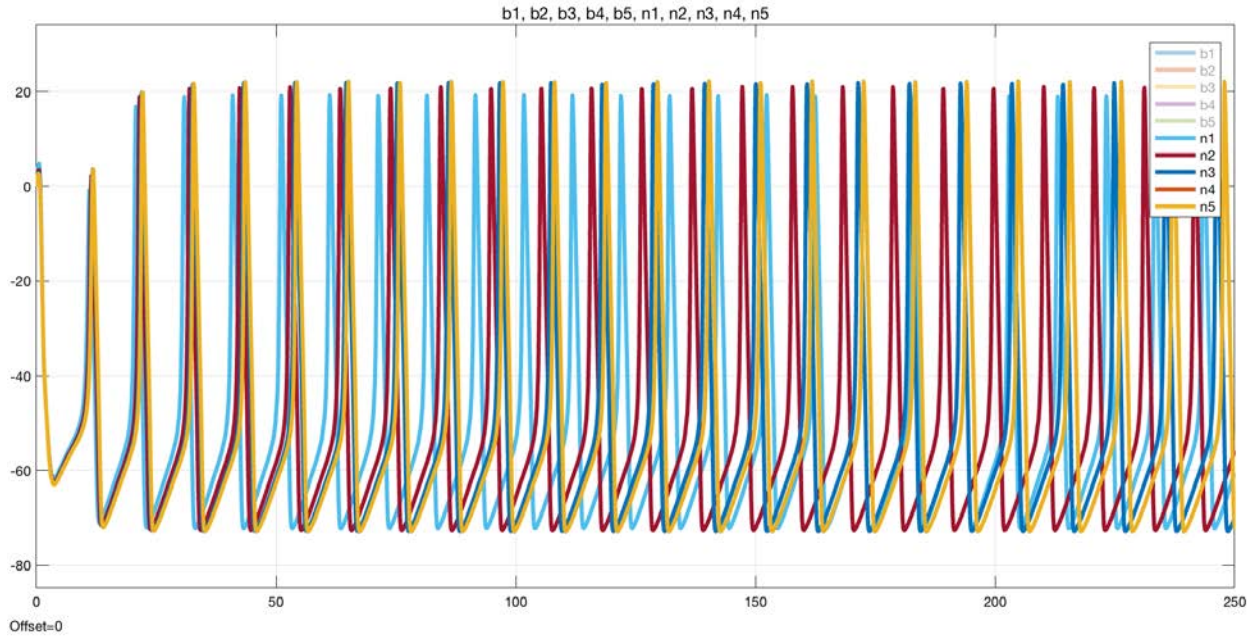


Figure 5-53: Five-neuron Hodgkin-Huxley interneuron winner-take-all network with low-pass filter feedback where  $\tau = 10$ ;  $I_1 = 30, I_2 = 27, I_3 = 25.5, I_4 = I_5 = 25$ .

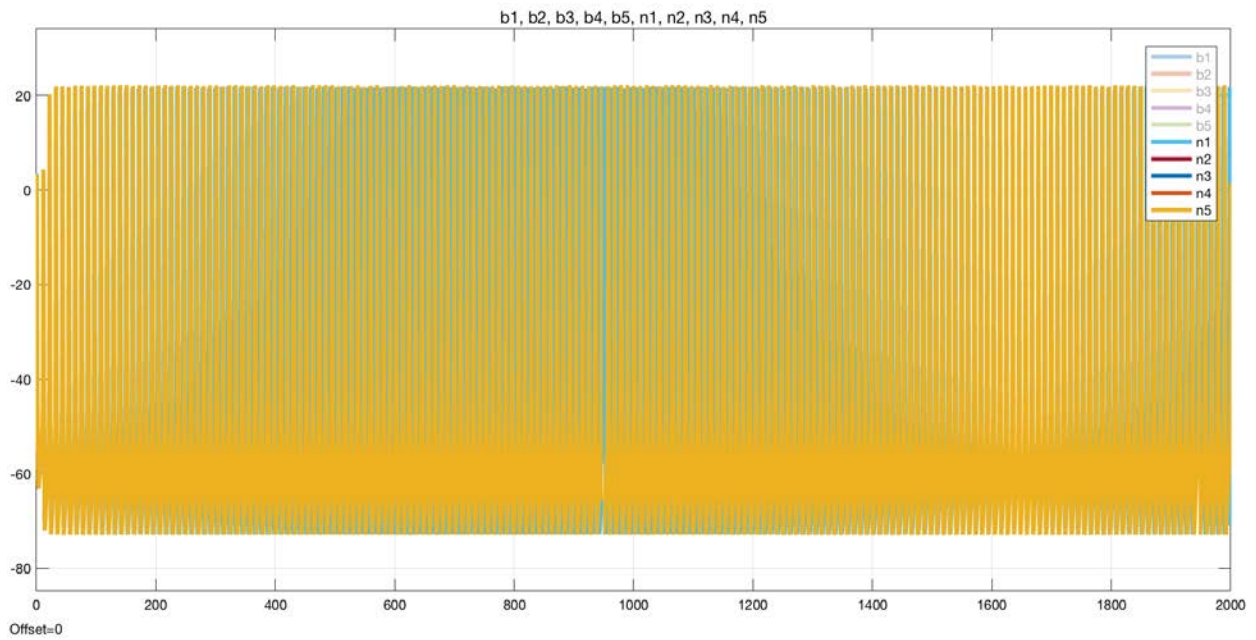


Figure 5-54: Five-neuron Hodgkin-Huxley interneuron winner-take-all network with low-pass filter feedback where  $\tau = 100$ ;  $I_1 = 25.5, I_2 = I_3 = I_4 = I_5 = 25$ .

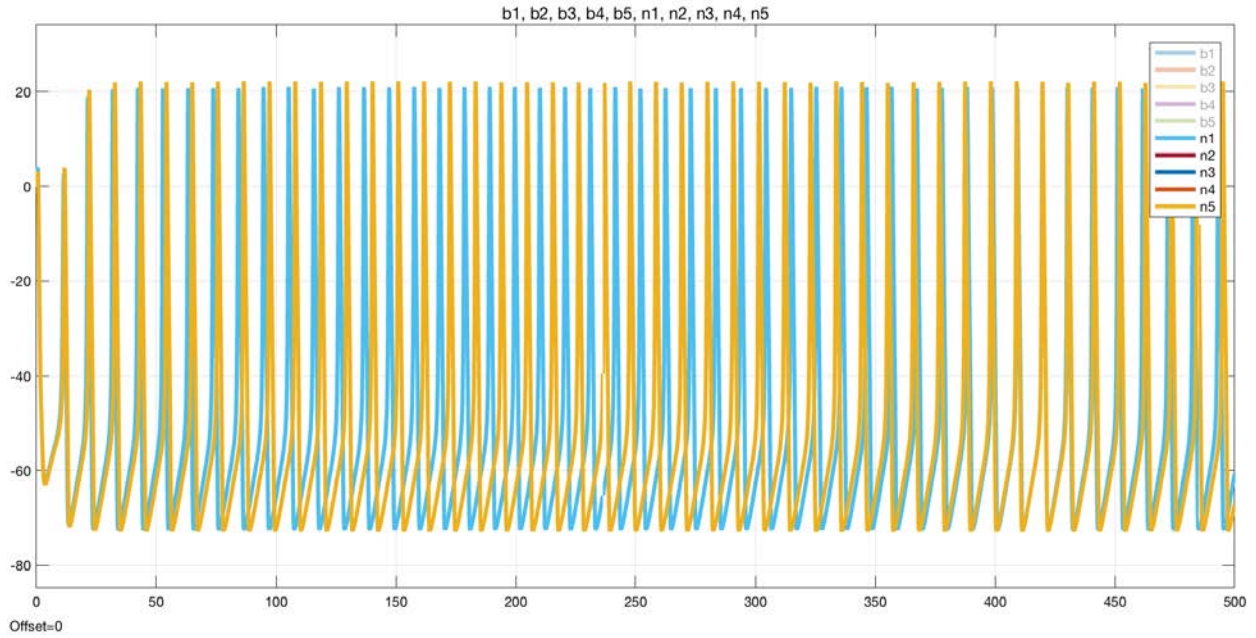


Figure 5-55: Five-neuron Hodgkin-Huxley interneuron winner-take-all network with low-pass filter feedback where  $\tau = 100$ ;  $I_1 = 27, I_2 = I_3 = I_4 = I_5 = 25$ .

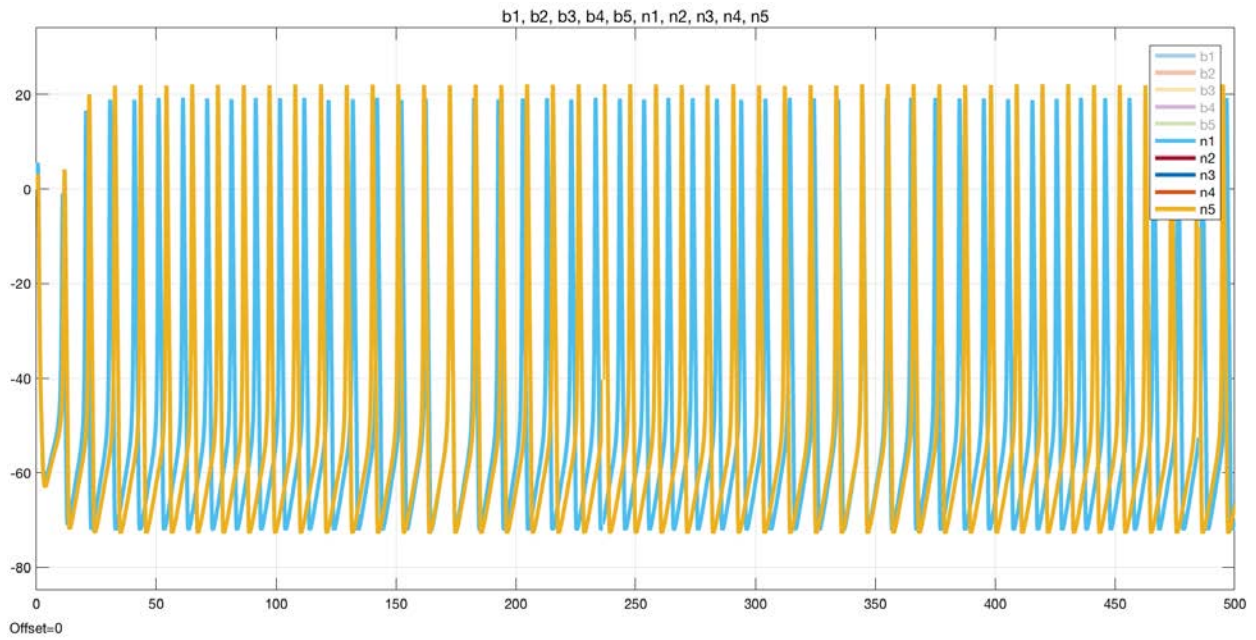


Figure 5-56: Five-neuron Hodgkin-Huxley interneuron winner-take-all network with low-pass filter feedback where  $\tau = 100$ ;  $I_1 = 30, I_2 = I_3 = I_4 = I_5 = 25$ .

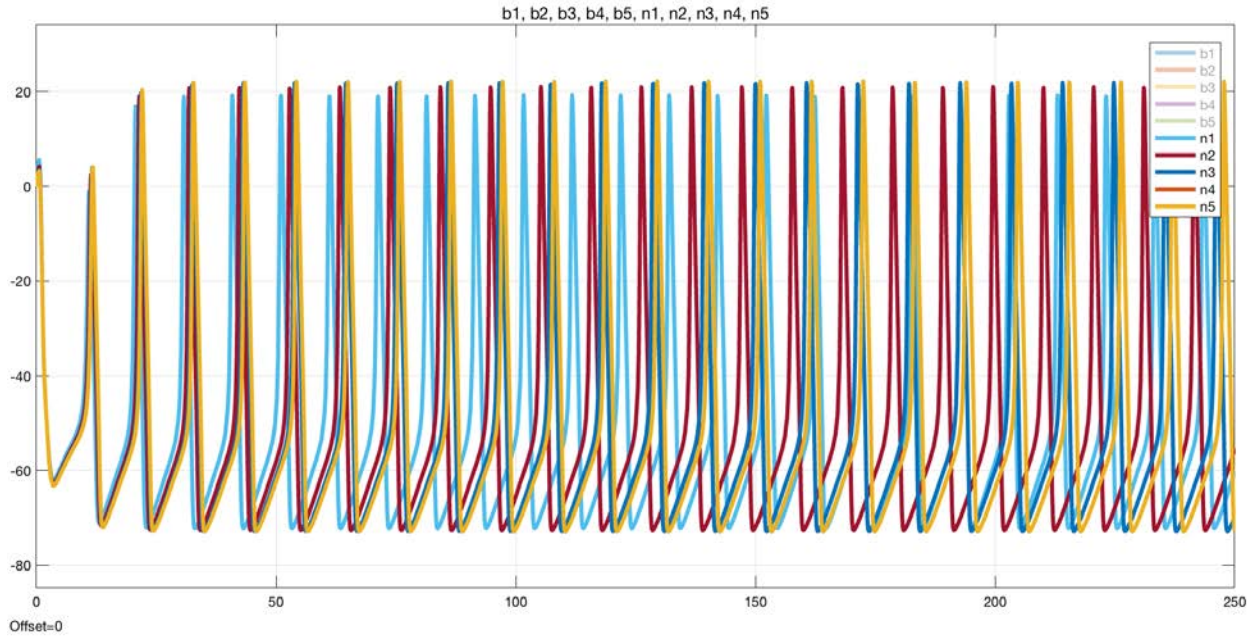


Figure 5-57: Five-neuron Hodgkin-Huxley interneuron winner-take-all network with low-pass filter feedback where  $\tau = 100$ ;  $I_1 = 30, I_2 = 27, I_3 = 25.5, I_4 = I_5 = 25$ .

### 5.5 Fitzhugh-Nagumo

Referring to the model equations of the Fitzhugh-Nagumo model, more specifically equation (1.13), the following values were chosen for the parameters:

Table 5-2: Fitzhugh-Nagumo Parameters

Parameter	Value
$\beta$	0.08
$\gamma$	0.064

According to simulations tested, the Fitzhugh-Nagumo neuron operates within an input range of about 0.1 to 0.5. For these experiments, the input current values used range from 0.1 to 0.5. Just as before with the Hodgkin-Huxley model, weights for the feedback will range from 0.1

to 1 and time-constant values will range from 0.1 to 100. Figure 5-58 through Figure 5-61 again show the behavior of the individual uncoupled neurons. The input current of neuron 2 remains constant while the input current to neuron 1 is increased. In this model, the frequency of neuron 1 decreases as its input current increases.

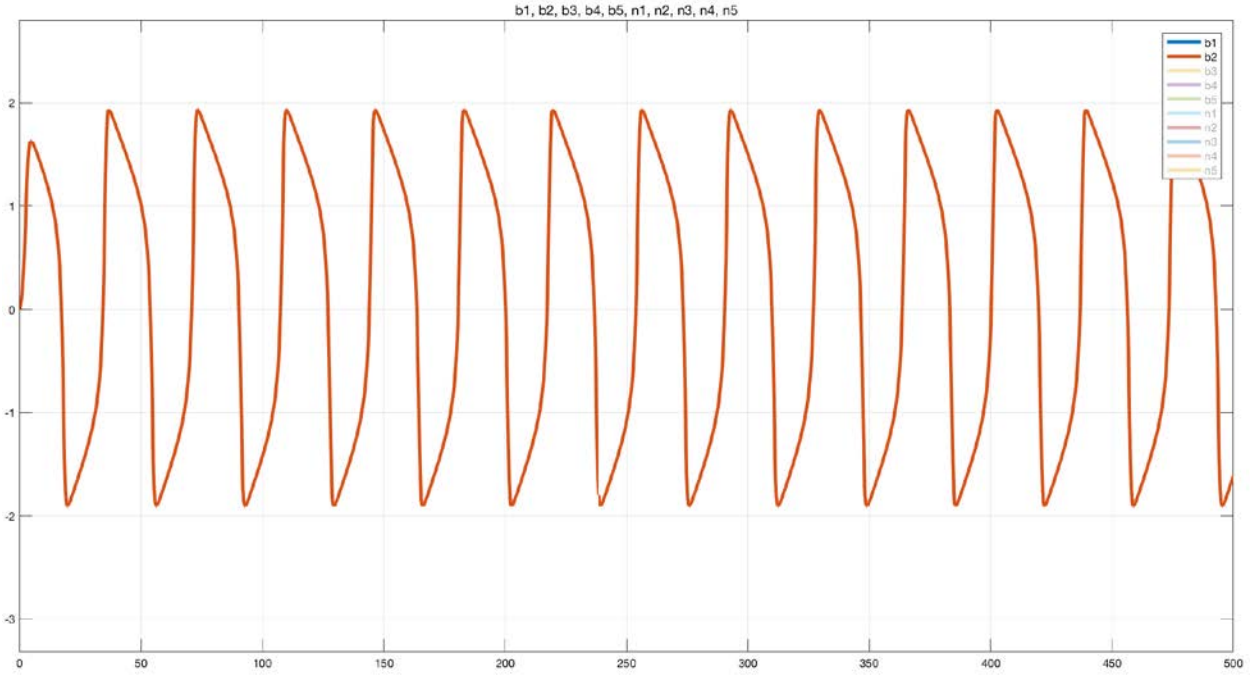


Figure 5-58: Two uncoupled Fitzhugh-Nagumo neurons where  $I_1 = I_2 = 0.1$ .

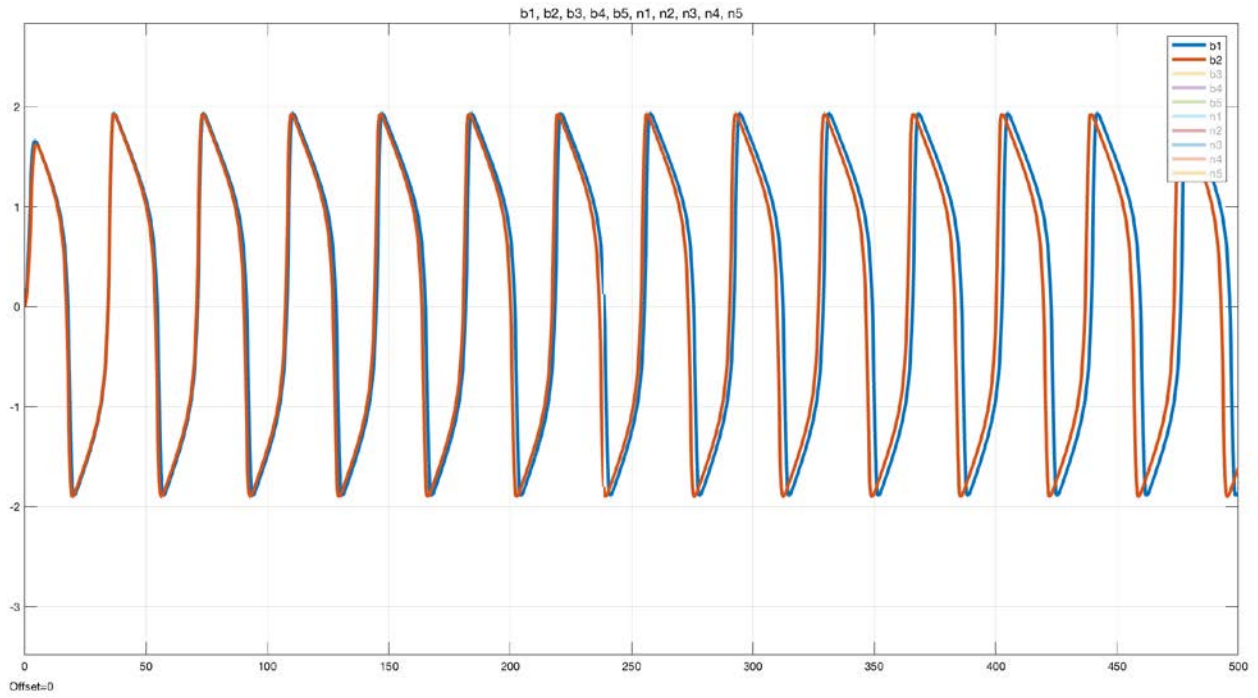


Figure 5-59: Two uncoupled Fitzhugh-Nagumo neurons where  $I_1 = 0.15$ ;  $I_2 = 0.1$ .

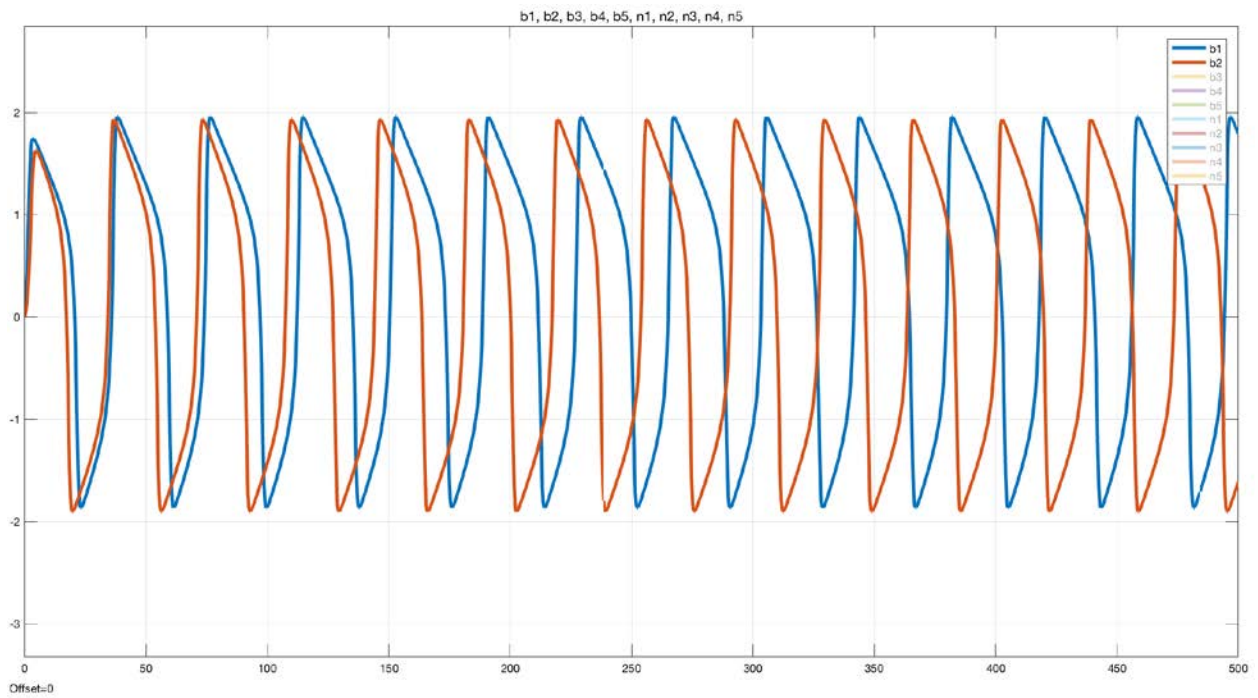


Figure 5-60: Two uncoupled Fitzhugh-Nagumo neurons where  $I_1 = 0.3$ ;  $I_2 = 0.1$ .

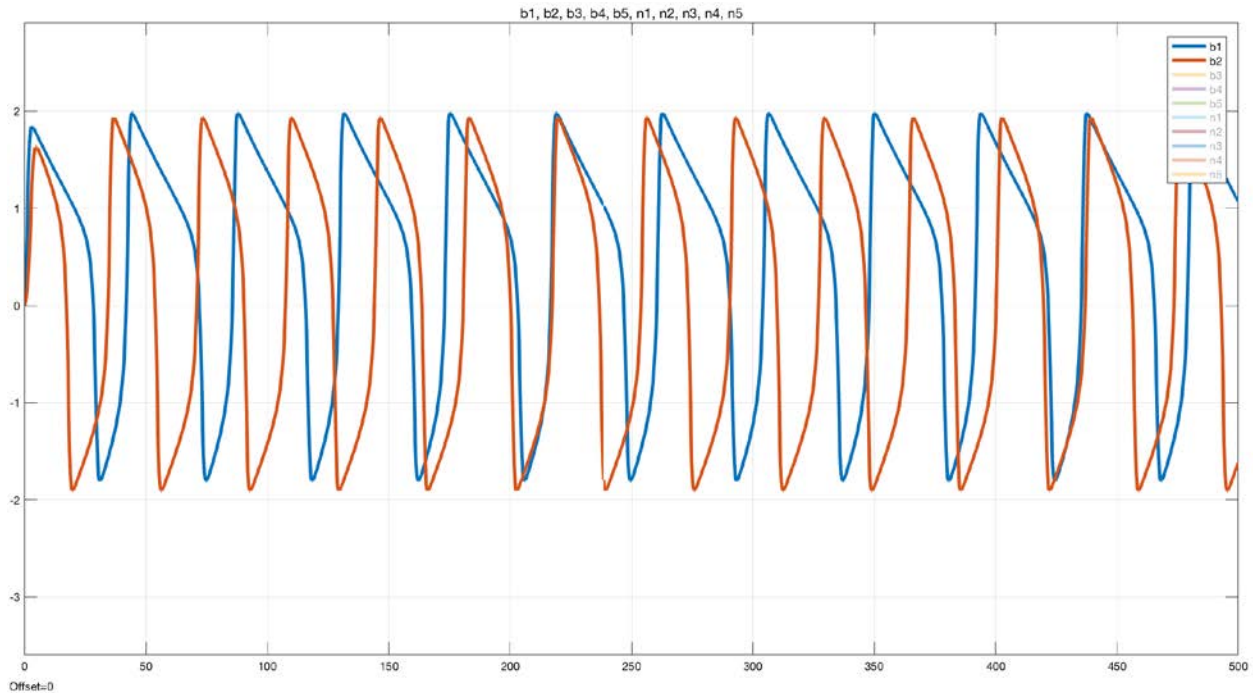


Figure 5-61: Two uncoupled Fitzhugh-Nagumo neurons where  $I_1 = 0.5$ ;  $I_2 = 0.1$ .

### 5.5.1 Lateral Inhibition Weighted Feedback

Figure 5-62 through Figure 5-64 show simulation results of a 5-neuron weighted feedback network with a weight of 1. The network synchronizes immediately with a 90-degree phase shift, unlike the Hodgkin-Huxley model where the phase shift is gradual. As the input current to neuron 1 increases, its pulse width gets wider, while maintaining the phase-shift. The pulse width of the rest of the network remains about the same but is pushed because of the change in the behavior of neuron 1. Decreasing the weight of the feedback to 0.5 as in Figure 5-66 through Figure 5-68, it is observed that the pulse widths of the neurons are narrower since they have less impact on the network with a lower weight. The pulse widths still increase, however, as the input current of neuron 1 is increased while maintaining the phase shift. When the weights are decreased further

to 0.1, the neuron outputs have even less impact on the network. The wave forms for neuron 1 and neuron 2 are more similar, besides the jitter during the first cycle. There is still a 90-degree shift.

Figure 5-65, Figure 5-69, and Figure 5-73 show simulations for varying input currents for feedback weight values of 1, 0.5, and 0.1, respectively. They show that the weight of the feedback does have some impact on the behavior of the network. In Figure 5-65 and Figure 5-69, neuron 1 and neuron 2 are closely synchronized, almost indistinguishable, and spike first. However, neuron 4 and neuron 5 appear to spike ahead of neuron 3. Figure 5-73 initially shows the corresponding spikes in the order of the winners. Then, neuron 2 and neuron 3 spike similarly ahead of neuron 1.

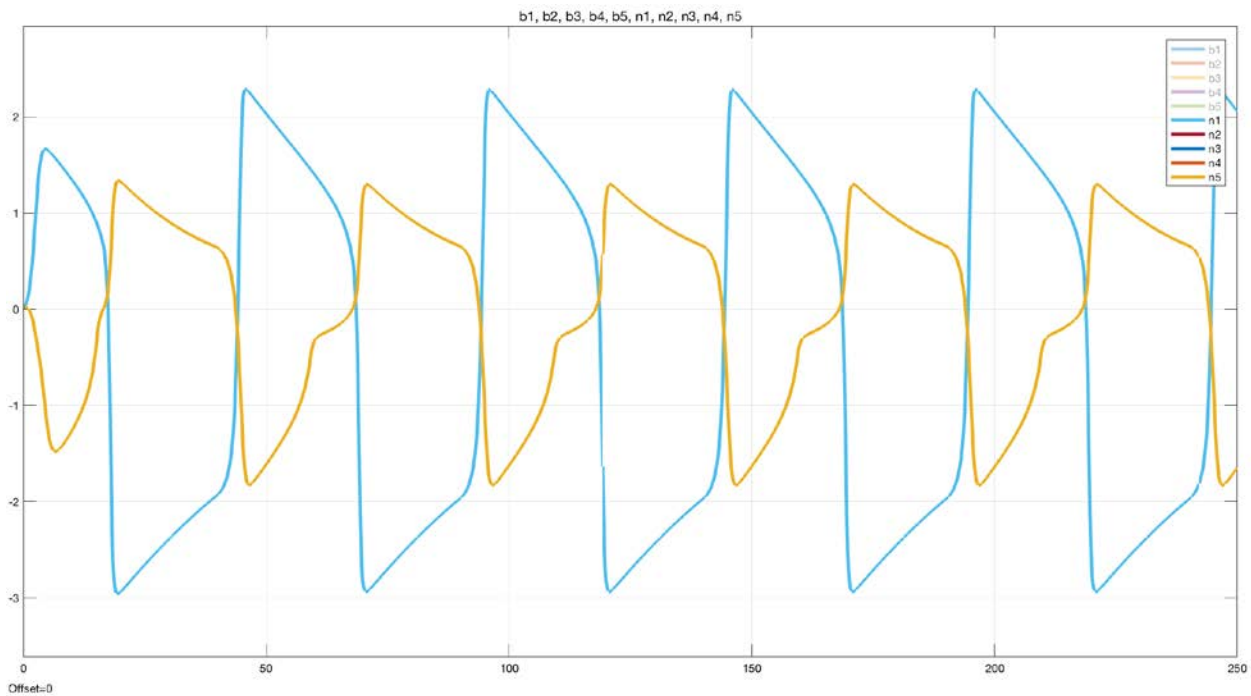


Figure 5-62: Five-neuron Fitzhugh-Nagumo inhibition winner-take-all network with weighted feedback of 1 where  $I_1 = 0.15$ ;  $[I_2, I_3, I_4, I_5] = 0.1$ .

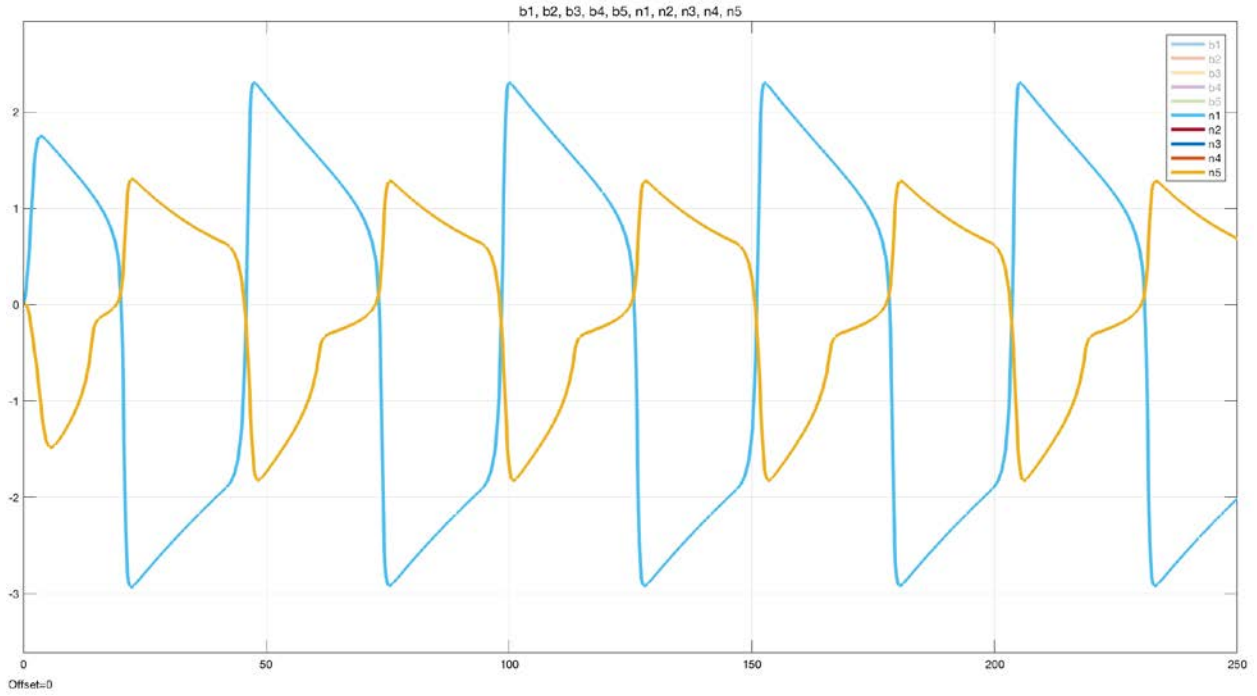


Figure 5-63: Five-neuron Fitzhugh-Nagumo inhibition winner-take-all network with weighted feedback of 1 where  $I1 = 0.3$ ;  $[I2, I3, I4, I5] = 0.1$ .

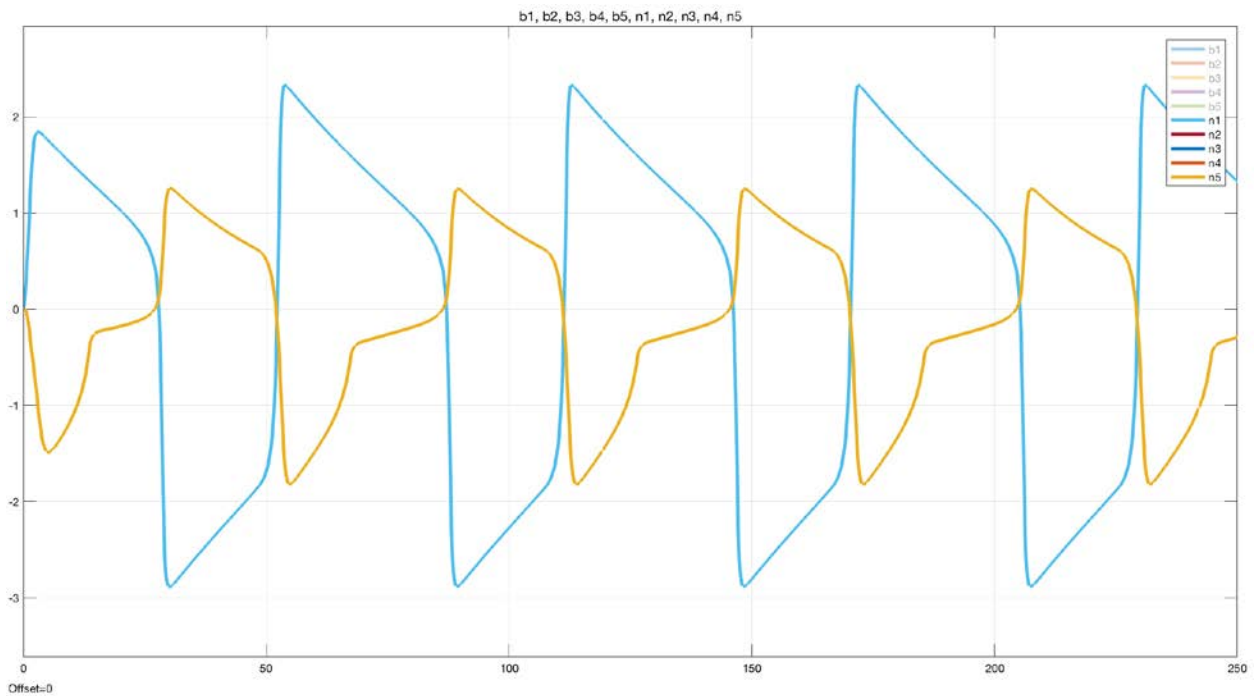


Figure 5-64: Five-neuron Fitzhugh-Nagumo inhibition winner-take-all network with weighted feedback of 1 where  $I1 = 0.5$ ;  $[I2, I3, I4, I5] = 0.1$ .

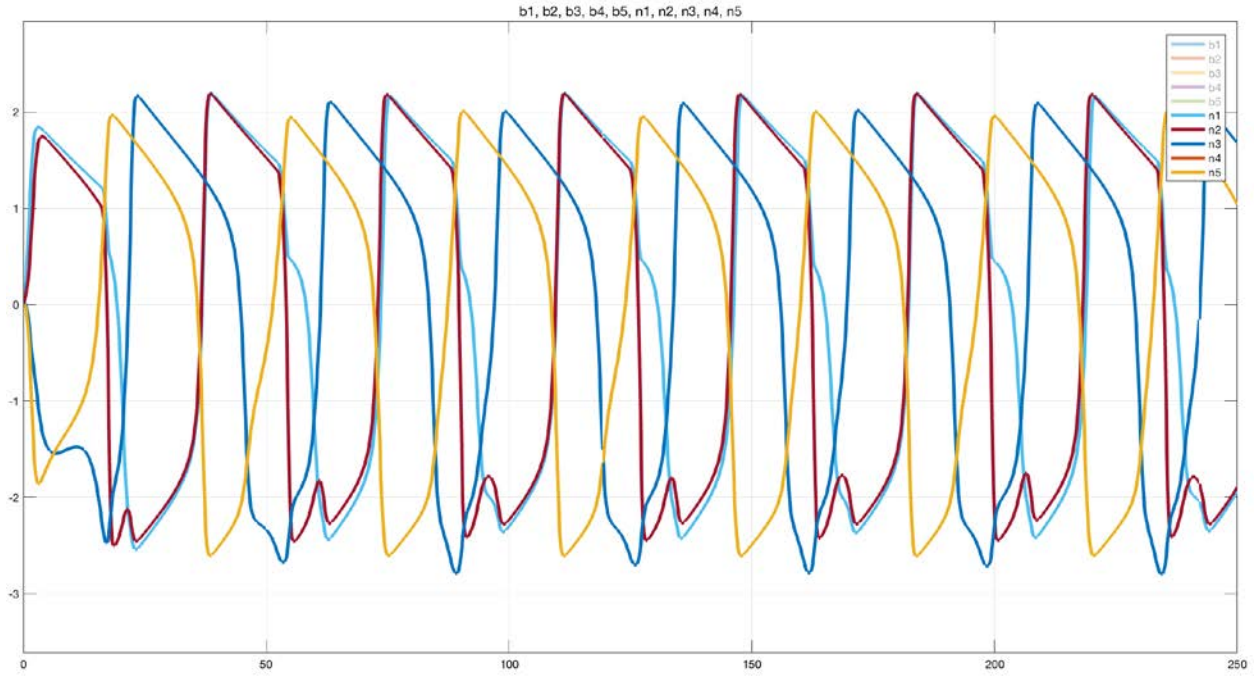


Figure 5-65: Five-neuron Fitzhugh-Nagumo inhibition winner-take-all network with weighted feedback of 1 where  $I_1 = 0.5$ ;  $I_2 = 0.3$ ;  $I_3 = 0.15$ ;  $[I_4, I_5] = 0.1$ .

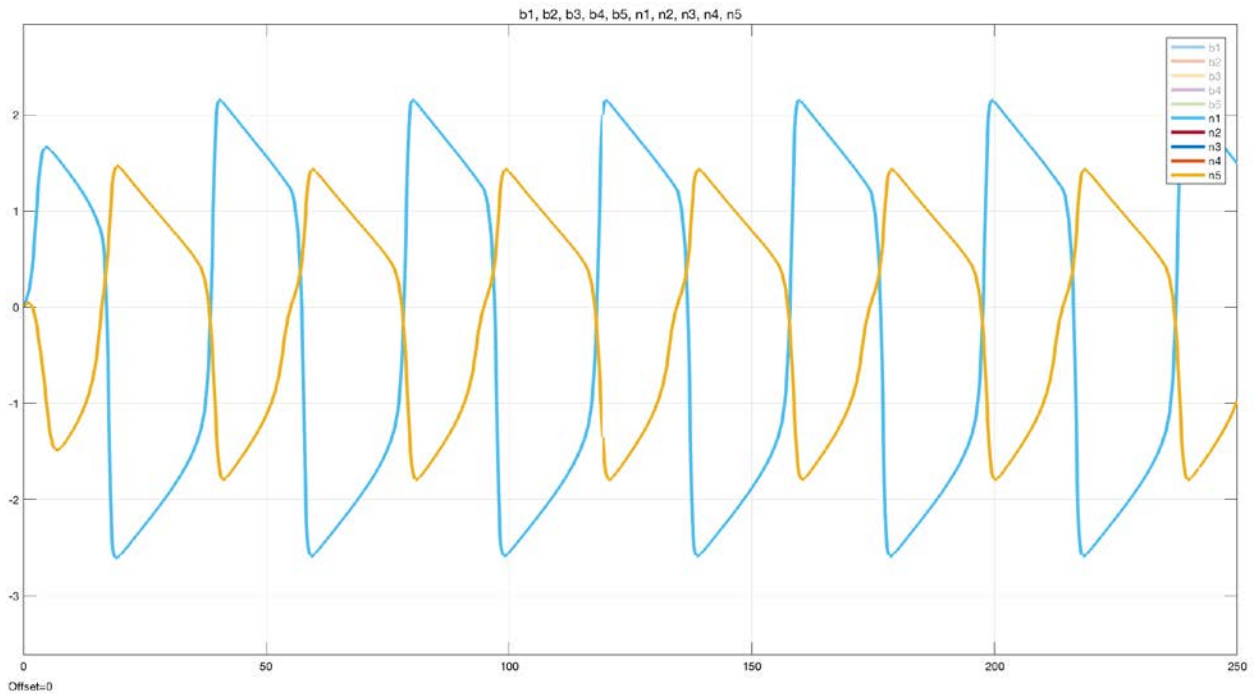


Figure 5-66: Five-neuron Fitzhugh-Nagumo inhibition winner-take-all network with weighted feedback of 0.5 where  $I_1 = 0.15$ ;  $[I_2, I_3, I_4, I_5] = 0.1$ .

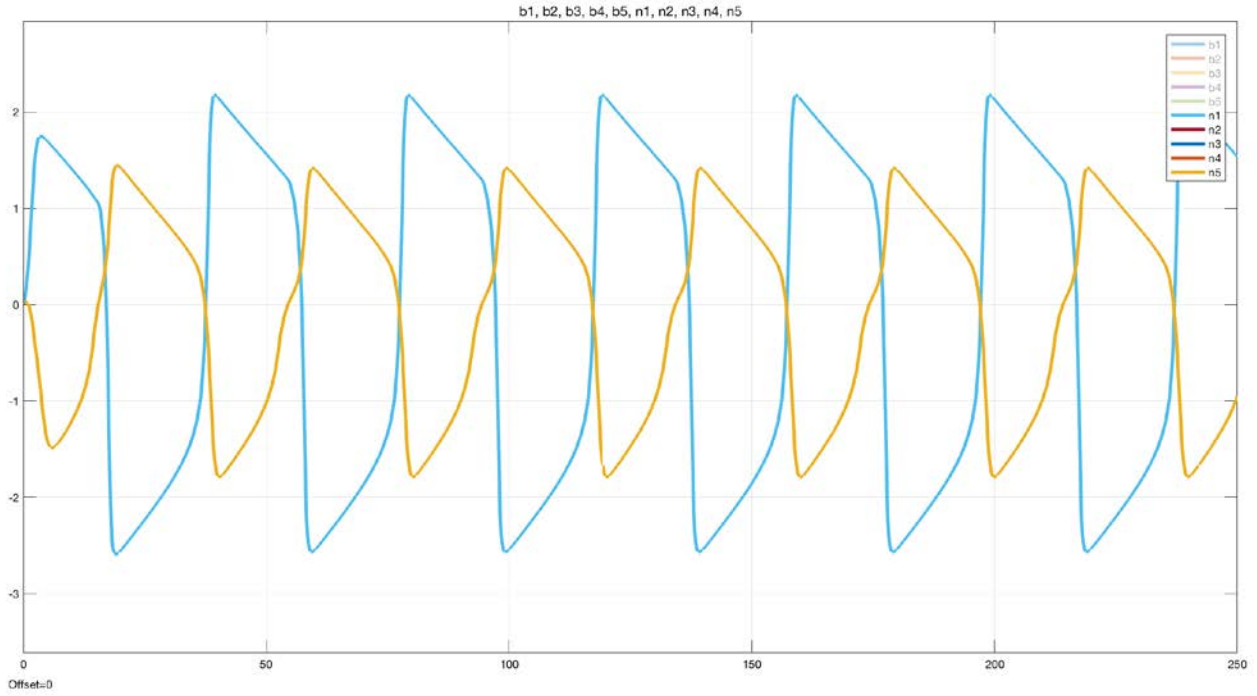


Figure 5-67: Five-neuron Fitzhugh-Nagumo inhibition winner-take-all network with weighted feedback of 0.5 where  $I1 = 0.3$ ;  $[I2, I3, I4, I5] = 0.1$ .

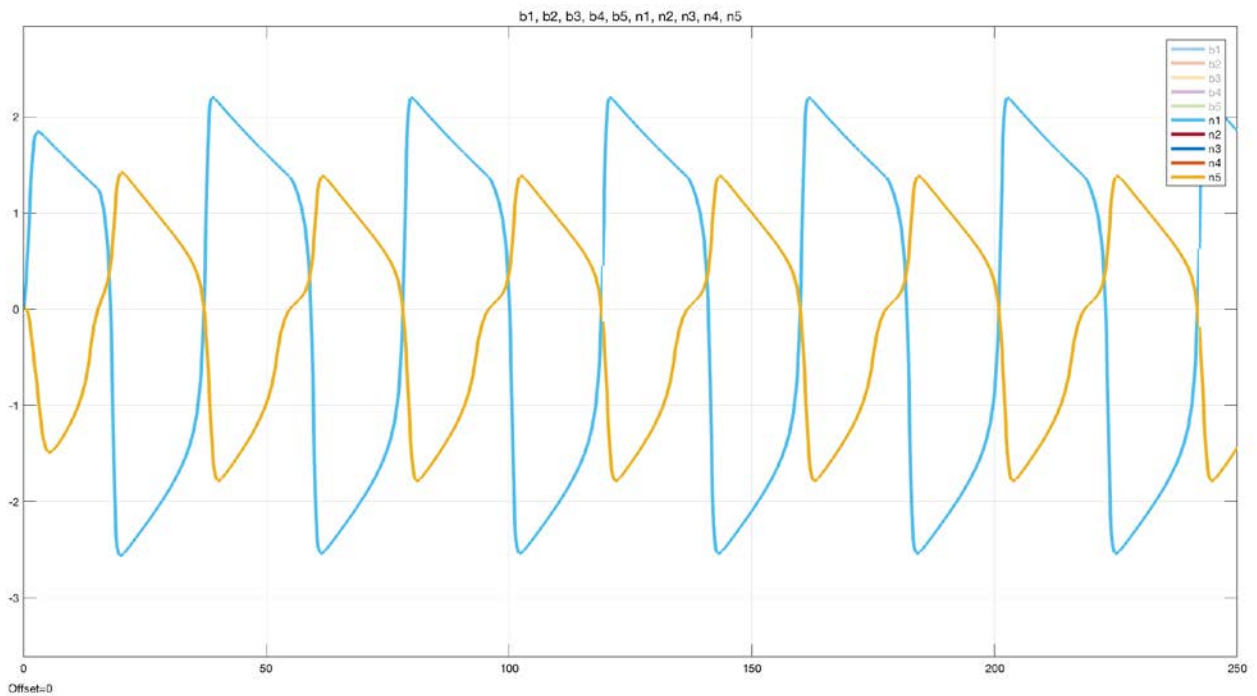


Figure 5-68: Five-neuron Fitzhugh-Nagumo inhibition winner-take-all network with weighted feedback of 0.5 where  $I1 = 0.5$ ;  $[I2, I3, I4, I5] = 0.1$ .

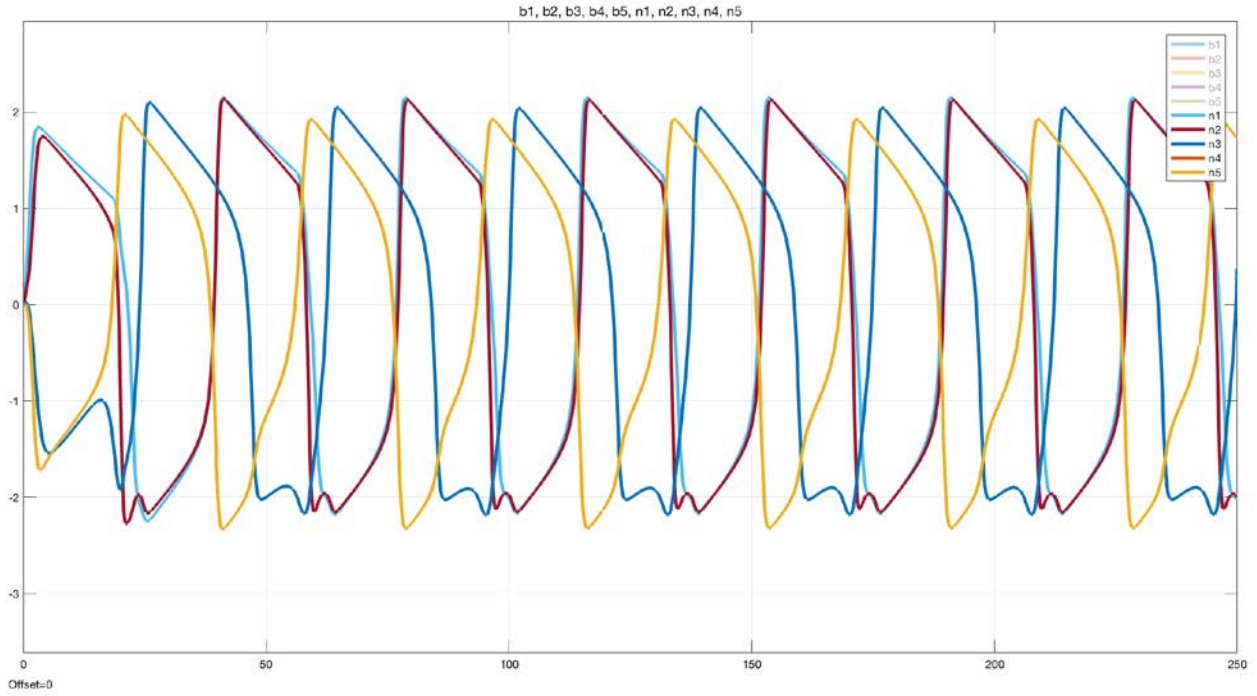


Figure 5-69: Five-neuron Fitzhugh-Nagumo inhibition winner-take-all network with weighted feedback of 0.5 where  $I1 = 0.5$ ;  $I2 = 0.3$ ;  $I3 = 0.15$ ;  $[I4, I5] = 0.1$ .

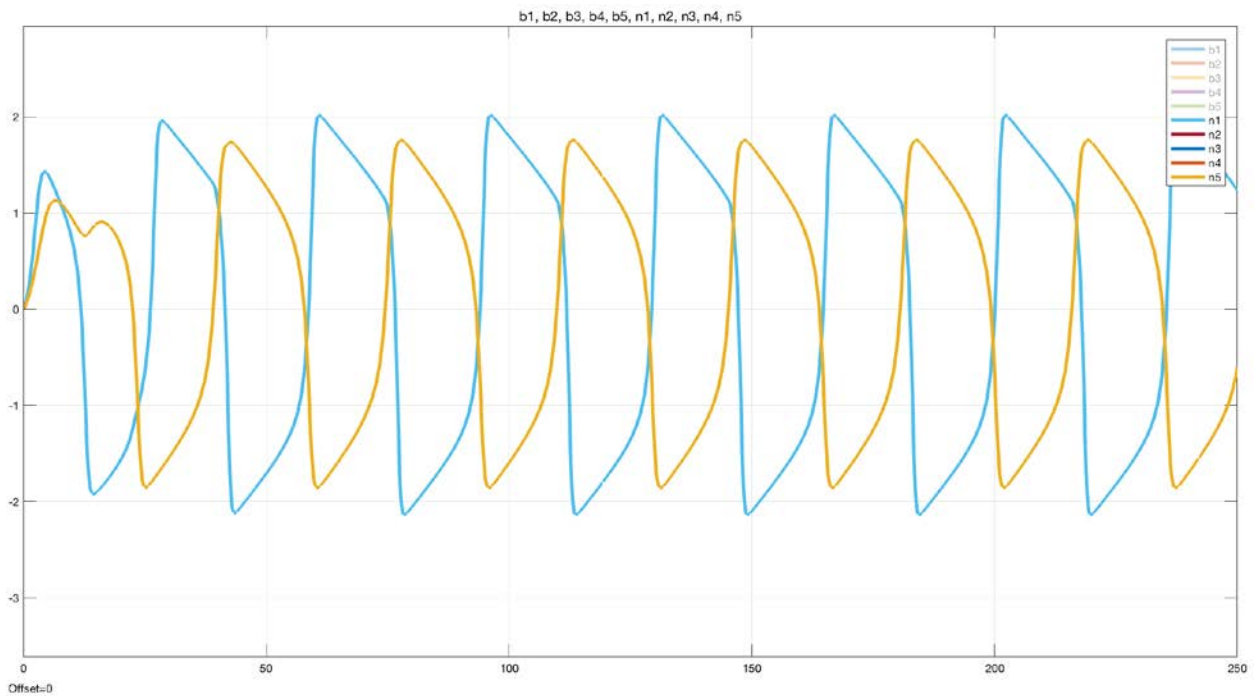


Figure 5-70: Five-neuron Fitzhugh-Nagumo inhibition winner-take-all network with weighted feedback of 0.1 where  $I1 = 0.15$ ;  $[I2, I3, I4, I5] = 0.1$ .

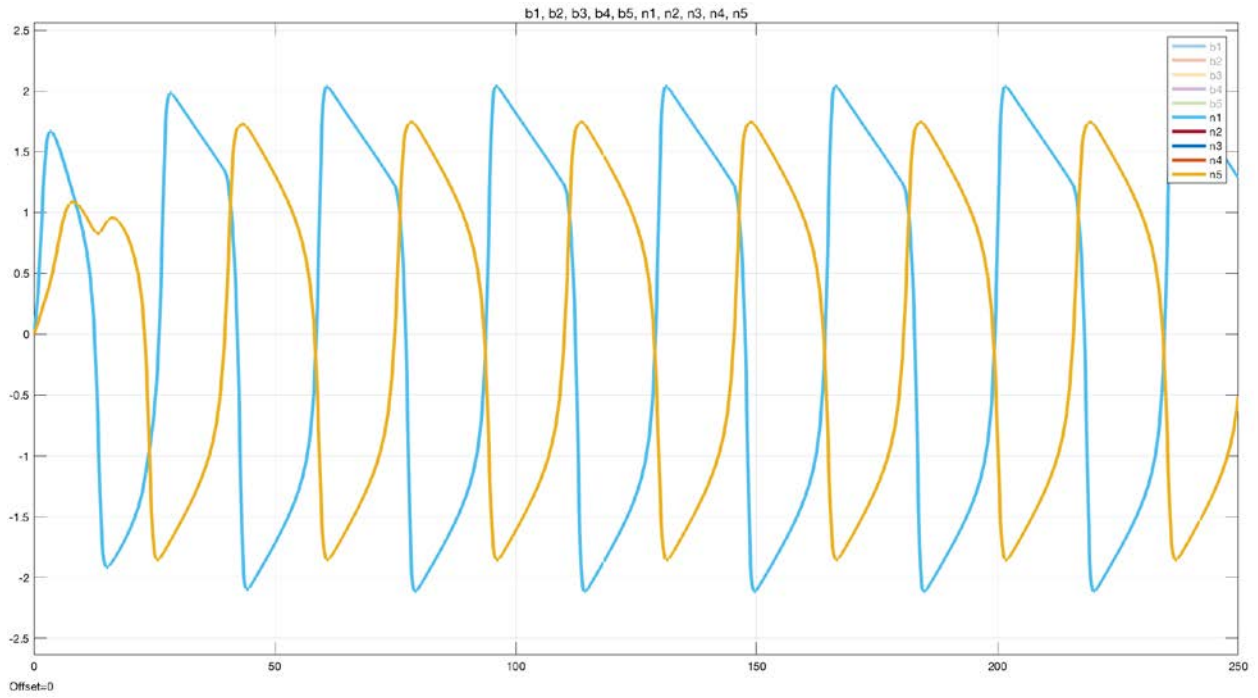


Figure 5-71: Five-neuron Fitzhugh-Nagumo inhibition winner-take-all network with weighted feedback of 0.1 where  $I1 = 0.3$ ;  $[I2, I3, I4, I5] = 0.1$ .

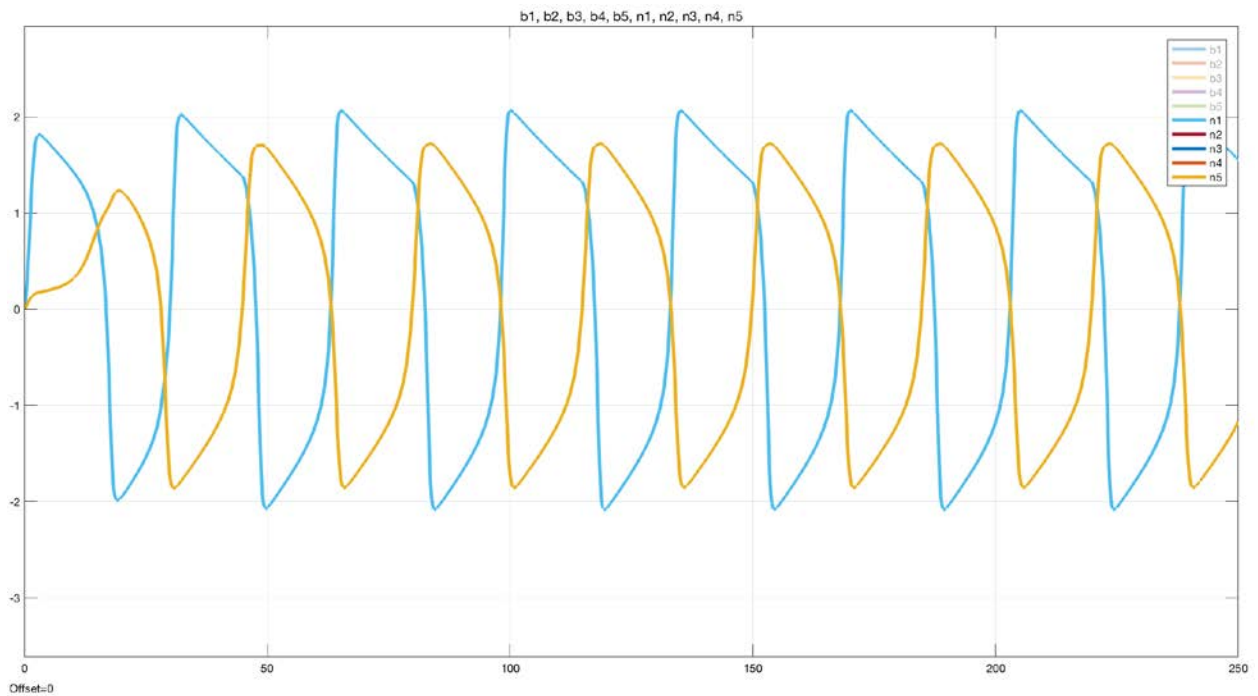


Figure 5-72: Five-neuron Fitzhugh-Nagumo inhibition winner-take-all network with weighted feedback of 0.1 where  $I1 = 0.5$ ;  $[I2, I3, I4, I5] = 0.1$ .

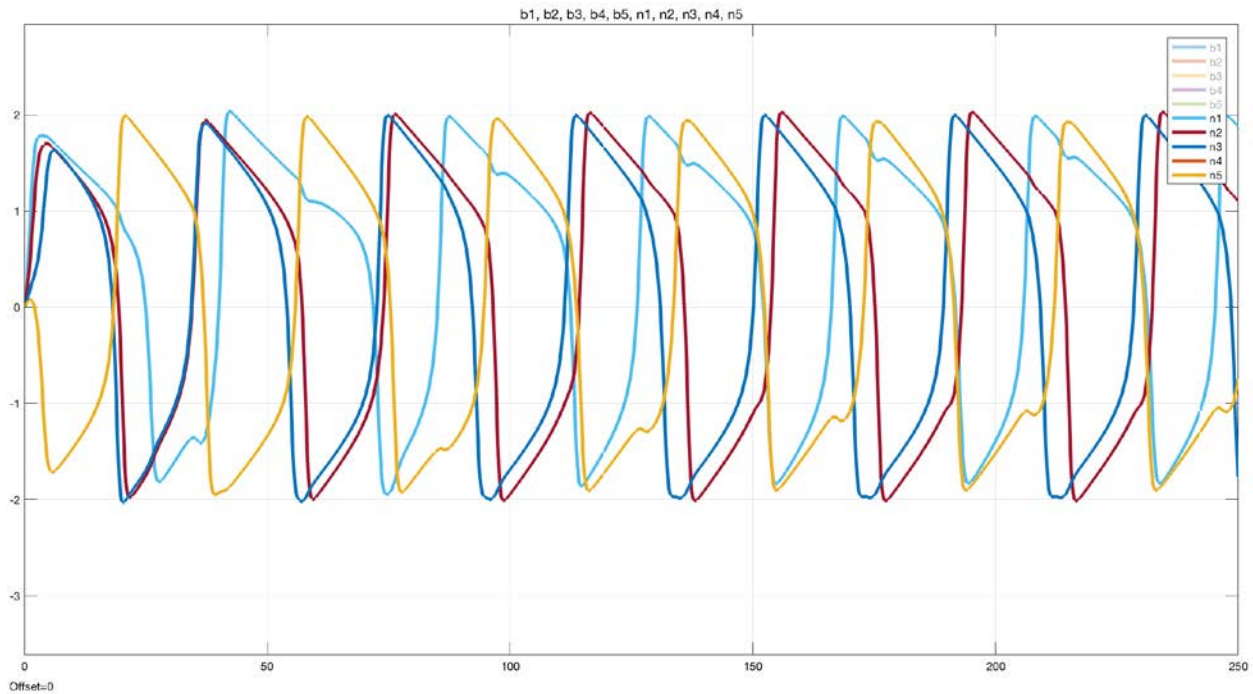


Figure 5-73: Five-neuron Fitzhugh-Nagumo inhibition winner-take-all network with weighted feedback of 0.1 where  $I_1 = 0.5$ ;  $I_2 = 0.3$ ;  $I_3 = 0.15$ ;  $[I_4, I_5] = 0.1$ .

### 5.5.2 Lateral Inhibition Low-Pass Filter Feedback

Figure 5-74 through Figure 5-76 show simulation results of a 5-neuron low-pass feedback network with a time constant value of 0.1. There is an immediate phase shift of 90 degrees, however the spiking of neuron 1, is significantly larger than the spiking of the rest of the network. The pulse width of neuron 1 increases as its input current is increased. The pulse width of the rest of the network remains the same but is shifted as the width of neuron 1 is increased. When the time-constant is increased to 10, as shown in Figure 5-78 through Figure 5-80, the network becomes unstable. In fact, after more simulations were done, the network begins to experience this behavior when the time-constant is between about 1 and 25. Time-constant values greater than that

result in stable behaviors similar to Figure 5-82 through Figure 5-84, which show simulations with a time constant value of 100. The network behaves similar to the Hodgkin-Huxley model in that the phase shift occurs gradually. In addition, the shift is not as large as for smaller time-constants.

Figure 5-77, Figure 5-81, and Figure 5-85 show simulations for varying input currents for time-constant values of 0.1, 10, and 100, respectively. Similar to the simulations with the weighted feedback, the time-constant values impact the order of the winners.

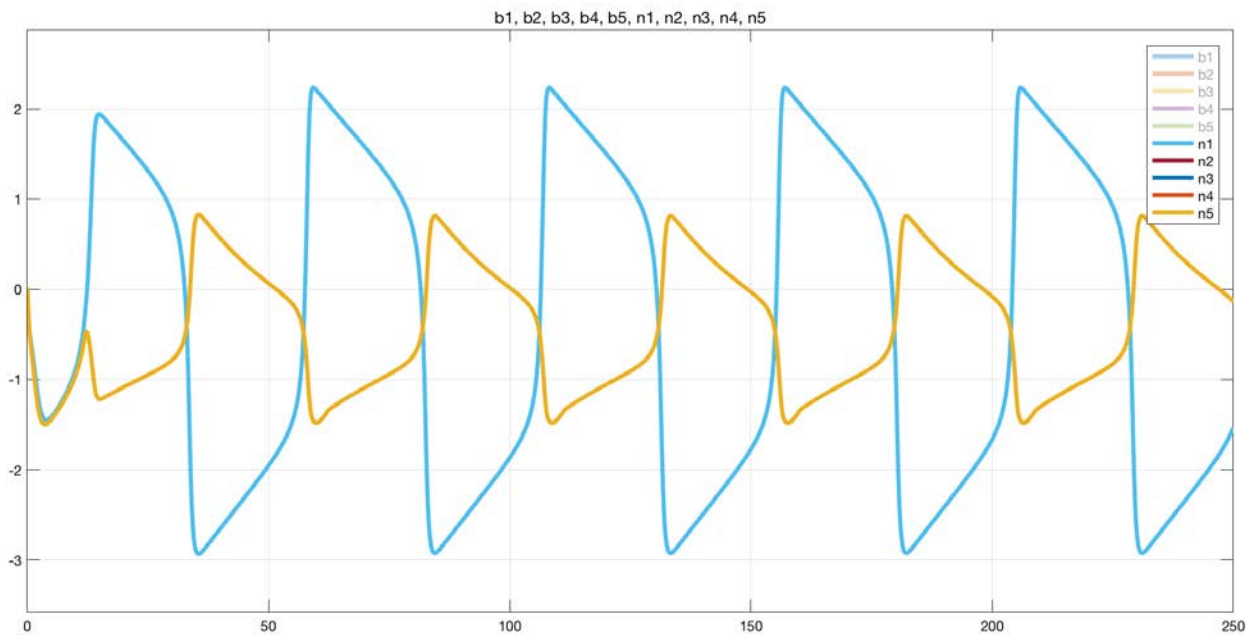


Figure 5-74: Five-neuron Fitzhugh-Nagumo inhibition winner-take-all network with low-pass filter feedback where  $\tau = 0.1$ ;  $I_1 = 0.15$ ;  $[I_2, I_3, I_4, I_5] = 0.1$ .

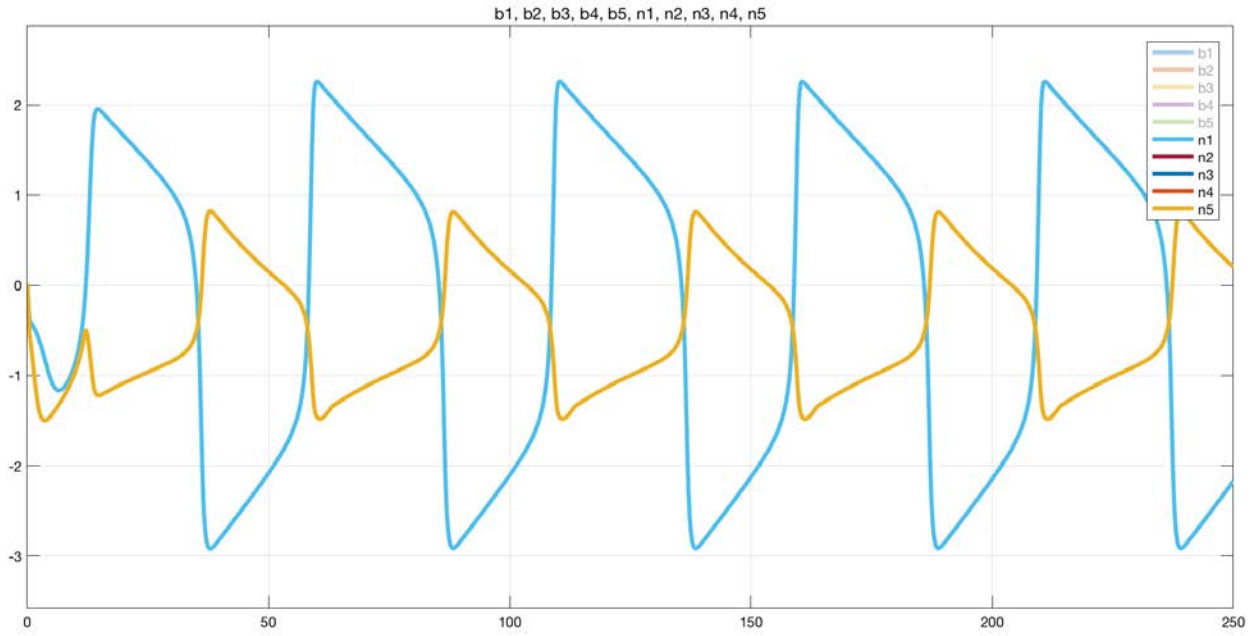


Figure 5-75: Five-neuron Fitzhugh-Nagumo inhibition winner-take-all network with low-pass filter feedback where  $\tau = 0.1$ ;  $I_1 = 0.3$ ;  $[I_2, I_3, I_4, I_5] = 0.1$ .

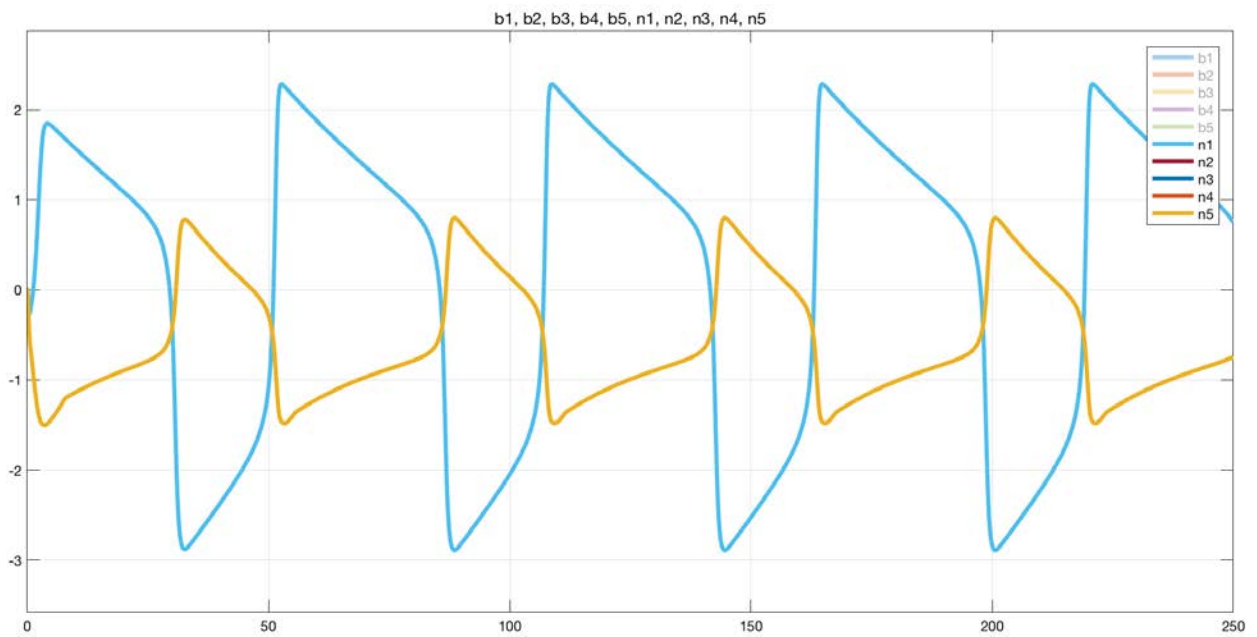


Figure 5-76: Five-neuron Fitzhugh-Nagumo inhibition winner-take-all network with low-pass filter feedback where  $\tau = 0.1$ ;  $I_1 = 0.5$ ;  $[I_2, I_3, I_4, I_5] = 0.1$ .

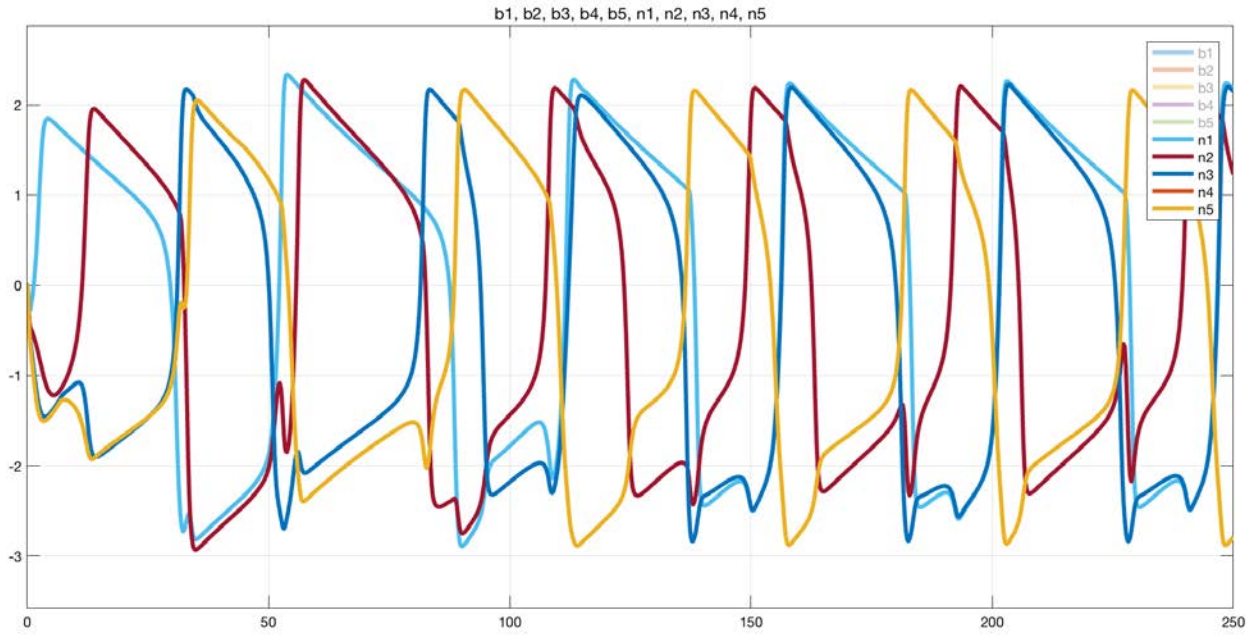


Figure 5-77: Five-neuron Fitzhugh-Nagumo inhibition winner-take-all network with low-pass filter feedback where  $\tau = 0.1$ ;  $I_1 = 0.5$ ;  $I_2 = 0.3$ ;  $I_3 = 0.15$ ;  $[I_4, I_5] = 0.1$ .

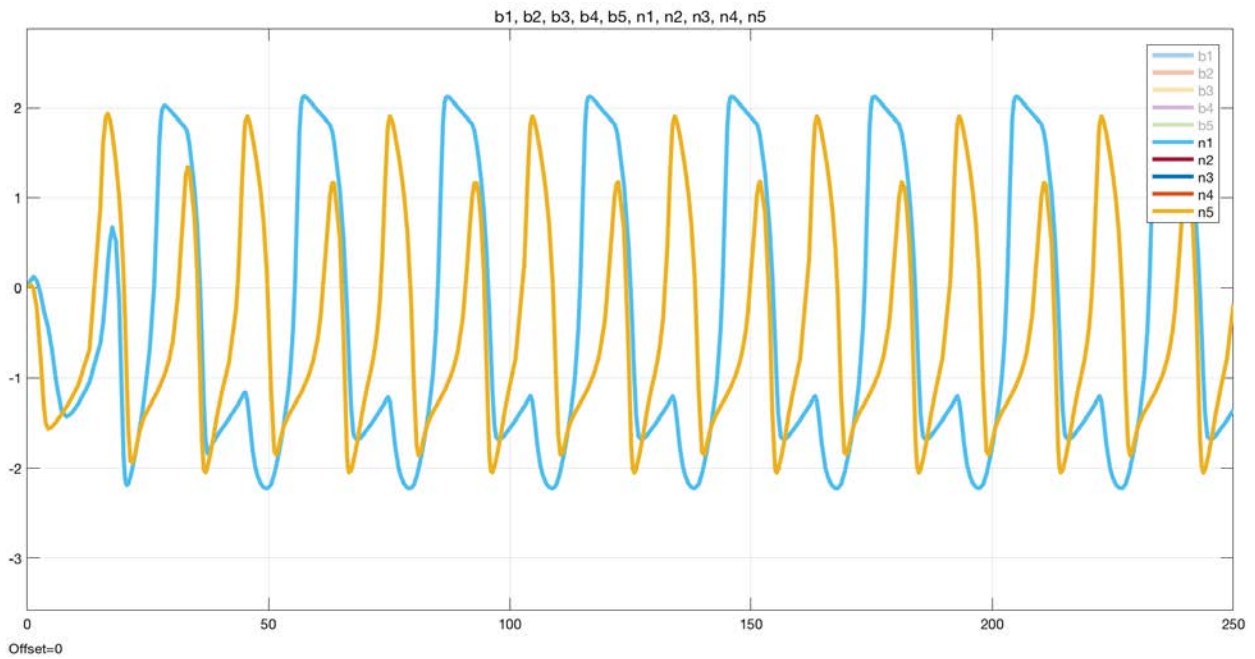


Figure 5-78: Five-neuron Fitzhugh-Nagumo inhibition winner-take-all network with low-pass filter feedback where  $\tau = 10$ ;  $I_1 = 0.15$ ;  $[I_2, I_3, I_4, I_5] = 0.1$ .

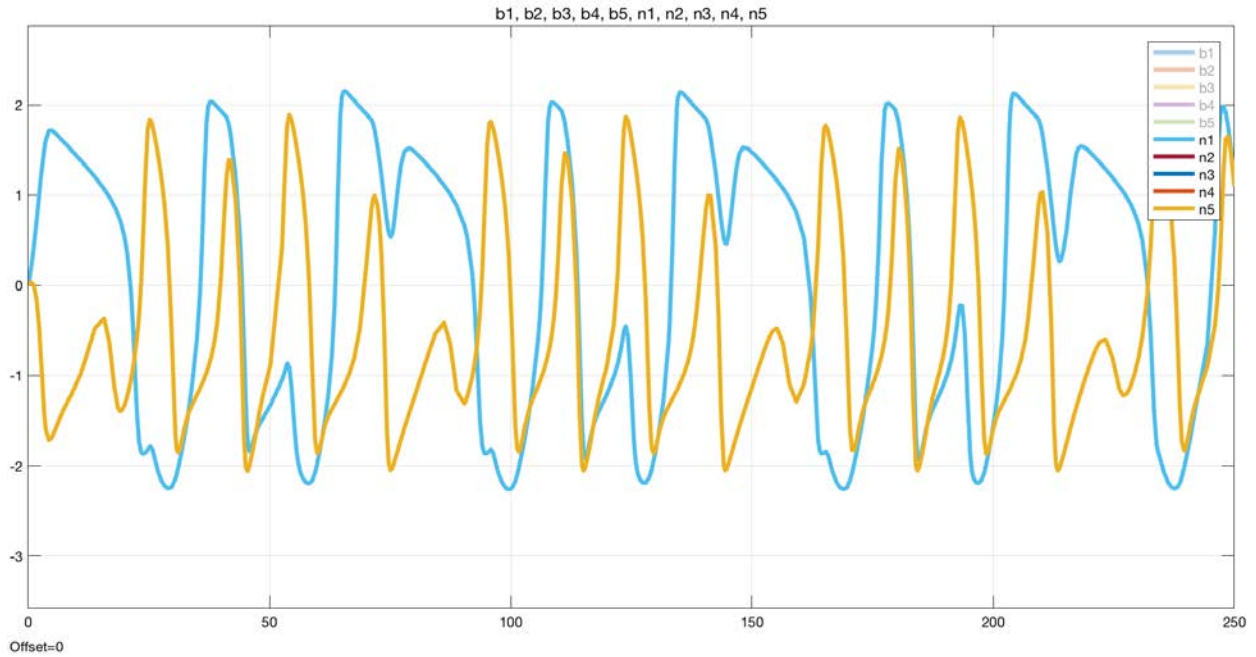


Figure 5-79: Five-neuron Fitzhugh-Nagumo inhibition winner-take-all network with low-pass filter feedback where  $\tau = 10$ ;  $I_1 = 0.3$ ;  $[I_2, I_3, I_4, I_5] = 0.1$ .

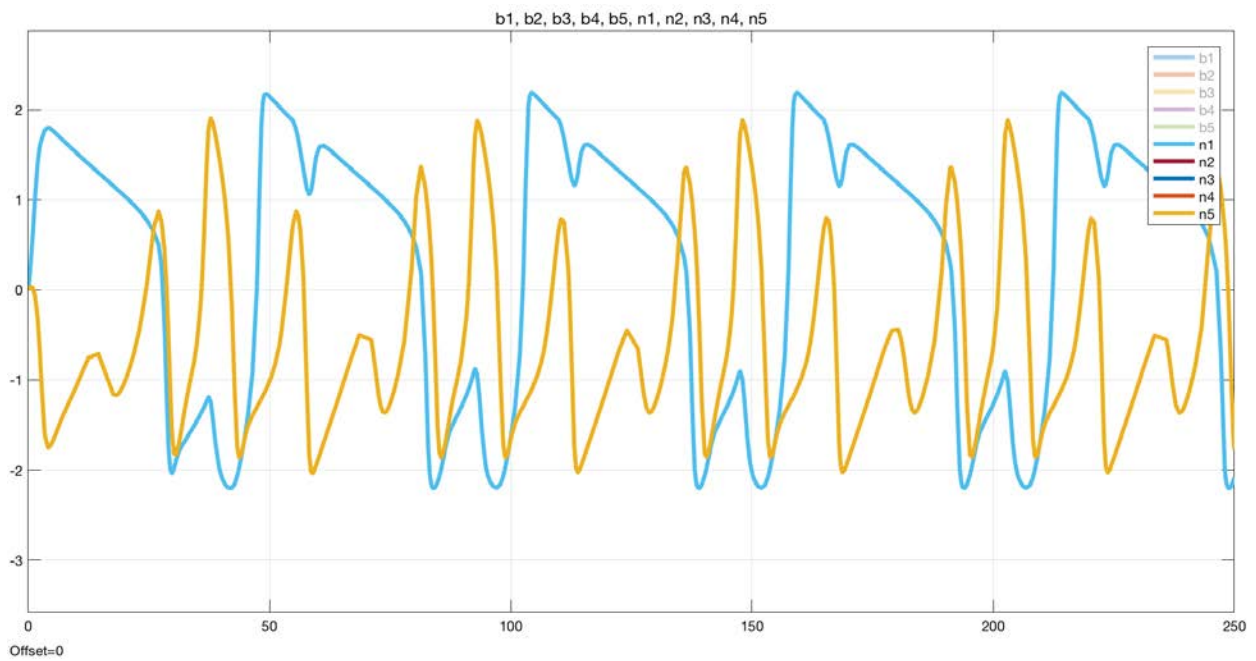


Figure 5-80: Five-neuron Fitzhugh-Nagumo inhibition winner-take-all network with low-pass filter feedback where  $\tau = 10$ ;  $I_1 = 0.5$ ;  $[I_2, I_3, I_4, I_5] = 0.1$ .

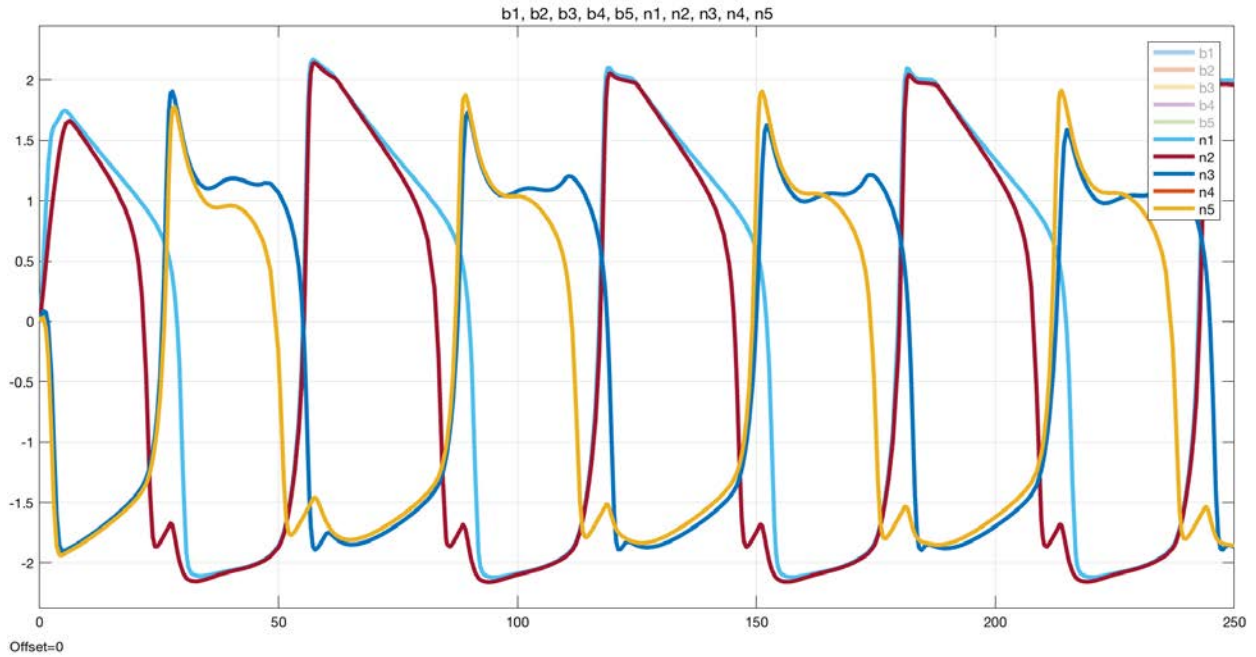


Figure 5-81: Five-neuron Fitzhugh-Nagumo inhibition winner-take-all network with low-pass filter feedback where  $\tau = 10$ ;  $I_1 = 0.5$ ;  $I_2 = 0.3$ ;  $I_3 = 0.15$ ;  $[I_4, I_5] = 0.1$ .

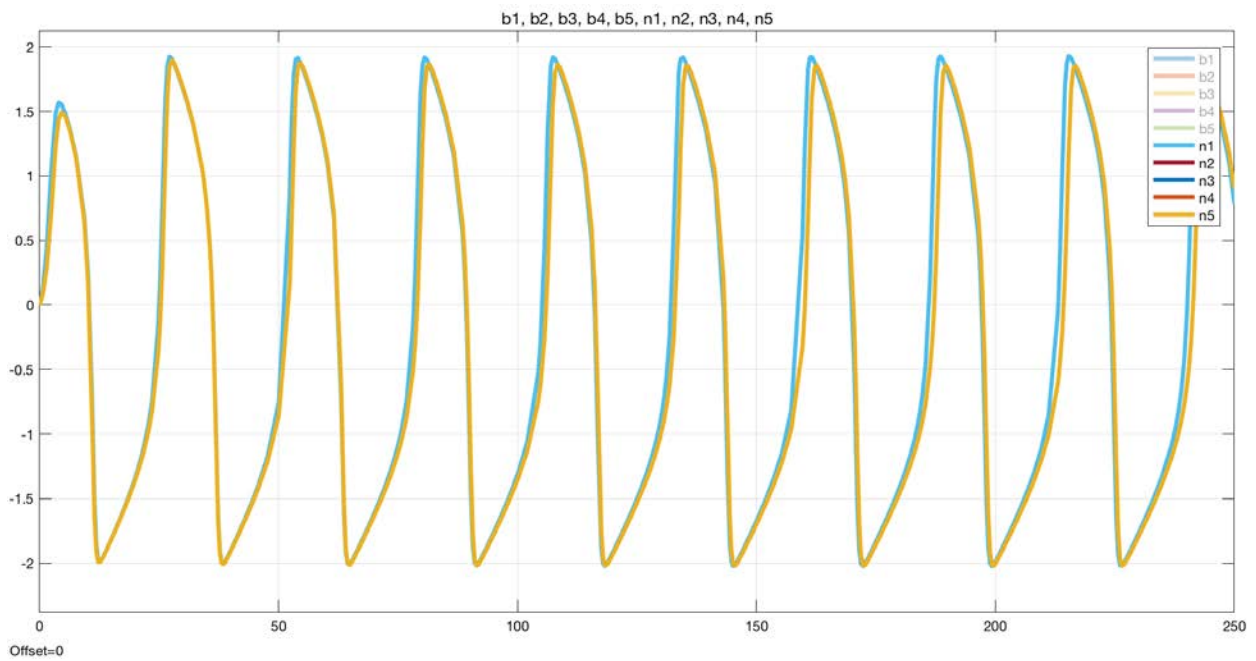


Figure 5-82: Five-neuron Fitzhugh-Nagumo inhibition winner-take-all network with low-pass filter feedback where  $\tau = 100$ ;  $I_1 = 0.15$ ;  $[I_2, I_3, I_4, I_5] = 0.1$ .

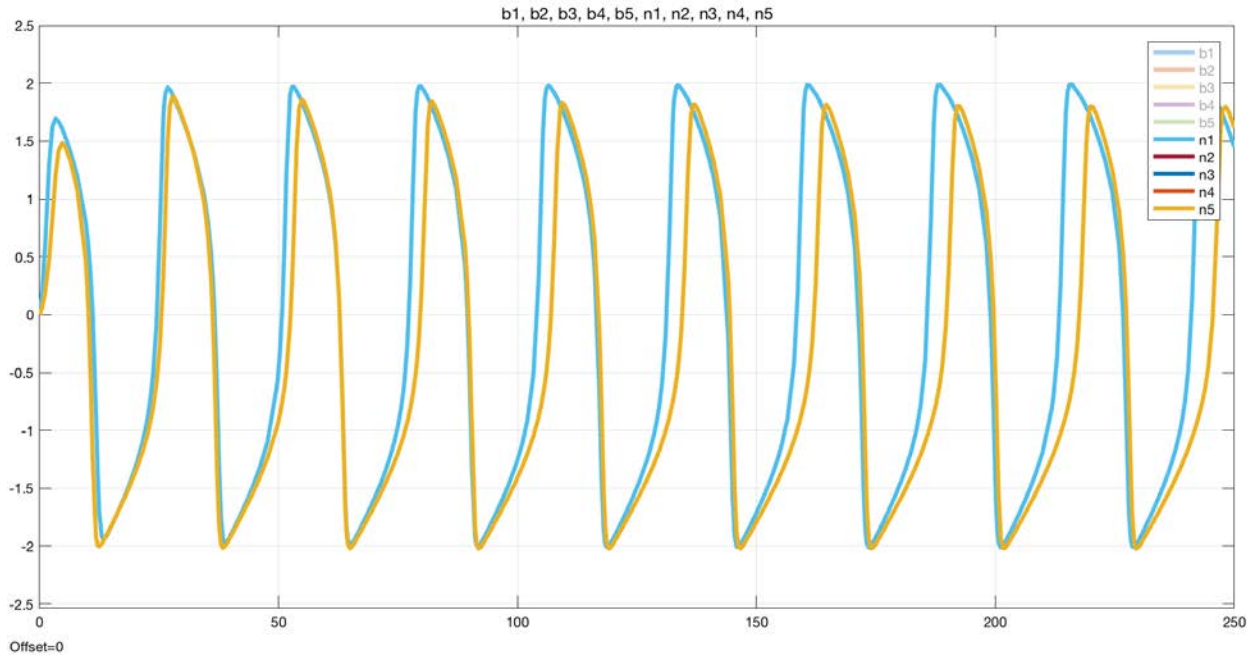


Figure 5-83: Five-neuron Fitzhugh-Nagumo inhibition winner-take-all network with low-pass filter feedback where  $\tau = 100$ ;  $I_1 = 0.3$ ;  $[I_2, I_3, I_4, I_5] = 0.1$ .

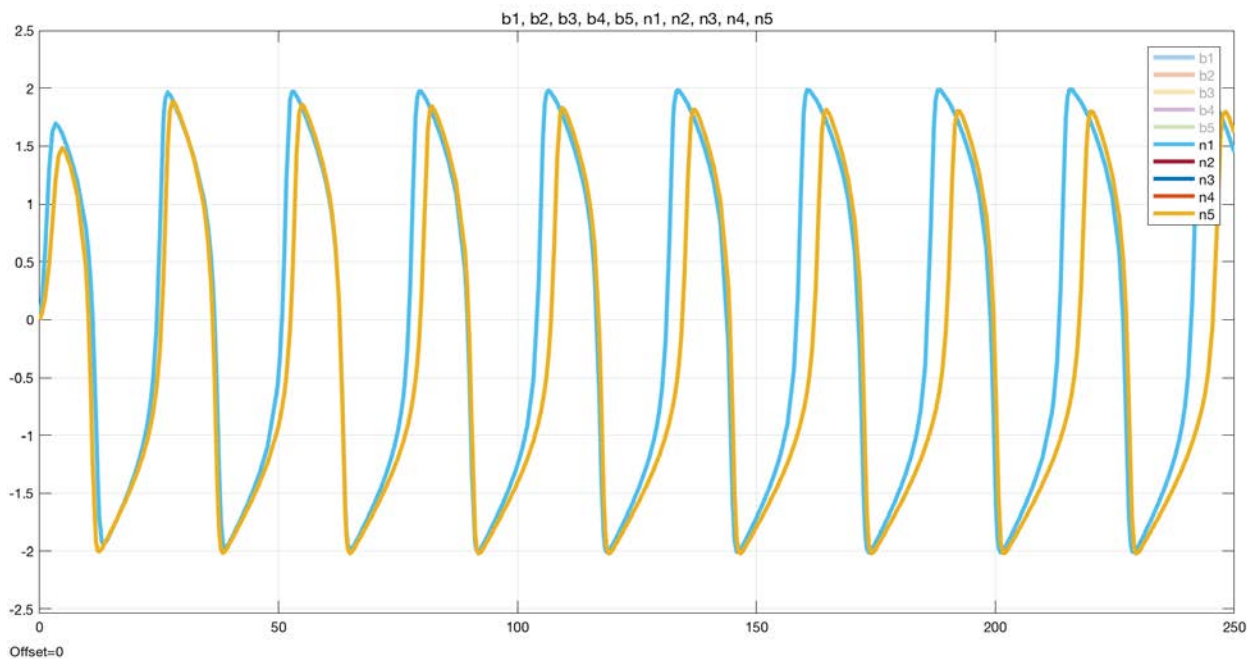


Figure 5-84: Five-neuron Fitzhugh-Nagumo inhibition winner-take-all network with low-pass filter feedback where  $\tau = 100$ ;  $I_1 = 0.5$ ;  $[I_2, I_3, I_4, I_5] = 0.1$ .

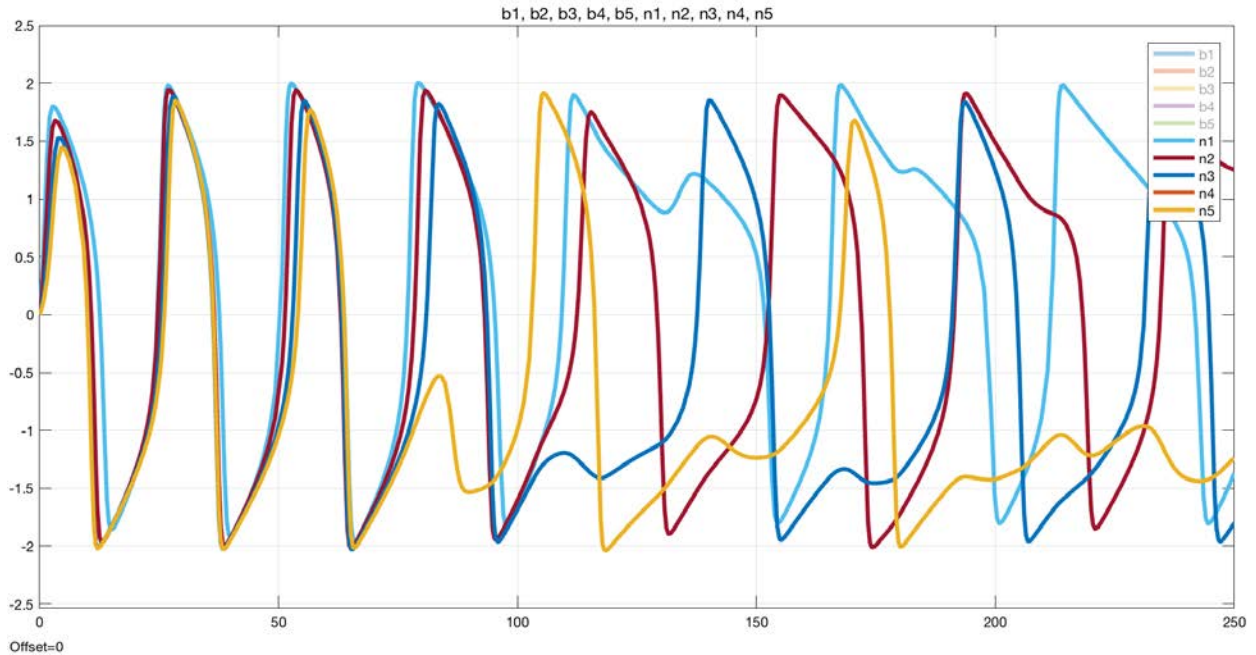


Figure 5-85: Five-neuron Fitzhugh-Nagumo inhibition winner-take-all network with low-pass filter feedback where  $\tau = 100$ ;  $I_1 = 0.5$ ;  $I_2 = 0.3$ ;  $I_3 = 0.15$ ;  $[I_4, I_5] = 0.1$ .

### 5.5.3 Global Interneuron Weighted Feedback

Figure 5-86 through Figure 5-88 show simulations of a 5-neuron weighted feedback network with a weight of 1. The network synchronizes with a 90-degree phase shift, where the spiking of neuron 1 is greater than the rest of the network. As the input current to neuron 1 is increased, the frequency of the neuron oscillations is increased proportionally, and the phase-shift is maintained. When the feedback weights are decreased, as in Figure 5-90 through Figure 5-92, the same observations can be made, with a slight difference in that the oscillation of the losers is increased nominally. Decreasing the weights of the feedback even further to 0.1, as shown in Figure 5-94 through Figure 5-96, again shows the same phase-shift and the amplitude of neuron 2 increasing.

Figure 5-89, Figure 5-93, and Figure 5-97 show simulations for varying input currents for feedback weight values of 1, 0.5, and 0.1, respectively. They show again that for varying input currents, the behavior of network changes for different values of feedback weights.

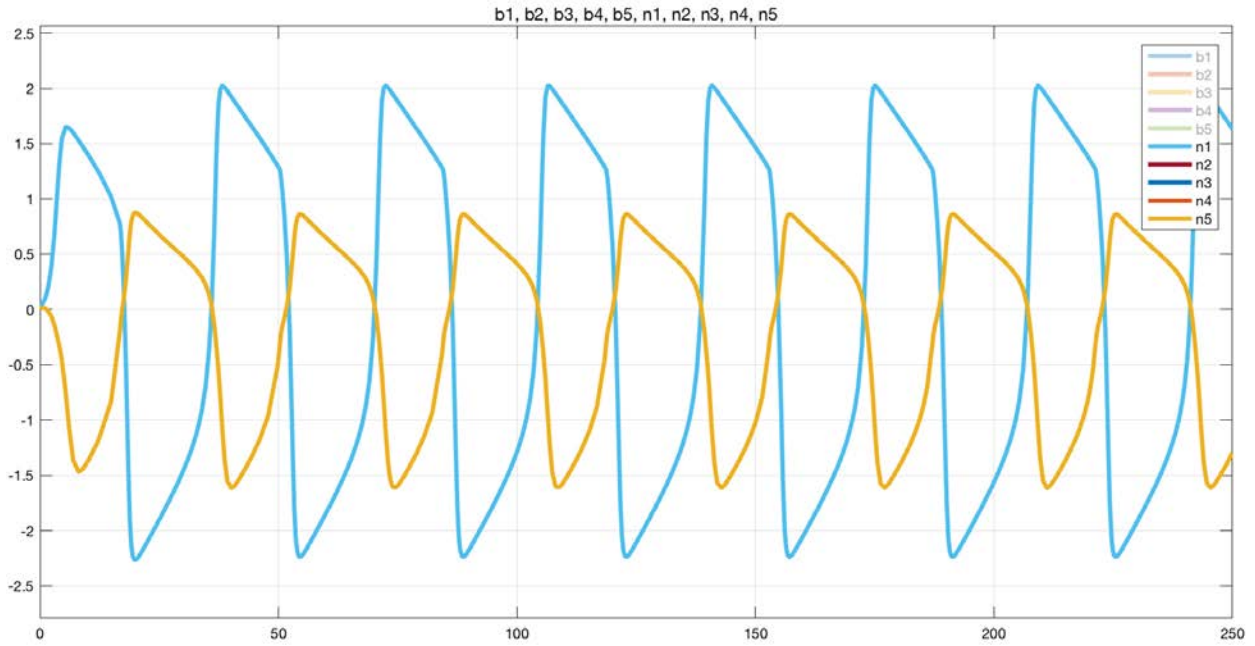


Figure 5-86: Five-neuron Fitzhugh-Nagumo interneuron winner-take-all network with weighted feedback of 1 where  $I_1 = 0.15$ ;  $[I_2, I_3, I_4, I_5] = 0.1$ .

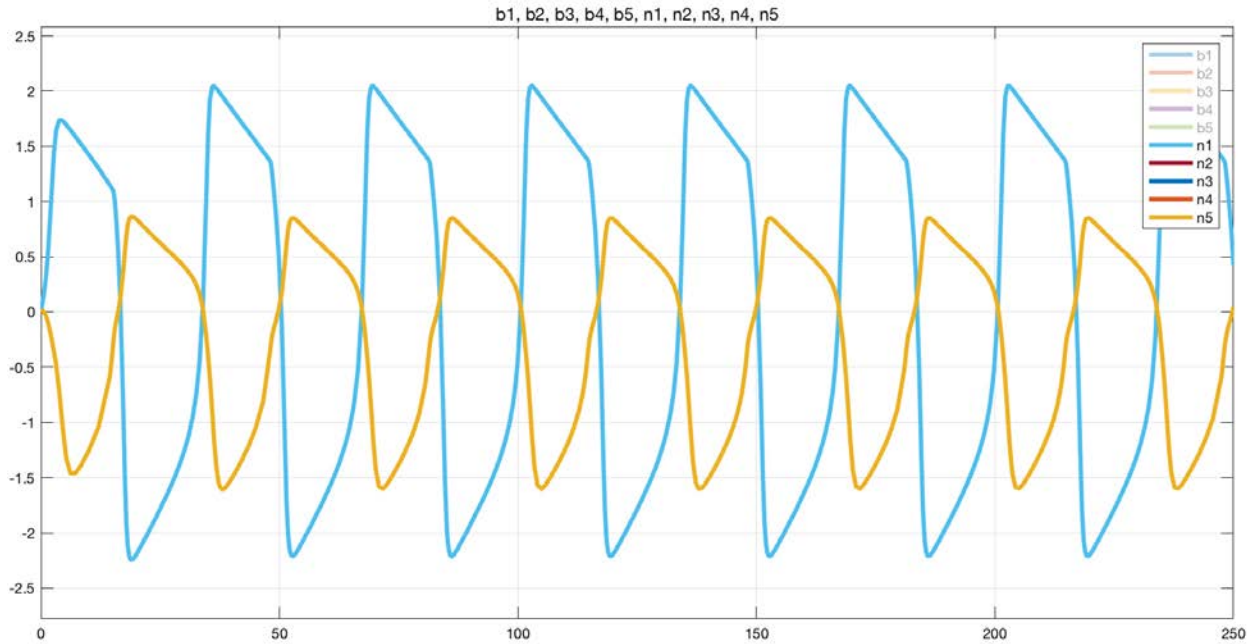


Figure 5-87: Five-neuron Fitzhugh-Nagumo interneuron winner-take-all network with weighted feedback of 1 where  $I1 = 0.3$ ;  $[I2, I3, I4, I5] = 0.1$ .

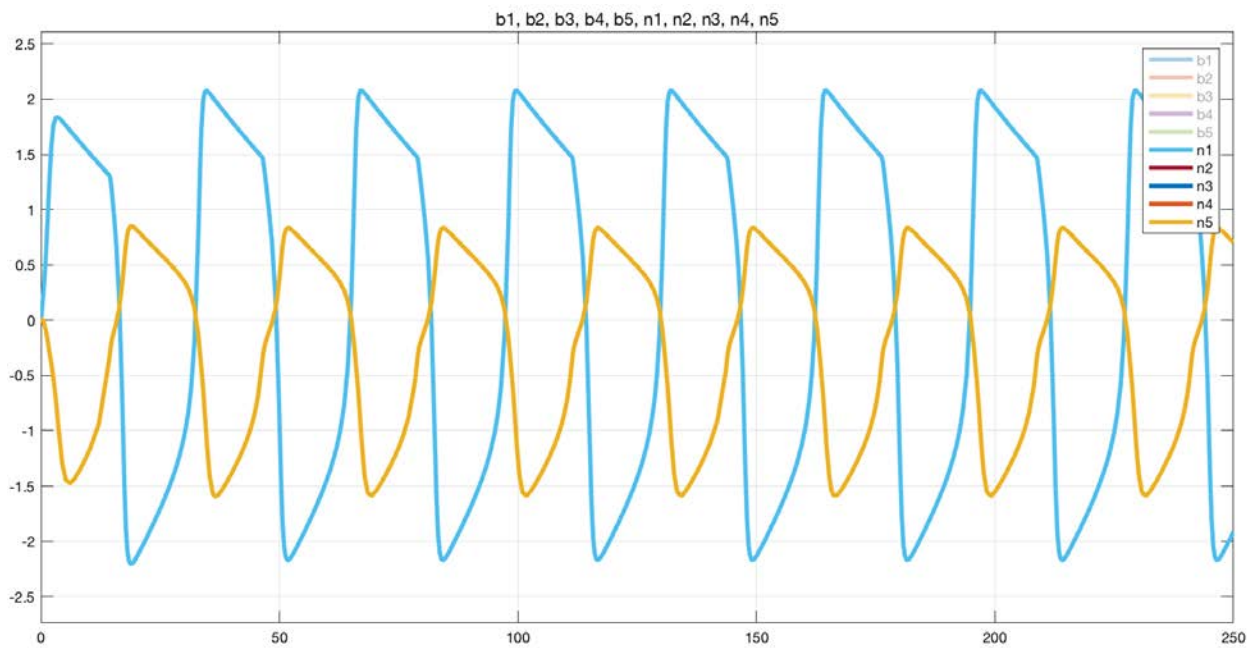


Figure 5-88: Five-neuron Fitzhugh-Nagumo interneuron winner-take-all network with weighted feedback of 1 where  $I1 = 0.5$ ;  $[I2, I3, I4, I5] = 0.1$ .

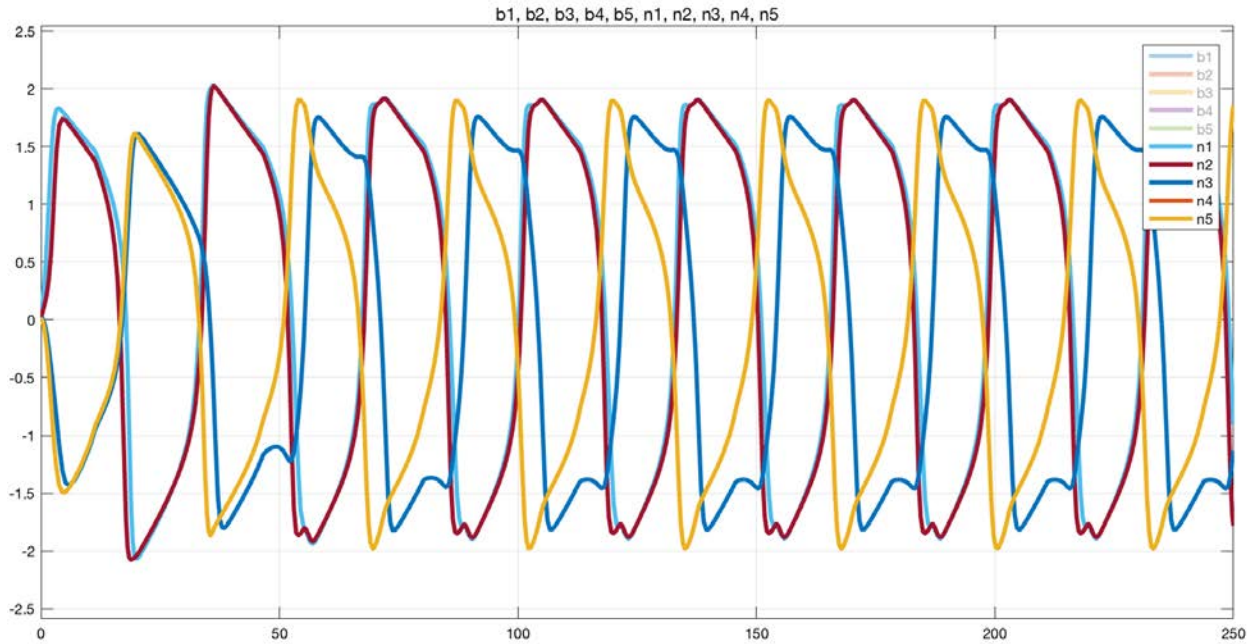


Figure 5-89: Five-neuron Fitzhugh-Nagumo interneuron winner-take-all network with weighted feedback of 1 where  $I1 = 0.5$ ;  $I2 = 0.3$ ;  $I1 = 0.15$ ;  $[I4, I5] = 0.1$ .

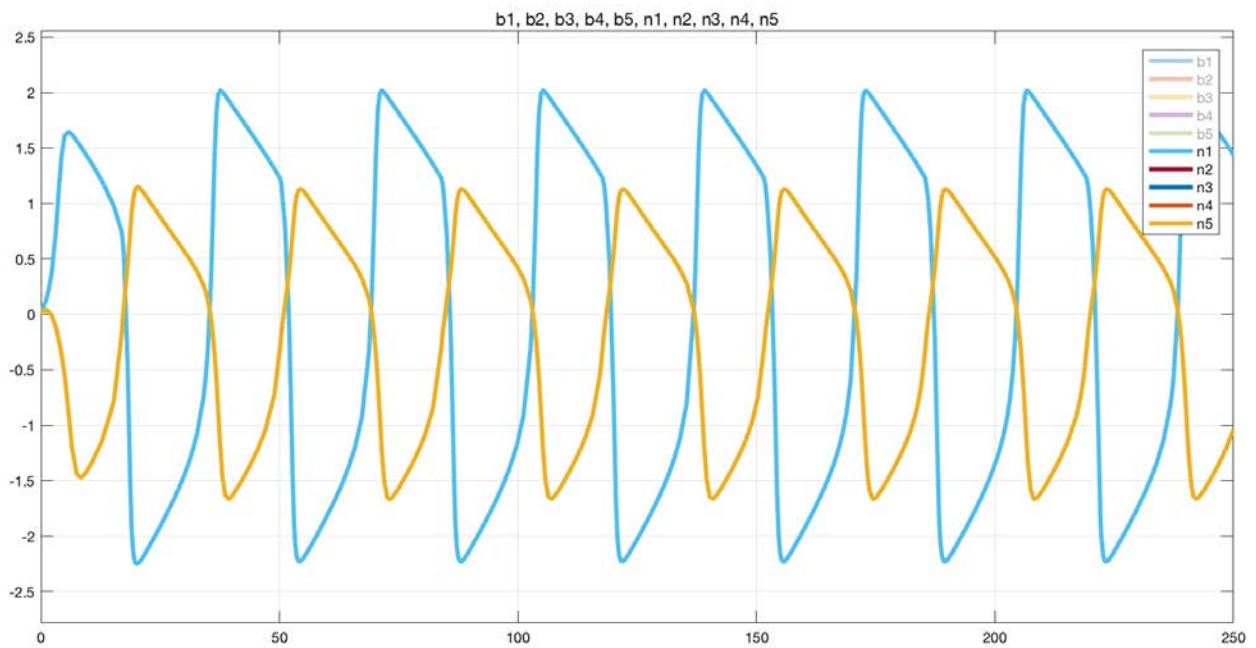


Figure 5-90: Five-neuron Fitzhugh-Nagumo interneuron winner-take-all network with weighted feedback of 0.5 where  $I1 = 0.15$ ;  $[I2, I3, I4, I5] = 0.1$ .

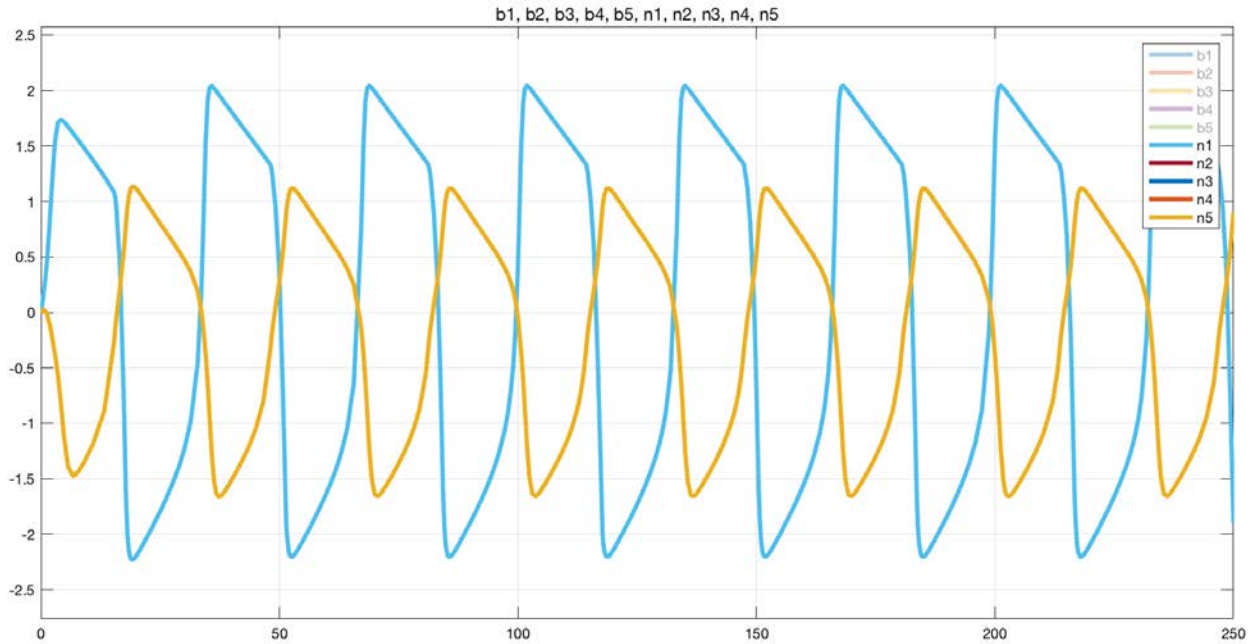


Figure 5-91: Five-neuron Fitzhugh-Nagumo interneuron winner-take-all network with weighted feedback of 0.5 where  $I1 = 0.3$ ;  $[I2, I3, I4, I5] = 0.1$ .

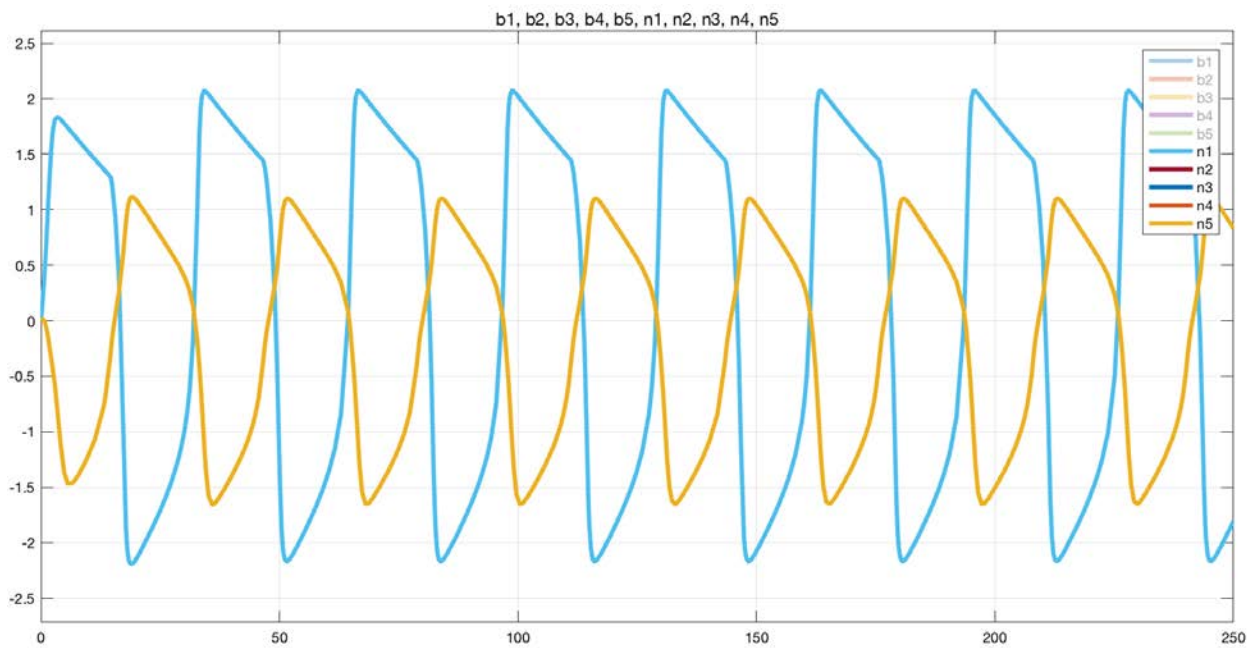


Figure 5-92: Five-neuron Fitzhugh-Nagumo interneuron winner-take-all network with weighted feedback of 0.5 where  $I1 = 0.5$ ;  $[I2, I3, I4, I5] = 0.1$ .

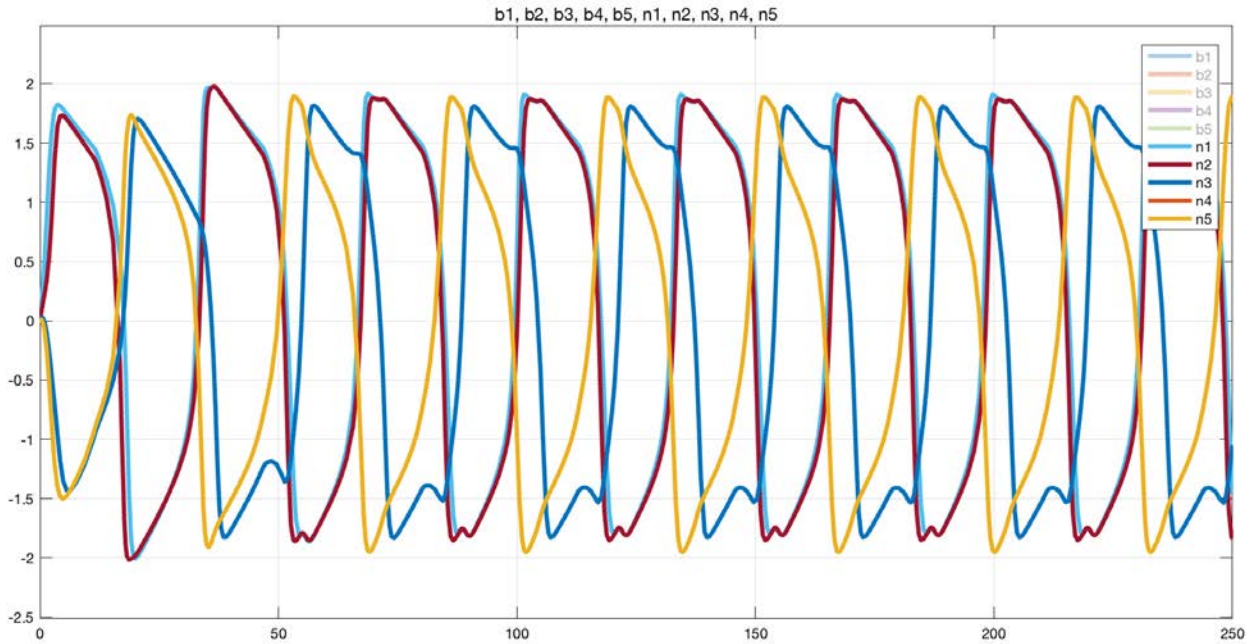


Figure 5-93: Five-neuron Fitzhugh-Nagumo interneuron winner-take-all network with weighted feedback of 0.5 where  $I1 = 0.5$ ;  $I2 = 0.3$ ;  $I1 = 0.15$ ;  $[I4, I5] = 0.1$ .

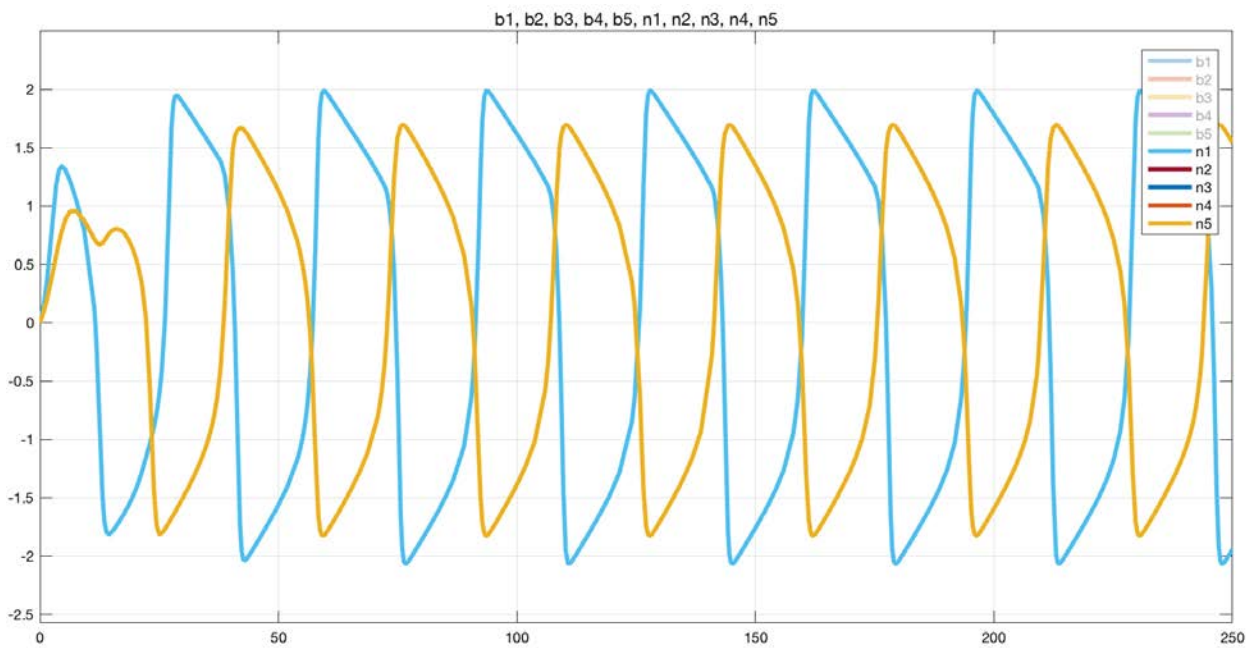


Figure 5-94: Five-neuron Fitzhugh-Nagumo interneuron winner-take-all network with weighted feedback of 0.1 where  $I1 = 0.15$ ;  $[I2, I3, I4, I5] = 0.1$ .

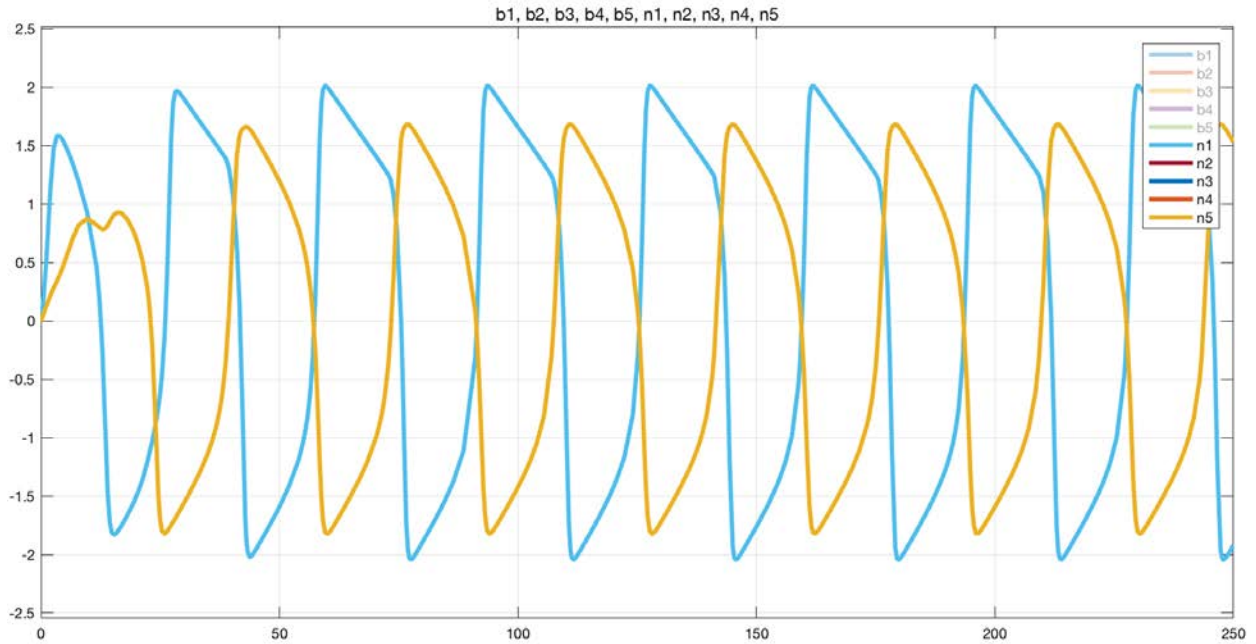


Figure 5-95: Five-neuron Fitzhugh-Nagumo interneuron winner-take-all network with weighted feedback of 0.1 where  $I1 = 0.3$ ;  $[I2, I3, I4, I5] = 0.1$ .

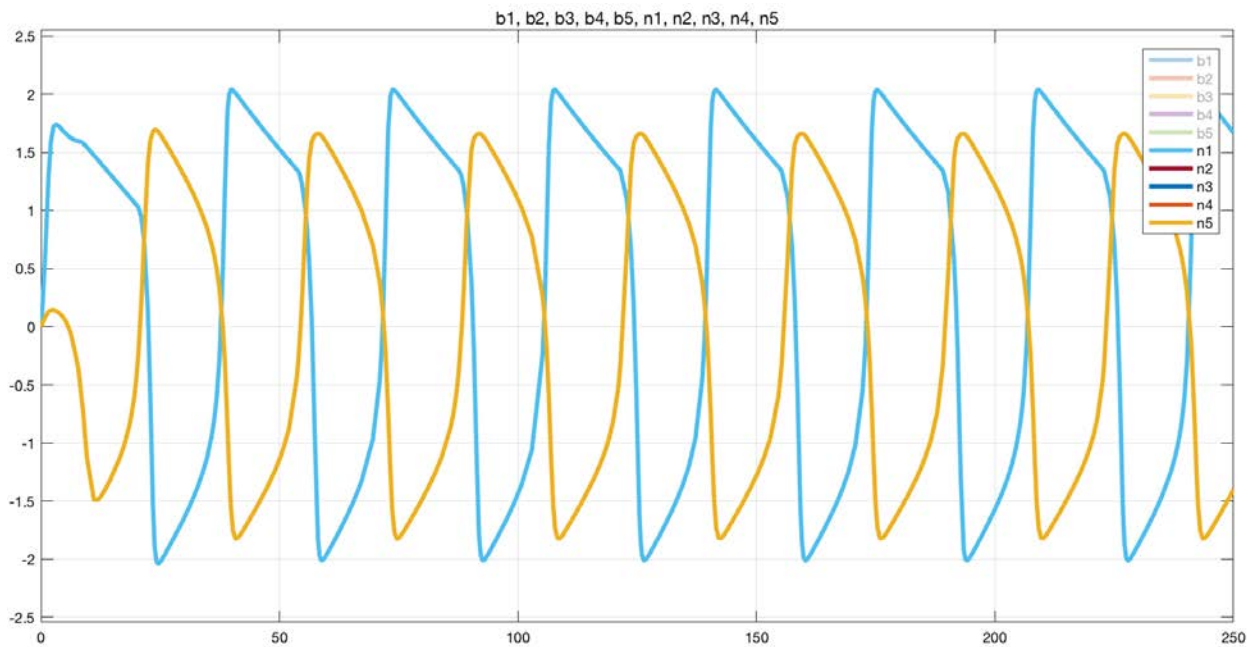


Figure 5-96: Five-neuron Fitzhugh-Nagumo interneuron winner-take-all network with weighted feedback of 0.1 where  $I1 = 0.5$ ;  $[I2, I3, I4, I5] = 0.1$ .

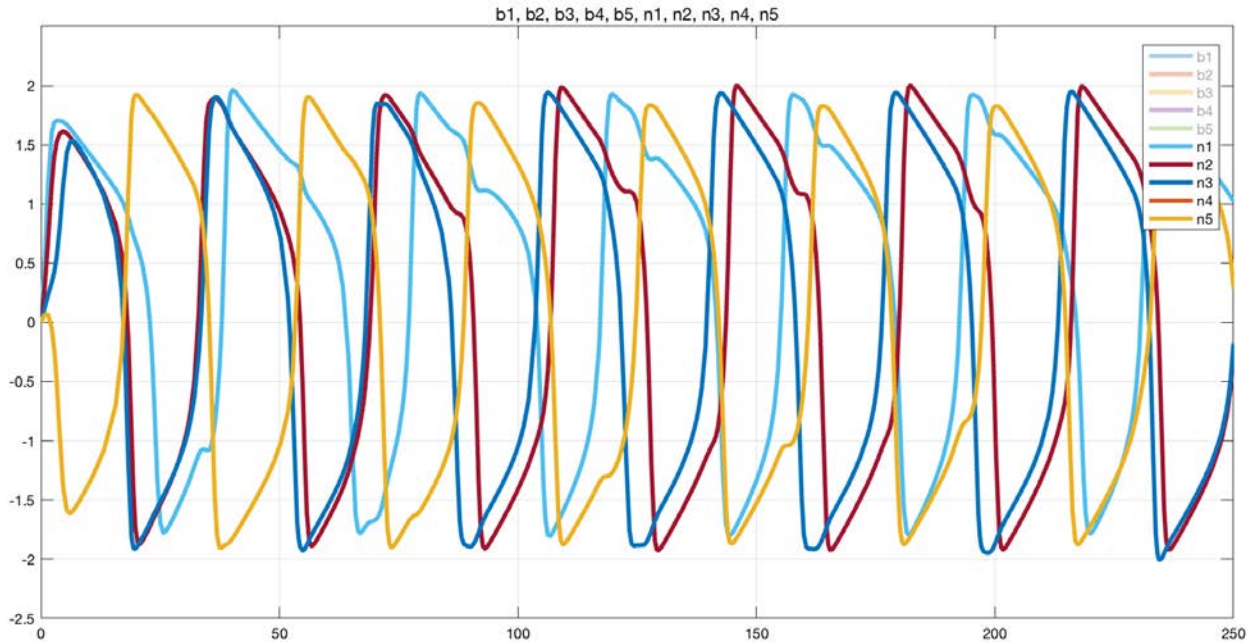


Figure 5-97: Five-neuron Fitzhugh-Nagumo interneuron winner-take-all network with weighted feedback of 0.1 where  $I_1 = 0.5$ ;  $I_2 = 0.3$ ;  $I_3 = 0.15$ ;  $[I_4, I_5] = 0.1$ .

#### 5.5.4 Global Interneuron Low-Pass Filter

Figure 5-98 through Figure 5-100 show simulations of a 5-neuron low-pass feedback network with a time constant value of 0.1. It can be observed that there is not much impact increasing the input current of neuron 1 has on the network. There is still a 90-phase shift between the winner and losers. Figure 5-102 through Figure 5-104 show that after increasing the time-constant to 10, the network has a difficult time distinguishing between winners and losers. They appear to be synchronized in the same phase with the same frequency. Though as the input current to neuron 1 is increased, it does shift slightly ahead of the rest of the network. Figure 5-106 through Figure 5-108 show similar results, in that for close input current values, a winner is indistinguishable. As the input current increases, there gradually becomes a phase-shift. Figure

5-101, Figure 5-105, and Figure 5-109 show simulation results for varying input currents for time-constant values of 0.1, 10, and 100, respectively. They show that for smaller time-constants, the network does not synchronize, but as the time-constant increases, the network becomes more stable and the phase-shift of the neuron outputs corresponds to the order of the winners.

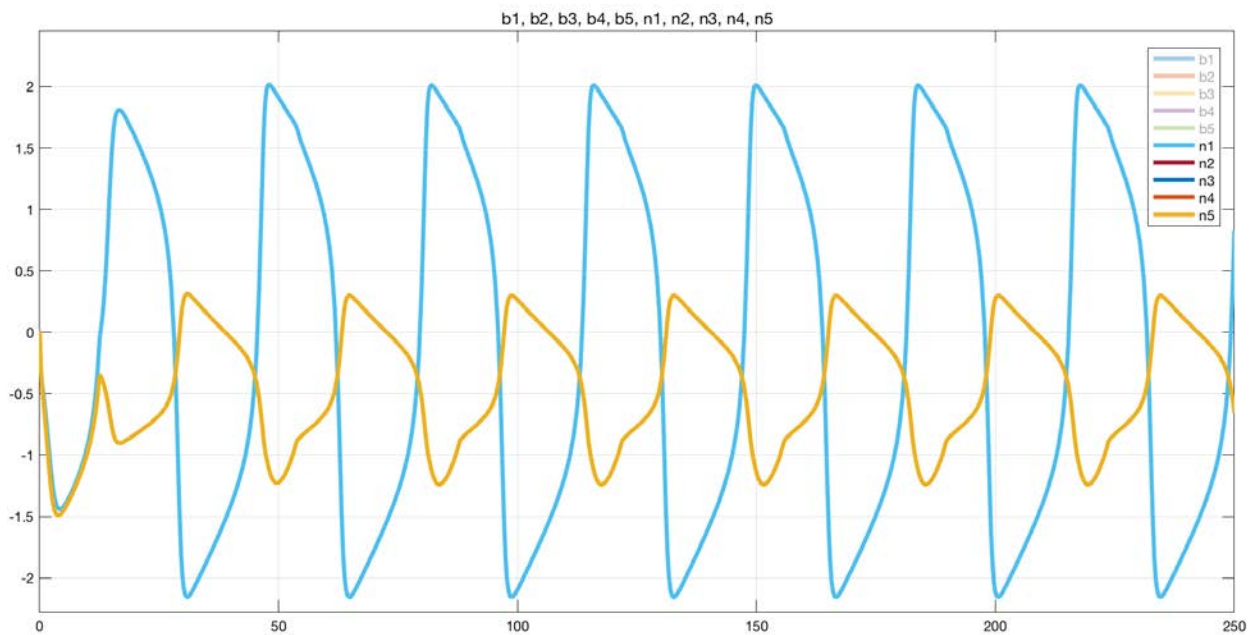


Figure 5-98: Five-neuron Fitzhugh-Nagumo interneuron winner-take-all network with low-pass filter feedback where  $\tau = 0.1$ ;  $I_1 = 0.15$ ;  $[I_2, I_3, I_4, I_5] = 0.1$ .

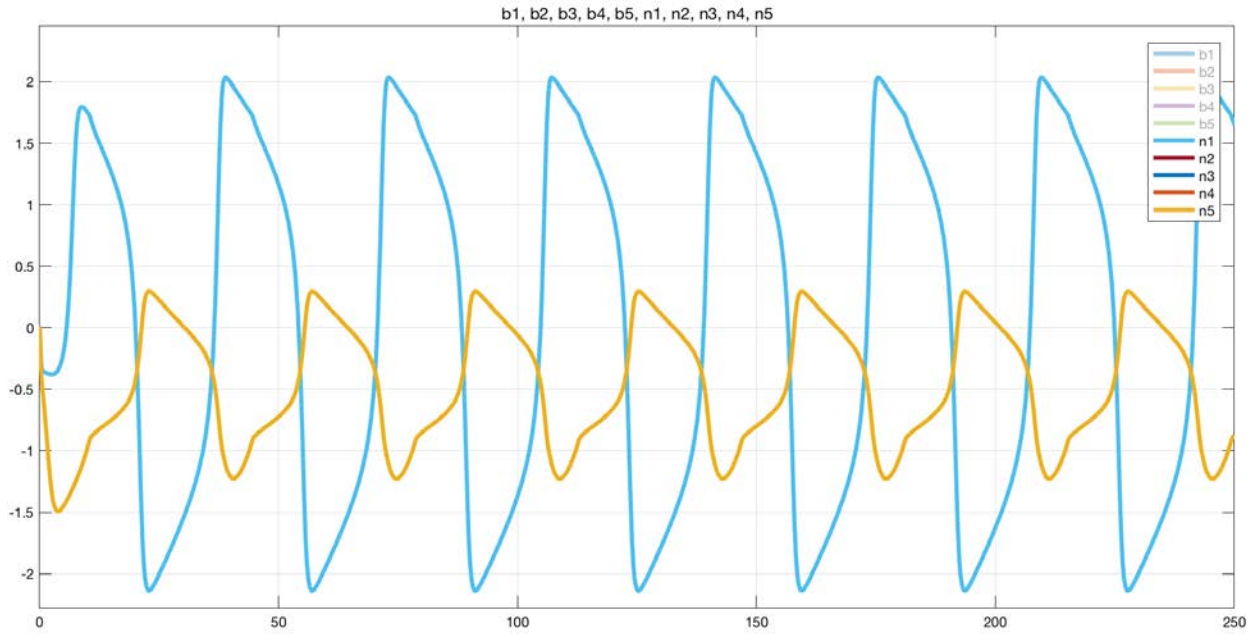


Figure 5-99: Five-neuron Fitzhugh-Nagumo interneuron winner-take-all network with low-pass filter feedback where  $\tau = 0.1$ ;  $I_1 = 0.3$ ;  $[I_2, I_3, I_4, I_5] = 0.1$ .

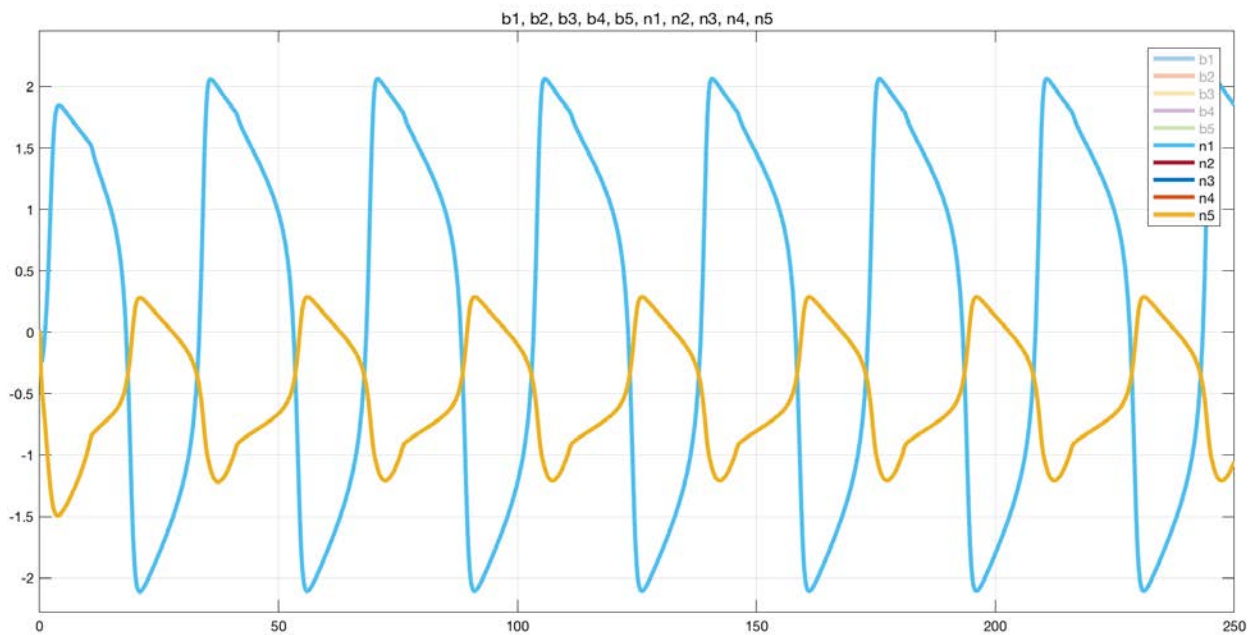


Figure 5-100: Five-neuron Fitzhugh-Nagumo interneuron winner-take-all network with low-pass filter feedback where  $\tau = 0.1$ ;  $I_1 = 0.5$ ;  $[I_2, I_3, I_4, I_5] = 0.1$ .

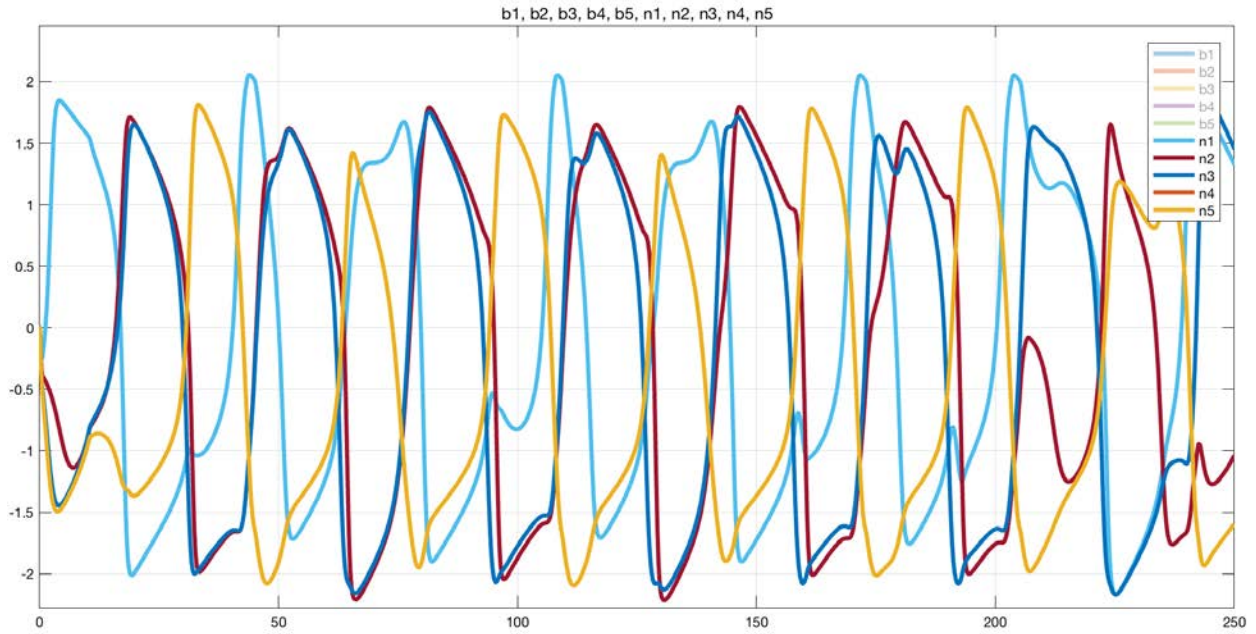


Figure 5-101: Five-neuron Fitzhugh-Nagumo interneuron winner-take-all network with low-pass filter feedback where  $\tau = 0.1$ ;  $I_1 = 0.5$ ;  $I_2 = 0.3$ ;  $I_3 = 0.15$ ;  $[I_4, I_5] = 0.1$ .

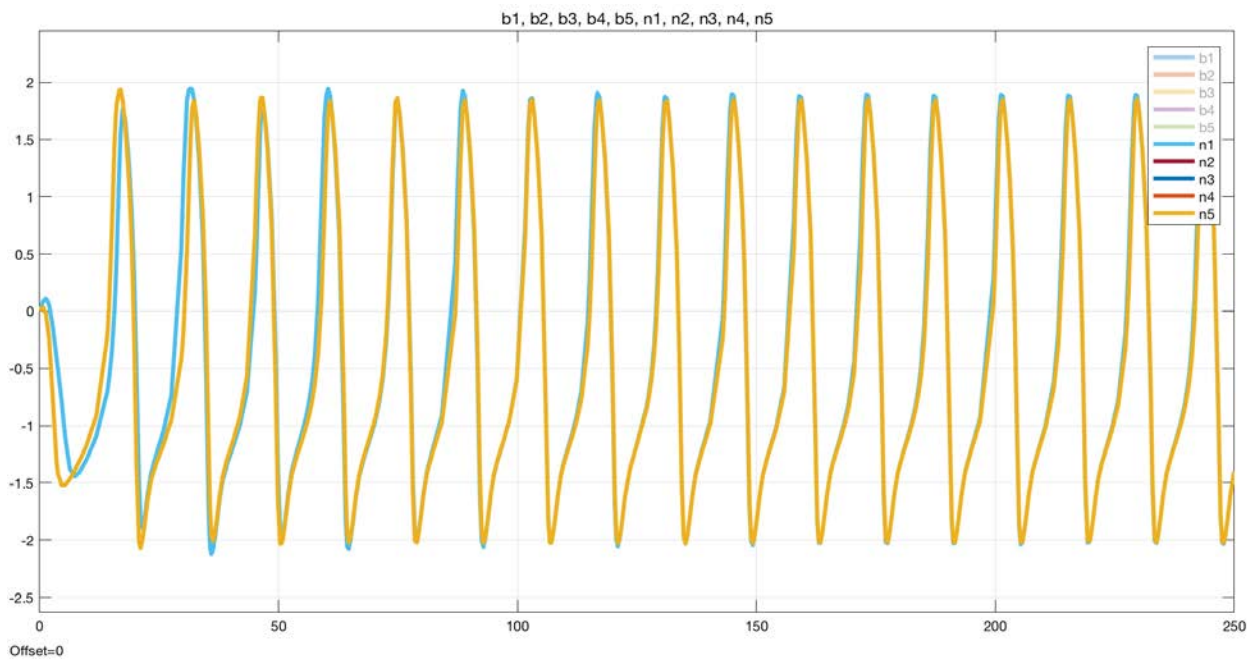


Figure 5-102: Five-neuron Fitzhugh-Nagumo interneuron winner-take-all network with low-pass filter feedback where  $\tau = 10$ ;  $I_1 = 0.15$ ;  $[I_2, I_3, I_4, I_5] = 0.1$ .

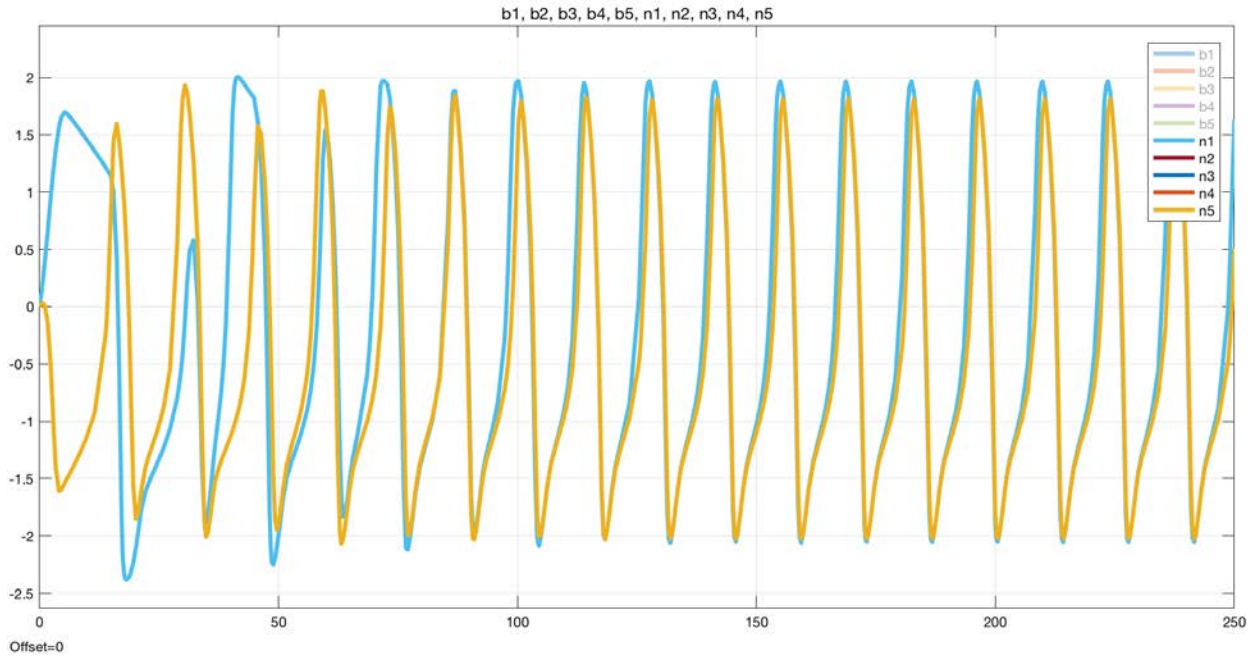


Figure 5-103: Five-neuron Fitzhugh-Nagumo interneuron winner-take-all network with low-pass filter feedback where  $\tau = 10$ ;  $I_1 = 0.3$ ;  $[I_2, I_3, I_4, I_5] = 0.1$ .

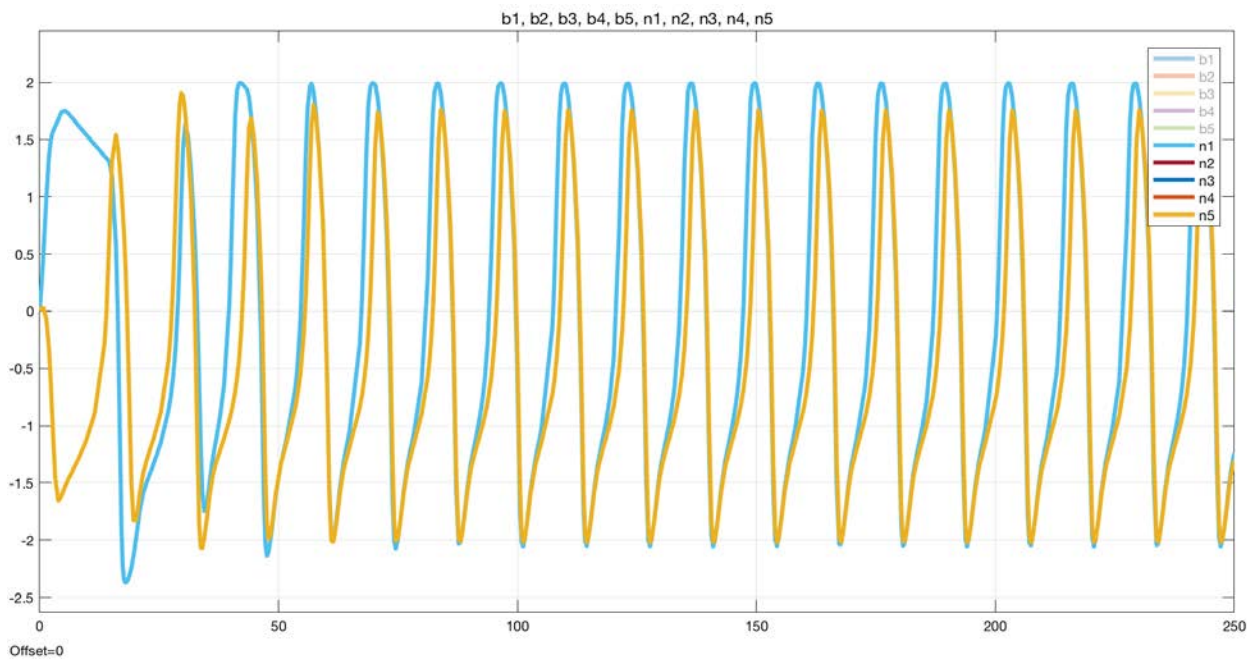


Figure 5-104: Five-neuron Fitzhugh-Nagumo interneuron winner-take-all network with low-pass filter feedback where  $\tau = 10$ ;  $I_1 = 0.5$ ;  $[I_2, I_3, I_4, I_5] = 0.1$ .

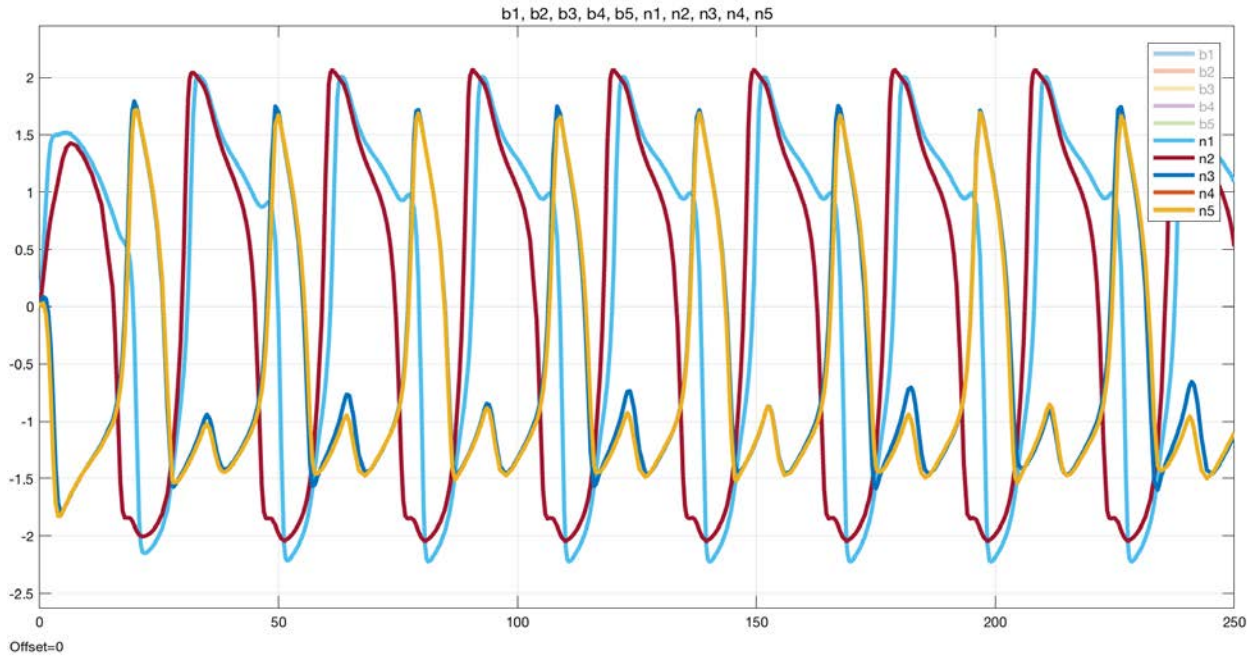


Figure 5-105: Five-neuron Fitzhugh-Nagumo interneuron winner-take-all network with low-pass filter feedback where  $\tau = 10$ ;  $I_1 = 0.5$ ;  $I_2 = 0.3$ ;  $I_3 = 0.15$ ;  $[I_4, I_5] = 0.1$ .

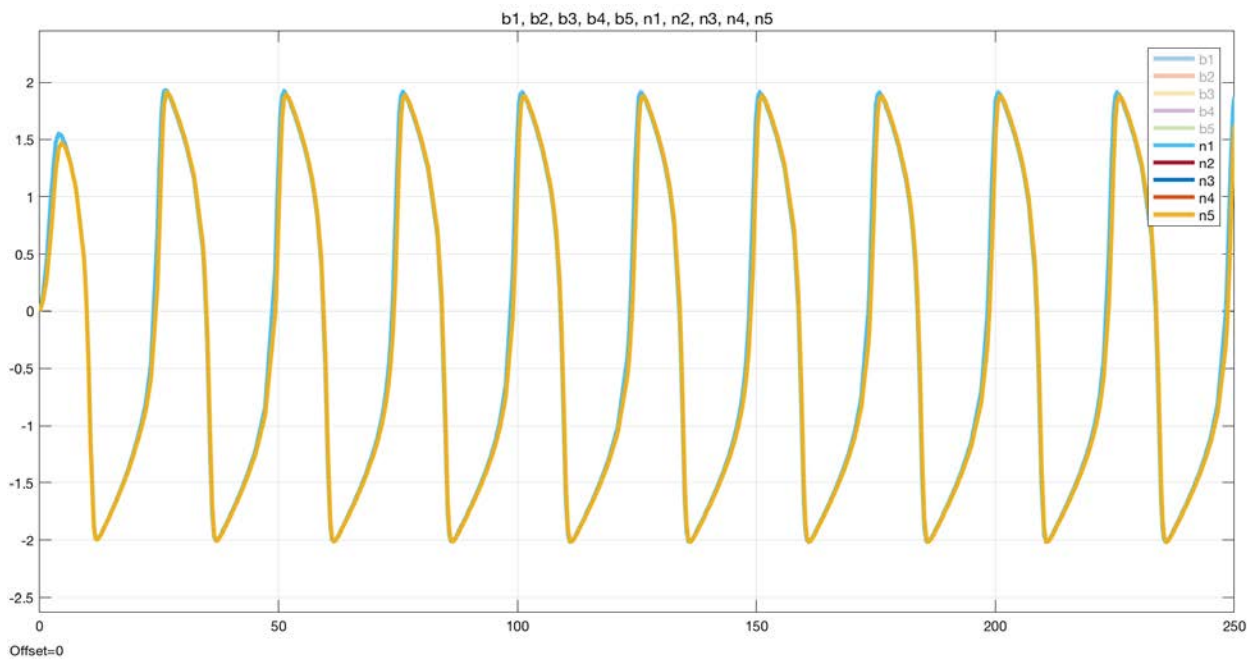


Figure 5-106: Five-neuron Fitzhugh-Nagumo interneuron winner-take-all network with low-pass filter feedback where  $\tau = 100$ ;  $I_1 = 0.15$ ;  $[I_2, I_3, I_4, I_5] = 0.1$ .

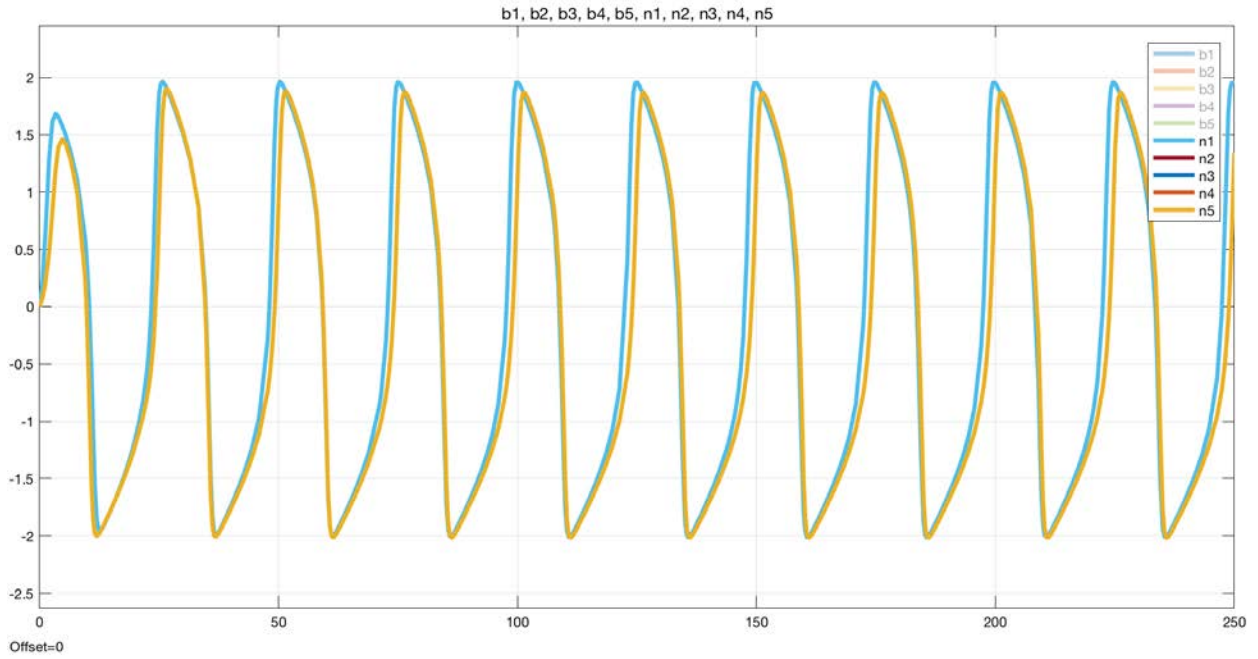


Figure 5-107: Five-neuron Fitzhugh-Nagumo interneuron winner-take-all network with low-pass filter feedback where  $\tau = 100$ ;  $I_1 = 0.3$ ;  $[I_2, I_3, I_4, I_5] = 0.1$ .

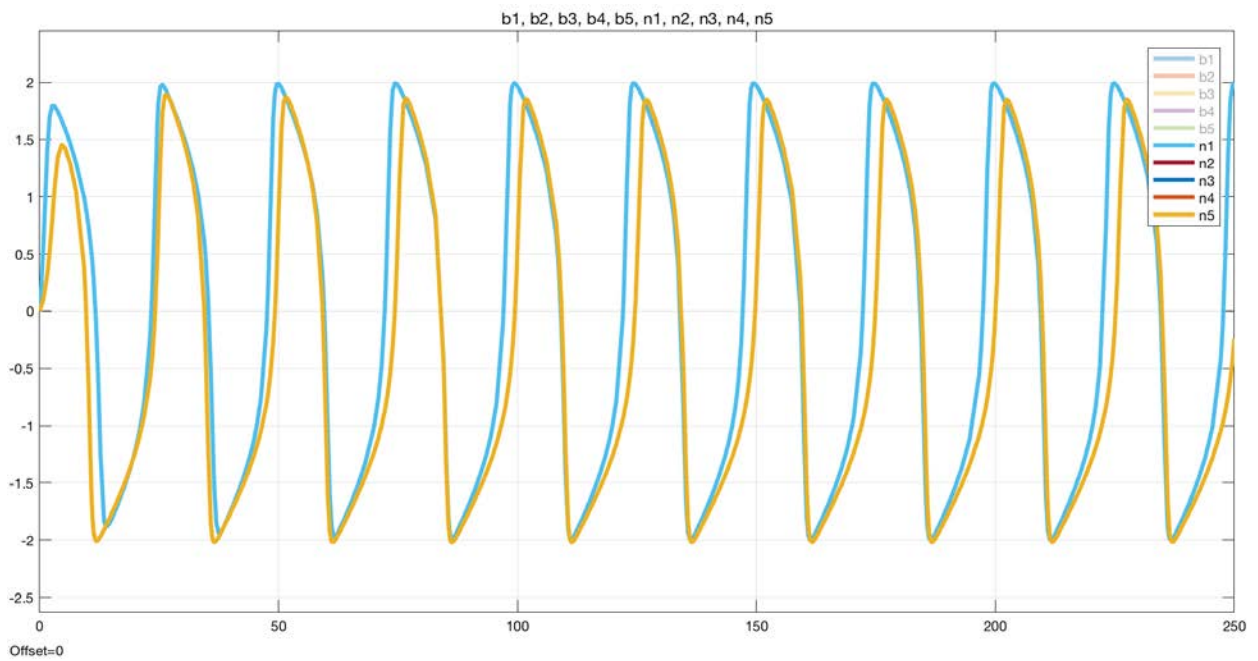


Figure 5-108: Five-neuron Fitzhugh-Nagumo interneuron winner-take-all network with low-pass filter feedback where  $\tau = 100$ ;  $I_1 = 0.5$ ;  $[I_2, I_3, I_4, I_5] = 0.1$ .

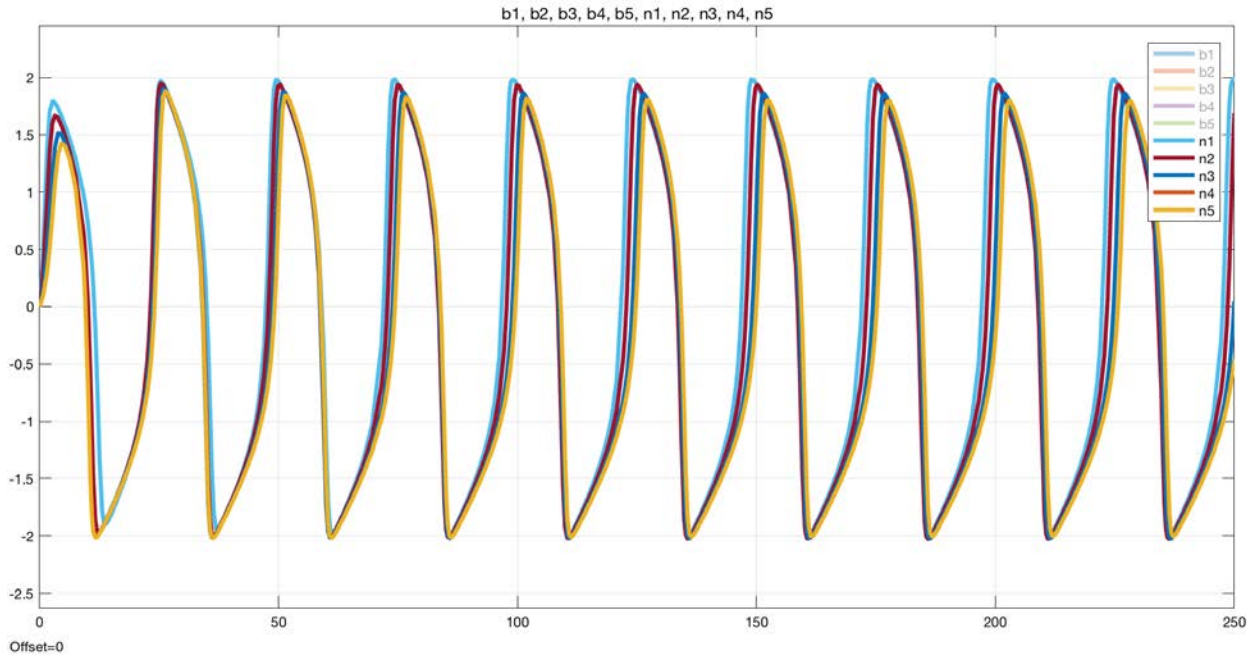


Figure 5-109: Five-neuron Fitzhugh-Nagumo interneuron winner-take-all network with low-pass filter feedback where  $\tau = 100$ ;  $I_1 = 0.5$ ;  $I_2 = 0.3$ ;  $I_3 = 0.15$ ;  $[I_4, I_5] = 0.1$ .

## 6.0 Conclusions

As interest and importance grows in the neuronal network space, it becomes critical to creatively and effectively model different types of networks to understand their behavior. There is a very broad range of applications for neuronal networks such as associative memory, neuromorphic computing, artificial intelligence, and image and audio processing. Neuronal networks are also important in regard to biology, as being able to develop accurate biologically plausible neuronal networks enable for the study of various neurological diseases and conditions.

In this dissertation multiple models of winner-take-all based on both lateral inhibition and interneuron have been simulated and analyzed. Previous work analyzing the dynamics of winner-take-all based on postsynaptic membrane potential was reviewed and then reproduced to compare the original model based on lateral inhibition with a different model with an interneuron topology. What was shown was that despite the difference in the amount of feedback, or inhibition, the models provided, their behavior was quite similar.

This dissertation also examined biologically plausible winner-take-all models based on two different types of neurons, the Hodgkin-Huxley neuron and the Fitzhugh-Nagumo neuron. The Hodgkin-Huxley neuronal model is valuable in that it is a model derived from an actual neuron from a squid. However, its dimensionality made it particularly complex to theoretically analyze and simulate so the Fitzhugh-Nagumo model simplified it. In this dissertation the Fitzhugh-Nagumo neuron was theoretically analyzed to gather insight about its behavior in a winner-take-all-network.

Unlike other works on lateral inhibition based winner-take-all that focus on inhibition in the sense of the suppression of other signals in a network, both biological models were simulated

and analyzed in terms of their ability synchronize in phase. In addition, each biological model was simulated using two different types of feedback. One was a weighted feedback that essentially simulated the strength of neuronal connections. The other was a low-pass filter, that with a sufficient time-constant, behaves like a DC signal, i.e. external current.

What was observed was using a simple summation of the feedback, similar to the firing rate model, both models were able to synchronize and differ by a shift in phase depending on the winner and the parameters of the models. There was also an observed difference between the way the complex Hodgkin-Huxley model synchronized and the simpler Fitzhugh-Nagumo model synchronized. The Hodgkin Huxley model took much more time to synchronize than the Fitzhugh-Nagumo. The Fitzhugh-Nagumo model was generally more definitive in terms of a winner than the Hodgkin-Huxley. In addition to simulating the lateral inhibition using the biological neuronal models, this dissertation also simulated the interneuron variant. These simulations were then compared to the lateral inhibition.

Because of the simplicity of the postsynaptic model, it is clearly more capable of discerning a winner. Operating as a function of firing rate, it is able to compute winner-take-all without the complexities of a true biological model. There is some, though relatively small, difference between the lateral inhibition variant and the global interneuron variant. Though this provides a simple and functioning model of winner-take-all, it is not a biologically plausible model which could be used in applications that need to consider biological aspects of neurons such as neuronal membrane potential and ionic channels. Future work of this dissertation may include observing the impact of biological parameters on synchronization behavior. The models used in this work, use “normal” parameter settings, but do not look at how, for example, the ratio of the ionic channels in the Hodgkin-Huxley model would impact the network behavior. In addition, further analysis of the

Fitzhugh-Nagumo model could be done to address some of the anomalies in the behavior, such as the stability of the system for particular input currents. Considering the simplicity and low-dimensional nonbiological models such as the postsynaptic model, it would be worth researching how to achieve simpler winner-take-all neuronal network that can retain the relevant biological attributes needed for particular applications.

# Appendix A

## Simulink Block Diagrams

This appendix shows diagrams of the neuron models in Simulink.

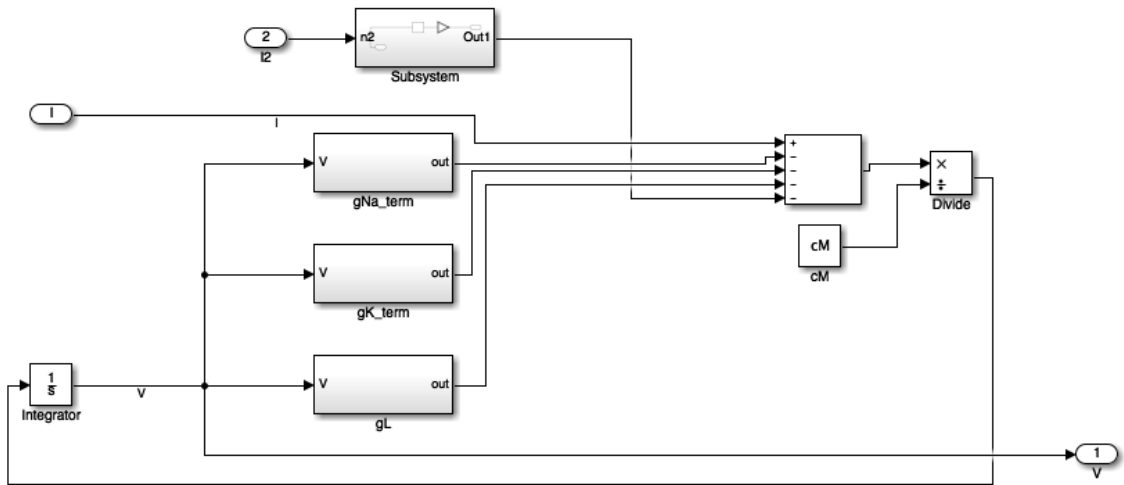


Figure 6-1: Hodgkin-Huxley neuron with feedback.

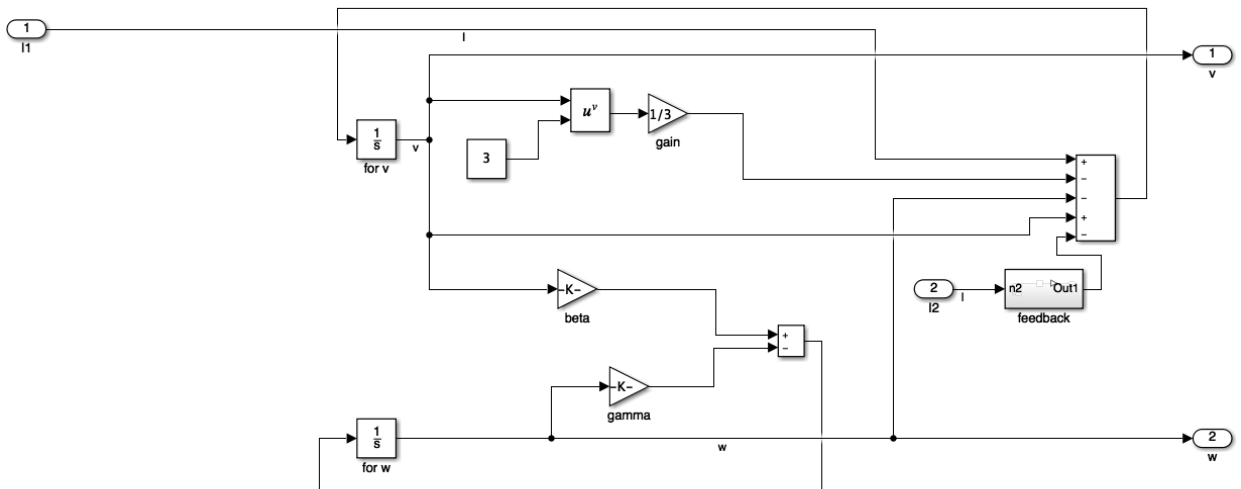


Figure 6-2: Fitzhugh-Nagumo neuron with feedback.

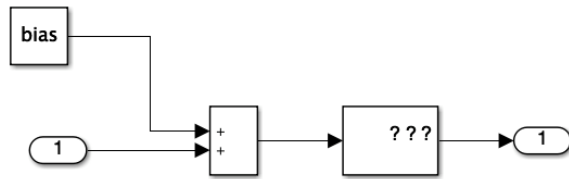


Figure 6-3: Low-pass filter feedback.

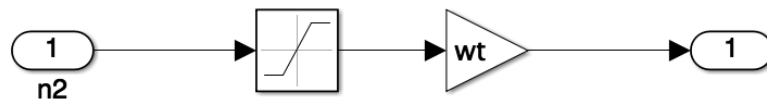


Figure 6-4: Weighted feedback.

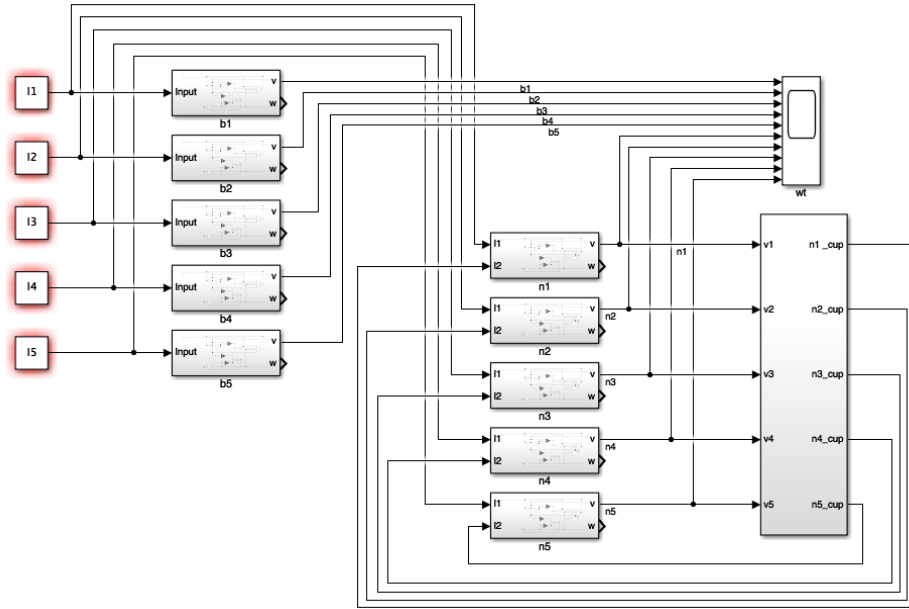


Figure 6-5: Five-neuron network

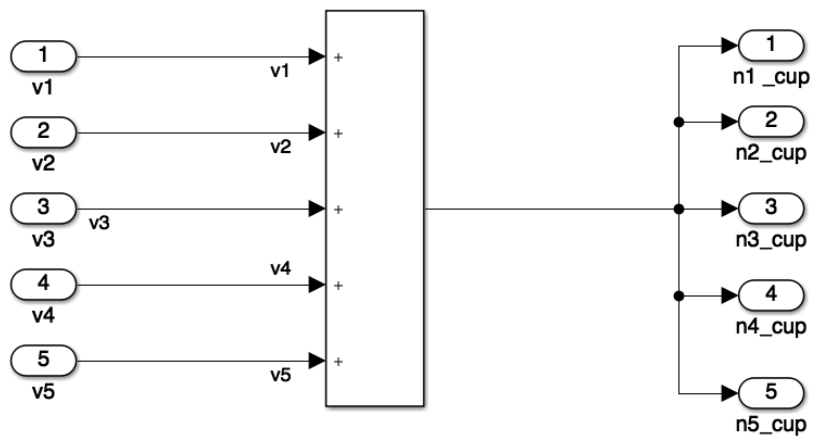


Figure 6-6: Interneuron coupling.

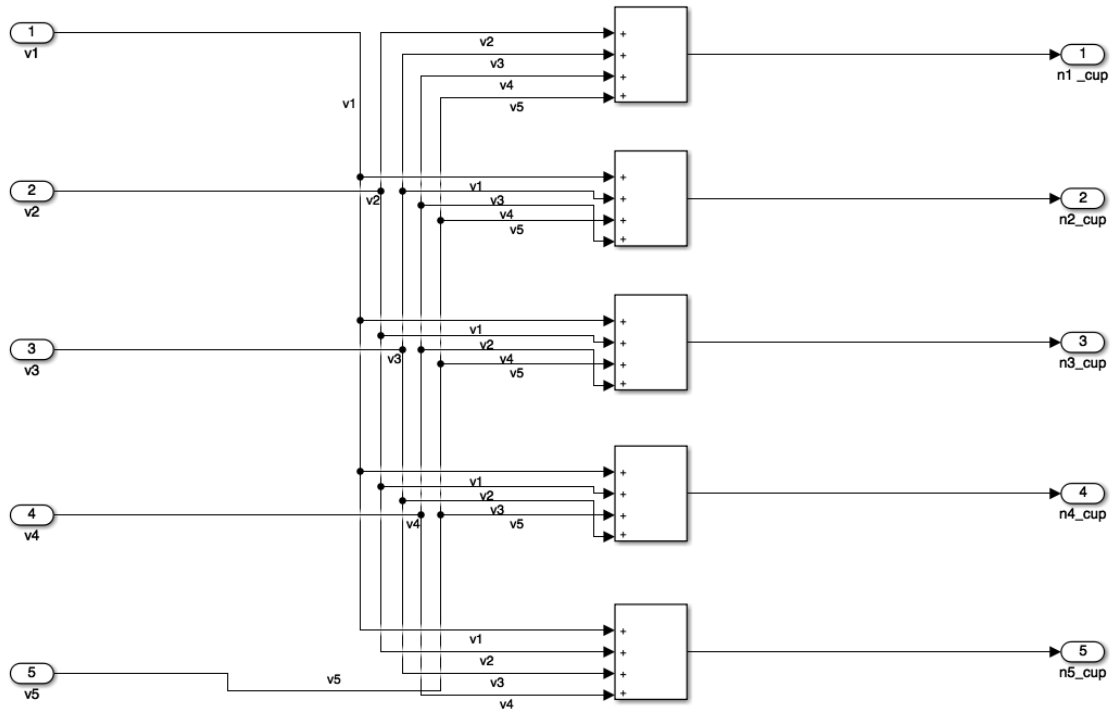


Figure 6-7: Inhibitory coupling.

## Appendix B

### Proofs and Theorems

**Condition 6.1** *The neuronal activation  $f_i(u)$ , where  $i = 1, \dots, n$ , is continuous and nonnegative for any  $u \in (-\infty, +\infty)$ . Furthermore,  $f_i(u)$  has continuous first derivative, and  $\dot{f}_i(u)$  is nonnegative for any  $u \in (-\infty, +\infty)$ .*

**Proposition 6.1** *The network of (4.1) and (4.2) has at least one equilibrium.*

**Proof:** Denote  $h_i(x) = d_i - \sum_{k \neq i} v_k f_k(x_k)$  and  $h(x) = [h_1(x), \dots, h_n(x)]^T$ . Consider a compact convex set  $D = [d_1 - \sum_{k \neq 1} v_k f_k(d_k), d_1] \times \dots \times [d_n - \sum_{k \neq n} v_k f_k(d_k), d_n]$ . For any  $x \in D$ ,  $h_i(x)$  is no greater than  $d_i$  due to  $f_k(x_k) \geq 0$  for any  $k$ , and  $h_i(x)$  is no less than  $d_i - \sum_{k \neq i} v_k f_k(d_k)$  due to  $f_k(x_k) \leq f_k(d_k)$  for any  $k$  (this is because  $f_k(\cdot)$  is monotone nondecreasing and  $x_k \leq d_k$ ). Therefore,  $h(x) \in D$  for any  $x \in D$ . According to Brouwer Fixed Point Theorem [70],  $x = h(x)$  has a fixed point in  $D$ , which implies that the network of (4.1) and (4.2) has at least one equilibrium. **Q.E.D.**

**Lemma 6.1** *For*

$$A = \begin{bmatrix} 1 & a_2 & \cdots & a_{n-1} & a_n \\ a_1 & 1 & \cdots & a_{n-1} & a_n \\ \vdots & \vdots & \ddots & \vdots & \vdots \\ a_1 & a_2 & \cdots & 1 & a_n \\ a_1 & a_2 & \cdots & a_{n-1} & 1 \end{bmatrix},$$

*where  $n \geq 2$ , the determinant of  $A$  equals*

$$\det A = \prod_{k=1}^n (1 - a_k) + \sum_{i=1}^n a_i \prod_{k \neq i} (1 - a_k). \quad (6.1)$$

**Proof:** It can be easily verified that (6.1) holds for  $n = 2$  and  $n = 3$ . In the following, we consider  $n \geq 4$ .

Subtracting the first row from the other rows of  $A$ , we get a new matrix

$$A_1 = \begin{bmatrix} 1 & a_2 & a_3 & \cdots & a_n - 2 & a_n - 1 & a_n \\ a_1 - 1 & 1 - a_2 & 0 & \cdots & 0 & 0 & 0 \\ a_1 - 1 & 0 & 1 - a_3 & \cdots & 0 & 0 & 0 \\ \vdots & \vdots & \vdots & \ddots & \vdots & \vdots & \vdots \\ a_1 - 1 & 0 & 0 & \cdots & 1 - a_{n-2} & 0 & 0 \\ a_1 - 1 & 0 & 0 & \cdots & 0 & 1 - a_{n-1} & 0 \\ a_1 - 1 & 0 & 0 & \cdots & 0 & 0 & 1 - a_n \end{bmatrix}.$$

According to the property of the determinant of a matrix [79],  $\det A$  equals  $\det A_1$ .

Further using the Laplace expansion by minors along the first row of  $A_1$  [79], we have

$$\begin{aligned} \det A &= \det A_1 \\ &= (-1)^{1+1} \begin{vmatrix} 1 - a_2 & 0 & \cdots & 0 & 0 \\ 0 & 1 - a_3 & \cdots & 0 & 0 \\ \vdots & \vdots & \ddots & \vdots & \vdots \\ 0 & 0 & \cdots & 1 - a_{n-1} & 0 \\ 0 & 0 & \cdots & 0 & 1 - a_n \end{vmatrix} \\ &\quad + (-1)^{1+2} a_2 \begin{vmatrix} a_1 - 1 & 0 & \cdots & 0 & 0 \\ a_1 - 1 & 1 - a_3 & \cdots & 0 & 0 \\ \vdots & \vdots & \ddots & \vdots & \vdots \\ a_1 - 1 & 0 & \cdots & 1 - a_{n-1} & 0 \\ a_1 - 1 & 0 & \cdots & 0 & 1 - a_n \end{vmatrix} \end{aligned}$$

$$\begin{aligned}
& + \sum_{i=3}^{n-1} (-1)^{1+i} a_i \begin{vmatrix} a_1 - 1 & 1 - a_2 & \cdots & 0 & 0 & 0 & \cdots & 0 \\ a_1 - 1 & 0 & \cdots & 0 & 0 & 0 & \cdots & 0 \\ \vdots & \vdots & \ddots & \vdots & \vdots & \vdots & \ddots & \vdots \\ a_1 - 1 & 0 & \cdots & 0 & 1 - a_{i-1} & 0 & \cdots & 0 \\ a_1 - 1 & 0 & \cdots & 0 & 0 & 0 & \cdots & 0 \\ a_1 - 1 & 0 & \cdots & 0 & 0 & 1 - a_{i+1} & \cdots & 0 \\ \vdots & \vdots & \ddots & \vdots & \vdots & \vdots & \ddots & \vdots \\ a_1 - 1 & 0 & \cdots & 0 & 0 & 0 & \cdots & 1 - a_n \end{vmatrix} \\
& + (-1)^{1+n} a_n \begin{vmatrix} a_1 - 1 & 1 - a_2 & \cdots & 0 & 0 \\ a_1 - 1 & 0 & \cdots & 0 & 0 \\ \vdots & \vdots & \ddots & \vdots & \vdots \\ a_1 - 1 & 0 & \cdots & 0 & 1 - a_{n-1} \\ a_1 - 1 & 0 & \cdots & 0 & 0 \end{vmatrix}.
\end{aligned}$$

For each determinant except the first one in the above equation, we use the Laplace expansion by minors along the first column of the determinant. Then we have

$$\begin{aligned}
\det A &= \prod_{k=2}^n (1 - a_k) + (-1) a_2 (a_1 - 1) \prod_{k=3}^n (1 - a_k) \\
&+ \sum_{i=3}^{n-1} (-1)^{1+i} a_i (-1)^{1+i-1} (a_1 - 1) \prod_{k=2}^{i-1} (1 - a_k) \prod_{k=i+1}^n (1 - a_k) \\
&+ (-1)^{1+n} a_n (-1)^{1+n-1} (a_1 - 1) \prod_{k=2}^{n-1} (1 - a_k) \\
&= \prod_{k=2}^n (1 - a_k) + \sum_{i=2}^n a_i \prod_{k \neq i} (1 - a_k) = \prod_{k=1}^n (1 - a_k) + \sum_{i=1}^n a_i \prod_{k \neq i} (1 - a_k).
\end{aligned}$$

**Q.E.D.**

**Proposition 6.2** *Let  $x^*$  be an equilibrium of (4.1) and (4.2). If*

$$\prod_{k=1}^n [1 - v_k \dot{f}_k(x_k)] + \sum_{i=1}^n v_i \dot{f}_i(x_i^*) \prod_{k \neq i} [1 - v_k \dot{f}_k(x_k^*)] \neq 0. \quad (6.2)$$

Then  $x^*$  is an isolated equilibrium.

**Proof:** Since  $\dot{f}_i(x_i)$  is continuous for any  $i = 1, \dots, n$ , Inequality (6.2) implies that there exists an  $\epsilon > 0$  and an open set  $S(x^*, \epsilon) \equiv \{x \mid |x_i - x_i^*| < \epsilon \text{ for any } i = 1, \dots, n\}$  such that  $\prod_{k=1}^n [1 - v_k \dot{f}_k(x_k)] + \sum_{i=1}^n v_i \dot{f}_i(x_i) \prod_{k \neq i} [1 - v_k \dot{f}_k(x_k)]$  is not equal to 0 for any  $x \in S(x^*, \epsilon)$ .

Next, we prove that  $x^*$  is the only equilibrium in  $S(x^*, \epsilon)$ . Assume that there exists another equilibrium  $x' \in S(x^*, \epsilon)$ . Apparently,  $x'$  satisfies  $x_i' = d_i - \sum_{k \neq i} v_k f_k(x_k')$  for any  $i = 1, \dots, n$ . Let  $u = x' - x^*$  and substitute  $x' = x^* + u$  into the above equilibrium equation for  $x'$ :  $x_i^* + u_i = d_i - \sum_{k \neq i} v_k f_k(x_k^* + u_k)$ . According to the mean value theorem [70] and the fact that  $\dot{f}$  is continuous, there exist  $\eta_i, i = 1, \dots, n$  such that  $f_i(x_i^* + u_i) = f_i(x_i^*) + \dot{f}_i(x_i^* + \eta_i u_i) u_i$  where  $0 \leq \eta_i \leq 1$ . Therefore, we have  $x_i^* + u_i = d_i - \sum_{k \neq i} v_k [f_k(x_k^*) + \dot{f}_k(x_k^* + \eta_k u_k) u_k]$ , which becomes  $u_i = -\sum_{k \neq i} v_k \dot{f}_k(x_k^* + \eta_k u_k) u_k, i = 1, \dots, n$ . Denote  $a_i = v_i \dot{f}_i(x_i^* + \eta_i u_i)$ , and write the above equations in matrix form  $Au = 0$  where

$$A = \begin{bmatrix} 1 & a_2 & \cdots & a_{n-1} & a_n \\ a_1 & 1 & \cdots & a_{n-1} & a_n \\ \vdots & \vdots & \ddots & \vdots & \vdots \\ a_1 & a_2 & \cdots & 1 & a_n \\ a_1 & a_2 & \cdots & a_{n-1} & 1 \end{bmatrix}.$$

Since  $x' = x^* + u \in S(x^*, \epsilon)$  and  $0 \leq \eta_i \leq 1$  for any  $i = 1, \dots, n$ , we have  $(x_i^* + \eta_1 u_1, \dots, x_n^* + \eta_n u_n)^T \in S(x^*, \epsilon)$ . Thus  $\prod_{k=1}^n (1 - a_k) + \sum_{i=1}^n a_i \prod_{k \neq i} (1 - a_k) \neq 0$ . According

to **Lemma 6.1**,  $\det A$  is not equal to 0. Hence  $Au = 0$  has only one solution, i.e.,  $u = 0$ , which implies  $x' = x^*$ . So, there is only one equilibrium in the open set  $S(x^*, \epsilon)$  containing  $x^*$ . In other words,  $x^*$  is an isolated equilibrium. **Q.E.D.**

Corollary 6.1 *Let  $x^*$  be an equilibrium of (4.1) and (4.2). If*

$$v_i \dot{f}_i(x_i^*) < 1 \text{ for any } i = 1, \dots, n, \quad (6.3)$$

or

$$v_i \dot{f}_i(x_i^*) > 1 \text{ for any } i = 1, \dots, n, \quad (6.4)$$

then  $x^*$  is an isolated equilibrium.

**Proof:** We only need to show that Condition (6.3) or (6.4) implies (6.2).

If Condition (6.3) is satisfied (note that  $v_i \dot{f}_i(x_i^*)$  is also nonnegative for any  $i = 1, \dots, n$ ), then we have  $\prod_{k=1}^n [1 - v_k \dot{f}_k(x_k)] + \sum_{i=1}^n v_i \dot{f}_i(x_i) \prod_{k \neq i} [1 - v_k \dot{f}_k(x_k)]$ , so Inequality (6.2) is satisfied.

If Condition (6.4) is satisfied, then  $\frac{v_i \dot{f}_i(x_i^*)}{1 - v_i \dot{f}_i(x_i^*)}$  is less than  $-1$  for any  $i = 1, \dots, n$ . Hence

$$1 + \frac{v_1 \dot{f}_1(x_1^*)}{1 - v_1 \dot{f}_1(x_1^*)} + \dots + \frac{v_n \dot{f}_n(x_n^*)}{1 - v_n \dot{f}_n(x_n^*)} < 0,$$

and thus

$$\prod_{k=1}^n [1 - v_k \dot{f}_k(x_k^*)] + \sum_{i=1}^n v_i \dot{f}_i(x_i^*) \prod_{k \neq i} [1 - v_k \dot{f}_k(x_k^*)]$$

$$= \left\{ \prod_{k=1}^n [1 - v_k \dot{f}_k(x_k^*)] \right\} \left( 1 + \frac{v_1 \dot{f}_1(x_1^*)}{1 - v_1 \dot{f}_1(x_1^*)} + \dots + \frac{v_n \dot{f}_n(x_n^*)}{1 - v_n \dot{f}_n(x_n^*)} \right) \neq 0.$$

So, Inequality (6.2) is also satisfied. **Q.E.D.**

Proposition 6.3 *The network of (4.1) and (4.2) has only one equilibrium if there exists  $M_i$  such that  $\dot{f}_i(x_i) \leq M_i$  for any  $x_i$  and*

$$v_i M_i < 1 \tag{6.5}$$

for any  $i = 1, \dots, n$ .

**Proof:** Let  $x^*$  be an equilibrium and assume that there exists another equilibrium  $x'$ . Then following similar steps as in the proof of Proposition 6.2, we may prove  $x' = x^*$ . **Q.E.D.**

It turns out, the condition provided by Proposition 6.3 actually is a sufficient condition of uniqueness of equilibrium for the network, as well as Proposition 6.5 later detailed. In fact, if it were such that  $v_i$  equals  $v$  and  $M_i$  equals  $M$  for  $i = 1, \dots, n$ , the results from general recurrent network theory [56][57] could be used to show conservative this proposition truly is. From [75][73], the network of (4.1) and (4.2) has only one equilibrium if

$$(n - 1)vM < 1. \tag{6.6}$$

Comparing to Proposition 6.3 ( $vM < 1$ ) to (6.6), it is clear that Proposition 6.3 is significantly less conservative than (6.6).

Proposition 6.4 *Let  $x^*$  be an equilibrium of (4.1) and (4.2). If  $v_i \dot{f}_i(x_i^*) < 1$  for any  $i = 1, \dots, n$ , then  $x^*$  is an asymptotically stable equilibrium.*

**Proof:** Given  $x$ , denote  $u = x - x^*$  and  $u_i = x_i - x_i^*$  for  $i = 1, \dots, n$ . Furthermore, denote  $g_i(u_i) = f_i(x_i) - f_i(x_i^*) = f_i(x_i^* + u_i) - f_i(x_i^*)$  and

$$M_v = \frac{1}{2} + \frac{\max_i \{v_i \dot{f}_i(x_i^*)\}}{2}.$$

Apparently,  $M_v$  is strictly greater than  $v_i \dot{f}_i(x_i^*)$  for any  $i = 1, \dots, n$  and strictly less than 1, since  $v_i \dot{f}_i(x_i^*)$  is less than 1. Because  $\dot{f}_i(x_i^*)$  is continuous and  $M_v$  is strictly greater than  $\max_i \{v_i \dot{f}_i(x_i^*)\}$ , there exists an  $\epsilon > 0$  and a domain containing  $x^*$ ,  $S(x^*, \epsilon) \equiv \{x \mid |x_i - x_i^*| < \epsilon \text{ for any } i = 1, \dots, n\}$ , such that  $v_i \dot{f}_i(x_i)$  is less than  $M_v$  for any  $x \in S(x^*, \epsilon)$  and for any  $i = 1, \dots, n$ . Correspondingly, denote  $D = \{u \mid u + x^* \in S(x^*, \epsilon)\}$ . Therefore,

$$v_i \dot{g}_i(u_i) < M_v \text{ for any } u \in D. \quad (6.7)$$

We use a Lure-type Lyapunov function [76][73]

$$V(u) = \frac{1}{2} \sum_{i=1}^n c u_i^2 + \sum_{i=1}^n \int_0^{u_i} v_i g_i(s) ds, \quad (6.8)$$

where  $c$  is a positive constant satisfying

$$c < \frac{4}{n}(1 - M_v). \quad (6.9)$$

Obviously,  $V(0)$  equals 0 and  $V(u)$  is greater than 0 for any  $u \in D$  except for  $u = 0$ .

In the following, we want to show  $\frac{dV}{dt} < 0$  for any  $u \in D$  and  $u \neq 0$ . If this is true, then we can

claim that  $u = 0$ , i.e.  $x = x^*$ , is asymptotically stable, according to [76] (Theorem 3.1, Page 100).

Let us first calculate  $\tau \frac{du_i}{dt} \cdot \tau \frac{du_i}{dt} = \tau \frac{dx_i}{dt} = -x_i - \sum_{k \neq i} v_k f_k(x_k) + d_i = -x_i^* - u_i -$

$\sum_{k \neq i} v_k [f_k(x_k^*) + g_k(u_k)] + d_i = -u_i - \sum_{k \neq i} v_k g_k(u_k)$ . Then we have

$$\begin{aligned} \tau \frac{dV}{dt} &= \sum_{i=1}^n cu_i \left( \tau \frac{du_i}{dt} \right) + \sum_{i=1}^n v_i g_i(u_i) \left( \tau \frac{du_i}{dt} \right) \\ &= \sum_{i=1}^n cu_i \left[ -u_i - \sum_{k \neq i} v_k g_k(u_k) \right] + \sum_{i=1}^n v_i g_i(u_i) \left[ -u_i - \sum_{k \neq i} v_k g_k(u_k) \right] \\ &= \sum_{i=1}^n [cu_i + v_i g_i(u_i)] \left[ -u_i - \sum_{k \neq i} v_k g_k(u_k) \right] \\ &= \sum_{i=1}^n [cu_i + v_i g_i(u_i)] \left\{ -[u_i - v_i g_i(u_i)] - \sum_{k=1}^n v_k g_k(u_k) \right\} \\ &= - \sum_{i=1}^n [cu_i + v_i g_i(u_i)] [u_i - v_i g_i(u_i)] - \sum_{i=1}^n [cu_i + v_i g_i(u_i)] \sum_{k=1}^n v_k g_k(u_k). \end{aligned}$$

Note that

$$\sum_{i=1}^n [cu_i + v_i g_i(u_i)] \sum_{k=1}^n v_k g_k(u_k)$$

$$\begin{aligned}
&= \sum_{i=1}^n cu_i \sum_{k=1}^n v_k g_k(u_k) + \left[ \sum_{k=1}^n v_k g_k(u_k) \right]^2 \\
&= \sum_{i=1}^n \left\{ cu_i \sum_{k=1}^n v_k g_k(u_k) + \frac{1}{n} \left[ \sum_{k=1}^n v_k g_k(u_k) \right]^2 \right\} \\
&= \sum_{i=1}^n \left\{ \frac{c^2 n}{4} u_i^2 + cu_i \left[ \sum_{k=1}^n v_k g_k(u_k) \right] + \frac{1}{n} \left[ \sum_{k=1}^n v_k g_k(u_k) \right]^2 \right\} - \sum_{i=1}^n \frac{c^2 n}{4} u_i^2 \\
&= \sum_{i=1}^n \left\{ \frac{c\sqrt{n}}{2} u_i + \frac{1}{\sqrt{n}} \left[ \sum_{k=1}^n v_k g_k(u_k) \right] \right\}^2 - \sum_{i=1}^n \frac{c^2 n}{4} u_i^2 \\
&\geq - \sum_{i=1}^n \frac{c^2 n}{4} u_i^2.
\end{aligned}$$

Therefore,

$$\tau \frac{dV}{dt} \leq - \sum_{i=1}^n [cu_i + v_i g_i(u_i)][u_i - v_i g_i(u_i)] + \sum_{i=1}^n \frac{c^2 n}{4} u_i^2.$$

According to (6.7) and the definition of  $M_v$ , for any  $u \in D$  we have (i)  $0 \leq v_i g_i(u_i) \leq M_v u_i$  when  $u_i > 0$  and (ii)  $M_v u_i \leq v_i g_i(u_i) \leq 0$  when  $u_i < 0$ . Since  $M_v < 1$ , we have  $0 \leq v_i g_i(u_i) < u_i$  for  $u_i > 0$  and  $u_i < v_i g_i(u_i) \leq 0$  for  $u_i < 0$ . Thus  $v_i g_i(u_i)[u_i - v_i g_i(u_i)]$  is no less than 0 for any  $u \in D$ . Therefore,

$$\begin{aligned}
&\tau \frac{dV}{dt} \leq - \sum_{i=1}^n [cu_i + v_i g_i(u_i)][u_i - v_i g_i(u_i)] + \sum_{i=1}^n \frac{c^2 n}{4} u_i^2 \\
&= - \sum_{i=1}^n cu_i [u_i - v_i g_i(u_i)] - \sum_{i=1}^n v_i g_i(u_i) [u_i - v_i g_i(u_i)] + \sum_{i=1}^n \frac{c^2 n}{4} u_i^2
\end{aligned}$$

$$\begin{aligned}
&\leq -\sum_{i=1}^n cu_i[u_i - v_i g_i(u_i)] + \sum_{i=1}^n \frac{c^2 n}{4} u_i^2 \\
&\leq -\sum_{i=1}^n cu_i[u_i - M_v u_i] + \sum_{i=1}^n \frac{c^2 n}{4} u_i^2 \\
&= -\sum_{i=1}^n \left[ c(1 - M_v) - \frac{c^2 n}{4} \right] u_i^2.
\end{aligned}$$

According to (6.9),  $c(1 - M_v) - \frac{c^2 n}{4}$  is strictly greater than 0, so  $\frac{dV}{dt}$  is strictly negative for any  $u \in D$  except for  $u = 0$ . **Q.E.D.**

It turns out that the constraints of Condition 6.1 on the types of activation functions that can be used can be loosened since what was learned from the proof of Proposition 6.4 can be applied more generally. This gives

**Condition 6.2** *The neuronal activation  $f_i(u)$ , where  $i = 1, \dots, n$ , is nonnegative for any  $u \in (-\infty, +\infty)$ . In addition,  $f_i(u)$  is globally Lipschitz continuous, i.e.,*

$$0 \leq \frac{f_i(u_1) - f_i(u_2)}{u_1 - u_2} \leq M_i \tag{6.10}$$

for any two different  $u_1, u_2$ .

Since it is apparent that a globally Lipschitz continuous activation function may be non-differentiable and unbounded, this leads to:

Proposition 6.5 Let  $f_i(\cdot)$  satisfy Condition 6.2 and the constant  $M_i$  in (6.10) is constrained by  $v_i M_i < 1$  for any  $i = 1, \dots, n$ . Then the network of (4.1) and (4.2) has a unique equilibrium, which is globally asymptotically stable.

**Proof:** Following the proof of Condition 6.1 The neuronal activation  $f_i(u)$ , where  $i = 1, \dots, n$ , is continuous and nonnegative for any  $u \in (-\infty, +\infty)$ . Furthermore,  $f_i(u)$  has continuous first derivative, and  $\dot{f}_i(u)$  is nonnegative for any  $u \in (-\infty, +\infty)$ .

**Proposition 6.1** The network of (4.1) and (4.2) with activation functions described as above has at least one equilibrium. Let  $x^*$  be such an equilibrium. Denote  $u_i = x_i - x_i^*$  and  $g_i(u_i) = f_i(x_i) - f_i(x_i^*) = f_i(x_i^* + u_i) - f_i(x_i^*)$  for  $i = 1, \dots, n$ .

Define an energy function  $V(u)$  in the form of (6.8, where  $c$  is a positive constant satisfying  $c < \min_i \left\{ \frac{4}{n} (1 - v_i M_i) \right\}$ . Obviously,  $V(0)$  equals 0,  $V(u)$  is greater than 0 for any  $u \neq 0$ , and  $V(u)$  approaches positive infinity as  $\|u\| \rightarrow \infty$ . Furthermore, following the similar steps as in the proof of Proposition 6.4, we may show that  $\frac{dV}{dt}$  is strictly negative for any  $u \neq 0$ . Then we can claim that  $u = 0$ , i.e.  $x = x^*$  is globally asymptotically stable, according to [76] (Theorem 3.2, Page 110). Obviously,  $x^*$  has to be the unique equilibrium of the network of (4.1) and (4.2). **Q.E.D.**

**Condition 6.3** The neuronal activation  $f(u)$  is nonnegative and globally Lipschitz continuous, i.e.,

$$0 \leq \frac{f(u_1) - f(u_2)}{u_1 - u_2} \leq M_i \quad (6.11)$$

for any two different  $u_1, u_2$ .

Consider  $x_i^* < x_j^*$  when  $d_i < d_j$ , where  $i, j \in \{1, \dots, n\}$ .

**Proposition 6.6** *The network of (4.10) always has an equilibrium  $x^*$  that is order preserving with respect to the network inputs.*

**Proof:** Without loss of generality, let  $d_1 \leq d_2 \leq \dots \leq d_n$ .

Denote  $h_i(x) = d_i - \sum_{k \neq i} v f(x_k)$  and  $h(x) = [h_1(x), \dots, h_n(x)]^T$ . Consider a compact convex set  $D = \{x \mid d_i - \sum_{k \neq i} v f(d_k) \leq x_i \leq d_i, i = 1, \dots, n, \text{ and } x_1 \leq \dots \leq x_n\}$ . Similar to the proof of Condition 6.1 *The neuronal activation  $f_i(u)$ , where  $i = 1, \dots, n$ , is continuous and nonnegative for any  $u \in (-\infty, +\infty)$ . Furthermore,  $f_i(u)$  has continuous first derivative, and  $\dot{f}_i(u)$  is nonnegative for any  $u \in (-\infty, +\infty)$ .*

**Proposition 6.1**, it can be shown that for any  $x \in D$ ,  $h_i(x)$  is no greater than  $d_i$  and no less than  $d_i - \sum_{k \neq i} v f(d_k)$ . Furthermore, for any  $i < j$  (and thus  $d_i \leq d_j$ ), we have  $h_i(x) - h_j(x) = d_i - d_j + v f(x_i) - v f(x_j) \leq 0$ , because  $d_i \leq d_j$  and  $f(x_i) \leq f(x_j)$  (since  $f$  is monotone nondecreasing and  $x_i$  is no greater than  $x_j$  due to  $i < j$  and  $x \in D$ ). Therefore,  $h(x) \in D$  for any  $x \in D$ . According to Brouwer Fixed Point Theorem [70],  $x = h(x)$  has a fixed point in  $D$ , which implies that (6.2 has at least one equilibrium, say  $x^*$ , such that  $x_1^* \leq x_2^* \leq \dots \leq x_n^*$ .

For any  $d_i < d_j$ , we have  $x_i^* \leq x_j^*$  and thus  $f(x_i^*) \leq f(x_j^*)$ . Therefore,  $x_i^* - x_j^* = d_i - d_j + vf(x_i^*) - vf(x_j^*) \leq d_i - d_j < 0$ , so  $x_i^*$  is strictly less than  $x_j^*$ . Hence, we proved that  $x^*$  is order preserving with respect to the network inputs. **Q.E.D.**

Proposition 6.7 *The network of (4.10) has only one equilibrium,  $x^*$ , if  $f(\cdot)$  satisfies Condition 6.3 and the constant  $M$  in (4.11) is constrained by*

$$vM < 1. \tag{6.12}$$

*This equilibrium is globally asymptotically stable. Furthermore,  $x^*$  is order preserving with respect to the network inputs, and  $x_i^*$  equals  $x_j^*$  whenever  $d_i$  equals  $d_j$ .*

**Proof:** First show that an equilibrium of (4.10, say  $x^*$ , has to be order preserving. Prove this by contradiction. If for some  $d_i < d_j$  we have  $x_i^* \geq x_j^*$ , then we can get  $0 \leq x_i^* - x_j^* = d_i - d_j + vf(x_i^*) - vf(x_j^*) \leq d_i - d_j + vM(x_i^* - x_j^*)$ , which implies  $0 \leq (1 - vM)(x_i^* - x_j^*) \leq d_i - d_j < 0$ , causing contradiction. Therefore,  $x^*$  has to be order preserving. Similarly, we may prove  $x_i^* = x_j^*$  if  $d_i = d_j$ .

Next show that (4.10) has unique equilibrium and the equilibrium is globally asymptotically stable. This directly follows Proposition 6.5. Here we want to show an alternative proof of the uniqueness of equilibrium without using the Lure-type Lyapunov function. This proof is via contradiction. Assume that the network has more than one equilibrium and let  $x^{(1)} \neq x^{(2)}$  be two of the equilibria. Without loss of generality, assume  $d_1 \leq d_2 \leq \dots \leq d_n$ . According to the above argument, we have  $x_1^{(1)} \leq \dots \leq x_n^{(1)}$  and  $x_1^{(2)} \leq \dots \leq x_n^{(2)}$ . Let  $i$  be the smallest integer

such that  $x_i^{(1)} \neq x_i^{(2)}$ , which implies  $x_j^{(1)} = x_j^{(2)}$  for any  $j < i$  if  $i > 1$ . Without loss of generality, let  $x_i^{(1)} < x_i^{(2)}$ . Thus  $x_i^{(1)} = d_i - \sum_{k \neq i} v f(x_k^{(1)}) < x_i^{(2)} = d_i - \sum_{k \neq i} v f(x_k^{(2)})$ , and therefore  $\sum_{k \neq i} f(x_k^{(1)}) > \sum_{k \neq i} f(x_k^{(2)})$ . Then there exists at least one  $k > i$  such that  $f(x_k^{(1)}) > f(x_k^{(2)})$ . Obviously,  $x_k^{(1)} > x_k^{(2)}$ . Now we have  $x_i^{(1)} < x_i^{(2)} \leq x_k^{(2)} < x_k^{(1)}$ .

Consider simple calculation as follows:

$$\begin{aligned}
& x_k^{(1)} - x_k^{(2)} + x_i^{(2)} - x_i^{(1)} \\
&= \left( d_k - \sum_{j \neq k} v f(x_j^{(1)}) \right) - \left( d_k - \sum_{j \neq k} v f(x_j^{(2)}) \right) + \left( d_i - \sum_{j \neq k} v f(x_j^{(2)}) \right) \\
&\quad - \left( d_i - \sum_{j \neq k} v f(x_j^{(1)}) \right) \\
&= -v f(x_i^{(1)}) + v f(x_i^{(2)}) - v f(x_k^{(2)}) + v f(x_k^{(1)}) \\
&= v \left( f(x_i^{(2)}) - f(x_i^{(1)}) \right) + v \left( f(x_k^{(1)}) - f(x_k^{(2)}) \right) \\
&\leq vM(x_i^{(2)} - x_i^{(1)}) + vM(x_k^{(1)} - x_k^{(2)}) \\
&< x_i^{(2)} - x_i^{(1)} + x_k^{(1)} - x_k^{(2)},
\end{aligned}$$

which leads to contradiction and thus completes the proof of uniqueness. **Q.E.D.**

**Proposition 6.8** *Let  $x^*$  be an order preserving equilibrium of (4.10). If  $f(\cdot)$  is strictly monotone increasing, then for any  $d_i < d_j$  we have*

$$x_j^* - x_i^* > d_j - d_i > 0, \quad (6.13)$$

*i.e., expressed in another form,*

$$d_i - x_i^* > d_j - x_j^* \geq 0. \quad (6.14)$$

**Proof:** Since  $x^*$  is an order preserving equilibrium, we have  $x_i^* < x_j^*$  for any  $d_i < d_j$  and thus  $f(x_i^*) < f(x_j^*)$  because  $f(\cdot)$  is strictly monotone increasing. Therefore,  $x_j^* - x_i^* = d_j - d_i + vf(x_j^*) - vf(x_i^*) > d_j - d_i$ . So, we get (6.13). Expressing this inequality in another form, we have  $d_i - x_i^* > d_j - x_j^*$ . Inequality (4.7) guarantees  $d_j - x_j^* \geq 0$ . Then we get (6.14). **Q.E.D.**

**Condition 6.4** *The neuronal activation  $f(u)$ , is continuous, nonnegative, and strictly monotone increasing;  $\dot{f}(u)$  is continuous;  $\dot{f}(u)$  is monotone decreasing on  $[b, \infty)$  and monotone increasing on  $(-\infty, b]$  – this implies that  $\dot{f}(u)$  achieves its maximum at  $u = b$  and that  $f(u)$  is concave on the right side of  $u = b$  and convex on the left side of  $u = b$ .*

**Proposition 6.9** *Consider a network of (4.10) with neuronal activation function satisfying Condition 6.4. Let  $d_i$  and  $d_j$  be two inputs such that  $b < d_i < d_j$ , and let  $x^*$  be an order preserving equilibrium of (4.10). If neurons  $i$  and  $j$  are both active at  $x^*$ , i.e.,  $b < x_i^* < x_j^*$ , then there must be*

$$v\dot{f}(d_j) < 1, \quad (6.15)$$

$$x_j^* - x_i^* \geq \frac{d_j - d_i}{1 - v\dot{f}(d_j)}, \quad (6.16)$$

and

$$f(x_j^*) - f(x_i^*) \geq f(d_j) - f(d_i) + \frac{vf(d_j)\dot{f}(d_i)}{1 - vf(d_j)}(d_j - d_i). \quad (6.17)$$

**Proof:** First prove (6.15) and (6.16). Since  $f(\cdot)$  is continuous, we have

$$\begin{aligned} x_j^* - x_i^* &= d_j - d_i + vf(x_j^*) - vf(x_i^*) \\ &= d_j - d_i + v\dot{f}(\xi)(x_j^* - x_i^*), \end{aligned} \quad (6.18)$$

where  $\xi \in [x_i^*, x_j^*] \subset (b, d_j]$ , according to the mean value theorem [70]. Hence  $\dot{f}(\xi) \geq \dot{f}(d_j)$  ( $\dot{f}(\cdot)$  is monotone decreasing on  $[b, \infty)$ ). Because  $x_i^* < x_j^*$  and  $d_i < d_j$ , there must be  $v\dot{f}(\xi) < 1$ , otherwise we may derive  $x_j^* - x_i^* \geq d_j - d_i + x_j^* - x_i^*$  and thus  $d_j \leq d_i$ , causing contradiction. Therefore, we have  $v\dot{f}(d_j) \leq v\dot{f}(\xi) < 1$ , which leads to (6.15). Following (6.18, we further have

$$x_j^* - x_i^* = \frac{d_j - d_i}{1 - v\dot{f}(\xi)} \geq \frac{d_j - d_i}{1 - v\dot{f}(d_j)},$$

which leads to (6.16).

Next prove (6.17). According to (6.16), the fact that  $b < x_i^* < x_j^* \leq d_j$ , and that  $f(\cdot)$  is strictly monotone increasing and  $\dot{f}(\cdot)$  is monotone decreasing on  $[b, \infty)$ , we have

$$f(x_j^*) - f(x_i^*) \geq f(d_j) - f(d_j - (x_j^* - x_i^*)) \geq f(d_j) - f(d_j - \frac{d_j - d_i}{1 - v\dot{f}(d_j)})$$

$$\begin{aligned}
&= f(d_j) - f\left(d_i - \frac{vf(d_j)(d_j - d_i)}{1 - vf(d_j)}\right) \\
&\geq f(d_j) - f(d_i) + \dot{f}(d_i) \frac{vf(d_j)(d_j - d_i)}{1 - vf(d_j)} \\
&= f(d_j) - f(d_i) + \frac{vf(d_j)\dot{f}(d_i)}{1 - vf(d_j)}(d_j - d_i),
\end{aligned}$$

complete the proof. **Q.E.D.**

Corollary 6.2 Consider a network of (4.10) with neuronal activation function satisfying Condition 6.4. Let  $d_j$  and  $d_i$  be the largest and second largest inputs, respectively, with  $b < d_i < d_j$ , and  $x^*$  an order preserving equilibrium of (4.10). If

$$vf(d_j) \geq 1, \tag{6.19}$$

or if

$$vf(d_j) < 1 \text{ and } d_j - b < \frac{d_j - d_i}{1 - vf(d_j)}, \tag{6.20}$$

then the network has at most one active neuron at  $x^*$ .

**Proof:** The proof directly follows Proposition 6.9. **Q.E.D.**

## Bibliography

- [1] Horvath, A., Synchronization in cellular spin torque oscillator arrays. Cellular Nanoscale Networks and their applications (CNNA), 13th International Workshop on. IEEE, 2012.
- [2] Shibata, T., et al., (2012). CMOS supporting circuitries for nano-oscillator-based associative memories. 13th International Workshop on Cellular Nanoscale Networks and their Applications (CNNA), 1-5. Turin, Italy, August 29-31, 2012.
- [3] Hoppensteadt F.C. and Izhikevich E.M. (2001) Synchronization of MEMS Resonators and Mechanical Neurocomputing. IEEE Transactions on Circuits and Systems I, 48:133-138.
- [4] Nikonov, Dmitri E., Ian A. Young, and George I. Bourianoff. "Convolutional Networks for Image Processing by Coupled Oscillator Arrays." arXiv preprint arXiv: 1409.4469 (2014).
- [5] D. M. Chiarulli, B. Jennings, Y. Fang, and A. Steel, and S. P. Levitan, "A Computational Primitive for Convolution based on Coupled Oscillator Arrays", ISVLSI 2015
- [6] Jennings, Brandon (2016) An Analysis of Oscillator-Based Computations for Image Processing. Master's Thesis, University of Pittsburgh.
- [7] Christiaan Huygens, "Horologium Oscillatorium", 1673.
- [8] D. Rairigh, "Limits of CMOS technology scaling and technologies beyond-CMOS," [http://www.drlock.com/papers/cmos\\_survey.pdf](http://www.drlock.com/papers/cmos_survey.pdf).
- [9] Nagumo, J., Arimoto, S., and Yoshizawa, S. (1962) An Active Pulse Transmission Line Simulating Nerve Axon, Proc. Inst. Radio Engineers, 50:2061-2070
- [10]Fitzhugh, R.A. (1961) Impulses and Physiological States in Theoretical Models of Nerve Membrane, Biophys. J., 1:445-466
- [11]Hodgkin, A.L., and Huxley, A.F. (1952) A Quantitative Description of Membrane Current and its Application to Conduction and Excitation in Nerve, J. Physiol., 117:500.
- [12]Grossberg, S. (1978) Competition, Decision, and Consensus, Journal of Mathematical Analysis and Applications, 66:470-493
- [13]Indiveri, G. (2000) A 2D Neuromorphic VLSI Architecture for Modeling Selective Attention, IEEE-INNS-ENNS International Joint Conference on Neural Networks (IJCNN'00) vol.4, July 24-27, Como, Italy
- [14]Wei Wang, Jean-Jacques E. Slotine, Fast computation with neural oscillators, In Neurocomputing, Volume 69, Issues 16–18, 2006, Pages 2320-2326, ISSN 0925-2312.

- [15]Faghieh R.T., Savla K, Dahleh M.A., Brown E.N. “The Fitzhugh- Nagumo Model: Firing Modes with Time Varying Parameters and Parameter Estimation,” Annual International Conference of the IEEE Engineering in Medicine and Biology Society, Buenos Aires, Argentina, p. 4116-4119, Summer 2010.
- [16]G. Indiveri, BA current-mode hysteretic winner-take-all network, with excitatory and inhibitory coupling, *Analog Integr. Circuits Signal Process.*, vol. 28, no. 3, pp. 279–291, 2001
- [17]Kaski, S., and Kohonen, T. 1994. Winner-take-all networks for physiological models of competitive learning. *Neural Networks* **7**, 973–984.
- [18]Linares-Barranco B et al. (1991), A CMOS implementation of Fitzhugh-Nagumo neuron model. *IEEE Journals of Solid-State Circuits*, vol. 26, no. 7, pp 956-965
- [19]Sase, T., Katori, Y., Komuro, M., & Aihara, K. (2017). Bifurcation Analysis on Phase-Amplitude Cross-Frequency Coupling in Neural Networks with Dynamic Synapses. *Frontiers in Computational Neuroscience*, *11*, 18.
- [20]Jian-Wei Shuai, Dominique M. Durand, Phase synchronization in two coupled chaotic neurons, In *Physics Letters A*, Volume 264, Issue 4, 1999, Pages 289-297
- [21]B. Jennings, et al, “HMAX Image Processing Pipeline with Coupled Oscillator Acceleration”, *IEEE International Workshop on Signal Processing Systems (SiPS 2014)*, Oct 20-22, 2014
- [22]Gambuzza, L. V., Gómez-Gardeñes, J., & Frasca, M. (2016). Amplitude dynamics favors synchronization in complex networks. *Scientific Reports*, *6*, 24915.
- [23]Y. Fang, V. V. Yashin, D. M. Chiarulli, and S. P. Levitan, “A Simplified Phase Model for Oscillator Based Computing,” In: *ISVLSI: IEEE Computer Society*, pp. 231-236 (2015)
- [24]V. Syrjala, M. Valkama, L. Anttila, T. Riihonen, and D. Korpi, “Analysis of oscillator phase-noise effects on self-interference cancellation in full-duplex OFDM radio transceivers,” *IEEE Trans. Wireless Commun.*, vol. 13, no. 6, pp. 2977-2990, Jun. 2014.
- [25]Urazhdin, S., Tabor, P., Tiberkevich, V., Slavin, A.: Fractional synchronization of spin-torque nano-oscillators. *Phys. Rev. Lett.* *105*, 104101 (2010).
- [26]Lawrence Perko. 1991. *Differential Equations and Dynamical Systems*. Springer-Verlag New York, Inc., New York, NY, USA.
- [27][www.ugr.es/~jtorres/FNtema7.pdf](http://www.ugr.es/~jtorres/FNtema7.pdf)
- [28]Nelson, M. (2004). “Electrophysiological models,” in *Databasing the Brain: From Data to Knowledge*, ed. S. H. Koslow (New York: Wiley), 285–301.

- [29]Mahbub, K. (2013). *Exitable Media & Fitzhugh-Nagumo Model*. Department of Mathematical Sciences, Liverpool University, Liverpool, United Kingdom.
- [30]M. Lemmon and B. V. K. V. Kumar, "Competitive learning with generalized winner-take-all activation," in *IEEE Transactions on Neural Networks*, vol. 3, no. 2, pp. 167-175, March 1992.
- [31]Bechara, Antoine (2005). "Decision Making, Impulse Control and Loss of Willpower to Resist Drugs: A Neurocognitive Perspective." *Nature Neuroscience* 8(11): 1458-1463.
- [32][https://en.wikipedia.org/wiki/Hyperbolic\\_equilibrium\\_point](https://en.wikipedia.org/wiki/Hyperbolic_equilibrium_point)
- [33][https://en.wikipedia.org/wiki/Center\\_manifold](https://en.wikipedia.org/wiki/Center_manifold)
- [34]<http://www.sosmath.com/diffeq/system/linear/eigenvalue/real/real.html>
- [35][https://en.wikipedia.org/wiki/Limit\\_cycle](https://en.wikipedia.org/wiki/Limit_cycle)
- [36]<http://www.math.pitt.edu/~bdoiron/assets/ermentrout-and-terman-ch-1.pdf>
- [37] Mao, Zhi-Hong. (2006). Modeling the role of the basal ganglia in motor control and motor programming.
- [38]Yantis, Steven (2014). *Sensation and Perception*. New York, NY: Worth Publishers. p. 77.
- [39]Moini, Alireza. *Vision chips*. Boston, Springer US, 2000.
- [40]Sendhoff, Bernhard. *Artificial Neural Networks - ICANN 96: 6th International Conference*, Bochum, Germany, July 16 - 19, 1996. Proceedings. Germany, Springer, 1996.
- [41]Marcus Jacobson (1993). *Foundations of neuroscience* (2nd ed.). Springer. p. 277.
- [42]H. K. Hartline, H. C. Wagner, and F. Ratliff. Inhibition in the eye of *Limulus*. *Journal of General Physiology*, 39:651–673, 1956
- [43]R. F. Lyon, "The optical mouse, and an architectural methodology for smart digital sensors," *CMU Conference on VLSI Systems and Computations*, pp. 1-19, 1981.
- [44]J. G. Nicholls, A. R. Martin, B. G. Wallace, and P. A. Fuchs. *From Neuron to Brain* (4th ed.). Sinauer Associates, Inc., Sunderland, MA, 2001.
- [45]R. M. Arthur, R. R. Pfeiffer, and N. N. Suga. Properties of "two-tone inhibition" in primary auditory neurones. *Journal of Physiology*, 212:593–609, 1971.
- [46]A. Kaneko. Physiological and morphological identification of horizontal, bipolar and amacrine cells in goldfish retina. *Journal of Physiology*, 207:623–633, 1970.

- [47]R. J. Sayer, M. J. Friedlander, and S. J. Redman. The time course and amplitude of EPSPs evoked at synapses between pairs of CA3/CA1 neurons in the hippocampal slice. *Journal of Neuroscience*, 10:826–836, 1990.
- [48]Yantis, Steven. *Sensation and Perception*. New York, NY: Worth Publishers, 2014.
- [49]Roska B, Nemeth E, Orzo L, Werblin FS (1 March 2000). "Three levels of lateral inhibition: A space-time study of the retina of the tiger salamander". *J Neurosci*. 20 (5): 1941–51.
- [50]J. W. Mink. The basal ganglia: focused selection and inhibition of competing motor programs. *Progress in Neurobiology*, 50:381–425, 1996.
- [51]Stocco A, Lebiere C, Anderson JR. Conditional routing of information to the cortex: a model of the basal ganglia's role in cognitive coordination. *Psychol Rev*. 2010;117(2):541-74.
- [52]Chakravarthy, V. S.; Joseph, Denny; Bapi, Raju S. (2010). "What do the basal ganglia do? A modeling perspective". *Biological Cybernetics*. 103 (3): 237–53.
- [53]J. Carr. Tremor in Parkinson's disease. *Parkinsonism and Related Disorders*, 8:223–234, 2002.
- [54]D. Knopman and M. J. Nissen. Procedural learning is impaired in Huntington's disease: from the serial reaction time task. *Neuropsychologia*, 29:245–254, 1991.
- [55]Perez-Costas E, Melendez-Ferro M, Roberts RC. Basal ganglia pathology in schizophrenia: dopamine connections and anomalies. *J Neurochem*. 2010;113(2):287-302.
- [56]J. J. Hopfield. Neural networks and physical systems with emergent collective computational abilities. *Proc. Nat. Acad. Sci.*, 79:2554–2558, 1982.
- [57]J. J. Hopfield. Neurons with graded response have collective computational properties like those of two-state neurons. *Proc. Nat. Acad. Sci.*, 81:3088–3092, 1984.
- [58]Gregor, K., Szlam, A., and LeCun, Y. (2011b). Structured sparse coding via lateral inhibition. In *Advances in Neural Information Processing Systems (NIPS 2011)*, volume 24.
- [59]Cao, C., Wang, Z., Wang, L., et al.: Lateral Inhibition-inspired Convolutional Neural Network for Visual Attention and Saliency Detection. *Association for the Advancement of Artificial Intelligence (2018)*
- [60]Xu M., Zhang H., Yang J. (2018) Prohibited Item Detection in Airport X-Ray Security Images via Attention Mechanism Based CNN. In: Lai JH. et al. (eds) *Pattern Recognition and Computer Vision. PRCV 2018. Lecture Notes in Computer Science*, vol 11257. Springer, Cham

- [61]R. Coultrip, R. Granger, and G. Lynch. A cortical model of winner-take-all competition via lateral inhibition. *Neural Networks*, 5:47–54, 1992.
- [62]B. Ermentrout. Complex dynamics in winner-take-all neural nets with slow inhibition. *Neural Networks*, 5:415–431, 1992.
- [63]T. Fukai and S. Tanaka. A simple neural network exhibiting selective activation of neuronal ensembles: from winner-take-all to winners-share-all. *Neural Computation*, 9:77–97, 1997.
- [64]X. Xie, R. H. R. Hahnloser, and H. S. Seung. Selectively grouping neurons in recurrent networks of lateral inhibition. *Neural Computation*, 14:2627–2646, 2002.
- [65]J. A. Feldman and D. H. Ballard. Connectionist models and their properties. *Cognitive Science*, 6:205–254, 1982.
- [66]C. Koch and S. Ullman. Shifts in selective visual attention: towards the underlying neural circuitry. *Human Neurobiology*, 4:219–227, 1985.
- [67]E. Majani, R. Erlanson, and Y. Abu-Mostafa. On the K-winners-take-all network. In D. S. Touretzky, editor, *Advances in Neural Information Processing Systems I*, pages 634–642. Morgan Kaufmann, Cambridge, MA, 1989.
- [68]J. P. F. Sum and P. K. S. Tam. Note on the Maxnet dynamics. *Neural Computation*, 8:491–499, 1996.
- [69]A. L. Yuille and N. M. Grzywacz. Winner-take-all networks. In M. A. Arbib, editor, *The handbook of brain theory and neural networks* (2nd ed.), pages 1228–1231. MIT Press, Cambridge, 2003.
- [70]K. Ito. *Encyclopedic Dictionary of Mathematics* (2nd ed.). MIT Press, Cambridge, MA, 1993.
- [71]K. Gurney, T. J. Prescott, and P. Redgrave. A computation model of action selection in the basal ganglia (I): a new functional anatomy. *Biological Cybernetics*, 84:401–410, 2001.
- [72]K. Gurney, T. J. Prescott, and P. Redgrave. A computation model of action selection in the basal ganglia (II): analysis and simulation of behaviour. *Biological Cybernetics*, 84:411–423, 2001.
- [73]M. Forti and A. Tesi. New conditions for global stability of neural networks with application to linear and quadratic programming problems. *IEEE Trans. Circuits and Systems I*, 42(7):354–366, 1995.
- [74]J. R. Wickens and D. E. Oorschot. Neural dynamics and surround inhibition in the neostriatum: a possible connection. In R. Miller and J. R. Wickens, editors, *Brain*

Dynamics and the Striatal Complex, pages 141–150. Harwood Academic Publishers, Australia, 2000.

- [75]Z.-H. Guan, G. Chen, and Y. Qin. On equilibria, stability, and instability of Hopfiled neural networks. *IEEE Trans. Neural Networks*, 11:534–540, 2000.
- [76]H. K. Khalil. *Nonlinear Systems* (2nd ed.). Prentice Hall, Upper Saddle River, NJ, 1996.
- [77]P. M. Groves. A theory of the functional organization of the neostriatum and the neostriatal control of movement. *Brain Research*, 286:109–132, 1983.
- [78]B. J. T. Fernandes, G. D. C. Cavalcanti, and T. I. Ren, “Lateral inhibition pyramidal neural network for image classification,” *IEEE Trans. Cybern.*, vol. 43, no. 6, pp. 2082–2092, Dec. 2013
- [79]R. A. Horn and C. R. Johnson. *Matrix Analysis*. Cambridge University Press, Cambridge, UK, 1985.
- [80]R. L. T. Hahnloser. On the piecewise analysis of networks of linear threshold neurons. *Neural Networks*, 11:691–697, 1998.
- [81]W. J. Wolfe, D. Mathis, C. Anderson, J. Rothman, M. Gottler, G. Brady, R. Walker, G. Duane, and G. Alagband. K-winner networks. *IEEE Trans. Neural Networks*, 2:310–315, 1991.
- [82]J. C. Yen and S. Chang. Improved winner-take-all neural networks. *Electronics Letter*, 28:662–664, 1992.
- [83]Z.-H. Guan, G. Chen, and Y. Qin. On equilibria, stability, and instability of Hopfiled neural networks. *IEEE Trans. Neural Networks*, 11:534–540, 2000.
- [84]H. Mostafa, L. K. Muller, and G. Indiveri. Recurrent networks of coupled winner-take-all oscillators for solving constraint satisfaction problems. In C.J.C. Burges, L. Bottou, M. Welling, Z. Ghahramani, and K.Q. Weinberger, editors, *Advances in Neural Information Processing Systems (NIPS)*, volume 26, pages 719–727, 2013.
- [85]Fukai T. and Tanaka S. (1997) A simple neural network exhibiting selective activation of neuronal ensembles: From Winner-take-all to Winners-Share-all. *Neural Computation* 9, 77-97.
- [86]S. Haykin, *Neural Networks: A Comprehensive Foundation*, 2nd ed. Englewood Cliffs, NJ: Prentice-Hall, 1999.
- [87]Fukushima, K.: Cognitron: a self-organizing multilayered neural network. *Biol.Cybernetics*20, 121-136(1975)
- [88]Spratling, M. W., & Johnson, M. H. (2002). Pre-integration lateral inhibition enhances unsupervised learning. *Neural Computation*, 14(9), 2157–2179.

- [89]Jain, A. K. and Mao, J. 1996. Artificial neural networks: A tutorial. *IEEE Computer* 29 (Mar.), 31–44.
- [90]J. Rinzel. Models in neurobiology. In R.H. Enns, B.L. Jones, R.M. Miura, and S.S. Rangnekar, editors, *Nonlinear Phenomena in Physics and Biology*, pages 345367. Plenum Press, New York, 1981.
- [91]Nagumo J., Arimoto S., and Yoshizawa S. (1962) An active pulse transmission line simulating nerve axon. *Proc IRE*. 50:20612070.
- [92]Ermentrout G. B., Terman D. H. *Mathematical Foundations of Neuroscience*. New York: Springer; 2010.
- [93]Stiefel, K. M., & Ermentrout, G. B. (2016). Neurons as oscillators. *Journal of Neurophysiology*, 116, 2950–2960.
- [94]Catterall, W. A., Raman, I. M., Robinson, H. P., Sejnowski, T. J., and Paulsen, O. (2012). The Hodgkin-Huxley heritage: from channels to circuits. *J. Neurosci.* 32, 14064–14073.
- [95]Izhikevich E (2007) *Dynamical systems in neuroscience: the geometry of excitability and bursting*. Cambridge (Massachusetts): MIT Press.
- [96]Winfree AT. *The Geometry of Biological Time*. Springer Verlag, Berlin 1980.